Chapter 2: Observations: Atmosphere and Surface

Coordinating Lead Authors: Dennis L. Hartmann (USA), Albert Klein Tank (Netherlands), Matilde Rusticucci (Argentina)

Lead Authors: Lisa Alexander (Australia), Stefan Broennimann (Switzerland), Yassine Abdul-Rahman Charabi (Oman), Frank Dentener (EU / Netherlands), Ed Dlugokencky (USA), David Easterling (USA), Alexey Kaplan (USA), Brian Soden (USA), Peter Thorne (USA / UK), Martin Wild (Switzerland), Panmao Zhai (China)

Contributing Authors: Robert Adler (USA), Richard Allan (UK), Robert Allan (UK), Donald Blake (USA), Owen Cooper (USA), Aiguo Dai (USA), Robert Davis (USA), Sean Davis (USA), Markus Donat (Australia), Vitali Fioletov (Canada), Erich Fischer (Switzerland), Leopold Haimberger (Austria), Ben Ho (USA), John Kennedy (UK), Stefan Kinne (Germany), James Kossin (USA), Norman Loeb (USA), Cathrine Lund-Myre (Norway), Carl Mears (USA), Christopher Merchant (UK), Steve Montzka (USA), Colin Morice (UK), Joel Norris (USA), David Parker (UK), Bill Randel (USA), Andreas Richter (Germany), Matthew Rigby (UK), Ben Santer (USA), Dian Seidel (USA), Tom Smith (USA), David Stephenson (UK), Ryan Teuling (Netherlands), Junhong Wang (USA), Xiaolan Wang (Canada), Ray Weiss (USA), Kate Willett (UK), Simon Wood (UK)

Review Editors: Jim Hurrell (USA), Jose Marengo (Brazil), Fredolin Tangang (Malaysia), Pedro Viterbo (Portugal)

Date of Draft: 5 October 2012

Notes: TSU Compiled Version

Table of Contents

Executive Summary

Observations of the atmosphere and surface indicate the following changes:

Atmospheric Composition

It is *virtually certain* that atmospheric burdens of long-lived greenhouse gases controlled by the Kyoto Protocol increased from 2005 to 2011. Annual increases in global mean CO_2 and N_2O mole fractions were at rates comparable to those observed over the previous decade. Atmospheric CH_4 began increasing again in 2007 after remaining nearly constant from 1999 to 2006. HFCs, PFCs, and SF_6 all continue to increase rapidly, but their relative contributions to radiative forcing are small.

For ozone depleting gases, whose production and emissions are controlled by the Montreal Protocol, it is *virtually certain* that the global mean mole fractions of major CFCs are decreasing and HCFCs are increasing. Atmospheric burdens of CFC-11, CFC-12, CFC-113, CCl_4, CH_3CCl_3, and halons have decreased since 2005. HCFCs, which are transitional substitutes for CFCs, continue to increase, but the distribution of their emissions is changing.

Global satellite measurements of stratospheric water vapour (an important radiative forcing component), show substantial variability for 1992–2011 with a step-like decrease after 2000 and increases since 2005, but with *high confidence* the net change during 1992–2011 is small.

Stratospheric ozone has declined from ~1980 through the mid-1990s, partially recovered to ~2000, and remained constant until 2010 at a level 2.5% below the 1964–1980 mean (*high confidence*).

Surface observations, balloon soundings and satellite retrievals indicate tropospheric ozone trends over the past few decades, but the trends and the confidence attached to them vary from region to region. Almost all East Asian surface sites show increasing ozone, supported by satellite column ozone observations. In North America and Europe the trends are mixed (*medium confidence*).

Satellite observations of NO_x and CO indicate strong regional differences of ozone precursor gas trends, with increases of more than a factor 2 in Asia (NO_2), decreases in Europe and North America (30–50%), and an overall small global decline of CO (*medium confidence*).

Ground and satellite-based remotely sensed measurements of Aerosol Optical Depth (AOD), a measure of integrated columnar aerosol load, indicate positive trends in Eastern and Southern Asia, and negative trends in Europe and Eastern USA during the 1990s and 2000s, in qualitative agreement with a host of observations showing declining particulate matter air pollution at surface stations in Europe and the USA (*high confidence*). No reliable AOD trend can be detected in other regions of the world.

Radiation Budgets

Satellite records of top of the atmosphere radiation fluxes indicate a *likely* continuation of the decadal variations in the tropical radiation budget. Globally, no significant changes in the global planetary albedo are apparent since 2000. The variability in the Earth's energy imbalance at the top of the atmosphere that is related to El Niño-Southern Oscillation (ENSO) is consistent with ocean heat content records.

The evidence for widespread decadal changes in surface solar radiation (dimming until the 1980s and subsequent brightening) has been substantiated. *Confidence is high* because these changes are in line with observed changes in related variables, such as sunshine duration and hydrological quantities. There is *medium confidence* for increasing downward thermal and net radiation at the surface in recent decades.

Temperature

Globally averaged near surface temperatures have increased since 1901. This warming is *virtually certain* and has been particularly marked since the 1970s. The global combined land and ocean temperature data show an increase of about 0.8°C over the period 1901–2010 and about 0.5 °C over the period 1979–2010 when described by a linear trend. The warming from 1886–1905 (early-industrial) to 1986–2005 (reference period for the modelling chapters and the Atlas in Annex 1) is 0.66°C ± 0.06°C (5 to 95% confidence interval).

It is *virtually certain* that globally averaged land surface air temperatures have risen since the late 19th Century. Several independently analyzed data records of global and regional land surface air temperature obtained from station observations support this conclusion.

It is *likely* that urban heat-island effects and land use change effects have not raised the centennial global land surface air temperature trends by more than 10% of the observed trend. This is an average value; in some regions that have rapidly developed urban heat island and land use change impacts on regional trends have been substantially larger.

Confidence in the reported decrease in diurnal temperature range *is medium-to-low,* as recent analyses of the raw data on which previous analyses were based point to the potential for pervasive biases that differently affect maximum and minimum temperatures.

It is *virtually certain* that the global average sea surface temperatures have increased since the beginning of the 20th Century. Intercomparisons of new data records obtained by different measurement methods, including satellite data, have resulted in better understanding of errors and biases in the records.

Based upon multiple independent analyses of measurements from radiosondes and satellite sensors it is *virtually certain* that globally the troposphere has warmed since the mid 20th Century. There is only *medium to low confidence* in the rate of change and its vertical structure. Estimates of tropospheric warming rates encompass surface temperature warming rate estimates.

While it is *virtually certain* that globally the lower stratosphere has cooled since the mid 20th Century and the whole stratosphere since 1979, there is only *low confidence* in the cooling rate and vertical structure.

Hydrological Cycle

Confidence in global precipitation change over land *is low* prior to 1950 and *medium* afterwards because of data incompleteness. When virtually all the land area is filled in using a reconstruction method, the resulting time series shows little change in land-based precipitation since 1900. This is different from AR4, which reported that global precipitation averaged over land areas has increased, with most of the increase occurring in the early to mid 20th Century.

The mid-latitudes and higher latitudes of the NH do show an overall increase in precipitation from 1900–2010, however *confidence is low* because of much uncertainty in the data records for the early 20th Century. Insufficient evidence exists to define a long-term temporal change of precipitation in the mid-latitudes of the SH. Precipitation in the tropics has *likely* increased over the last decade, reversing the drying trend that occurred from the mid-1970s to mid-1990s reported in AR4.

In most regions analyzed, it is *likely* that decreasing numbers of snowfall events are occurring where increased winter temperatures have been observed. Antarctica is the exception, where increased snowfall is occurring with observed higher temperatures that are still below freezing. *Confidence is low* for the changes in snowfall over Antarctica. Changes in the area covered by snow are assessed in Chapter 4.

The most recent and most comprehensive analyses of river runoff which include newly assembled observational records do not support the AR4 conclusion that global runoff increased during the 20th Century. Average runoff has not changed in the majority of rivers, but year-to-year variability has increased.

As reported in AR4, absolute moistening of the atmosphere near the surface has been widespread across the globe since the 1970s, with *very high confidence*. However, during recent years this has abated over land, coincident with greater warming over land relative to the oceans. As a result, fairly widespread decreases in relative humidity near the surface have been observed over the land areas recently. Radiosonde, GPS and satellite observations indicate increases in tropospheric water vapour at continental scales, which are consistent with the observed increase in atmospheric temperature aloft. It is *very likely* that tropospheric specific humidity has increased since the 1970s. Because tropospheric temperatures have also increased, significant trends in tropospheric relative humidity have not been observed.

While trends of cloud cover are consistent between independent data sets in certain regions, substantial ambiguity and therefore *low confidence* remains in the observations of global-scale cloud variability and trends.

Extreme Events

Recent analyses of extreme events generally support the AR4 and SREX conclusions. It is *very likely* that the overall number of cold days and nights has decreased and the overall number of warm days and nights has increased on the global scale between 1951 and 2010 (with warming trends between 2.48 ± 0.64 and 5.75 ± 1.33 days per decade dependent on index). Globally, there is *medium confidence* that the length of warm spells, including heat waves, has increased since the middle of the 20th Century.

Consistent with AR4 conclusions, it is *likely* that the number of heavy precipitation events (e.g., 95th percentile) has increased significantly in more regions than it has decreased since 1950. *Confidence is highest* for North America where the most consistent trends towards heavier precipitation events are found.

There continues to be insufficient evidence and thus *low confidence* for consistent trends in the magnitude or frequency of floods on a global scale.

New results indicate that the AR4 conclusions regarding global increasing trends in hydrological droughts since the 1970s are no longer supported. Not enough evidence exists at present to suggest anything else than *low confidence* in observed large-scale trends in dryness (lack of rainfall), due to lack of direct observations, dependencies of inferred trends on the index choice and geographical inconsistencies in the trends.

Recent re-assessments of tropical cyclone data do not support the AR4 conclusions of an increase in the most intense tropical cyclones or an upward trend in the potential destructiveness of all storms since the 1970s. There is *low confidence* that any reported long-term changes are robust, after accounting for past changes in observing capabilities. However over the satellite era, increases in the intensity of the strongest storms in the Atlantic appear robust.

There is still *insufficient evidence* to determine whether robust global trends exist in small-scale severe weather events such as hail or tornadoes.

Atmospheric Circulation and Indices of Variability

Large variability on interannual to decadal time scales and remaining differences between data sets hamper robust conclusions on long-term changes in large-scale atmospheric circulation. *Confidence is high* that some trend features that appeared from the 1950s or earlier to the 1990s reported in AR4 (e.g., an increase in the mid-latitude westerly winds and the NAO index or a weakening of the Pacific Walker circulation) have been largely offset by more recent changes.

Nevertheless, it is *likely* that, in a zonal mean sense, circulation features have moved poleward (widening of the tropical belt, poleward shift of storm tracks and jet streams, contraction of the polar vortex) since the 1970s.

Finally, the evidence of climate change from observations of the atmosphere and surface has grown significantly during recent years, but at the same time new and improved ways of characterizing and quantifying uncertainty have highlighted the challenges that remain for developing long-term and climate quality data records for every region of the world.

2.1 Introduction

This chapter assesses the scientific literature on atmospheric and surface observations since AR4 (IPCC, 2007a). The most likely changes in physical climate variables or climate forcing agents are identified based on current knowledge, following the IPCC AR5 uncertainty guidance.

As described in AR4 (Trenberth et al., 2007), the climate varies over all spatial and temporal scales: from the diurnal cycle, to interannual variability such as El Niño, to multi-decadal and millennial variations. Climate change is considered to be statistically significant variations in either the mean state of the climate or in its variability, persisting for an extended period of time. In this chapter, climate change is examined for the period with instrumental observations, since about 1850. Observed change prior to this date is assessed in Chapter 5. Trends have been assessed for the periods starting in 1880, 1901, 1951, 1979, 1998 and ending in 2011 provided that data are available. For many variables derived from satellite data, information is available for 1979-2011 only. Where possible, the time interval 1961-1990 has been chosen as the climatological reference period (or normal period) for averaging. This choice enables direct comparisons with AR4. The word 'trend' is used to designate a long-term movement in a time series which may be regarded, together with the oscillation and random component, as generating the observed values (see Annex III: Glossary). Where numerical values are given, they are equivalent linear changes (Box 2.2), though more complex non-linear changes in the variable will often be clear from the description and plots of the time series.

In recent decades, advances in the global climate observing system have contributed to improved monitoring capabilities. The results of new observation techniques, in particular satellites, provide additional measures for climate change, which have been assessed in this and subsequent chapters together with more traditional measures. Dynamical reanalysis data sets of the global atmosphere are also used (Box 2.3). Developing homogeneous long-term records from these different sources remains a challenge.

The longest observational series are land surface air temperatures and sea surface temperatures (Section 2.4). Like all physical climate system measurements they suffer from non-climatic artefacts that must be taken into account (Box 2.1). The global mean surface air temperature remains an important climate change measure for several reasons. Climate sensitivity is typically assessed in the context of global surface temperature responses to a doubling of CO_2 (Chapter 8) and global mean surface temperature is thus a key metric in the climate change policy framework. Also, because it extends back in time farther than any other instrumental series, global mean surface air temperature is key to understanding both the causes of change and the patterns, role and magnitude of natural variability (Chapter 10). Starting at various points in the 20th Century, additional observations, including balloon-borne measurements, satellite measurements and reanalysis products, allow analyses of indicators such as atmospheric composition (Section 2.2), radiation budgets (Section 2.3), hydrological cycle changes (Section 2.5), extreme event characterizations (Section 2.6, FAQ 2.2) and circulation indices (Section 2.7). A full understanding of the climate system characteristics and changes requires analyses of all such variables as well as ocean (Chapter 3) and cryosphere (Chapter 4) indicators. Through such a holistic analysis, a clearer and more robust assessment of the changing climate system emerges (FAQ 2.1).

Observations of the abundances of greenhouse gases (GHGs) and of aerosols are also included in this chapter (Section 2.2). Global trends in GHGs are indicative of the imbalance between sources and sinks in GHG budgets, and play an important role in emissions verification on a global scale. The radiative forcing effects of GHGs and aerosols are assessed in Chapter 8. Aerosol-cloud interactions are assessed in Chapter 7.

Besides global averages of climate variables, this chapter also focuses on the changes over large regions (typically latitudinal bands or continents) and on a limited number of preferred patterns (or modes) of variability, which determine the main seasonal and longer-term climate anomalies at the regional scale. Trends in these patterns are discussed in Section 2.7. The regional changes associated with global warming can be complex and perhaps even counter-intuitive, such as changes in planetary waves in the atmosphere that result in regional cooling (Trenberth et al., 2007).

Changes in variability and extremes are also assessed (Section 2.6). As illustrated in SREX (Seneviratne et al., 2012a), extremes of weather and climate, such as droughts and wet spells, are important because of their

large impacts on society and the environment. The nature of variability at different spatial and temporal scales is vital to our understanding of extremes.

As described in AR4, many different drivers for the observed changes may exist. It is important to note that the question of whether the observed changes are outside the possible range of natural internal climate variability and consistent with the climate effects from changes in atmospheric composition is not addressed in this Chapter, but rather in Chapter 10. No attempt to further interpret the observed changes in terms of multidecadal oscillatory (or low frequency) variations, (long-term) persistence and/or secular trends (e.g., as in Wu et al., (2011) has been attempted either, because the results of such analyses depend entirely on the null hypothesis one formulates (Cohn and Lins, 2005; Mann, 2011; Mills, 2010). In this Chapter, the robustness of the observed changes is assessed in relation to various sources of observational uncertainty (Box 2.1). In addition, the reported trend significance and statistical confidence intervals provide an indication of how large the observed trend is compared to the range of observed variability. The chapter also examines the physical consistency across different observations, which helps to provide additional confidence in the reported changes (Section 2.8). Additional information about data sources and methods are described in Appendix 2.A.

[START BOX 2.1 HERE]

Box 2.1: Uncertainty in Observational Records

The vast majority of historical (and modern) weather observations were not made for climate monitoring purposes. Measurements have changed in nature as data demands, observing practices and technologies have evolved. These changes almost always alter the characteristics of observational records, changing their mean, their variability or both, such that it is necessary to process the raw measurements before they can be considered useful for assessing the true climate evolution. This is true of all observing techniques that measure physical atmospheric quantities. The uncertainty in observational records encompasses instrumental / recording errors, errors of representation (e.g., exposure, observing frequency or timing), as well as errors due to physical changes in the instrumentation (such as station relocations or new satellites). All further processing steps (gridding, interpolating, averaging) have their own particular uncertainties. Since there is no unique, unambiguous, way to identify and account for non-climatic artefacts in the vast majority of records, there must be a degree of uncertainty as to how the climate system changed.The only exceptions are certain atmospheric composition and flux measurements that are directly tied to internationally recognized absolute measurement standards (e.g., the CO_2 record at Manua Loa (Keeling et al., 1976)).

Uncertainty in data set production can result from the choice of parameters within a particular analytical framework, parametric uncertainty, or from the choice of overall analytical framework, structural uncertainty. Structural uncertainty is best estimated by having multiple independent groups assess the same data using distinct approaches. More analyses assessed now than at the time of AR4 include a published estimate of parametric or structural uncertainty. It is important to note that the literature includes a very broad range of approaches. Great care has been taken in comparing the published uncertainty ranges as they almost always do not constitute a like-for-like comparison. In general, studies that account for multiple potential error sources in a rigorous manner yield larger uncertainty ranges. This yields an apparent paradox in interpretation as one might think that smaller uncertainty ranges should indicate a better product. However, in many cases this would be an incorrect inference as the smaller uncertainty range may instead reflect that the published estimate considered only a subset of the plausible sources of uncertainty.

To conclude, the vast majority of the raw observations used to monitor the state of the climate contain residual non-climatic influences. Removal of these influences cannot be done definitively and neither can the uncertainties be unambiguously defined. Therefore, care is required in interpreting both data products and their stated uncertainty estimates. Confidence can be built from: redundancy in efforts to create products; product heritage; and cross-comparisons of variables that would be expected to co-vary for physical reasons, such as land surface temperatures and sea surface temperatures around coastlines. Finally, trends are often quoted as a way to synthesize the data into a single number. Uncertainties that arise from such a process and the choice of technique used within this Chapter are described in more detail in Box 2.2.

[END BOX 2.1 HERE]

2.2 Changes in Atmospheric Composition

2.2.1 Long-Lived Greenhouse Gases

AR4 (IPCC, 2007a) concluded that increasing atmospheric burdens of long-lived greenhouse gases (LLGHG) resulted in a 9% increase in their radiative forcing from 1998 to 2005. While the atmospheric abundances of many LLGHG increased since 2005, there were decreases in the burdens of some ozone depleting substances (ODS) whose production and emissions were controlled by the Montreal Protocol on Substances that Deplete the Ozone Layer (1987; hereafter, 'Montreal Protocol'). Based on updated in situ observations, this assessment concludes that these trends continue, resulting in a 7.5% increase in radiative forcing from 2005 to 2011, with CO_2 contributing 80% of the increase. Of note is an increase in the average growth rate of atmospheric CH_4 from ~0.5 ppb yr^{-1} during 1999 to 2006 to ~6 ppb yr^{-1} from 2007 through 2011. Current observation networks are sufficient to quantify global annual mean burdens used to calculate radiative forcing and to constrain global emission rates, but they are not sufficient for accurately estimating regional scale emissions and how they are changing with time.

The globally, annually averaged LLGHG mole fractions reported here are used in Chapter 8 to calculate radiative forcing, which totals 2.79 W m^{-2} since 1750. A direct, inseparable connection exists between observed changes in atmospheric composition and their emissions and losses (discussed in Chapter 6 for CO_2, CH_4, and N_2O). A global GHG budget consists of the total atmospheric burden, total global rate of production or emission (i.e., sources), and the total global rate of destruction or removal (i.e., sinks). Precise, accurate systematic observations from independent globally distributed measurement networks are used to estimate global annual mean LLGHG mole fractions at Earth's surface, and these allow estimates of global burdens. Emissions are predominantly from surface sources, which are described in Chapter 6 for CO_2, CH_4, and N_2O. Direct use of observations of LLGHGs to model their regional budgets can also play an important role in emissions verification (Nisbet and Weiss, 2010).

Systematic measurements of LLGHGs in ambient air began at various times during the last six decades, with earlier atmospheric histories being reconstructed from measurements of air trapped in polar ice cores or in firn. In contrast to the physical meteorological parameters discussed elsewhere in this chapter, measurements of LLGHGs are reported relative to standards developed from fundamental SI base units (SI = International System of Units) as dry-air mole fractions, a unit that is conserved with changes in temperature and pressure. This eliminates dilution by H_2O vapour, which can reach 4% of total atmospheric composition. Here, the following abbreviations are used: ppm = µmol mol^{-1}; ppb = nmol mol^{-1}; and ppt = pmol mol^{-1}. Unless noted otherwise, globally, an average of NOAA and AGAGE annually averaged surface mean mole fractions are described in Section 2.2.1; see Appendix 2.A for further species not listed here.

Table 2.1 summarizes globally, annually averaged LLGHG mole fractions from four independent measurement programs. Sampling strategies and techniques for estimating global means and their uncertainties vary among programs. Differences among measurement programs are relatively small and will not add significantly to uncertainty in radiative forcing. Time series of the LLGHGs are plotted in Figures 2.1 (CO_2), 2.2 (CH_4), 2.3 (N_2O), and 2.4 (halogen-containing compounds).

Table 2.1: Global annually averaged surface dry air mole fractions and their change since 2005 (columns labelled 2011–2005) for LLGHGs from four measurement networks. Units are ppt (parts per trillion) except where noted (ppm = parts per million; ppb = parts per billion). Uncertainties are 90% confidence intervals.[a] GWP = Global Warming Potential from Chapter 8.

	Lifetime	GWP	UCI	UCI	SIO[b]/AGAGE	SIO/AGAGE	NOAA	NOAA
Species	(year)	(100 year)	2011	2011–2005	2011	2011–2005	2011	2011–2005
CO_2 (ppm)	---	1	---	---	390.48 ± 0.28	11.67 ± 0.37	390.44 ± 0.16	11.66 ± 0.13
CH_4 (ppb)	~9	25	1798.1 ± 0.6	26.6 ± 0.9	1803.1 ± 4.8	28.9 ± 6.8	1803.2 ± 1.2	28.6 ± 0.9
N_2O (ppb)	120	298	---	---	324.0 ± 0.1	4.7 ± 0.2	324.3 ± 0.1	5.24 ± 0.14

SF_6	3200	22,800	---	---	7.26 ± 0.02	1.65 ± 0.03	7.31 ± 0.02	1.64 ±0.01
CF_4	50000	7,390	---	---	79.0 ± 0.1	4.0 ± 0.2	---	---
C_2F_6	10000	12,200	---	---	4.16 ± 0.02	0.50 ± 0.03	---	---
HFC-125	29	3,500	---	---	9.58 ± 0.04	5.89 ± 0.07	---	---
HFC-134a	14	1,430	63.4 ± 0.9	27.7 ± 1.4	62.4 ± 0.3	28.2 ± 0.4	63.0 ± 0.6	28.2 ± 0.1
HFC-143a	47.1	4,470	---	---	12.04 ± 0.07	6.39 ± 0.10	---	---
HFC-152a	1.4	124	---	---	6.4 ± 0.1	3.0 ± 0.2	---	---
HFC-23	222	14,800	---	---	24.0 ± 0.3	5.2 ± 0.6	---	---
CFC-11	45	4,750	237.9 ± 0.8	–13.2 ± 0.8	236.9 ± 0.1	–12.7 ± 0.2	238.5 ± 0.2	–13.0 ± 0.1
CFC-12	100	10,900	525.3 ± 0.8	–12.8 ± 0.8	529.5 ± 0.2	–13.4 ± 0.3	527.4 ± 0.4	–14.1 ± 0.1
CFC-113	85	6,130	74.9 ± 0.6	–4.6 ± 0.8	74.29 ± 0.06	–4.25 ± 0.08	74.40 ± 0.04	–4.35 ±0.02
HCFC-22	12	1,810	209.0 ± 1.2	41.5 ± 1.4	213.4 ± 0.8	44.6 ± 1.1	213.2 ± 1.2	44.3 ± 0.2
HCFC-141b	9.3	725	20.8 ± 0.5	3.7 ± 0.5	21.38 ± 0.09	3.70 ± 0.1	21.4 ± 0.2	3.76 ± 0.03
HCFC-142b	17.9	2,310	21.0 ± 0.5	4.9 ± 0.5	21.35 ± 0.06	5.72 ± 0.09	21.0 ± 0.1	5.73 ± 0.04
CCl_4	26	1,400	87.8 ± 0.6	–6.4 ± 0.5	85.0 ± 0.1	–6.9 ± 0.2	86.5 ± 0.3	–7.8 ± 0.1
CH_3CCl_3	5	146	6.8 ± 0.6	–14.8 ± 0.5	6.3 ± 0.1	–11.9 ± 0.2	6.35 ± 0.07	–12.1 ± 0.1

Notes:
AGAGE = Advanced Global Atmospheric Gases Experiment; NOAA = National Oceanic and Atmospheric Administration, Earth System Research Laboratory, Global Monitoring Division; SIO = Scripps Institution of Oceanography, University of California, San Diego; UCI = University of California, Irvine, Department of Chemistry.
HFC-125 = CHF_2CF_3; HFC-134a = CH_2FCF_3; HFC-143a = CF_3CH_3; HFC-152a = CH_3CHF_2; HFC-23 = CHF_3; CFC-11 = $CFCl_3$; CFC-12 = CF_2Cl_2; CFC-113 = $CF_2ClCFCl_2$; HCFC-22 = CHF_2Cl; HCFC-141b = CH_3CFCl_2; HCFC-142b = CH_3CF_2Cl.
(a) Each program uses different methods to estimate uncertainties. (b) SIO reports only CO_2; all other values reported in these columns are from AGAGE.
Budget lifetimes are shown; for CH_4 and N_2O, perturbation lifetimes (12 year for CH_4 and 114 year for N_2O) are used to estimate global warming potentials.
Pre-industrial (1750) values determined from air extracted from ice cores are below detection limits for all species except CO_2 (278 ± 2 ppm), CH_4 (722 ± 25 ppb), N_2O (270 ± 7 ppb) and CF_4 (34.7 ± 0.2 ppt).

[INSERT FIGURE 2.1 HERE]
Figure 2.1: a) Globally averaged CO_2 dry air mole fractions from Scripps Institution of Oceanography (SIO) at monthly time resolution based on measurements from Mauna Loa, Hawaii and South Pole (red) and NOAA/ESRL/GMD at quasi-weekly time resolution (blue). SIO values are deseasonalized. b) Instantaneous growth rates for globally averaged atmospheric CO_2 using the same colour code as in (a). Growth rates are calculated as the time derivative of the deseasonalized global averages.

[INSERT FIGURE 2.2 HERE]
Figure 2.2: a) Globally averaged CH_4 dry air mole fractions from UCI (green), AGAGE (red), and NOAA/ESRL/GMD (blue) b) Instantaneous growth rate for globally averaged atmospheric CH_4 using the same colour code as in (a). Growth rates were calculated as in Figure 2.1.

[INSERT FIGURE 2.3 HERE]
Figure 2.3: a) Globally averaged N_2O dry air mole fractions from AGAGE (red) and NOAA/ESRL/GMD (blue). b) Instantaneous growth rates for globally averaged atmospheric N_2O. Growth rates were calculated as in Figure 2.1.

[INSERT FIGURE 2.4 HERE]

Figure 2.4: Globally averaged dry air mole fractions at Earth's surface of the major halogen-containing LLGHGs. These are derived mainly using monthly mean measurements from the AGAGE and NOAA/ESRL/GMD networks. For clarity, only the most abundant chemicals are shown in different compound classes and results from different networks have been combined when both are available. While differences exist, different network measurements agree reasonably well (except for CCl_4 (differences of 2–4% between networks) and HCFC-142b (differences of 3–6% between networks)) (see also WMO, 2011; Chapter 1).

2.2.1.1 Kyoto Protocol Gases (CO_2, CH_4, N_2O, HFCs, PFCs, and SF_6)

2.2.1.1.1 Carbon dioxide (CO_2)

Precise, accurate systematic measurements of atmospheric CO_2 at Mauna Loa, Hawaii and South Pole were started by C. D. Keeling from Scripps Institution of Oceanography in the late-1950s (KEELING et al., 1976a; Keeling et al., 1976b). The pre-industrial (1750) globally averaged abundance of atmospheric CO_2 based on measurements of air extracted from ice cores and from firn is 278 ± 2 ppm (Etheridge et al., 1996). Globally averaged CO_2 mole fractions since the start of the instrumental record are plotted in Figure 2.1. The main features in the contemporary CO_2 record are the long-term increase and the seasonal cycle resulting from seasonal photosynthesis and respiration by the terrestrial biosphere, mostly in the NH. The main contributors to increasing atmospheric CO_2 abundance are fossil fuel combustion and land use change. Multiple lines of observational evidence suggest that during the past few decades, most of the increasing atmospheric burden of CO_2 is from fossil fuel combustion (Tans, 2009). Since the last year for which the AR4 reported (2005), CO_2 has increased by 11.7 ppm to 390.5 ppm in 2011 (Table 2.1). From 1980 to 2011, the average annual increase in globally averaged CO_2 (from 1 Jan in one year to 1 Jan in the next year) was 1.68 ppm yr^{-1} (1 standard deviation = 0.55 ppm yr^{-1}). Since 2001, CO_2 has increased at 2.0 ppm yr^{-1} (1 standard deviation = 0.30 ppm yr^{-1}). The CO_2 growth rate varies significantly from year to year; since 1980, the range in annual increase is 0.67 ± 0.14 ppm in 1992 to 2.90 ± 0.14 ppm in 1998. Most of this interannual variability (IAV) in growth rate is driven by small changes in the balance between photosynthesis and respiration on land, each having global fluxes of ~100 PgC yr^{-1} (see Chapter 6).

2.2.1.1.2 Methane (CH_4)

Globally averaged CH_4 in 1750 was 722 ± 25 ppb (after correction to the NOAA-2004 CH_4 standard scale)(Dlugokencky et al., 2005; Etheridge et al., 1998), although human influences on the global CH_4 budget may have began much earlier than the industrial era (Ferretti et al., 2005; Ruddiman, 2003; Ruddiman, 2007). Direct atmospheric measurements of CH_4 of sufficient spatial coverage to calculate global annual means began in 1978 and are plotted through 2011 in Figure 2.2a. This time period is characterized by a decreasing rate of increase (Figure 2.2b) from the early 1980s until 1998, stabilization from 1999 to 2006, and an increasing global CH_4 burden from 2007 to 2011 (Dlugokencky et al., 2009; Rigby et al., 2008). Assuming no long-term trend in [OH], the observed decrease in CH_4 growth rate from the early-1980s through 2006 indicates an approach to steady state where total global emissions have been approximately constant at ~550 Tg CH_4 yr^{-1}. Superimposed on the long-term pattern is significant IAV; studies of this variability are used to improve understanding of the global CH_4 budget (see Chapter 6). The most likely drivers of increased atmospheric CH_4 were anomalously high temperatures in the Arctic in 2007 and greater than average precipitation in the tropics during 2007 and 2008 (Bousquet, 2011; Dlugokencky et al., 2009). Observations of the difference in CH_4 between zonal averages for northern and southern polar regions (53°–90°) (Dlugokencky et al., 2009; Dlugokencky et al., 2011) suggest that, so far, it is unlikely that Arctic CH_4 emissions from wetlands and shallow sub-sea CH_4 clathrates have measurably increased.

Reaction with OH is the main loss process for CH_4 (and for HFCs and HCFCs), and it is the largest term in the global CH_4 budget. Therefore, trends and IAV in [OH] significantly impact our understanding of changes in CH_4 emissions. AR4 reported no detectable trend in [OH] from 1979 to 2004, and there is no evidence from this assessment to change that conclusion for 2005 to 2011. Montzka et al., (2011a) analyzed 6 tracers whose atmospheric loss is predominantly by reaction with OH to show that IAV in global annual mean [OH] of more than a few percent is unlikely.

2.2.1.1.3 Nitrous oxide (N_2O)

Globally averaged N_2O in 2011 was 324.2 ppb, an increase of 5.0 ppb over the value reported for 2005 in AR4 (Table 2.1). This is an increase of 20% over the value estimated for 1750 from ice cores, 270 ± 7 ppb. Measurements of N_2O and its isotopic composition in firn air suggest the increase, at least since the early 1950s, is dominated by emissions from soils treated with nitrogen fertilizer and manure (Davidson, 2009;

Ishijima et al., 2007; Syakila and Kroeze, 2011). Since systematic measurements began in the late 1970s, N_2O has increased at an average rate of ~0.75 ppb yr^{-1} (Figure 2.3); this, combined with a decreasing atmospheric burden of CFC-12 makes it the third most important LLGHG contributing to radiative forcing (Elkins and Dutton, 2011).

There are persistent latitudinal gradients in annually averaged N_2O at background surface sites, with maxima in the northern subtropics, values about 1.7 ppb lower in the Antarctic, and values about 0.4 ppb lower in the Arctic (Huang et al., 2008). These persistent gradients contain information about anthropogenic emissions from fertilizer use at northern mid-latitudes and natural ocean emissions in upwelling regions of the tropics. N_2O time series also contain seasonal variations with peak-to-peak amplitudes of about 1 ppb in high latitudes of the NH and about 0.4 ppb at high southern and tropical latitudes. In the NH, exchange of air between the stratosphere (where N_2O is destroyed by photochemical processes) and troposphere is the dominant contributor to observed seasonal cycles, not seasonality in emissions (Jiang et al., 2007). Nevison et al. (2011) found correlations between the magnitude of detrended N_2O seasonal minima and lower stratospheric temperature providing evidence for a stratospheric influence on the timing and amplitude of the seasonal cycle at surface monitoring sites. In the SH, observed seasonal cycles are also affected by stratospheric influx, and by ventilation and thermal out-gassing of N_2O from the oceans.

2.2.1.1.4 HFCs, PFCs, and SF_6

The budgets of HFCs, PFCs, and SF_6 were recently reviewed in Chapter One of the Scientific Assessment of Ozone Depletion: 2010 (Montzka et al., 2011b), so only a brief description is given here. The current atmospheric abundances of these species are summarized in Table 2.1 and plotted in Figure 2.4.

Atmospheric HFC abundances are low and their contribution to radiative forcing is relatively small. However, as they replace CFCs and HCFCs phased out by the Montreal Protocol, their contribution to future climate forcing is projected to grow considerably in the absence of controls on global production (Velders et al., 2009).

HFC-134a is a replacement for CFC-12 in automobile air conditioners and is also used in foam blowing applications. In 2011, it reached 62.5 ppt, an increase of 22.8 ppt since 2005. Based on analysis of high-frequency measurements, the largest emissions occur in N. America, Europe, and East Asia (Stohl et al., 2009).

HFC-23 is a by-product of HCFC-22 production. Direct measurements of HFC-23 in ambient air from 5 sites began in 2007. The 2005 global annual mean used to calculate the increase since AR4 in Table 2.1, 5.2 ppt, is based on an archive of air collected at Cape Grim, Tasmania (Miller et al., 2010). In 2011, atmospheric HFC-23 was at 24.0 ppt. Its growth rate peaked in 2006 as emissions from developing countries increased, then declined as emissions were reduced through abatement efforts under the Clean Development Mechanism (CDM) of the UNFCCC. Estimates of total global emissions based on atmospheric observations and bottom-up inventories agree within uncertainties (Miller et al., 2010; Montzka et al., 2010). Currently, the largest emitter of HFC-23 is China (Kim et al., 2010; Stohl et al., 2010; Yokouchi et al., 2006); developed countries emit <20% of the global total. Keller et al. (2011) found that emissions from developed countries may be larger than those reported to the UNFCCC, but their contribution is small. The lifetime of HFC-23 was revised from 270 to 222 years since AR4 (WMO, 2011).

After HFC-134a and HFC-23, the next most abundant HFCs are HFC-143a at 12.04 ppt in 2011, 6.39 ppt greater than in 2005; HFC-125 (O'Doherty et al., 2009) at 9.58 ppt , increasing by 5.89 ppt since 2005; HFC-152a (Greally et al., 2007) at 6.4 ppt with a 3.0 ppt increase since 2005; and HFC-32 at 4.92 ppt in 2011, 3.77 ppt greater than in 2005. Since 2005, all of these are increasing exponentially except for HFC-152a, whose growth rate slowed considerably in ~2007 (Figure 2.4). HFC-152a has a relatively short atmospheric lifetime of 1.5 years, so its growth rate will respond quickly to changes in emissions. Its major uses are as a foam blowing agent and aerosol spray propellant while HFC-143a, HFC-125, and HFC-32 are mainly used as components in refrigerant blends. The reasons for slower growth in HFC-152a since ~2007 are unclear. Total global emissions of HFC-125 estimated from the observations are within ~20% of emissions reported to the UNFCCC, after accounting for estimates of emissions from East Asia.

CF_4 and C_2F_6 (PFCs) have lifetimes of 50 kyr and 10 kyr, respectively, and they are emitted as by-products of aluminium production and used in plasma etching of electronics. CF_4 has a natural lithospheric source (Deeds et al., 2008) with a pre-industrial level (about 1750) determined from Greenland and Antarctic firn air of 34.7 ± 0.2 ppt (Muhle et al., 2010; Worton et al., 2007). In 2011, atmospheric abundances were 79.0 ppt for CF_4, increasing by 4.0 ppt since 2005, and 4.16 ppt for C_2F_6, increasing by 0.50 ppt. The sum of emissions of CF_4 reported by aluminium producers and for non-aluminium production in EDGAR (Emission Database for Global Atmospheric Research) v4.0 only accounts for about half of global emissions inferred from atmospheric observations (Muhle et al., 2010). For C_2F_6, emissions reported to the UNFCCC are also substantially lower than those estimated from atmospheric observations (Muhle et al., 2010).

The main sources of atmospheric SF_6 emissions are electricity distribution systems, magnesium production, and semi-conductor manufacturing. Global annual mean SF_6 in 2011 was 7.28 ppt, increasing by 1.65 ppt since 2005. SF_6 has a lifetime of 3200 years, so its emissions accumulate in the atmosphere and can be estimated directly from its observed rate of increase. Levin et al. (2010) and Rigby et al. (2010) showed that SF_6 emissions decreased after 1995, most likely because of emissions reductions in developed countries, but then increased after 1998. During the past decade, they found that actual SF_6 emissions from developed countries are at least twice the reported values.

2.2.1.2 Montreal Protocol Gases (CFCs, Chlorocarbons, HCFCs, and Halons)

CFC atmospheric abundances are decreasing (Figure 2.4) because of the successful reduction in emissions resulting from the Montreal Protocol. By 2010, emissions from ODSs had been reduced by ~11 $PgCO_2$-eq yr^{-1} (after reductions for stratospheric O_3 depletion and use of HFCs); this is 5 to 6 times the reduction target of the first commitment period (2008–2012) of the Kyoto Protocol (2 $PgCO_2$-eq yr^{-1}) (Velders et al., 2007). Recent observations in Arctic and Antarctic firn air further confirm that emissions of CFCs are entirely anthropogenic (Martinerie et al., 2009; Montzka et al., 2011b). CFC-12 has the largest atmospheric abundance and GWP-weighted emissions of the CFCs. Its tropospheric abundance peaked during 2000–2004. Since AR4, its global annual mean mole fraction declined 13.7 ppt to 528.4 ppt in 2011. CFC-11 continued the decrease that started in the mid-1990s, by 12.8 ppt since 2005. In 2011, CFC-11 was 237.7 ppt. CFC-113 decreased by 4.3 ppt since 2005 to 74.3 ppt in 2011. A discrepancy exists between top-down and bottom-up methods for calculating CFC-11 emissions (Montzka et al., 2011b). Emissions calculated using top-down methods come into agreement with bottom-up estimates when a lifetime of 64 years is used for CFC-11 in place of the accepted value of 45 years; this longer lifetime (64 years) is at the upper end of the range estimated by Douglass et al. (2008) in a study of the CFC-11 lifetime with models that more accurately simulate stratospheric circulation. Future emissions of CFCs will largely come from 'banks' (i.e., material residing in existing equipment or stores) rather than current production.

The mean decrease in globally, annually averaged CCl_4 based on NOAA and AGAGE measurements since 2005 was 7.4 ppt, with an atmospheric abundance of 85.7 ppt in 2011; decreases reported by each lab do not agree within their stated uncertainties (Table 2.1). The observed rate of decrease and interhemispheric difference of CCl_4 suggest that emissions determined from the observations are on average greater and less variable than bottom-up emission estimates, although large uncertainties in the CCl_4 lifetime result in large uncertainties in the top-down estimates of emissions (Montzka et al., 2011b). CH_3CCl_3 has declined exponentially for about a decade, decreasing by 12.0 ppt since 2005 to 6.3 ppt in 2011. Because its atmospheric loss is dominated by reaction with hydroxyl radical (OH), CH_3CCl_3 has been used extensively to estimate globally averaged OH concentrations (e.g., Prinn et al., 2005). Montzka et al. (2011a) exploited the exponential decrease and small emissions in CH_3CCl_3 to show that interannual variations in OH concentration from 1998 to 2007 are 2.3 ± 1.5%, which is consistent with estimates based on other species including CH_4, C_2Cl_4, CH_2Cl_2, CH_3Cl, and CH_3Br.

HCFCs are classified as 'transitional substitutes' by the Montreal Protocol, so their global production and use will ultimately be phased out, but their global production is not currently capped and, based on changes in observed spatial gradients, there has likely been a shift in emissions within the NH from regions north of about 30°N to regions south of 30°N (Montzka et al., 2009). As a result, global levels of the three most abundant HCFCs in the atmosphere continue to increase. HCFC-22 increased by 44.5 ppt since 2005 to 213.0 ppt in 2011. Developed country emissions of HCFC-22 are decreasing, and the trend in total global emissions is driven by large increases from South and Southeast Asia (Saikawa et al., 2012). HCFC-141b

increased by 3.7 ppt since 2005 to 21.4 ppt in 2011, and for HCFC-142b, the increase was 5.73 ppt to 21.1 ppt in 2011. The rates of increase in these 3 HCFCs increased since 2004, but the change in HCFC-141b growth rate was smaller and less persistent than for the others, which approximately doubled from 2004 to 2007 (Montzka et al., 2009).

2.2.2 Short-Lived Greenhouse Gases and Other Climate Relevant Gases

This section covers observed trends in stratospheric water vapour; stratospheric and tropospheric ozone (O_3); the O_3 precursor gases, nitrogen dioxide (NO_2) and carbon monoxide (CO); and column and surface aerosol. Since trend estimates from the cited literature are used here, issues such as data records of different length, potential lack of comparability among measurement methods, and different trend calculation methods, add to the uncertainty in assessing trends.

2.2.2.1 Stratospheric H_2O Vapour

Stratospheric H_2O vapour has an important role in the Earth's radiative balance and in stratospheric chemistry. Increased stratospheric H_2O vapour causes the troposphere to warm and the stratosphere to cool (Solomon et al., 2010), and also causes increased rates of stratospheric O_3 loss. Stratospheric water vapour mainly enters across the cold tropical tropopause, causing extreme dryness and a large annual cycle in stratospheric H_2O. Other contributions include oxidation of methane within the stratosphere, and possibly direct injection of H_2O vapour in overshooting deep convection (Schiller et al., 2009). AR4 reported that stratospheric H_2O vapour showed significant long-term variability and an upward trend over the last half of the 20th Century, but no net increase since 1996. This updated assessment finds a significant decrease in stratospheric H_2O from 2000 to 2001 and a subsequent increase since 2005 that have been observed by independent measurement techniques.

The longest continuous time series of stratospheric water vapour abundance is from in situ measurements made with frost point hygrometers starting in 1980 over Boulder, USA (40°N, 105°W) (Scherer et al., 2008). These observations have been complemented by long-term global satellite observations from SAGE II (1984–2005; Stratospheric Aerosol and Gas Experiment II), HALOE (1991–2005; HALogen Occultation Experiment (RUSSELL et al., 1993)), Aura MLS (2004–present; Microwave Limb Sounder (Read et al., 2007)) and Envisat MIPAS Michelson Interferometer for Passive Atmospheric Sounding for 2002–2012 (Milz et al., 2005; von Clarmann et al., 2009)). Some discrepancies in water vapour mixing ratios from these different instruments can be attributed to differences in the vertical resolution of measurements. For example, offsets of up to 0.5 ppm in lower stratospheric water vapour mixing ratios exist between the most current versions of HALOE (v20) and Aura MLS (v3.3) retrievals during their 16-month period of overlap (2004 to 2005), although such biases can be adjusted to generate long-term records.

Observed anomalies in stratospheric H_2O from the near-global combined HALOE+MLS record (1992–2011) (Figure 2.5) include effects linked to the stratospheric quasi-biennial oscillation (QBO), plus a step-like drop after 2001 (noted in AR4), and an increasing trend since 2005. Variability during 2001–2011 was large yet there were small changes from 1992 through 2011. These inter-annual water vapour variations for the satellite record are closely linked to observed changes in tropical tropopause temperatures (Fueglistaler and Haynes, 2005; Randel et al., 2006; Rosenlof and Reid, 2008; Randel, 2010), providing reasonable understanding of observed changes. The longer record of Boulder balloon measurements (1980–2011) has been updated and revised (Scherer et al., 2008; Hurst, 2011), showing decadal-scale variability and a long-term stratospheric (16–26 km) increase of 1.0 ± 0.2 ppm for 1980–2010. Agreement between inter-annual changes inferred from the Boulder and HALOE+MLS data is good for the period since 2000 but was poor during 1992–1996. About 30% of the positive trend during 1980–2010 determined from frost point hygrometer data (Hurst, 2011; Fujiwara et al., 2010) can be explained by increased production of H_2O from CH_4 oxidation (Rohs et al., 2006), but the remainder can not be explained by changes in tropical tropopause temperatures (Fueglistaler and Haynes, 2005).

Since AR4, new studies characterize the uncertainties in measurements from individual types of *in situ* H_2O sensors (Vomel et al., 2007a; Vomel et al., 2007b; Weinstock et al., 2009), but discrepancies between different instruments (50 to 100% at H_2O mixing ratios less than 10 ppm), particularly for high-altitude measurements from aircraft, remain largely unexplained.

In summary, near-global satellite measurements of stratospheric H_2O for 1992–2011 show substantial variability, with a step-like decrease after 2000 and increases since 2005, but the net change during 1992–2011 is small. There is good understanding of the relationship between the satellite-derived H_2O variations and tropical tropopause temperature changes. Stratospheric H_2O changes from temporally sparse balloon-borne observations at one location (Boulder, Colorado) are in good agreement with satellite observations from 2000 to present, but a discrepancy exists for changes during the 1990s. Long-term balloon measurements from Boulder indicate a net increase of 1.0 ± 0.2 ppm over 16–26 km for 1980–2010, although these long-term increases cannot be fully explained by changes in tropical tropopause temperatures and methane oxidation.

[INSERT FIGURE 2.5 HERE]

Figure 2.5: Top: De-seasonalized near-global water vapour anomalies in the lower stratosphere (16–19 km) from merged HALOE (black) and MLS (blue) measurements (updated from (Randel, 2010). Bottom: Balloon-borne measurements of stratospheric water vapour from Boulder, Colorado (green dots, with green curve showing smoothed variations), compared with monthly HALOE+MLS satellite measurements over 30–50°N. Both data sets have been de-seasonalized and normalized for the period 2000–2011.

2.2.2.2 Stratospheric Ozone

AR4 briefly discussed stratospheric ozone trends, and reported the radiative forcing of stratospheric ozone between pre-industrial and 2005 to be –0.05 ± 0.10 W m^{-2}, with medium scientific understanding.

Total ozone is a good proxy for stratospheric ozone, since tropospheric ozone accounts for only about 10% of the total ozone column. Long-term total ozone changes over various latitudinal belts, derived from Weber et al. (2012), are illustrated in Figure 2.6 (a-d). Annually averaged total column ozone declined during the 1980s and early 1990s and has remained constant for the past decade, about 3.5% below the 1964–1980 average for the entire globe, and 2.5% for 60°S–60°N. There is no statistically significant ozone trend in the tropics. SH and NH mid-latitude (30°–60°) annual mean total column ozone amounts have remained at the same level for the past decade, approximately 6% and 3.5% below the 1964–1980 average respectively. In theNH, a minimum about 5.5% below the 1964–1980 average was reached in 1993 and was primarily caused by ozone loss through heterogeneous reactions on volcanic aerosols from Mt. Pinatubo.

There are two altitude regions mainly responsible for long-term changes in total column ozone (Douglass et al., 2011). In the upper stratosphere (35–45 km), which is subject to halogen-catalyzed O_3 loss from ODSs, there was a strong and statistically significant decline (6–8% per decade) up to the mid-1990s and a near-zero or slightly positive trend thereafter. The lower stratosphere, between 20 and 25 km over mid-latitudes, also experienced a statistically significant decline of about 4 to 5% per decade (7–8% total decline) between 1979 and the mid-1990s, followed by stabilization or a slight (2–3%) ozone increase.

Springtime averages of total ozone poleward of 60° latitude in the Arctic and Antarctic are shown in Figure 2.6e. Inter-annual variability in polar stratospheric ozone abundance and chemistry is driven by variability in temperature and transport due to year-to-year differences in dynamics. This variability is particularly large in the Arctic where large depletion occurred in 2011 (Manney et al., 2011).

There is *high confidence* in the observed stratospheric ozone declines from ~1980 through the mid-1990s, a partial recovery to ~2000, followed by stratospheric O_3 remaining constant until 2010, but still 2.5% below the 1964–1980 mean. For further discussion regarding changes in stratospheric dynamics see Section 2.7.7 and Chapter 8 for radiative forcing resulting from stratospheric ozone change.

[INSERT FIGURE 2.6 HERE]

Figure 2.6: Zonally averaged, annual mean total column ozone in Dobson Units (DU; 1 DU = 2.69×10^{16} O_3 cm^{-2}) of ground-based measurements combining Brewer, Dobson, and filter spectrometer data (red), merged BUV/SBUV/TOMS/OMI MOD V8 (blue) and GOME/SCIAMACHY/GOME-2, 'GSG' (green), for a) 60°S–60°N, b) 30°N–60°N (NH), c) 15°S–15°N (tropics), and d) 30°S–60°S (SH). e) March and October polar total column ozone in the NH and SH, respectively. Adapted from Weber et al. (2012).

2.2.2.3 Tropospheric Ozone

Tropospheric ozone is a short-lived trace gas that either originates in the stratosphere or is produced in situ by precursor gases and sunlight. Tropospheric ozone is an important climate forcer (Chapter 8) and elevated levels of surface ozone impact human health and vegetation. The paucity of long-term measurements and its average atmospheric lifetime of a few weeks make the assessment of long-term global ozone trends challenging. AR4 reported regional and seasonal long-term ozone trends varying in magnitude and sign. Since AR4 new studies have provided an improved understanding of global tropospheric ozone distribution and long-term regional trends, with some time series beginning in the 1950s, but most in the 1990s. New time-series for Eastern Asia are now available.

Satellite-based tropospheric column ozone (TCO) in the tropics and mid-latitudes show a greater burden in the NH than the SH. In the NH ozone peaks during summer at 35°–40° with the strongest enhancements stretching from the eastern USA to southern Europe, and from East Asia into the western North Pacific. The SH peak occurs in Austral spring at 25°–30° within a band stretching from Brazil eastward to Australia (Ziemke et al., 2011). TCO trend analyses are few, however an analysis of the Pacific Ocean found no trend in the tropics but significant positive trends in the mid-latitudes of both hemispheres during 1979–2003 (Ziemke et al., 2005). Consistently, Beig and Singh (2007) did not find TCO trends across much of the tropical Pacific for 1979–2005, but did find significant positive trends across broad regions of the tropical South Atlantic, India, southern China, Southeast Asia, Indonesia and the northern tropics downwind of China.

Tropospheric ozone also varies with altitude, a property difficult to assess with satellite retrievals. Presently, long-term trends at the surface and at specific levels in the free troposphere are only available from sites with high quality in situ measurements. Many sites are clustered in just a few regions, while large areas, especially the tropics and SH are sparsely sampled. An overview of surface and free tropospheric ozone trends measured around the globe is presented in Appendix 2.A. Ozone time series from several sites that are regionally representative (i.e., not strongly influenced by local emissions) of tropospheric chemical composition are shown in Figure 2.7. Annual average ozone levels range from less than 20 ppb at Samoa to more than 70 ppb at Mt Happo, Japan. The largest ozone increases have occurred at northern mid-latitudes where anthropogenic emissions are concentrated.

[INSERT FIGURE 2.7 HERE]

Figure 2.7: Annually averaged surface ozone mixing ratios from regionally representative monitoring sites around the world. Top: Europe with trend lines fit through the data prior to 2000 when ozone was generally increasing. Middle: East Asia and western North America. Bottom: Remote sites in the NH and SH. Time series include data from all times of day and trend lines are linear regressions described in Parrish et al. (2012).

Many surface sites exhibit no significant ozone trend. These sites tend to sample air masses with little recent influence from anthropogenic emissions (Appendix 2.A). Surface sites with significantly increasing ozone are not always associated with regional increases in anthropogenic emissions. In East Asia, where emissions are growing faster than any other region on Earth, almost all surface sites show increasing ozone. However, in the western USA where emissions are decreasing, springtime ozone is increasing at rural coastal sites and at many of the available inland rural sites, possibly due to its location downwind of Asia (Cooper, 2012; Jacob et al., 1999). Ozone is generally increasing in winter at nearly half of the rural sites in the eastern USA for as yet unknown reasons (Cooper, 2012). Ozone increased in Europe from the 1950s and 1970s until approximately 2000. Emissions increased in Europe and North America up until the 1980s, then levelled off and began to decrease in the 1990s. The continued increase of ozone during the 1990s is unexpected considering Europe's decreasing emissions (Logan et al., 2012). Smaller surface ozone increases have also been detected in remote locations such as the Canadian Arctic (Alert), Hawaii (Mauna Loa), the Western North Atlantic (Bermuda) in winter and summer, the South Atlantic mid-latitudes, the Eastern South Atlantic tropics, and southern Australia (Cape Grim).

Significant regional decreases in surface ozone have occurred where there have been strong decreases in local emissions: Europe since 2000; median values in rural eastern USA in spring and summer since 1990; and highest ozone values at many urban sites across the USA since 1980 (Lefohn et al., 2010).

In the free troposphere, ozone trends are difficult to assess on a global basis due to the limited number of measurement sites, but increasing ozone has been detected more generally than decreasing ozone, with regional summaries given in Appendix 2.A.

2.2.2.4 Carbon Monoxide (CO) and Nitrogen Dioxide (NO_2)

Emissions of CO, VOCs and (NO_x = NO + NO_2) do not have a direct effect on radiative forcing, but indirectly influence OH, CH_4 and tropospheric O_3 abundance. Due to space limitations, trends in VOCs have not been assessed in this section.

AR4 did not assess current trends in atmospheric CO based on observations. The major sources of atmospheric CO are in situ production by oxidation of hydrocarbons (mostly CH_4 and isoprene) and direct emission resulting from incomplete combustion of biomass and fossil fuels. An analysis of MOPITT and AIRS satellite data suggest a clear decline of CO columns for the period 2002–2010 over a number of polluted regions in Europe, North America and Asia with a global trend of about –1% yr^{-1} (Fortems-Cheiney et al., 2011; Worden et al., 2012b; Yurganov et al., 2010). Recent analysis of MOPITT and AIRS including TES and IASI data for recent overlapping years shows qualitatively similar decreasing trends (Worden et al., 2012a), but the magnitude of trends remains uncertain due to the presence of instrument drifts. Small CO decreases observed in the NOAA and AGAGE networks are consistent with slight declines in global anthropogenic CO emissions over the same time (Appendix 2.A).

Due to its short atmospheric lifetime (hours), NO_x concentrations are highly variable in time and space. AR4 described the potential of satellite observations of NO_2 to verify and improve NO_x emission inventories and their trends and reported strong NO_2 increases by 50% over the industrial areas of China from 1996–2004. An extension of this analysis reveals increases between a factor of 1.7 and 3.2 over parts of China, while over Europe and the US NO_2 has decreased by 30 to 50% between 1996 and 2010.

Figure 2.8 shows the changes relative to 1996 in satellite derived tropospheric NO_2 columns, with a strong upward trend over Central Eastern China and an overall downward trend in Europe and the US. Decreases over Western Europe and Poland are only observed until 2003, with only small changes afterwards. In contrast, NO_2 reductions in the US are most pronounced after 2004, related to differences in effectiveness of NO_x emission abatements in the US and Europe. Increasingly, satellite data are used to derive trends in anthropogenic NO_x emissions (Castellanos and Boersma, 2012), reporting overall increases in global emissions, driven by Asian emission increases of up to 29% yr^{-1} (1996–2006), while moderate decreases up to 7% yr^{-1} (1996–2006) are reported for North America and Europe.

[INSERT FIGURE 2.8 HERE]

Figure 2.8: Relative changes in tropospheric NO_2 column amounts, normalized for 1996, derived from two instruments, the Global Ozone Monitoring Experiment (GOME) from 1996 to 2002 and the Scanning Imaging Spectrometer for Atmospheric Cartography (SCIAMACHY) from 2003 to 2010. Updated from (Richter et al., 2005).

2.2.3 Aerosols

This section assesses trends in aerosol resulting from both anthropogenic and natural emissions. Chapter 7 provides additional discussion of aerosol properties, Chapter 8 evaluates the radiative forcing of aerosol, and Chapter 11 assesses air quality-climate change interactions. Due to the short lifetime (days to weeks) of aerosol, trends in anthropogenic aerosol are mainly confined to polluted regions in the NH. Natural aerosols (such as desert dust, sea salt, volcanic and biogenic aerosols) are important in both hemispheres, and are also important for both direct and indirect aerosol interactions. Changes in natural aerosols are likely to result from climate and land-use use change (Carslaw et al., 2010). However, data on the trends in natural aerosols are even more limited compared to those for anthropogenic aerosols (Mahowald et al., 2010).

2.2.3.1 Aerosol Optical Depth (AOD) from Remote Sensing

AOD is a measure of the integrated columnar aerosol load and an important parameter for evaluating aerosol direct radiative forcing. AR4 described early attempts to retrieve AOD from satellites but did not provide

estimates on temporal changes in tropospheric aerosol. Better aerosol satellite sensors and ground-based sun-photometer networks provide an opportunity to assess local and regional AOD trends for the last 15 years.

AOD can be relatively accurately determined with sun-photometers that measure the direct solar intensity during cloud-free conditions. AERONET (AErosol RObotic NETwork) is a global sun photometer network, with densest coverage over Europe and North America. AERONET AOD temporal trends at sun-photometer sites (Holben et al., 1998) were examined in independent studies (de Meij et al., 2012; Hsu et al., 2012; Yoon et al., 2012) , using different data selection and statistical methods. Table 2.2 summarizes AOD trends at regionally representative stations. For the last decade, AERONET data show increasing AOD trends over the Arabian Peninsula, and eastern and southern Asia. Handheld sun photometer time-series (Krishna Moorthy et al., 2012) confirm increasing AOD during the last decade over southern Asia. In contrast, de Meij et al (2012) reported decreasing AOD trends at more than 80% of European and North American sites. In Europe, AOD trends are less negative and even slightly positive near cities, whereas stronger decreasing AOD trends occur over rural sites. In India, however, increases are stronger in rural regions than in cities. Decreasing AOD trends are observed near the west coast of Africa, where aerosol loads are dominated by Saharan dust outflow. Large AOD trends, positive and negative, are detected in central Africa, associated with strong inter-annual variability related to wildfires and dust emissions.

Cloud screened, ground-based solar broadband radiometer measurements provide longer time-records than sub-spectral sun-photometer data, but they are less accurate. A recent study investigating multi-decadal records over Japan (Kudo et al., 2011) derived an AOD increase until the mid-1980s, followed by an AOD decrease until the late 1990s and almost constant AOD in the 2000s. Similar multi-decadal trends have been observed for urban-industrial regions of Europe and North America, linked to successful measures to reduce sulphate emissions since the mid-1980s.

Aerosol products from dedicated satellite sensors complement surface based AOD with global coverage. The accuracy of the AOD derived from satellites strongly depends on how well the retrieval removes scenes contaminated by clouds and correctly subtracts the surface (background) signal. The accuracy of retrieved AOD over oceans is usually better over ocean. AOD trends from 2000 to 2009 over oceans from carefully cloud-screened MODIS data (Zhang and Reid, 2010) are presented in Figure 2.9. For 2000–2009, strongly increasing AOD trends are displayed over southern and eastern Asia coastal waters, suggesting similar trends over adjacent land regions. Trends of increasing AOD are also observed over most tropical oceans. Negative AOD trends are rare and only observed over coastal regions of Europe and near the US east coast, in agreement with decreasing AOD trends from surface observations over Europe and the US. These regional changes are consistent with an analysis of AVHRR trends, updated from Mishchenko et al (Mishchenko et al., 2007a)**,** except over the Southern Ocean (45°S–60°S) where Zhang and Reid (2010) do not find significant trends. Increasing trends over a number of open ocean regions were also reported forATSRR-2 data (Thomas et al., 2010).

[INSERT FIGURE 2.9 HERE]

Figure 2.9: Trends in aerosol optical depth (AOD) for the ten-year period 2000–2009, based on de-seasonalized, conservatively cloud-screened MODIS aerosol data over oceans (Zhang and Reid, 2010). Negative AOD trends off Mexico are due to enhanced volcanic activity at the beginning of the record. Most non-zero trends are significant at 95% confidence levels (Zhang and Reid, 2010).

Recently, re-processed SeaWiFS AOD data over both oceans and land were evaluated from 1998 to 2010 (Hsu et al., 2012). Seasonal AOD trends of SeaWiFS are presented in Figure 2.10. The sign and magnitude of SeaWiFS continental AOD trends are in good agreement with almost all regional AOD trends suggested by ground-based sun-photometer data (Table 2.2). The strong positive AOD trend over the Arabian Peninsula occurs mainly during spring (MAM) and summer (JJA), during times of dust transport. The positive AOD trend over southern and eastern Asia is strongest during the dry seasons (DJF, MAM), when reduced wet deposition allows anthropogenic aerosol to accumulate in the troposphere. AOD trends over the Saharan outflow region off western Africa display the strongest regional AOD trend variability, with AOD increases only in spring but otherwise strong AOD decreases during the other seasons.

[INSERT FIGURE 2.10 HERE]

Figure 2.10: Trends in aerosol optical depth (AOD) using SeaWiFS data from 1998 to 2010 (Hsu et al., 2012).

Observed decreases in AOD over Europe and the US as well as observed increases in AOD over southern and eastern Asia (especially there during the dry season) are consistent with reported temporal trends in anthropogenic emissions. The analyses of more recent satellite and AERONET trends do not confirm a continuation of decreasing AOD trends over the oceans after 2000 (see Section 2.3 for a discussion on 'global brightening'), as suggested by earlier analyses of AVHRR sensor products (Cermak et al., 2010; Mishchenko et al., 2007a). However, analysis of longer over-lapping multi-annual time series is needed to corroborate this finding.

Recent ground and satellite based remote sensing of AOD reported both positive (eastern and southern Asia) and negative AOD trends for regions affected by anthropogenic pollution (Europe and Eastern USA) (*medium agreement, robust evidence*). Trends in regions with strong aerosol load inter-annual variability, e.g.,, due to wildfires or dust, are less robust. Vast regions of the world do not display significant aerosol trends over the last decades, and consequently no global tropospheric AOD trend can be detected.

Table 2.2: AERONET retrieved trend in Aerosol Optical Depth at selected ground-based monitoring sites worldwide from 3 studies (de Meij et al., 2012; Hsu et al., 2012; Yoon et al., 2012). Trends are ordered in magnitude intervals. Qualitative indication on change in aerosol size from Yoon et al. (2012) reported for Angstrom parameter change larger than 0.015 yr^{-1}. Hsu et al (2012) investigated AOD trends at 12 AERONET sites with data coverage of at least ten years. Yoon et al. . (2012) investigated trends at 14 AERONET sites with data coverage varying between four and twelve years. De Meij et al. (2012) investigated AOD trends at more than 60 AERONET sites for years from 2000 to 2009, mostly located in the USA (20) and Europe (20).

Trend Interval	Hsu et al (2012)	Yoon et al. (2012)	De Meij et al. (2012)	AERONET Site	Longitude	Latitude	Region	Aerosol Size
		AOD-trend [yr^{-1}]						
> +.0030 (strongly positive)	+.018[a]	+.008		Solar Village	46°E	25°N	Arabia	
		+.025[b]	+.003	Beijing/Xianghe	116°E	40°N	E. Asia	Increasing
		+.010[b]	+.023	Ouagadougou	1°W	12°N	Cent. Africa	Decreasing
	+.009[a]	+.003	+.013	Banizoumbou	3°E	14°N	Cent. Africa	
		+.007[b]		Mongu	23°E	15°S	S. Africa	
			+.006	Kanpur	80°E	27°N	S. Asia	
> +.0005 < +.0030 (weakly positive)	+.0014			La Paguera	67°W	18°N	Trop.Caribic	
	+.0013[a]			Nauru	167°E	1°S	Trop. Pacific	
	+.0012			Ascension Is.	14°W	8°S	Trop. Atlantic	
		+.0013[b]		Avignon	5°E	45°N	Europe	Decreasing
	+.0005		+.009	Alta Floresta	56°W	10°S	S. America	
< +.0005 > –.0005 (no trend)	+.0002			Tahiti	159°W	18°S	Trop.Pacific	
	+.0001	+.0007		Shiharama	135°E	34°N	Japan	Decreasing
		+.0000	–.003	MD-Science	77°W	39°N	East US	Increasing
< –.0005 > –.0030 (weakly negative)	–.0010			COVE	76°W	37°N	East US	
		–.002[b]	–.0012	Seviletta	107°W	34°N	West US	Increasing
		–.003[b]	–.0002	Sede Boker	35°E	31°N	Mid East	Increasing
< –.0030 (strongly negative)	–.004[a]	–.002	–.002	GSFC	77°W	39°N	East US	
			–.004	Tomsk	85°E	57°N	N. Asia	
	–.004[a]			Cape Verde	23°W	17°N	off W. Africa	
		–.005[b]		Dakar	17°W	14°N	W. Africa	Increasing
		–.005	–.011	Ispra	9°E	45°N	S. Europe	
	–.009[a]		–.008	Leipzig	12°E	51°N	Cent. Europe	
			–.012	Minsk	27°E	54°N	E. Europe	
			–.023	Ilorin	4°E	8°N	Cent. Africa	

Notes:
(a) significant at p=0.95
(b) 6 years or less data.

2.2.3.2 In Situ Surface Aerosol Measurememts

AR4 did not report trends in long-term surface-based *in situ* measurements of particulate matter, its components or properties. This section summarizes reported trends of PM10, PM2.5 (particulate matter with aerodynamic diameters <10 and 2.5 μm), sulphate, and equivalent black carbon/elemental carbon, from regionally representative measurement networks. An overview of current networks, acronyms and definitions pertinent to aerosol measurements is given in Appendix 2.A. Studies reporting trends representative for regional changes are presented in Table 2.3. Long-term data are almost entirely from North America and Europe, whereas a few individual studies on aerosol trends in India and China are reported in Appendix 2.A. Figure 2.11 gives an overview of observed PM10, PM2.5, and sulphate trends in North America and Europe for 1990–2009 and 2000–2009.

[INSERT FIGURE 2.11 HERE]
Figure 2.11: Trends in particulate matter (PM) and sulphate in Europe and USA. The trends are based on measurements from the EMEP (Torseth et al., 2012) and IMPROVE (Hand et al., 2011a) networks in Europe and USA, respectively. Sites with significant trends to p = 0.05 or better are shown in colour codes, the black dots are sites with non-significant trends.

In Europe, strong significant downward trends are observed for PM10, PM2.5 and sulphate from the rural stations in the EMEP network. PM2.5 shows an average reduction of 3.9% yr^{-1} for 6 stations with significant trends, while trends are not significant at 7 other stations. PM10 at 12 (out of 24) sites shows significant downward trends of 2.6% yr^{-1}. A strong significant reduction in sulphate of 3.1% yr^{-1} is observed from 1990-2009; 26 of 30 sites have significant reductions. For 2000–2009, the trends were weaker and less robust. This is consistent with reported emission reductions of 65% from 1990–2000 and 28% from 2001–2009 (EMEP, 2011; Torseth et al., 2012). Model analysis (Pozzoli et al., 2011) attributed the trends in large part to emission changes.

In the USA, the largest reductions in PM and sulphate are observed in the 2000s, rather than the 1990s as in Europe. PM2.5 measurements obtained in IMPROVE (Hand et al., 2011b) show significant downward trends of on average 4.0% yr^{-1} for 2000–2009 at sites with significant trends, and 2.1% yr^{-1} at all sites, and PM10 decreases of 3.1% yr^{-1} for 2000–2009. In Canada, annual mean PM2.5 at urban measurement sites decreased by 3.6% yr^{-1}, between 1985 and 2006 Canada (Canada, 2012) and Hidy and Pennell (2010) show remarkable agreement of PM2.5 and SO_4^{2-} declines in Canada, pointing to common emission sources of PM2.5 and SO_4^{2-}. IMPROVE sulphate declines are highly significant in the Eastern and South Western USA, and range from 2 to 6 % yr^{-1}, with average of 2.3 % yr^{-1} for the sites with significant negative trends for 1990–2009. However, four IMPROVE sites show strong SO_4^{2-} increases from 2000–2009, amounting to 11.9% yr^{-1}, at Hawaii (1225 m a.s.l), and 4–7% yr^{-1} at 3 sites in southwest Alaska. A recent study on long term trends in aerosol optical properties from 24 globally distributed sites (Collaud Coen et al., 2012)confirms these strong increases in absorption and scattering coefficients in the free troposphere at Mauna Loa, Hawaii (3400 m a.s.l). These findings are also supported by MODIS satellite-based observations of AOD shown in Figure 2.9. Possible explanations for these changes include the influence of increasing Asian emissions, and changes in clouds and removal processes. More and longer Asian time series are needed to corroborate these findings. Elsewhere trends in scattering and absorption are mostly insignificant. Aerosol number concentrations (Asmi et al., 2012) are significantly declining at most sites in Europe, North America, the Pacific and Caribic, but increasing at the South Pole.

Total carbon (=light absorbing carbon +organic carbon) measurements indicate highly significant downward trends of total carbon between 2.5 and 7.5% yr^{-1} along the east and west coasts of the USA, and smaller and less significant trends in other US regions from 1989–2008 (Hand et al., 2011b; Murphy et al., 2011). In Europe, Torseth et al. (Torseth et al., 2012) suggest a slight reduction in elemental carbon concentrations at two stations in Europe from 2001 to 2009, subject to large inter-annual variability. Collaud Coen et al. (2012) reported consistent negative trends in the aerosol absorption coefficient at stations in the continental US, Arctic and Antarctica, but mostly insignificant trends in Europe.

In the Arctic, changes in aerosol impact the atmosphere's radiative balance as well as snow and ice albedo. Similar to Europe and the USA, (Hirdman et al., 2010) reported downward trends in equivalent black carbon and SO_4^{2-} for two out of three stations and attributed them to emission changes.

Robust evidence from a host of *in situ* ground based aerosol measurements indicates downward trends in the last 2 decades of particulate matter (PM2.5) in parts of Europe (2–6% yr^{-1}) and the USA (1–2.5% yr^{-1}), and SO_4^{2-} (between 2 and 5% yr^{-1}). The strongest decreases were in the 1990s in Europe and in the 2000s in the USA. There is limited evidence from a variety of techniques for increases on the order of 10% yr^{-1} in the Pacific (different Hawaii sites; Table 2.3) in the last decade. Furthermore, there is consistent evidence on downward trends in the USA and the Arctic from long-term time series on light absorbing aerosol, while elsewhere in the world time series are lacking or not long enough to reach statistical significance.

[INSERT TABLE 2.3 HERE]

Table 2.3: Trends in various aerosol variables using data sets with at least 10 years of measurements. Unless otherwise noted, trends of individual stations were reported in % yr^{-1}, and significance level is $p < 0.05$. The standard deviation is determined from the individual trends of a set of regional stations. #Trend numbers refer to a subset of stations with significant changes over the time - generally in regions strongly influenced by anthropogenic emissions; Figure 2.11.

[START BOX 2.2 HERE]

Box 2.2: Quantifying Changes in the Mean: Trend Models and Estimation

Many statistical methods are available for estimating change in environmental time series (Chandler and Scott, 2011). The assessment of long-term changes in historical climate data requires trend models that are transparent and reproducible, and that can provide credible uncertainty estimates. In this box and the Appendix 2.A material it is shown that different methods give similar estimates of changes in the mean and associated sampling uncertainty for the global mean temperature time series. For simplicity, the quantification and visualisation of temporal changes are assessed in this Chapter using a linear trend procedure that allows for first order autocorrelation in the residuals (Santer et al., 2008). The 5 to 95% confidence interval quoted is solely that arising from trend fitting uncertainty. Structural uncertainties, to the extent sampled, are apparent from the range of estimates from different data sets. Parametric (and other remaining) uncertainties, which many groups include (and calculate in distinct ways), are not considered (Box 2.1).

Linear Trends

Historical climate trends are almost always described and quantified in climate science by estimating the linear component of the change with time (e.g., AR4). Such least squares linear trend modelling is simple and easy to communicate: it has broad acceptance and understanding based on its frequent and widespread use. This method is widely employed, and its strengths and weaknesses are well known (von Storch and Zwiers, 1999; Wilks, 2006). The greatest challenge arises in assessing the uncertainty in the trend and its dependence on the assumptions about the sampling distribution (bell shaped or different) and the serial correlation of the residuals about the trend line (one year correlated to the next; (Santer et al., 2008; Von Storch, 1999).

There is no *a priori* physical reason why the long-term trend in climate should be linear-in-time. Climatic time series often have trends for which a straight line is not a good approximation (e.g., Seidel and Lanzante, 2004). The residuals from a linear fit in time often do not follow a simple autoregressive or moving average process, and linear trend estimates can easily change when estimates are recalculated using data covering shorter or longer time periods or when new data are added. When linear trends for two parts of a longer time series are calculated separately, the trends calculated for two shorter periods may be very different (even in sign) from the trend in the overall longer period, if the time series exhibits significant nonlinear behavior in time (Box 2.2, Table 1).

Non-linear Trends

A more flexible approach is to use an objective method to estimate the smooth function that best fits the time series. Box 2.2, Figure 1 shows the linear least squares and a non-linear trend fit to the global annual surface

temperature values from the HadCRUT4 data set (see Section 2.4.3). The non-linear trend is obtained by fitting smoothing splines (Scinocca et al., 2010; Wood, 2006) while allowing for first order autocorrelation in the residuals (see Appendix 2.A).

[INSERT BOX 2.2, FIGURE 1 HERE]

Box 2.2, Figure 1: Top: Global mean surface temperature anomalies relative to a 1961–1990 climatology based on HadCRUT4 annual data (dots). The straight black lines are Least Squares trends for 1901–2011, 1901–1950 and 1951–2011. Bottom: Same data as top, with Smoothing Spline (solid curve) and the 90% confidence interval on the smooth curve (shading).

Box 2.2, Table 1 shows estimates of the change in the global mean temperature from the two methods. The methods give similar estimates with 90% confidence intervals that overlap one another for each of the changes. Appendix 2.A describes the details of these two methods and also compares the simple method used to compute linear trends throughout this chapter with more advanced methods.

Box 2.2, Table 1: Estimates of the mean change per decade in global mean temperature between 1901 and 2011, 1901 and 1950, and 1951 and 2011, obtained from the linear (Least Squares) and non-linear (Smoothing Spline) trend models. Approximate 90% confidence intervals in the estimates are also given for each trend model and are required to test if the changes are statistically significant.

Method	1901–2011	1901–1950	1951–2011
Least Squares	0.075 ± 0.013	0.107 ± 0.026	0.107 ± 0.028
Smoothing Spline	0.082 ± 0.010	0.070 ± 0.016	0.093 ± 0.019

[END BOX 2.2 HERE]

2.3 Changes in Radiation Budgets

The radiation budget of Earth is a central component of the climate system. On average, radiative processes warm the surface and cool the atmosphere, requiring the hydrological cycle and sensible heating to compensate. Spatial and temporal energy imbalances due to radiation and latent heating produce the general circulation of the atmosphere and oceans. Anthropogenic influence on climate (Chapter 8) occurs primarily through perturbations of the components of the Earth radiation budget.

The radiation budget at the top of atmosphere (TOA) includes the absorption of solar radiation by Earth, determined as the difference between the incident and reflected solar radiation at the TOA, as well as the thermal outgoing radiation emitted to space. The surface radiation budget takes into account the solar fluxes absorbed at Earth's surface, as well as the upwelling and downwelling thermal radiative fluxes emitted by the surface and atmosphere, respectively.

In view of new observational evidence since AR4, the long-term mean state as well as decadal changes of the surface and TOA radiation budgets are assessed in the following.

2.3.1 Global Mean Radiation Budget

Since AR4, knowledge on the radiative energy flows in the climate system has improved, requiring an update of the global annual mean energy balance diagram (Figure 2.12). Energy exchanges between Sun, Earth and space are measured with unprecedented accuracy from spaceborne platforms such as the Clouds and the Earth's Radiant Energy System (CERES, Wielicki et al., 1996) and the Solar Radiation and Climate Experiment (SORCE, Kopp and Lawrence, 2005) which began operation near the turn of the millennium. The total solar irradiance (TSI) incident at the TOA is now much better known, with the most recently launched SORCE Total Irradiance Monitor (TIM) reporting uncertainties as low as 0.035%,compared to 0.1% for other TSI instruments (Kopp et al., 2005). During the 2008 solar minimum, SORCE/TIM observed a solar irradiance of 1360.8 ± 0.5 Wm^{-2} compared to 1365.5 ± 1.3 $Wm^{-2}$for instruments launched prior to SORCE still operating in 2008 (Section 8.2.1). Kopp and Lean (2011) conclude that the SORCE/TIM value of TSI is the most credible value because it is validated by a National Institute of Standards and Technology

calibrated cryogenic radiometer). This revised TSI estimate corresponds to a solar irradiance close to 340 W m^{-2} globally averaged over Earth's sphere (Figure 2.12).

[INSERT FIGURE 2.12 HERE]

Figure 2.12: Global mean energy budget under present day climate conditions. Numbers state magnitudes of the individual energy flows in Wm^{-2}, adjusted within their uncertainty ranges to close the energy budgets. Numbers in parentheses attached to the radiative fluxes cover the range of values in line with observational constraints (based on Loeb et al., 2009; Stephens et al., in press; Trenberth and Fasullo, 2012; Wild et al., submitted).

The estimate for the reflected solar radiation at the TOA in Figure 2.12, 100 W m^{-2}, is a rounded value based on the CERES Energy Balanced and Filled (EBAF) satellite data product (Loeb et al., 2012; Loeb et al., 2009) for the period 2001–2010. This data set adjusts the solar and thermalTOA fluxes within their range of uncertainty to be consistent with independent estimates of the global heating ratebased upon in-situ ocean observations (Loeb et al., 2012). This leaves 240 W m^{-2} of solar radiation absorbed by Earth, which is nearly balanced by thermal emission to space of about 239 W m^{-2}(based on CERES EBAF), considering a global heat storage of 0.6 W m^{-2} (residual term in Figure 2.12) (Hansen et al., 2011; Loeb et al., 2012). The stated uncertainty in the solar reflected TOA fluxes from CERES due to uncertainty in absolute calibration alone is ~2% (2-sigma), or equivalently 2 W m^{-2}(Loeb et al., 2009). The uncertainty of the outgoing thermal flux at the TOA as measured by CERES due to calibration is ~3.7 W m^{-2} (2-sigma). In addition to this, there is uncertainty in unfiltering the radiances, in radiance-to-flux conversion, and in time-space averaging, which adds up to another 1 W m^{-2} or more (Loeb et al., 2009).

The components of the radiation budget at the surface are generally more uncertainthan their counterparts at the TOA, as they cannot be directly measured by passive satellite sensors. Since AR4, new estimates for the downward thermal infrared radiation at the surface have been established that incorporate criticalinformation on cloud base heights from space-born radar and lidar instruments (Kato et al., 2011; L'Ecuyer et al., 2008; Stephens et al., 2012). In line with earlier studies based on direct surface radiation measurements (Wild et al., 2001; Wild et al., 1998) these estimates suggest higher values of global mean downward thermal radiation than presented in previous IPCC assessments and typically found in climate models, exceeding 340 W m^{-2} (Figure 2.12). Estimates of global mean downward thermal radiation computed as a residual of other terms of the surface energy budget (Kiehl and Trenberth, 1997; Trenberth et al., 2009) are lower (324−333 W m^{-2}), highlighting the need for improved estimates of uncertainty in both radiative and non-radiative components of the surface energy budget.

Estimates of absorbed solar radiation at Earth's surface include considerable uncertainty. Global mean estimates derived from satellite retrievals, reanalyses and climate models range from below 160 W m^{-2} to above 170 W m^{-2}. Comparisons of climate models with surface observations as well as updated spectroscopic parameters and continuum absorption for water vapor favour values towards the lower bound of the range, near 160 W m^{-2}, and an atmospheric solar absorption close to 80 W m^{-2}(Kim and Ramanathan, 2008; Trenberth et al., 2009; Wild, 2008; Wild et al., submitted). Some of the satellite-derived products calculate asomewhat higher surface insolation (Kato et al., 2011; Stephens et al., in press).

The latent heat flux estimate, required toexceed 80 Wm^{-2} to close the surface energy balance in Figure 2.12, is higher than in previous IPCC assessments. A higher estimate is supported by the evidence for underestimation in the remotely-sensed precipitation estimates (the latent heat flux corresponds to the energy equivalent of evaporation, which globally equals precipitation, and its magnitude is derived from global precipitation estimates) (Berg et al., 2010; Ellis et al., 2009; Haynes et al., 2009; Stephens et al., in press; Trenberth and Fasullo, 2012). The magnitude of this underestimation is currently disputed. The 85 W m^{-2} attached to the latent heat flux in Figure 2.34 is considered as upper limit by Trenberth and Fasullo (2012), yet istowards the low end of the uncertainty range in Stephens et al. (in press), and fits well to observationally constrained surface radiation estimates (Wild et al., submitted). Relative uncertainty in the globally averaged sensible heat flux estimate remains high due to the very limited direct observational constaints (Stephens et al., in press; Trenberth et al., 2009).

2.3.2 Changes in Top of Atmosphere Radiation Budget

While the previous section emphasized the long term average state of the radiation budget, the forcus in the following is on the temporal (decadal) changes of its components. Variations in TSI are discussed in Chapter 8, Section 8.3.1. AR4 reported that large changes in tropical TOA radiation occurred between the 1980s and1990s. The results were based upon observations from the Earth Radiation Budget Experiment (ERBE, Barkstrom, 1984) Earth Radiation Budget Satellite (ERBS) Nonscanner Wide Field of View (WFOV) instrument (Wong et al., 2006). Net TOA radiation (net radiation absorbed by the climate system) increased by 1.4 W m^{-2}, reflected solar radiation decreased by 2.1 W m^{-2} and emitted thermal radiation increased by 0.7 W m^{-2} over the period 1985–1998. Since AR4, Andronova et al.(2009) extended the Wong et al. (2006) ERBS/WFOV record with observations from CERES (Wielicki et al., 1996) on the Terra satellite. The longer record shows a continuation of these trends with tropical net TOA flux increasing by 2 W m^{-2} between 1985 and 2005. By comparison, when thermal data based upon HIRS and ISCCP-FD are used in place of the ERBS/CERES thermal record, the net radiation increase is more pronounced, reaching 6 W m^{-2} for ISCCP-FD. ERBE and CERES employ broadband measurements that span most of the full solar and thermal spectrum.The HIRS and ISCCP-FD estimates employ measurements with much more limited spectral coverage. The change in net radiation for ERBS/CERES is associated with a 3 W m^{-2} decrease in reflected solar radiation and an increase of 1 W m^{-2} in thermal emission. Comparisons between ERBS/CERES thermal radiation and that derived from the NOAA High Resolution Infrared Radiation Sounder (HIRS) (Lee et al., 2007; Lee et al., 2004) show good agreement until approximately 1998, corroborating the reported rise of 0.7 W m^{-2}, after which HIRS thermal fluxes show much higher values. The discrepancy is likely due to changes in the channels used for HIRS/3 instruments launched after October 1998 compared to earlier HIRS instruments (Lee et al., 2007). While the underlying causes for the large decadal changes in tropical radiation remain uncertain, several studies have suggested links to decadal changes in atmospheric circulation(Allan and Slingo, 2002; Chen et al., 2002; Clement and Soden, 2005; Merrifield, 2011) (see Section 2.7).

The extended records of reflected solar radiation from CERES covering the period 2001–2010 suggestthat globally, the planetary albedo has been rather stable over the first decade of the 21st Century (Loeb et al., 2012).

On a global scale, interannual variations in net TOA radiation and ocean heating rate should be correlated, since oceans have a much larger heat capacity compared to land and the atmosphere and therefore serve as the main reservoir for heat added to the Earth-atmosphere system. Wong et al. (2006) showed that these two data sources are in good agreement for 1992–2003. In the ensuing 5 years, however, Trenberth and Fasullo (2010) note that the two diverge. The satellite observations show an increase of about 1 W m^{-2} in the rate of absorbed net radiation at the TOA while the ocean in-situ measurements show a slowing of the increase in global ocean heat content (Chapter 3). Loeb et al.(2012) point out that the apparent decline in ocean heating rate is not statistically robust. Differences in variations in ocean heating rate and satellite net TOA flux are well within the uncertainty of the measurements. The variability in Earth's energy imbalance, related to the El Niño-Southern Oscillation (Section 2.7) is found to be consistent within uncertainties among the satellite measurements, a reanalysis model simulation and a new analysis of the ocean heat content records (Johnson et al., 2011) (Figure 2.13).

[INSERT FIGURE 2.13 HERE]

Figure 2.13: Comparison of net TOA flux and upper ocean heating rates. Global annual average net TOA flux from (a) CERES observations (based upon the EBAFTOA_ Ed2.6 product) and (b) ERA Interim reanalysis are anchored to an estimate of Earth's heating rate for 2006–2010. The Pacific Marine Environmental Laboratory/Jet Propulsion Laboratory/Joint Institute for Marine and Atmospheric Research (PMEL/JPL/JIMAR) ocean heating rate estimates (a) use data from Argo and World Ocean Database 2009; The gray bar (b) corresponds to one standard deviation about the 2001–2010 average net TOA flux of 15 CMIP3 models. From Loeb et al.(2012).

2.3.3 Changes in Surface Radiation Budget

2.3.3.1 Surface Solar Radiation

Changes in radiative fluxes at the surface can be traced further back in time than the satellite-based TOA fluxes, although only at selected locations where long term records exist. Monitoring of radiative fluxes from surface stations began on a widespread basis in the mid-20th Century, predominantly measuring the

downwelling solar component (also known as global radiation or surface solar radiation, hereafter referred to as SSR).

Various processes have the potential to alter SSR, such as changes in cloud characteristics, aerosol and water vapour. First indications for substantial decadal changes in observational SSR records were reported in AR4. Specifically, a decline of SSR from the beginning of widespread measurements in the 1950s until the mid-1980s has been observed at many land-based sites (popularly known as 'global dimming' (popularly known as "global dimming", Liepert, 2002; Stanhill and Cohen, 2001), as well as a partial recovery from the 1980s onward ('brightening' ("brightening", Wild et al., 2005) (see the long-term SSR record of Potsdam, Germany, in Figure 2.14 as an illustrative example).

Since AR4, numerous studies have substantiated the findings of significant decadal SSR changes observed both at globally distributed sites (e.g., Dutton et al., 2006 ; Gilgen et al., 2009; Ohmura, 2009; Wild, 2009 and references therein) as well as in specific regions. Wild et al. (2008) estimated the SSRbrightening over land surfaces at 2 W m^{-2} per decade for the period 1986–2000. In Europe, Norris and Wild (2007) noted a dimming from 1971 until the mid-1980s of 2.0–3.1 W m^{-2} per decadeand subsequent brightening of 1.1–1.4 W m^{-2} per decade in a pan-European time series consisting of 75 sites. Similar tendencies were found at sites in northern Europe (Stjern et al., 2009), Estonia (Russak, 2009) and Moscow (Abakumova et al., 2008). Chiacchio and Wild (2010) pointed out that dimming and subsequent brightening in Europe is mainly seen in spring and summer. Brightening in Europe from the 1980s onward was further documented at sites in Switzerland, Germany and Greece (Ruckstuhl et al., 2008; Zerefos et al., 2009).

At continental US sites, Long et al. (2009) and Riihimaki et al. (2009)noteda significant brightening of SSR over the periods 1995–2007 and 1980–2007, respectively. The general pattern of dimming until the 1980s and brightening thereafter was also found at numerous sites in Japan (Norris and Wild, 2009; Ohmura, 2009; Wild et al., 2005). Analyses of observations from sites in China confirmed strong declines in SSR from the 1960s to 1980s on the order of 2–8 W m^{-2} per decade, which also did not persist in the 1990s (Che et al., 2005; Liang and Xia, 2005; Norris and Wild, 2009; Qian et al., 2006; Shi et al., 2008; Tang et al., 2011; Xia, 2010a). Dimming and subsequent brightening was not only found at sites on the NH, but also in New Zealand (Liley, 2009). On the other hand, persistent dimming since the mid-20th Century with no evidence for a trend reversal was noted at sites in India (Kumari and Goswami, 2010; Kumari et al., 2007; Wild et al., 2005), and in the Canadian Prairie (Cutforth and Judiesch, 2007).

The longest observational SSR records, extending back to the 1920s and 1930s at a few sites in Europe, further indicate some brightening during the first half of the 20th Century, known as 'early brightening' (Figure 2.14) (Ohmura, 2009; Wild, 2009). This suggests that the decline in SSR, at least in Europe, was confined to a period between the 1950s and 1980s.

Updates on latest SSR changes observed at Earth's surface since 2000 provide a less coherent picture (Wild, 2012). They suggest a continuation of brightening at sites in Europe, U.S., and parts of Asia, a levelling off at sites in Japan and Antarctica, and indications for a renewed dimming in China (Wild et al., 2009). Renewed dimming after 2000, particularly in the SH,is also seen in a satellite-derived SSR data set (Hatzianastassiou et al., 2012).

A number of issues remain, such as the quality and representativeness of some of the SSR data as well as the large scale significance of the phenomenon (Wild, 2012). The historic radiation records are of variable quality and rigorous quality control is necessary to avoid spurious trends (Dutton et al., 2006; Gilgen et al., 2009; Shi et al., 2008; Tang et al., 2011). Since the mid-1990s, high-quality data are becoming increasingly available from new sites of the Baseline Surface Radiation Network (BSRN) and Atmospheric Radiation Measurement (ARM) Program, which allow the determination of SSR variations with unprecedented accuracy (Ohmura et al., 1998). Alpert et al. (2005) and Alpert and Kishcha (2008) argued that the observed SSR decline between 1960 and 1990 is larger in densely populated than in rural areas. The magnitude of this 'urbanization effect' in the radiation data is not yet well quantified. Dimming and brightening is, however, also notable at remote and rural sites (Dutton et al., 2006; Karnieli et al., 2009; Liley, 2009; Russak, 2009; Wang et al., 2012b; Wild, 2009).

While extended areas of the globe are not covered by surface measurements and hamper a true global assessment, satellite-derived fluxes can provide a near global picture. Such estimates are available since the early 1980s (Hatzianastassiou et al., 2005; Hinkelman et al., 2009; Pinker et al., 2005). Since satellites do not directly measure the surface fluxes, they have to be infered from measurable top-of-atmosphere signals using empirical or physical models to remove atmospheric perturbations. Available satellite-derived products qualitatively agree on a brightening from the mid-1980s to 2000 averaged globallyas well as over oceans, on the order of 2–3 W m^{-2} per decade(Hatzianastassiou et al., 2005; Hinkelman et al., 2009; Pinker et al., 2005). Averaged over land, however, trends are positive or negative depending on the respective satellite product (Wild, 2009). Knowledge of the spatiotemporal variation of aerosol burdens and optical properties, required in satellite retrievals of SSR and considered relevant for dimming/brightening particularly over land, is very limited.

Reconstructions of SSR changes from more widely measured meteorological variables can help to increasetheir spatial and temporal coverage. Decadal SSR changes have been related to observed changes in sunshine duration, diurnal temperature range (DTR), and pan evaporation. Overall, these proxies provide independent evidence for the existence of large-scale decadal variations in SSR. Specifically, SSR dimmingfrom the 1950s to the 1980s obtained additional support from widespread observations of concurrent declines in pan evaporation (Roderick and Farquhar, 2002) and DTR (Wild et al., 2007). The trend reversal of DTR observed over global land surfaces during the 1980s (Section 2.4) fits to the transition from dimming to brightening (Wild et al., 2007). Over Europe, SSR dimming and subsequent brighteningis consistent with concurrent declines and increases in sunshine duration (Sanchez-Lorenzo et al., 2008; Wang et al., submitted), evaporation in energy limited environments (Teuling et al., 2009) and DTR (Makowski et al., 2009). The early brightening in the 1930s and 1940s seen in a few European records is in line with corresponding changes in sunshine duration (Sanchez-Lorenzo et al., 2008; Sanchez-Lorenzo and Wild, 2012). In China, the levelling off in SSR in the 1990s after decades of decline coincides with similar tendencies in the pan evaporation records, sunshine duration and DTR (Ding et al., 2007; Liu et al., 2004a; Liu et al., 2004b; Qian et al., 2006; Wang et al., 2012b). Dimming up to the 1980s and subsequent brightening is also indicated in a set of 237 sunshine duration records in South America (Raichijk, 2011).

[INSERT FIGURE 2.14 HERE]

Figure 2.14: Annual mean surface solar radiation (in W m^{-2}) as observed at Potsdam, Germany, from 1937 to 2010. Five year moving average in blue. Updated from Wild (2009) and Ohmura (2009).

2.3.3.2 Surface Thermal Exchanges and Net Radiation

Long-term measurements of the thermal surface components as well as surface net radiation are available at far fewer sites than SSR. Downward thermal radiation observations started to become availableduring the early 1990s with the initiation of BSRN at a limited number of worldwide distributed sites. From these records, Wild et al. (2008) determined an overall increase of 2.6 W m^{-2} per decade over the 1990s, in line with model projections and the expectations of an increasing greenhouse effect. Wang and Liang (2009) inferred an increase in downward thermal radiation of 2.2 W m^{-2} per decade over the period 1973–2008 from observations of temperature, humidity and cloud fraction. Prata (2008) estimated a slightly lower increase of 1.7 W m^{-2} per decade for clear sky conditions over the earlier period 1964–1990, based on radiative transfer calculations using observed temperature and humidity profiles from radiosondes. Philipona et al. (2004) measured increasing downward thermal fluxes since the mid-1990s in the Swiss Alps, corroborating an increasing greenhouse effect. A contribution from anthropogenic chlorofluorocarbons (CFCs) to the downward thermal radiation has been documented in spectral atmospheric radiation measurements by Evans and Puckrin(1995).There is limited information on changes in surface net radiation, in large part because measurements of upwelling fluxes at the surface are made at only a few sites and are not spatially representative. Wild et al. (2008; 2004) inferred a decline in land surface net radiation on the order of 2 W m^{-2} per decadefrom the 1960s to the 1980s, and an increase at a similar rate from the 1980s to 2000, respectively, based on estimated changes of the individual surface radiative components.

2.3.3.3 Implications from Observed Changes in Related Climate Elements

The observed decadal SSR variations cannot be explained by changes in TSI, which are an order of magnitude smaller (Willson and Mordvinov, 2003). They therefore have to originate from alterations in the

transparency of the atmosphere, which depends on the presence of clouds, aerosols, and radiatively active gases (e.g., Kim and Ramanathan, 2008; Kvalevag and Myhre, 2007). Cloud cover changes effectively modulate SSR on an interannual basis, but their contribution to the detected longer-term SSR trends is ambiguous. While cloud cover changes were found to explain the trends in some areas (e.g., Liley, 2009), this is not always the case particularly in relatively polluted regions such as Europe and China (Norris and Wild, 2007; Norris and Wild, 2009; Qian et al., 2006; Wild, 2009; Wild, 2012). SSR dimming and brightening has also been observed under cloudless atmospheres at various locations, pointing to a prominent role of atmospheric aerosols (Norris and Wild, 2007; Norris and Wild, 2009; Ohvril et al., 2009; Russak, 2009; Sanchez-Lorenzo et al., 2009; Wang et al., 2009a; Wild, 2009; Wild et al., 2005; Zerefos et al., 2009).

Aerosols can directly attenuate SSR by scattering and absorbing solar radiation, or indirectly, through their ability to act as cloud condensation nuclei, thereby increasing cloud reflectivity and lifetime (see Chapter 7). The trend reversal from SSR dimming to brightening in the 1980s is often reconcilable with trends in aerosol optical depth and anthropogenic emission histories, which also indicate a distinct reversal during the 1980s (Cermak et al., 2010; Mishchenko et al., 2007b; Ohvril et al., 2009; Stern, 2006; Streets et al., 2006; Streets et al., 2009; Wild, 2012; Wild et al., 2005).

However, direct aerosol effects alone may not be able to account for the full extent of the observed SSR changesin remote regions with low pollution levels (Dutton and Bodhaine, 2001; Schwartz, 2005). Aerosol indirect effects have not yet been well quantified, but have the potential to amplify aerosol-induced SSR trends, particularly in relatively pristine environments (Wild, 2012).

SSR trends are also in line with observed decadal warming trends, with generally less warming during phases of declining SSR, and more warming in phases of increasing SSR (Wild et al., 2007). This is seen more prominently on the relatively polluted NH than on the more pristine SH (Wild, 2012).For Europe, Vautard et al.(2009)find that adecline in the frequency of low-visibility conditions such as fog, mist and haze over the past 30 years and associated SSR increase may be responsible for 10–20% of Europe's recent daytime warming, and 50% of eastern European warming.

Reanalyses and observationally-based methodshave been used to show that increased atmospheric moisture with warming (Willett et al., 2008; cf. Section 2.5) enhances thermal radiative emission of the atmosphere to the surface (Allan, 2009; Philipona et al., 2009; Prata, 2008; Wang and Liang, 2009; Wild et al., 2008).

The surface radiative fluxes provide the energy for surface evaporation and thereby govern evaporation/precipitation and the intensity of the hydrological cycle on global scales(Ramanathan et al., 2001; Stephens et al., in press; Wild and Liepert, 2010). The observed decadal changes in surface radiation are in line with observed changes in precipitation over terrestrial surfaces (Wild, 2012; Wild et al., 2008).

2.3.4 Summary

Compared to AR4, satellite records of TOA radiation fluxes have been substantially extended, and indicate a continuation of the decadal variations in the tropical radiation budget with *high confidence*. Globally, no significant changes were measured in the planetary albedo since 2000 with *very high confidence*. The variability in the Earth's energy imbalance, related to ENSO, is consistent with a new analysis of ocean heat content records with *high confidence*.

Since AR4, the evidence for widespread decadal variations in solar radiation incident on land surfaces has been substantiated, with many of the observational records showing a decline from the 1950s to the 1980s ('dimming'), and a partial recovery thereafter ('brightening'). *Confidence* in these changes *is high* in regions with high station densities such as over Europe and parts of Asia. The changes are generally supported by observed changes in related, but more widely measured variables, such as sunshine duration and DTR, and often in line with aerosol emission patterns. Over some remote land areas and over the oceans, *confidence is low* due to the lack of direct observations, which hamper a true global assessment. Satellite-derived SSR fluxes support the existence of brightening also over oceans, but are less consistent over land surface where direct aerosol effects become more important. There are also indications with *medium to low confidence* for increasing downward thermal and net radiationat terrestrial stations in recent years.

[START BOX 2.3 HERE]

Box 2.3: Global Atmospheric Reanalyses

Dynamical reanalyses are increasingly used for assessing weather and climate phenomena. Given their more frequent use in this assessment compared to AR4, their characteristics are described in more detail here.

Reanalyses are distinct from, but complement, more 'traditional' statistical approaches to assessing the raw observations. They aim to produce continuous reconstructions of past atmospheric states that are consistent with all observations as well as with atmospheric physics as represented in a numerical weather prediction model, a process termed data assimilation. Unlike real-world observations, reanalyses are complete in space and time and provide non-observable variables (e.g., potential vorticity).

Several groups are actively pursuing reanalysis development at the global scale and many of these have produced several generations of reanalyses products (Box 2.3, Table 1). Since the first generation of reanalyses produced in the 1990s, substantial development has taken place. The MERRA and ERA-Interim reanalyses show improved tropical precipitation and hence better represent the global hydrological cycle (Dee et al., 2011). The NCEP/CFSR reanalysis uses a coupled ocean-atmosphere-land-sea-ice model (Saha et al., 2010). The 20th Century Reanalyses (20CR, Compo et al., 2011) is a 56 member ensemble and covers 140 years by assimilating only surface and sea-level pressure (SLP) information. This variety of groups and approaches provides some indication of the robustness.

Box 2.3, Table 1: Overview of global dynamical reanalysis data sets (ranked by start year). In addition to the global reanalyses listed here, several regional reanalyses exist or are currently being produced. A further description of reanalyses and their technical derivation is given in pp.S33-35 of Blunden et al. (2011).

Institution	Reanalysis	Period	Approximate Resolution at Equator	Reference
Cooperative Institute for Research in Environmental Sciences (CIRES), National Oceanic and Atmospheric Administration (NOAA), USA	20th Century Reanalysis, Vers. 2 (20CR)	1871–2008	320 km	Compo et al. (2011)
National Centers for Environmental Prediction (NCEP) and National Center for Atmospheric Research (NCAR), USA	NCEP/NCAR R1 (NNR)	1948–	320 km	Kistler et al. (2001)
European Centre for Medium Range Weather Forecasts (ECMWF)	ERA-40	1957–2002	125 km	Uppala et al. (2005)
NCEP, US Department of Energy, USA	NCEP/DOE R2	1979–	320 km	Kanamitsu et al. (2002)
Japanese Meteorological Agency (JMA)	JRA-25	1979–	190 km	Onogi et al. (2007)
National Aeronautics and Space Administration (NASA), USA	MERRA	1979–	75 km	Rienecker et al. (2011)
European Centre for Medium Range Weather Forecasts (ECMWF)	ERA-Interim	1979–	80 km	Dee et al. (2011)
NCEP, USA	CFSR	1979–	50 km	Saha et al. (2010)

Reanalyses products provide invaluable information on time scales ranging from daily to interannual variability. Their ability to characterize long-term trends remains an open question (Trenberth et al., 2011). Although reanalyses projects by definition use a 'frozen' assimilation system, there are many other sources of potential errors. In addition to model biases, changes in the observational systems (e.g., coverage, introduction of satellite data) and errors in the underlying observations or in the boundary conditions lead to step changes in time, even in latest generation reanalyses (Bosilovich et al., 2011).

Errors of this sort were ubiquitous in early generation reanalyses and rendered them of limited value for trend characterization (Thorne and Vose, 2010). Subsequent products have improved and uncertainties are better understood, but artefacts are still present. As a consequence, trend adequacy depends upon the variable under consideration, the time period and the region of interest. For example, surface air temperature trends

over land in the ERA-40 reanalysis compare well with quasi-independent observations (Simmons et al., 2010), but polar tropospheric temperature trends disagree with trends derived from radiosonde and satellite observations (Bitz and Fu, 2008; Grant et al., 2008; Graversen et al., 2008; Thorne, 2008).

[END BOX 2.3 HERE]

2.4 Changes in Temperature

2.4.1 Land-Surface Air Temperature

2.4.1.1 Large-Scale Records and their Uncertainties

AR4 concluded global land-surface air temperatures (LSAT) had increased, with the rate of change in the most recent 50 years being almost double that in the last 100 years. Since AR4, substantial developments have occurred including the production of revised data sets, more digital data records, and new data set efforts. These innovations have improved understanding of data issues and uncertainties and allowed better understanding of regional changes.

Improvements have been made to the global data sets of LSAT observations used in AR4. Global Historical Climatology Network (GHCN) V3 incorporates many improvements (Lawrimore et al., 2011b) but was found to be virtually indistinguishable at the global mean from version 2 (used in AR4). Goddard Institute of Space Studies (GISS) continues to provide an estimate based upon primarily GHCN. Improvements in accounting for urban impacts through nightlights adjustments have been documented (Hansen et al., 2010). CRUTEM4 (Jones et al., 2012b) incorporates additional series and also newly homogenized versions of many stations. A new data product from a group based predominantly at Berkeley (Rhode et al., submitted) uses a method that is substantially distinct from earlier efforts. The long-term variations and trends broadly agree among these various estimates, particularly after 1900 (Figure 2.15, Table 2.4) despite the range of approaches. In the early years, sampling is far from global so differences are larger and different groups have made different decisions as to when meaningful global coverage begins, reflected in the range of data set start dates. Uncertainties arising from choice of data set do not impact the conclusion that global LSAT has increased (Table 2.4).

[INSERT FIGURE 2.15 HERE]

Figure 2.15: Global annually averaged LSAT anomalies relative to a 1961–1990 climatology from the latest versions of four different data sets.

Table 2.4: Trend estimates and 5 to 95% confidence intervals (Box 2.2) for LSAT global average values over five common periods.

Data Set	1880–2011	1901–2011	1901–1950	1951–2011	1979–2011
CRUTEM4	0.085 ± 0.015	0.094 ± 0.020	0.097 ± 0.029	0.176 ± 0.038	0.263 ± 0.049
GHCNv3.1.0	0.084 ± 0.017	0.095 ± 0.022	0.086 ± 0.034	0.191 ± 0.033	0.277 ± 0.049
GISS	0.083 ± 0.017	0.081 ± 0.022	0.080 ± 0.034	0.180 ± 0.035	0.270 ± 0.054
Berkeley	0.091 ± 0.014	0.100 ± 0.018	0.108 ± 0.038	0.179 ± 0.028	0.257 ± 0.052

Since AR4, various theoretical challenges have been raised over the verity of global LSAT records (Pielke et al., 2007) and some studies have yielded somewhat different regional characteristics (Christy et al., 2009). However, most research since AR4 reinforces confidence in the reported globally averaged LSAT time series behaviour. Globally, sampling and methodological independence has been assessed through sub-sampling (Jones et al., 2012b; Parker et al., 2009), creation of an entirely new and structurally distinct product (Rhode et al., submitted) and a complete reprocessing of the GHCN product (Lawrimore et al., 2011b). None of these yielded more than minor perturbations to the global LSAT records since 1900. Willett et al. (2008) and Peterson et al. (2011) explicitly showed that changes in specific and relative humidity confirmed reported temperature trends, a result replicated in the ERA reanalyses (Simmons et al., 2010). Various investigators (Parker, 2011; Simmons et al., 2010; Vose et al., 2012a) showed that temperatures from modern reanalyses were in very good agreement with observed products.

Particular controversy since AR4 has surrounded the LSAT record over the United States. A new automated homogeneity assessment approach (Menne and Williams, 2009) was developed that has been shown to perform as well or better than other contemporary approaches (Venema et al., 2011). Current station siting has been well documented for the USA (Fall et al., 2011) where most sites exhibit poor modern siting (since replacement of Stevenson screens with maximum minimum temperature sensors in the 1980s at the majority of sites) and may be expected to suffer potentially large siting-induced absolute biases (Fall et al., 2011). This modern siting quality is very highly correlated with instrument type and overall biases for the network are likely dominated by instrument type, rather than siting, biases (Menne et al., 2010; Williams et al., 2012), and homogenization likely removes much of the bias (Fall et al., 2011; Menne et al., 2010; Muller et al., submitted; Williams et al., 2012). Williams et al. (2012) produced an ensemble of realisations and concluded through assessment against plausible test cases that there existed a propensity to under-estimate adjustments. When the identified biases are removed from the observations both minimum and maximum centennial-timescale United States LSAT trends increase. Since 1979 these adjusted data agree with a range of reanalyses products whereas the raw records do not (Fall et al., 2010; Vose et al., 2012a).

Regional analyses have not been limited to the United States. Various national and regional studies have undertaken assessments using a range of statistical approaches for Europe (Bohm et al., 2010; Tietavainen et al., 2010; van der Schrier et al., 2011), China (Li et al., 2009; QingXiang et al., 2010; Tang et al., 2010; Zhen and Zhong-Wei, 2009), India (Jain and Kumar, 2012), Australia (Trewin, 2012), Canada (Vincent et al., Submitted), and East Africa (Christy et al., 2009). These analyses have used a range of methodologies and, in many cases, more data and metadata than available to the global analyses. Despite the range of analysis techniques they are generally in broad agreement with the global products in characterizing the long-term changes in mean temperatures. Of specific importance for the early global records, large summertime warm bias adjustments for many European 19th Century and early 20th Century records were revisited and broadly confirmed by a range of approaches (Bohm et al., 2010; Brunet et al., 2011). Since AR4 efforts have also been made to interpolate Antarctic records from the sparse, predominantly coastal ground-based network (O'Donnell et al., 2011; Steig et al., 2009). Although these agree that Antarctica as a whole is warming, substantial differences in reconstructed magnitude and spatial trend structure yield only *low confidence* in Antarctic region LSAT changes.

2.4.1.2 Diurnal Temperature Range

In AR4 Diurnal Temperature Range (DTR) was found, globally, to have narrowed with minimum daily temperatures increasing faster than maximum daily temperatures. However significant multi-decadal variability was highlighted including a recent period of no change. Since AR4 uncertainties in DTR and its physical interpretation have become much more apparent.

No in-depth global analysis of DTR has been undertaken subsequent to (Vose et al., 2005a), reported in AR4 for the period 1950–2004. The Berkeley group note globally an apparent reversal since the mid-1980s; with DTR increasing since then (Rhode et al., submitted). Makowski et al. (2009) found that the long-term trend of annual DTR in Europe over 1950 to 2005 changed from a decrease to an increase in the 1970s in Western Europe and in the 1980s in Eastern Europe. Roy and Balling (2005) found significant increases in both maximum and minimum temperatures for India, but little change in DTR over 1931–2002. Christy et al. (2009) reported that for East Africa there has been no pause in the narrowing of DTR in recent decades.

Various investigators (e.g., Christy et al., (2009), Pielke and Matsui, (2005)) have raised doubts about the physical interpretation of minimum temperature trends. They hypothesize that microclimate and local atmospheric composition impacts are most apparent in minimum temperatures because the dynamical mixing is much reduced. Parker (2006) used the difference between calm and windy nights to address these posited issues with minimum temperature trends and found no difference between trends for calm and windy nights on a global average basis. If the data were affected in this way, then a trend difference would be expected. Using more complex boundary layer modelling techniques Steeneveld et al. (2011) and McNider et al. (2012) showed much lower sensitivity to windspeed variations than posited by Pielke and Matsui but both concluded that boundary layer understanding was key to understanding minimum temperature changes.

Real non-climatic data artefacts certainly affect maximum and minimum differently in the raw records for both recent (Fall et al., 2011; Williams et al., 2012) and older (Bohm et al., 2010; Brunet et al., 2011) records. Hence there could be issues over interpretation of apparent DTR trends and variability in many regions (Christy et al., 2009; Christy et al., 2006; Fall et al., 2011; Williams et al., 2012), particularly when accompanied by regional-scale Land Use / Land Cover changes (Christy et al., 2006). As most studies looking at DTR to date have considered data that had not been assessed for homogeneity, it is unclear to what extent the conclusions from such studies are afflicted by diurnally differentiated biases in the data yielding spurious time series behaviour in DTR. Hence there is only *low-to-medium confidence* in global DTR trends.

2.4.1.3 Land-Use Change and Urban Heat Island Effects

In AR4 Urban Heat Island (UHI) effects were concluded to be real local phenomena with negligible impact on changes in the global average. UHI and land-use land-cover change (LULC) effects arise mainly because the modified surface affects the storage and transfer of heat. For single discrete locations these impacts may dominate all other factors. Since AR4 there has been substantial further research in this area which has investigated the issue in a myriad of ways.

For UHI, regionally, most recent attention has focused upon China where in some regions that have rapidly developed, UHI and LULC impacts on regional trends have been substantial. A variety of investigations using methods as diverse as sea surface temperature comparisons (e.g., Jones et al., 2008), urban minus rural (e.g., Ren et al.,(2008) Yang et al.,(2011b)) and observations minus reanalysis (e.g., Yang et al., 2011b; Hu et al., 2010) broadly agree that the effect is approximately 20% in Eastern China and of the order 0.1°C per decade nationally (see Table 1 in Yang et al., 2011b) over the last 30 years. Fujibe (2009) implicitly ascribes about 25% of Japanese warming trends in 1979–2006 to urban development. Das et al. (2011) confirmed that many Japanese sites have experienced UHI warming up to double the background warming, but that apparently rural stations show plausibly unaffected behaviour. Conversely, Jones and Lister (2009) and Wilby et al. (2011) using data from London (UK) concluded that some sites which have always been urban and where the UHI has not grown in magnitude will exhibit regionally indicative trends and that UHI effects may exhibit multi-decadal trends driven primarily by synoptic variations. Almazroui et al. (Submitted) found no evidence for urban influences on Saudia Arabian temperatures despite rapid urbanization.

Estimates of large-scale temperature change have tended either to avoid urban observing sites, or adjusted their data to match regional rural trends (Hansen et al., 2010; Menne and Williams, 2009; Parker, 2010). For the US network, Hausfather et al. (Submitted) showed that the adjustments removed much of an apparent systematic difference between urban and rural locations, concluding that this arose from adjustment of biased urban location data rather than vice-versa. Globally, Hansen et al. (2010) used satellite-based nightlight radiances to estimate the worldwide influence on LSAT of local urban development. Adjustments only reduced the global 1900–2009 temperature change (averaged over land and ocean) from 0.71°C to 0.70°C. Wickham et al. (submitted) similarly used satellite data and a much larger network of stations and found that urban locations exhibited less warming than rural stations, although not statistically significantly so, over 1950 to 2010. Efthymiadis and Jones (2010) estimated an absolute upper limit on urban influence globally of 0.02°C per decade, or ~15% of the total trends, in 1951–2009 from trends of coastal land and sea surface temperature.

McKitrick and Michaels (2004) and de Laat and Maurellis (2006) assessed national socioeconomic and geographical indicators, concluding that UHI and related LULC have caused much of the observed LSAT warming. AR4 concluded the correlation ceases to be statistically significant if one takes into account the fact that the locations of greatest socioeconomic development are also those that have been most warmed by atmospheric circulation changes. AR4 provided no explicit evidence for this overall assessment result. Subsequently McKitrick and Michaels (2007) corroborated their earlier finding, concluding that about half the reported warming trend in global-average land surface air temperature in 1980–2002 resulted from local land-surface changes and faults in the observations. In contrast, Schmidt (2009) concluded that much of the reported correlation likely arose due to naturally occurring climate variability and model over-fitting and was not robust. Taking these factors into account, modified analyses by McKitrick (2010) and McKitrick and Nierenberg (2010) still yielded apparently significant evidence for such contamination of the record. McKitrick (Submitted) noted how such studies need not be contradictory and concluded that neither the

findings of Schmidt (2009) nor Parker (2006) invalidated the findings of the various earlier McKitrick and colleagues analyses. In contrast, several studies have shown the methodologically diverse set of modern reanalysis products and the various LSAT records at global and regional levels to be similar since at least the mid 20th Century (Ferguson and Villarini, 2012; Ferguson and Villarini, Submitted; Parker, 2011; Simmons et al., 2010; Vose et al., 2012a). These reanalysis products on average imply slightly more, rather than significantly less (as posited by socio-economic indicator regressions), warming than the observed data sets. A hypothesized residual significant warming artefact argued for by socioeconomic regressions is therefore physically inconsistent with many other components of the global observing system according to a range of data assimilation models (Box 2.3). These models do not directly utilize the LSAT measurements but rather infer LSAT estimates thus representing an independent estimate.

It is indisputable that UHI and LULC are confounding influences on raw temperature measurements. At question is the extent to which such issues remain in the global products (as residual biases). Analyses ranging from urban-rural comparisons, socio-economic indicator regressions, coastal land-sea contrasts, calm and windy conditions, and reanalyses comparisons have all been used to quantify these influences since AR4. It is important to note that no published study since AR4 has implied that all, or even the majority of, the recent LSAT warming trend can be accounted for by UHI and LULC effects. Based primarily upon the range of urban minus rural comparisons and the degree of agreement with a broad range of reanalyses products it is concluded that it is likely that residual biases account for no larger than 10% of the warming trend globally and 25% regionally in rapidly developing regions.

2.4.2 Sea Surface Temperature and Marine Air Temperature

AR4 concluded that 'recent' warming (since the 1950s) is strongly evident at all latitudes in sea surface temperatures (SST) over each ocean. Prominent spatio-temporal structures including the El Nino and Pacific Decadal variability patterns in the Pacific Ocean and a hemispheric asymmetry in the Atlantic Ocean were highlighted as contributors to the regional differences in surface warming rates, which in turn affect atmospheric circulation. Since AR4 the availability of metadata has increased, data completeness has improved and a number of new SST products have been produced. Inter-comparisons of data obtained by different measurement methods, including satellite data, have resulted in better understanding of errors and biases in the record.

2.4.2.1 Advances in Assembling Data Sets and in Understanding Data Error

2.4.2.1.1 In situ data records

Historically, most SST observations were obtained from moving ships. Buoy and satellite measurements comprise a significant and increasing fraction of SST measurements from the 1980s onward (Figure 2.17). Improvements in the understanding of uncertainty have been expedited by the use of metadata (Kent et al., 2007) and the recovery of observer instructions and other related documents. Early data were systematically biased cold because they were made using canvas or wooden buckets that, on average, lost a great deal of heat to the air before the measurements were taken (Folland and Parker, 1995). This effect has long been recognized, and prior to AR4 represented the only artefact adjusted in gridded SST products, like HadSST2 (Rayner et al., 2006). The adjustments, made using ship observations of night marine air temperature data (NMAT) and other sources, had a striking effect on the SST global mean estimates (see ICOADS, NMAT, and HadSST2 curves for 1850–1941 in Figure 2.16).

[INSERT FIGURE 2.16 HERE]

Figure 2.16: Global annually averaged SST and NMAT relative to a 1961-1990 climatology from gridded data sets of SST observations (HadSST2 and its successor HadSST3), the raw SST measurement archive (ICOADS, v2.5) and night marine air temperatures data set HadNMAT2 (Kent et al., Submitted). Both HadSST2 and HadSST3 are based on SST observations from versions of the ICOADS data set, where some measurement biases were corrected. Largest corrections are applied to the period before 1941 and are informed, in particular, by night marine air temperature data. In HadSST3 biases are adjusted for the entire period (Kennedy et al., 2011c).

Measurement methods with smaller biases and buckets of improved design came into use after 1941 (Figure 2.17, top); biases were reduced further in recent decades, but not eliminated (Figure 2.17, bottom). Increasing density of SST observations made possible the identification (Kennedy et al., 2011a; Reynolds et al., 2002a; Reynolds et al., 2010) and correction of these smaller biases (HadSST3, Kennedy et al., 2011c).

The difference between HadSST3 and HadSST2 global means (Figure 2.16) is particularly prominent in 1945–1970 period, where biases due to the ERI-to-bucket transition after the end of World War II (Thompson et al., 2008) are corrected in HadSST3. Some degree of independent check on the validity of these adjustments comes from a comparison to sub-surface temperature data (discussed further in Chapter 3 (Gouretski et al., Submitted)). For periods longer than a century the effect of HadSST3-HadSST2 differences on linear trend slopes is small relative to the trend estimation uncertainty (Table 2.5).

Table 2.5: Same as Table 2.4 but for two subsequent versions of the HadSST data set to show the impact of HadSST2 to HadSST3 changes on multi-decadal trend estimates through the overlap period ending in 2011. HadSST2 has been used in AR4; HadSST3 is used in this chapter.

Data Set	1880–2011	1901–2011	1901–1950	1951–2011	1979–2011
HadSST3	0.054 ± 0.012	0.067 ± 0.013	0.117 ± 0.028	0.074 ± 0.028	0.127 ± 0.030
HadSST2	0.050 ± 0.015	0.069 ± 0.013	0.084 ± 0.055	0.098 ± 0.018	0.125 ± 0.033

[INSERT FIGURE 2.17 HERE]

Figure 2.17: Temporal changes in the prevalence of different measurement methods in the ICOADS. Top: fractional contributions of observations made by different measurement methods: bucket observations (blue), ERI and hull contact sensor observations (green), moored and drifting buoys (red), and unknown (yellow). Bottom: Global annual average SST anomalies based on different kinds of data: engine room intake (ERI) and hull contact sensor (green), bucket (blue), buoy (red), and all (black). Averages are computed over all times and locations where both ERI and hull measurements, (but not necessarily buoy data) were simultaneously available. Adapted from Kennedy et al. (2011c).

The traditional approach to estimating random error of *in situ* SST data assumed the independence of individual measurements. Kent and Berry (2008) introduced platform-dependent biases, which are constant within the same 'platform' (e.g., an individual ship or buoy), but change from platform to platform in a random fashion. HadSST3 accounting for such correlated errors (Kennedy et al., 2011b) resulted in error estimates for global and hemispheric monthly means that are more than twice the estimates from HadSST2.

Datasets of MAT have traditionally been restricted to night-time series (NMAT) due to the direct solar heating effect on the daytime measurements, although corrected MAT records from 1973-present are already available (Berry and Kent, 2009). Other major biases, affecting both night-time and day-time MAT are due to increasing deck height with the general increase in the size of ships over time and non-standard measurement practices. Recently these biases were re-examined and explicit uncertainty calculation undertaken for NMAT by (Kent et al., Submitted) building confidence in the reality of multidecadal warming in the near surface air temperature above the sea surface since the late 19th Century.

2.4.2.1.2 Satellite SST data records

The majority of satellite SST data are collected by sensors primarily designed for meteorological purposes and have to be tuned to *in situ* observations. Satellite-based data sets describe global SST fields with a level of spatial detail unachievable with *in situ* data only. The principal IR sensor is the Advanced Very High Resolution Radiometer (AVHRR) series. Since AR4, the AVHRR time series has been reprocessed consistently back to March 1981 (Casey et al., 2010) to create the AVHRR Pathfinder v5.2 data set. Passive microwave data sets of SST are available since 1997 equatorward of 40^{o} and since 2002 near-globally (Gentemann et al., 2004; Wentz et al., 2000). They are generally less accurate than IR-based SST data sets, but their superior coverage in areas of persistent cloudiness provides SST estimates where the IR record has none (Reynolds et al., 2010).

The Along Track Scanning Radiometer (ATSR) series of three sensors was designed for climate monitoring of SST; its combined record starts in August 1991 and exceeds two decades. The ATSRs are 'dual-view' IR radiometers intended to support atmospheric effects removal without use of *in situ* observations. Since AR4, ATSR observations have been reprocessed with new estimation techniques (Embury and Merchant, 2011). The resulting SST product seem to be more accurate than many *in situ* observations (Embury et al., 2011). In terms of monthly global means, the agreement is illustrated in Figure 2.18. By analyzing AATSR and *in situ*

data together, Kennedy at al. (2011a) verified and extended existing models for biases and random errors of *in situ* data.

[INSERT FIGURE 2.18 HERE]

Figure 2.18: Global monthly mean SST anomaly from satellites (ATSRs) and *in situ* records (HadSST3). Black lines: the 100 member HadSST3 ensemble. Red lines: ATSR night-time $SST_{0.2m}$ estimates from the ATSR Reprocessing for Climate (ARC) project. Retrievals based on three spectral channels (D3, solid line) are more accurate than retrievals based on only two (D2, dotted line). Contributions of the three different ATSR missions to the curve shown are indicated at the bottom. The *in situ* and satellite records were co-located within 5° × 5° monthly grid boxes: only those where both data sets had data in the same month were used in the comparison. Adapted from Merchant et al. (Submitted).

2.4.2.2 Interpolated SST Products and Trends

SST datasets form major part of global surface temperature analyses considered in this assessment report. To use an SST data set as a boundary condition for atmospheric reanalyses products (Box 2.3) and in atmosphere only climate models considered in Chapter 9 onwards, a gridded data set with complete coverage over the global ocean is typically needed too. They are usually produced by a form of kriging (optimal interpolation) procedure. For the pre-satellite era (generally, before October 1981) only *in situ* data are used; for the later period some products use the satellite data as well. Figure 2.19 intercompares interpolated SST data sets that extend back to the 19th century with the uninterpolated HadSST3 product and the MAT HadNMAT2 product. Linear trend estimates for global mean SSTs from those products updated through 2011 are presented in Table 2.6.

[INSERT FIGURE 2.19 HERE]

Figure 2.19: Global annually averaged SST and NMAT relative to a 1961–1990 climatology from state of the art datasets. Interpolated products are shown by solid lines; non-interpolated products by dashed lines.

Table 2.6: Same as Table 2.4 but for SST data sets. Trends for periods for which a time series is incomplete are not shown.

Data Set	1880–2011	1901–2011	1901–1950	1951–2011	1979–2011
HadISST1	0.042 ± 0.008	0.052 ± 0.007	0.067 ± 0.024	0.064 ± 0.015	0.074 ± 0.025
COBE-SST		0.058 ± 0.008	0.066 ± 0.032	0.072 ± 0.014	0.075 ± 0.021
ERSSTv3b	0.053 ± 0.016	0.070 ± 0.012	0.096 ± 0.049	0.088 ± 0.018	0.109 ± 0.031
HadSST3	0.054 ± 0.012	0.067 ± 0.013	0.117 ± 0.028	0.074 ± 0.028	0.127 ± 0.030

2.4.3 Global Combined Land and Ocean Surface Temperature

AR4 concluded that the global average surface temperature had increased, especially since 1950. Independently produced data sets were found to be consistent. Subsequent developments in land and SST have led to better understanding of the data and their uncertainties as discussed in preceding sections. This improved understanding has led to revised global products.

Changes have been made to all three data sets that were used in AR4 (Hansen et al., 2010; Morice et al., 2012; Vose et al., 2012b). These are now in somewhat better agreement with each other over recent years, in large part because HadCRUT4 now better samples the NH high latitude land regions (Morice et al., 2012; Simmons et al., 2010). Global mean surface temperatures have increased since the late 19th Century. Warming has not been linear; most warming occurred in two periods: c.1900 to c.1940 and c.1970 onwards. Starting in the 1980s each decade has been significantly warmer than all preceding decades in HadCRUT4 which explicitly quantifies a large number of sources of uncertainty (Figure 2.20). All ten of the warmest years have occurred since 1997, with 2010 and 2005 effectively tied for the warmest year on record in all three products. However, uncertainties on individual annual values are sufficiently large that the top ten or so years are statistically indistinguishable from one another. Using HadCRUT4 according to its published

uncertainty estimate method, the warming from 1886-1905 (early-industrial) to 1986-2005 (reference period for the modelling chapters and the Atlas in Annex 1) is 0.66°C ± 0.06°C (5 to 95% confidence interval).

[INSERT FIGURE 2.20 HERE]

Figure 2.20: Decadal mean temperature anomalies (white vertical lines) and their uncertainties (5–95 percentile ranges as coloured blocks) based upon the LSAT and SST combined HadCRUT4 ensemble (Morice et al., 2012). Anomalies are relative to a 1961–1990 climatology. 1850s indicates the period 1850-1859, and so on. NCDC MLOST and GISS dataset best-estimates are also shown.

Differences between data sets are much smaller than both inter-annual variability and the long-term trend (Figure 2.21). However, there are some decadal timescale differences. Much interest has focussed on differences in the period since 1998 and an apparent flattening in HadCRUT3 trends. Various investigators have pointed out the limitations of such short-term trend analysis in the presence of auto-correlated series variability and that several other similar length phases of no warming exist in all the observational records and in climate model simulations (Easterling and Wehner, 2009; Grant Foster and Stefan, 2011; Peterson et al., 2009; Santer et al., 2011). This issue is discussed in the context of model behaviour and natural variability in Chapter 10. Regardless, changes to HadCRUT4 (Morice et al., 2012), primarily as a result of incorporation of more high-latitude NH land data, mean that all products now show a warming trend since 1998 (0.055°C per decade (HadCRUT4); 0.042°C per decade (MLOST); 0.093C/decade (GISS), none of these are statistically significant). Differences between data sets are larger in earlier periods that have received less focus, particularly prior to c.1945 when observational sampling is much more geographically incomplete (and many of the well sampled areas may have been globally unrepresentative (Bronnimann, 2009)), the data errors and subsequent methodological impacts are larger (Thompson et al., 2008), and the different ways of accounting for data void regions become more important (Vose et al., 2005b).

[INSERT FIGURE 2.21 HERE]

Figure 2.21: Global mean surface temperature anomalies relative to a 1961–1990 climatology from the latest version of the three combined LSAT and SST data sets.

Since 1901 almost the whole globe has experienced surface warming (Figure 2.22, left hand panels). This warming is generally greater over land than oceans and greater in mid- to high-latitude regions. Over the satellite era most of the globe again experienced warming (Figure 2.22, right hand panels), but over this shorter period a greater proportion of the globe exhibits cooling, in particular over the oceans. Shorter periods are noisier and so proportionately less of the sampled globe exhibits statistically significant trends at the gridbox level in this period. The global mean warming rate has been much greater in this recent period and global trends are significant for all multi-decadal periods considered here (Table 2.7).

[INSERT FIGURE 2.22 HERE]

Figure 2.22: Trends in surface temperature from the three global datasets for 1901–2011 (left hand panels) and 1979–2011 (right hand panels). Trends have been calculated only for those grid boxes with greater than 70% complete records and more than 20% data availability in first and last decile of the period. Grid boxes where the trend is significant at the 10% level are indicated by a +. Differences in coverage primarily reflect the degree of interpolation undertaken by the dataset providers ranging from none (HadCRUT4) to substantial (GISS).

Table 2.7: Same as Table 2.4, but for combined surface temperature global average values over five common periods.

Data Set	1880–2011	1901–2011	1901–1950	1951–2011	1979–2011
HadCRUT4	0.062 ± 0.012	0.075 ± 0.013	0.107 ± 0.026	0.107 ± 0.028	0.161 ± 0.032
NCDC MLOST	0.061 ± 0.015	0.077 ± 0.014	0.094 ± 0.040	0.116 ± 0.022	0.154 ± 0.032
GISS	0.060 ± 0.010	0.070 ± 0.012	0.079 ± 0.027	0.113 ± 0.022	0.157 ± 0.034

2.4.4 Upper Air Temperature

AR4 concluded that globally the troposphere was warming at a rate indistinguishable from reported surface trends over the common period of record. Trends in the tropics were concluded to be more uncertain although even this region was concluded to be warming. Globally, the stratosphere was concluded to be

cooling over the satellite era starting in 1979. New advances since AR4 have highlighted the substantial degree of uncertainty in both satellite and weather balloon records.

2.4.4.1 Advances in Multi-Decadal Observational Records

The major global radiosonde records extend back to 1958 with temperatures, measured as the balloon ascends, reported at pressure levels. Satellites have monitored tropospheric and lower stratospheric temperature trends since late 1978 through the Microwave Sounding Unit (MSU) and its follow-on Advanced Microwave Sounding Unit (AMSU) since 1998. These measures of upwelling radiation represent bulk (volume averaged) atmospheric temperature (Figure 2.23). The 'Mid-Tropospheric' (MT) MSU channel that most directly corresponds to the troposphere has 10–15% of its signal from both the skin temperature of the Earth's surface and the stratosphere. Two alternative approaches have been suggested for removing the stratospheric component based upon differencing of view angles (LT) and statistical recombination (*G) with the 'Lower Stratosphere' (LS) channel (Fu et al., 2004; Spencer and Christy, 1992). The MSU satellite series also included a Stratospheric Sounding Unit (SSU) that measured at higher altitudes (Seidel, 2011).

[INSERT FIGURE 2.23 HERE]

Figure 2.23: Vertical weighting functions for those satellite temperature retrievals discussed in this chapter (modified from Seidel et al. (2011)). The dashed line indicates the typical maximum altitude achieved in the historical radiosonde record. The three SSU channels are denoted by the designated names 25, 26 and 27. LS (Lower Stratosphere) and MT (Mid Troposphere) are two direct MSU measures and LT (Lower Troposphere) and *G (Global Troposphere) are derived quantities from one or more of these that attempt to remove the stratospheric component from MT.

At the time of AR4 there were only two radiosonde data sets that included treatment of homogeneity issues: RATPAC (Free et al., 2005) and HadAT (Thorne et al., 2005). Three additional estimates have appeared since AR4; these are based on novel and distinct approaches. In addition, a systematic effort has been made to understand uncertainty in the HadAT product. A group at the University of Vienna have produced RAOBCORE and RICH (Haimberger, 2007; Haimberger et al., 2008; Haimberger et al., 2012) using ERA reanalysis products (Box 2.3). Sherwood and colleagues developed an iterative universal kriging approach for radiosonde data to create IUK (Sherwood et al., 2008) and concluded that non-climatic data issues remained in the deep tropics even after homogenisation. The HadAT group created an automated version, undertook systematic experimentation and concluded that the parametric uncertainty was of the same order of magnitude as the apparent climate signal (McCarthy et al., 2008; Thorne et al., 2011a). A similar ensemble approach has also been applied to the RICH product (Haimberger et al., 2012). These various ensembles exhibited more tropospheric warming / less stratospheric cooling than existing products at all levels. Globally the radiosonde records all imply the troposphere has warmed and the stratosphere cooled since 1958 but with uncertainty in the rate of change that grows with height. This uncertainty is much greater outside the better sampled NH extra-tropics (Haimberger et al., 2012; Thorne et al., 2011a), and even here is of the order 0.1°C per decade.

For MSU, AR4 considered estimates produced from three groups: UAH (University of Alabama in Huntsville); RSS (Remote Sensing Systems) and VG2 (now deprecated). A new product has been created by NOAA labelled STAR. The new STAR analysis used a fundamentally distinct approach for the critical inter-satellite warm target calibration step (Zou et al., 2006a). STAR exhibits more warming / less cooling at all levels than UAH and RSS. For MT and LS (Zou and Wang, 2010) concluded that this does not primarily relate to use of the inter-satellite calibration technique but rather differences in other processing steps. RSS also produced a comprehensive model of their parametric uncertainty (Box 2.1) employing a Monte-Carlo approach allowing methodological inter-dependencies to be fully expressed (Mears et al., 2011). For large-scale trends dominant effects were inter-satellite offset determinations and, for tropospheric channels, diurnal drift. Uncertainties in resulting trend estimates were concluded to be of the order 0.1°C per decade at the global mean for both tropospheric channels (where it is of comparable magnitude to the long-term trends) and the stratospheric channel.

SSU provides the only long-term near-global temperature data above the lower stratosphere, with the series terminating in 2006. Until recently only one SSU data set existed (Nash and Edge, 1989), updated by Randel et al. (2009). Liu and Weng (2009) have produced an intermediate analysis for Channels 25 and 26 (but not channel 27), and Wang et al. (2012c) have produced a more complete analysis. Differences between the independent estimates, documented in Seidel et al. (2011) and Wang et al. (2012c) are much larger than

differences between MSU records or radiosonde records at lower levels, with substantial inter-decadal time series behaviour departures and trend differences of the order 0.5°C per decade (Wang et al., 2012c). Although all SSU data sets agree that the stratosphere is cooling, there is therefore *low confidence* in the details above the lower stratosphere.

2.4.4.2 Intercomparisons of Various Long-Term Radiosonde and MSU Products

Since AR4 there have been a large number of intercomparisons between radiosonde and MSU data sets. Interpretation is complicated, as most studies considered data set versions that have since been superseded. Several studies compared UAH and RSS products to local, regional or global raw / homogenized radiosonde data (Christy, 2010; Christy and Norris, 2006; Christy and Norris, 2009; Christy et al., 2007; Christy et al., 2011; Mears et al., Submitted; Po-Chedley and Fu, 2012; Randall and Herman, 2008). Early studies focussed upon the time of transition from NOAA-11 to NOAA-12 (early 1990s), which indicated an apparent issue in RSS. Christy et al. (2007) noted that this coincided with the Mount Pinatubo eruption and that RSS was the only product, either surface or tropospheric, that exhibited tropical warming immediately after the eruption when cooling would be expected. Using reanalyses data Bengtsson and Hodges (2011) also found evidence of a potential jump in RSS in 1993 over the tropical oceans. Mears et al. (Submitted) cautioned that an El Nino event quasi-simultaneous with Pinatubo complicates interpretation. Mears et al. (Submitted) also highlighted several other periods of disagreement between radiosonde records and MSU records. Po-Chedley and Fu (2012) highlighted an apparent artefact in UAH earlier in the record associated with NOAA-9; although their interpretation of its size and significance was disputed by Christy and Spencer (Submitted). All MSU records were most uncertain when satellite orbits are drifting rapidly (Christy and Norris, 2006; Christy and Norris, 2009) and it was cautioned that there were potential common residual biases (of varying magnitudes) in the MSU and radiosonde records (Christy and Norris, 2006; Christy and Norris, 2009; Mears et al., Submitted). Mears et al. (2011) found that trend differences between RSS and other data sets could not be explained in many cases by parametric uncertainties in RSS alone. McKitrick et al (2010) found no statistical difference between the average of all satellite and all radiosonde products.

The data clearly indicate warming of the troposphere and cooling of the stratosphere. However, the differences among the data sets, all of which are uncertain, means there can only be *low confidence* in the details of the upper air temperature trends.

2.4.4.3 Additional Evidence from Other Technologies and Approaches

Global Positioning System (GPS) radio occultation (RO) currently represents the only self-calibrated SI traceable raw satellite measurements (Anthes, 2011; Anthes et al., 2008). The fundamental observation is time delay of the occulted signal's phase traversing the atmosphere. The time delay is a function of several atmospheric physical state variables. Subsequent analysis converts the time delay to temperature and other parameters, which inevitably adds some degree of uncertainty to the temperature data, which is not the directly measured quantity. Intercomparisons of GPS-RO products show that differences are largest for derived geophysical parameters (including temperature), but are still small relative to other observing technologies (Ho et al., Submitted). Comparisons to MSU and radiosondes (Baringer et al., 2010; He et al., 2009; Kuo et al., 2005; Sun et al., 2010) Ho et al. (2009a; 2009b; 2007) and Ladstadter et al. (2011) show substantive agreement in interannual behaviour, but also some multi-year drifts that require further examination before this additional data source can usefully arbitrate between different MSU and radiosonde products trends.

Atmospheric winds are driven by thermal gradients. Radiosonde winds are far less obviously affected by time-varying biases than their temperatures (Gruber and Haimberger, 2008; Sherwood et al., 2008). Allen and Sherwood (2007) initially used radiosonde wind to infer temperatures within the Tropical West Pacific warm pool region, then extended this to a global analysis (Allen and Sherwood, 2008) yielding a distinct tropical upper tropospheric warming trend maximum within the vertical profile, but with large uncertainty. Winds can only quantify relative changes and require an initialization (location and trend at that location) (Allen and Sherwood, 2008). The large uncertainty range was predominantly driven by this initialization choice, a finding later confirmed by Christy et al. (2010), who in addition questioned the stability given the sparse geographical sampling, particularly in the tropics, and possible systematic wind speed bias sampling effects amongst other potential issues. Initializing closer to the tropics tended to reduce or remove the

appearance of a tropical upper tropospheric warming trend maximum (Allen and Sherwood, 2008; Christy et al, 2010). There is only *low confidence* in trends inferred from thermal winds given the relative immaturity of the analyses of this field and their large uncertainties.

2.4.4.4 Synthesis of Free Atmosphere Temperature Estimates

Global-mean lower tropospheric temperatures have increased since the mid 20th Century (Figure 2.24, bottom). Structural uncertainties are larger than at the surface but it can still be concluded that globally the troposphere has warmed. Uncertainty relates to the rate rather than sign of long-term changes, at least at the global mean (Table 2.8). On top of this long-term trend are super-imposed short-term variations that are highly correlated with those at the surface but of slightly greater amplitude. Global mean lower stratospheric temperatures have decreased since the mid-20th Century punctuated by short-lived warming events associated with explosive volcanic activity (Figure 2.24, top). Uncertainties are larger still than for the troposphere but these uncertainties again impact understanding of rate but not sign of long-term changes. Cooling rates are on average greater from radiosonde data sets than MSU data sets. This *very likely* relates to widely recognized cooling biases in radiosondes (Mears et al., 2006) which all data set producers explicitly caveat are *likely* to remain to some extent in their final products (Free and Seidel, 2007; Haimberger et al., 2008; Sherwood et al., 2008; Thorne et al., 2011a). Since the mid-1990s little net change has occurred in lower stratospheric temperatures.

[INSERT FIGURE 2.24 HERE]

Figure 2.24: Global average lower stratospheric (top) and lower tropospheric (bottom) temperature anomalies relative to a 1981–2010 climatology from different data sets. STAR does not produce a lower tropospheric temperature product. Note that the y-axis resolution differs between the two panels.

Table 2.8: Same as Table 2.4 but for radiosonde and MSU data set global average values over the radiosonde and satellite periods (Layers are depicted in Figure 2.23). Satellite records only start in 1979 and STAR do not produce an LT product.

Data Set	1958–2011			1979–2011		
	LT	MT	LS	LT	MT	LS
HadAT2	0.161 ± 0.040	0.095 ± 0.036	–0.341 ± 0.089	0.167 ± 0.049	0.078 ± 0.061	–0.446 ± 0.214
RAOBCORE 1.5	0.157 ± 0.032	0.110 ± 0.030	–0.187 ± 0.090	0.143 ± 0.051	0.080 ± 0.057	–0.273 ± 0.240
RICH-obs	0.159 ± 0.032	0.103 ± 0.029	–0.285 ± 0.090	0.163 ± 0.048	0.084 ± 0.055	–0.343 ± 0.246
RICH-tau	0.169 ± 0.033	0.111 ± 0.031	–0.282 ± 0.088	0.163 ± 0.049	0.084 ± 0.054	–0.355 ± 0.249
RATPAC	0.136 ± 0.029	0.078 ± 0.028	–0.338 ± 0.097	0.130 ± 0.047	0.042 ± 0.053	-0.478 ± 0.235
UAH				0.138 ± 0.048	0.049 ± 0.044	–0.384 ± 0.210
RSS				0.139 ± 0.045	0.083 ± 0.045	–0.303 ± 0.181
STAR					0.130 ± 0.048	–0.324 ± 0.187

Global-average analyses hide interesting geographical trend variability (Figure 2.25). In comparison to the surface (Figure 2.22), tropospheric layers exhibit much smoother geographic trends with warming dominating cooling north of approximately 45°S and greatest warming in high northern latitudes. The lower stratosphere cooled almost everywhere but this cooling also exhibits substantial structure. Cooling is greatest in the highest southern latitudes and smallest in high northern latitudes. There are secondary stratospheric cooling maxima in the mid-latitude regions of each hemisphere.

[INSERT FIGURE 2.25 HERE]

Figure 2.25: Trends in MSU upper air temperature over 1979 to 2011 from UAH (left hand panels) and RSS (right hand panels) and for LS (top row) and LT (bottom row). Data are temporally complete within the sampled domains for each dataset. Grid boxes where the trend is significant at the 10% level are highlighted by a +.

Available global and regional trends from radiosondes since 1958 (Figure 2.26) show agreement that the troposphere has warmed and the stratosphere cooled over this period. While there is little ambiguity in the sign of the changes, the rate and vertical structure of change are distinctly data set dependent, particularly in

the stratosphere. Differences are greatest in the tropics and SH extra-tropics where the historical radiosonde data coverage is poorest. Not shown in the figure for clarity are estimates of parametric data set uncertainties or trend-fit uncertainties – both of which are of the order at least 0.1°C per decade.

[INSERT FIGURE 2.26 HERE]

Figure 2.26: Linear temperature trend estimates for all available radiosonde data products that contain records for 1958–2010 for the globe (top) and tropics (20°N–20°S) and extra-tropics (bottom). The bottom panel trace in each case is for trends on distinct pressure levels. Note that the pressure axis is not linear. The top panel points show MSU layer equivalent measure trends. MSU layer equivalents have been processed using the method of Thorne et al. (2005). No attempts have been made to sub-sample to a common data mask.

Differences between available radiosonde data sets are greater during the satellite era than for the full radiosonde period of record in all regions and at most levels (Figure 2.27, c.f. Figure 2.26). The RAOBCORE product exhibits greater vertical trend gradients than other data sets and it has been posited that this relates to its dependency upon reanalysis fields (Christy et al., 2010; Sakamoto and Christy, 2009). MSU trend estimates in the troposphere are generally bracketed by the radiosonde range. In the stratosphere MSU deep layer estimates tend to show slightly less cooling. Over both 1958–2011 and 1979–2011 there is some evidence in the radiosonde products taken as a whole that the tropical tropospheric trends increase with height. But the magnitude and the structure is highly data set dependent.

[**INSERT FIGURE 2.27 HERE]**

Figure 2.27: As Figure 2.26 except for the satellite era 1979–2010 period and including MSU products.

2.4.5 Summary

It is *virtually certain* that global near surface temperatures have increased. Globally averaged near-surface combined land and ocean temperatures, according to several independent analyses, are consistent in exhibiting warming since 1901, much of which has occurred since 1979. Super-imposed upon the long-term changes are short-term climatic variations, so warming is not monotonic and trend estimates at decadal or shorter timescales tend to be dominated by short-term variations. Confidence in long-term temperature trends has increased with redundancy in measurement and analysis techniques and multiple published sensitivity and uncertainty studies.

It is *virtually certain* that globally averaged land surface air temperatures have risen since the late 19th Century and that this warming has been particularly marked since the 1970s. Several independently analyzed global and regional land surface temperature data products support this conclusion. There is *low confidence* in changes prior to 1880 owing to the reduced number of estimates, the greater spread among the estimates, and particularly the much reduced observational sampling. Since AR4 significant efforts have been undertaken to identify and adjust for data issues and new estimates have been produced. These innovations have strengthened confidence in the land temperature records.

Based primarily upon the substantial number of independent urban minus rural comparisons and the degree of agreement with a broad range of reanalyses products it is concluded that it is *likely* that residual biases arising from Urban Heat Islands and Land-Use Land-Cover changes account for no more than 10% of the land surface air temperature warming trend globally and 25% regionally in rapidly developing regions.

New insights regarding the likelihood of differential bias impacts between minimum and maximum temperatures in many station records have reduced confidence in reported Diurnal Temperature Range (DTR) changes at the global and regional levels to medium-to-low. To date these DTR changes almost exclusively rely upon analysing the raw, bias impacted, data.

It is *virtually certain* that global average sea surface temperatures have increased since the beginning of the 20th Century. Since AR4, major improvements in availability of metadata and data completeness have been made, and a number of new global SST records have been produced. Intercomparisons of data obtained by different measurement methods, including satellite data, have resulted in better understanding of errors and biases in the record. While these innovations have helped highlight and quantify uncertainties and alter our understanding of the character of changes since the mid 20th Century, they do not alter the conclusion that global SSTs have increased both since the 1950s and since the late 19th Century.

Based upon multiple independent analyses from weather balloons and satellites it is *virtually certain* that globally the troposphere has warmed since the mid 20th Century. However, there is only *medium to low confidence* in the rate and vertical structure. There is *medium confidence* in the rate of change and its vertical structure in the NH extra-tropics, while elsewhere *confidence is low*, particularly in the tropical upper troposphere and over the shorter period since 1979. Through construction of several additional data sets, detailed intercomparisons among data sets, and better understanding of uncertainties in pre-existing data sets, the large uncertainty has become much more apparent since AR4. Estimates of tropospheric warming rates encompass surface warming estimates.

While it is *virtually certain* that globally the stratosphere has cooled since the mid 20th Century, there is only *low confidence* in the cooling rate and vertical structure. Cooling of the lower stratosphere is consistently estimated to have levelled off in the past decade. *Confidence is low* in temperature changes in the mid- and upper stratosphere where data sets are both substantially less mature and poorly documented.

[START FAQ 2.1 HERE]

FAQ 2.1: How do We Know the World is Warming?

Evidence for a warming world comes from multiple climate indicators, from high up in the atmosphere to the depths of the oceans. They include changes in surface, atmospheric, and oceanic temperatures, glaciers, snow cover, sea ice, sea level, and atmospheric water vapour. Scientists from all over the world have independently verified this evidence many times. That the world has warmed since the nineteenth century is unequivocal.

Discussion around warming often centres on biases in temperature records from land-based weather stations. These records are very important, but they only represent one indicator of changes in the climate system. Broader evidence for a warming world comes from a wide range of physically-consistent measurements of many other, strongly interlinked, elements of the climate system (FAQ 2.1, Figure 1).

[INSERT FAQ 2.1, FIGURE 1 HERE]
FAQ 2.1, Figure 1: Repeated analyses of independently measured components of the climate system which would be expected to change in a warming world, exhibit trends consistent with warming (arrow direction denotes the sign of the change), as shown in FAQ 2.1, Figure 2.

A rise in global average surface temperatures is the best-known indicator of climate change. Although each year and even decade is not always warmer than the last, global surface temperatures have warmed substantially since 1900.

Warming land temperatures correspond closely with the observed warming trend over the oceans. Warming oceanic air temperatures, measured from aboard ships, and temperatures of the sea surface itself also coincide, as borne out by many independent analyses.

The atmosphere and ocean are both fluid bodies, so if the warming at the surface is real, it should also be seen in the lower atmosphere, and down into the upper oceans, and observations confirm that this is indeed the case. Analyses of measurements made by weather balloons and satellites consistently show warming of the troposphere, the active weather layer of the atmosphere.

More than 90 per cent of the energy absorbed by the climate system since at least the 1970s has been stored in the oceans as evidenced in global records of ocean heat content going back to the 1950s. As the oceans warm, the water itself expands. This expansion is one of the main drivers of the independently observed rise in sea levels over the past century. Melting of glaciers and ice sheets also contribute, as do changes in land storage of water.

A warmer world is also a moister one, because on average, warmer air holds more water vapour. Global analyses show that specific humidity, which measures the amount of water vapour in the atmosphere, has increased over both the land and the oceans.

The icy parts of the planet – known collectively as the cryosphere – affect, and are affected by, local changes in temperature. The amount of ice stored in glaciers globally has been declining every year for more than 20 years, and the lost mass contributes to the observed rise in sea level. Snow cover is sensitive to changes in temperature, particularly during the spring, when snow starts to melt. Spring snow cover has shrunk across the Northern Hemisphere since the 1950s. Substantial losses in Arctic sea ice have been observed since satellite records began, particularly at the time of the summer minimum extent. By contrast, comparatively little change in Antarctic sea ice has been observed.

Individually, any single analysis might be unconvincing, but analysis of these different indicators and independent data sets has led many independent research groups to *all* reach the same conclusion. From the deep oceans to the top of the troposphere, the evidence of warmer air and oceans, of melting ice and rising seas, of increasing water vapour, all points unequivocally to one thing: the world has warmed (FAQ 2.1, Figure 2).

[INSERT FAQ 2.1, FIGURE 2 HERE]

FAQ 2.1, Figure 2: Multiple redundant indicators of a changing global climate. Each line represents an independently-derived estimate of change in the climate element. All publicly-available, documented, datasets known to the authors have been used in this latest version. In each panel all datasets have been normalized to a common period of record. Further details are given in Arndt et al. (2010). A full detailing of which source datasets go into which panel is given in Appendix 2.A.

[END FAQ 2.1 HERE]

2.5 Changes in Hydrological Cycle

Changes in the hydrological cycle are less easily measured than changes in temperature, but can have large and long-lasting effects on the climate system as well as society. Changes in atmospheric water vapour affect both the hydrological cycle and the energy balance (Section 2.3), as water vapour is the source for precipitation and also the most important greenhouse gas. Long-term measurements of precipitation are available only for land areas and do not provide full global coverage. Satellite estimates of precipitation do provide near global coverage since they include both ocean and land areas, but are only available since about 1979. This section covers the main aspects of the hydrological cycle including large-scale average precipitation, stream flow and runoff, soil moisture, atmospheric water vapour, and clouds. Meteorological drought is assessed in Section 2.6. A more detailed discussion of issues with measurements of precipitation, and climate impacts of the hydrological cycle including aerosols and the energy balance and other impacts are contained in Section 3.3 of AR4 (Trenberth et al., 2007) and are not repeated here.

2.5.1 Large Scale Changes in Precipitation

2.5.1.1 Global Land and Combined Land-Ocean Areas

AR4 included analysis of both the GHCN (Vose et al., 1992) and CRU (Harris et al., 2012) precipitation data sets for the globally averaged annual precipitation over land and concluded that the overall linear trend from 1900–2005 (1901–2002 for CRU) for both data sets was increasing but not statistically significant (Table 3.4 from AR4). Other periods covered in AR4 (1951–2005 and 1979–2005) showed a mix of negative and positive trends depending on the data set. Figure 2.28 shows the century-scale variations and trends on globally and zonally averaged annual precipitation using the GHCN data set updated through 2011 (Vose et al., 1992). Also plotted are the smoothed time series from a number of other data sets including the Global Precipitation Climatology Project (GPCP) (Adler et al., 2003), CRU (Harris et al., 2012) and the Global Precipitation Climatology Centre data set (Becker et al., 2012). A new global data set for monthly total precipitation that is included is a reconstructed data set by (Smith et al., 2010). This is a statistical reconstruction using Empirical Orthogonal Functions, similar to the NOAA global temperature product (Smith et al., 2008; Vose et al., Submitted) that does provide coverage for most of the global surface area from 1900–2008. The GHCN data set shows a small statistically insignificant increase with 2010 as the wettest year on record, but the GPCC and Smith data sets show little change since 1901.

[INSERT FIGURE 2.28 HERE]

Figure 2.28: Annual precipitation anomalies averaged over land areas for four latitudinal bands and the globe from GHCN (green bars) relative to a 1981–2000 climatology. Smoothed curves (see Appendix 3.A from Trenberth et al. (2007) for GHCN and other global precipitation data sets as listed.

The latitude band plots in Figure 2.28 suggest that precipitation in the tropics has increased over the last decade reversing the drying trend that occurred from the mid-1970s to mid-1990s. The mid-latitudes of the NH show an overall increase in precipitation from 1900–2010 and the high latitudes (60°N–90°N) also show an increase, however there is much uncertainty in the results for the early 20th Century owing to a lack of spatial coverage during this period (Wan et al., 2012). In the mid-latitudes of the SH there is much decadal variability but little evidence of long-term change.

2.5.1.2 Spatial Variability of Observed Trends

Maps of observed trends of annual precipitation in AR4 for 1901–2005 were calculated using GHCN interpolated to a 5° × 5° latitude/longitude grid. Trends were calculated for each grid box and showed quite a number of statistically significant changes, particularly increases in eastern and northwestern North America, and parts of Europe and Russia, and southern South America, and Australia, and declines in the Sahel region of Africa, and a few scattered declines elsewhere. The general pattern was increases in the mid- and high-latitudes, declines in the tropical regions.

Since AR4 global satellite observations for the 1979–2008 period (Allan et al., 2010) and land-based gauge measurements for the 1950–1999 period (Zhang et al., 2007a) both indicate that precipitation has increased over wet regions of the tropics and NH mid-latitudes, and decreased over dry regions of the subtropics. Additionally, Wentz et al. (2007) found increases in satellite-derived precipitation over ocean and land areas for the period 1987–2006. These patterns of precipitation change are consistent with that expected in response to the observed increase in tropospheric specific humidity (Section 2.5.6).

Figure 2.29 shows the spatial variability of long-term trends (mm per century, 1901–2009) and more recent trends (1979–2009) over land in annual precipitation using the CRU, GHCN, and GPCC, and data sets. The trends, only over land, are computed from grid box time series using each native data set grid resolution. Increases for the 1901–2009 period are seen in the mid- and higher-latitudes of both the NH and SH, although compared to the same figures in AR4 at the grid box statistically significant trends occur in most of the same areas, and the same can be said comparing results for the three data sets. The decrease in annual precipitation in the Sahel region of Africa continues to be a significant decline. Comparing the maps in Figure 2.29, many of the areas that showed statistically significant long-term trends in AR4 show opposite trends between the 1901–2009 period and 1979–2009 period (e.g., parts of North America, Russia, Africa).

For the shorter period maps (1979–2009) many of the areas that show statistically significant trends for the longer period also show significant trends for the shorter period . The GPCC map shows the most areas with significant trends possibly owing to the much larger number of observing stations in the GPCC data set. The Sahel region for this period continues to show a shorter-term increase, although not as strong as in AR4. Other regions that show a shift in sign between the longer-term trends and shorter term include the western US, parts of southern South America, southern Africa, northeastern Africa and Spain, and Iceland.

In summary, there is uncertainty and thus *low confidence* in the observed changes in globally averaged annual precipitation, particularly in the early 20th century owing to the lack of spatial coverage in many parts of the globe. Where long-term data are available, there are statistically significant changes, with continued increases in parts of the mid- and higher latitudes and decreases in lower latitudes compared to AR4. Over the more recent period, many areas have changed their trend sign, such as the Sahel region getting wetter, but some regions such as the southwest USA, continue to get drier.

[INSERT FIGURE 2.29 HERE]

Figure 2.29: Trends in precipitation from the CRU, GHCN and GPCC data sets for 1901–2009 (left hand panels) and 1979–2009 (right hand panels). Grid boxes with statistically significant trends at the 10% level are indicated by a +.

2.5.1.3 Changes in Snowfall

AR4 discussed changes in snowfall on a region-by-region basis, but mainly focussed on North America and Eurasia. A general increase in winter precipitation in high latitudes was found, although subject to uncertainties, which remain. Statistically significant increases were found in most of Canada, parts of northern Europe and Russia. A number of areas showed a decline in the number of snowfall events, especially those where climatological averaged temperatures were close to 0°C, where warming led to earlier onset of spring. Also, an increase in lake-effect snowfall was found for areas near the North American Great Lakes. Studies since AR4 indicate that, in most regions analyzed, decreasing numbers of snowfall events are occurring where increased winter temperatures have been observed.

Since AR4, studies have confirmed that more winter-time precipitation is falling as rain rather than snow in the Western United States (Knowles et al., 2006), the Pacific Northwest and Central United States (Feng and Hu, 2007). Kunkel et al. (2009) analyzed trends in U.S. snowfall using a specially quality-controlled data set of snowfall observations over the contiguous U.S. and found that snowfall has been declining in the Western U.S., Northeastern U.S. and southern margins of the seasonal snow region, but increasing in the western Great Plains and Great Lakes regions.

Other regions that have been analyzed include Japan (Takeuchi et al., 2008), where warmer winters in the heavy snowfall areas on Honshu are associated with decreases in snowfall and precipitation in general. Shekar et al. (2010) found declines in total seasonal snowfall along with increases in maximum and minimum temperatures in the western Himalaya. Serquet et al. (2011) analyzed snowfall and rainfall days since 1961 and found the proportion of snowfall days to rainfall days in Switzerland was declining in association with increasing temperatures. Scherrer and Appenzeller (2006) found a trend in a pattern of variability of snowfall in the Swiss Alps that indicated decreasing snow at low altitudes relative to high altitudes. (van Ommen and Morgan, 2010) draw a link between increased snowfall in coastal East Antarctica and increased southwest Western Australia drought. However, Monaghan and Bromwich (2008) found an increase in snow accumulation over all Antarctica from the late 1950s to 1990, then a decline to 2004. Thus snowfall changes in Antarctica remain uncertain.

In summary, in most analysed regions, decreasing numbers of snowfall events are occurring where increased winter temperatures have been observed *(high confidence)*.

2.5.2 Streamflow and Runoff

River discharge is unique among water cycle components in that it both spatially and temporally integrates surplus waters upstream within a catchment (Shiklomanov et al., 2010), which makes it well suited for in-situ monitoring (Arndt et al., 2011). AR4 found that streamflow records for the world's major rivers show large decadal variability with small long-term change. Increased streamflow occurred in regions that had increased precipitation since about 1950. These regions included many parts of the United States and southeastern South America. However, decreased streamflow was reported over many Canadian river basins during the last 30–50 years in areas where precipitation decreased during the same period. Other changes included significant trends of more extreme flood events from 29 large river basins in one study, but others found increases, decreases, or no change in annual extreme flow from examining 195 river basins around the world. In summary, AR4 concludes that runoff and river discharge generally increased at high latitudes, with some exceptions.

It must be noted that many if not most large rivers have been impacted by human influences such as dam construction, so results must be interpreted with caution. Dai et al. (2009) assembled a data set of 925 most downstream stations on the largest rivers monitoring 80% of the global ocean draining land areas and capturing 73% of the continental runoff. Dai et al. (2009) found that only about one-third of the top 200 rivers (including the Congo, Mississippi, Yenisey, Paraná, Ganges, Columbia, Uruguay, and Niger) show statistically significant trends during 1948–2004, with the rivers having downward trends (45) outnumbering those with upward trends (19). The recent widespread drying trend and the effect of surface warming are qualitatively consistent with the observed decreases in streamflow over many low and mid-latitude river basins (Dai et al. (2009) such as the Yellow River in northern China since 1960s (Piao et al., 2010) where precipitation has decreased. However, increased streamflow during the later half of the 20th century also has been reported over many other regions with increased precipitation, such as many parts of the United States (Groisman et al., 2004), and in the Yangtze River in southern China (Piao et al., 2010).

At the higher latitudes, increasing winter base flow and mean annual stream flow resulted from possible permafrost thawing were reported in Northwest Canada (St. Jacques and Sauchyn, 2009). Rising minimum daily flows also have been detected in northern Eurasian rivers (Smith et al., 2007). For ocean basins other than the Arctic, and for the global ocean as a whole, the discharge data show small or downward trends, which are statistically significant for the Pacific (–9.4 km^3 yr^{-1}). Precipitation is a major driver for the discharge trends and large interannual-to-decadal variations. However, for the Arctic drainage areas, upward trends in streamflow are not accompanied by increasing precipitation, especially over Siberia, based on available data, although recent surface warming and associated downward trends in snow cover, soil ice content, and changes in evaporation over the northern high latitudes may have contributed to increased runoff in these regions (Adam and Lettenmaier, 2008).

Recently, Stahl et al. (2010) and Stahl and Tallaksen (2012) investigated streamflow trends based on a data set of near-natural streamflow records from more than 400 small catchments in 15 countries across Europe for 1962–2004. A regional coherent pattern of annual streamflow trends was revealed with negative trends in southern and eastern regions, and generally positive trends elsewhere. The most recent comprehensive analyses (Milliman et al., 2008; Dai et al., 2009) do not support earlier work (Labat et al., 2004) that reported an increasing trend in global river discharge associated with global warming during the 20th Century.

2.5.3 Soil Moisture

AR4 concluded that since historical records from in-situ measurements of soil moisture content are available only for limited regions in Eurasia and the U.S., and they are short in length (10–30 years) little can be said about long-term changes in direct soil moisture measurements. A rare 45-year record of soil moisture over Ukraine agricultural lands shows little change over three decades (Robock et al., 2005). Because of this, most studies have relied on simulations from land-surface models (LSMs), and owing to differences in the forcings (e.g., radiation, clouds, precipitation) estimates differ widely. Nevertheless, since AR4 these LSM soil moisture simulations, which often cover a whole continent or the global land and extend back to 1950 or 1900, have been increasingly used to document spatial and temporal variations and long-term changes in soil moisture in relation to drought (e.g., Andreadis and Lettenmaier, 2006; Sheffield and Wood, 2007; Sheffield and Wood, 2008), see Section 2.6.

2.5.4 Evapotranspiration Including Pan Evaporation

AR4 concluded that decreasing trends were found in records of pan evaporation over recent decades over the USA, India, Australia, New Zealand, China and Thailand and speculated on the causes including decreased surface solar radiation, sunshine duration, increased humidity and increased clouds. However, AR4 also reported that direct measurements of evapotranspiration over global land areas are scarce, and concluded that reanalysis evaporation fields are not reliable because they are not well constrained by precipitation and radiation. Since then gridded data sets have been developed that estimate actual evapotranspiration from either atmospheric forcing and thermal remote sensing, sometimes in combination with direct measurements (e.g., from FLUXNET, a global network of flux towers), or interpolation of FLUXNET data using regression techniques, providing an unprecedented look at global evapotranspiration (Mueller et al., 2011). The Fluxnet data-driven analysis of measured evapotranspiration and satellite observations showed increases in global evapotranspiration from 1982–1997, but the increase ceased thereafter due to decreased soil surface moisture supply (TRMM surface moisture data), particularly in semi-arid regions (Jung et al., 2010).

Since AR4, Zhang et al. (2007b) found decreasing pan evaporation at stations across the Tibetian Plateau, even with increasing air temperature. Similarly, decreases in pan evaporation were also found for northeastern India (Jhajharia et al., 2009) and the Canadian Praries (Burn and Hesch, 2007). A continuous decrease in reference and pan evaporation for the period 1960–2000 was reported by Xu et al. (2006a) for a humid region in China, consistent with reported continuous increase in aerosol levels over China (Qian et al., 2006). Roderick et al.(2007) examined the relationship between pan evaporation changes and many of the possible causes listed above using a physical model and conclude that many of the decreases (USA, China, Tibetian Plateau, Australia) cited above are related to declining wind speeds and to a lesser extent decreasing solar radiation. Fu et al. (2009a) provided a overview of pan evaporation trends and conclude the major

possible causes, changes in wind speed, humidity, and solar radiation, have been occurring, but the importance of each is regionally dependent.

The recent increase in incoming shortwave radiation in regions with decreasing aerosol concentrations (Wild et al. (2005) can explain positive evapotranspiration trends only in the humid part of Europe. In semi-arid and arid regions, trends in evapotranspiration largely follow trends in precipitation (Jung et al., 2010). Trends in surface winds (Vautard et al., 2010) and CO_2 also alter the partitioning of available energy into evapotranspiration and sensible heat. While surface wind trends may explain pan evaporation trends over Australia (Rayner, 2007; Roderick et al., 2007), their impact on actual evapotranspiration is limited due to the compensating effect of boundary-layer feedbacks (van Heerwaarden et al., 2010). In vegetated regions, where a large part of evapotranspiration comes from transpiration through plants' stomata, rising CO_2 concentrations can lead to reduced stomatal opening and evapotranspiration (Idso and Brazel, 1984; Leakey et al., 2006). Additional regional effects that impact evapotranspiration trends are lengthening of the growing season and land use change.

In summary, there is *medium confidence* that pan evaporation continues to decline in most regions studied since AR4 and is possibly related to changes in wind speed, solar radiation and humidity. On a global scale, evapotranspiration over land increased from the early 1980s up to the late 1990s (Jung et al., 2010; Wang et al., 2010; Wild et al., 2008) and Wang et al. (2010) found that global evpotransipitation increased at a rate of 0.6 W m^{-2} per decade for the period 1982–2002. After 1998, a lack of moisture availability in SH land areas, particularly decreasing soil moisture, has acted as a constraint to further increase of global evapotranspiration (Jung et al., 2010).

2.5.5 Surface Humidity

AR4 reported widespread increases in surface air moisture content, along with near-constant relative humidity over large scales though with some significant changes specific to region, time of day or season. Most of the conclusions of AR4 still stand, but since AR4 there have been advances in our knowledge and understanding of surface humidity through observations, reanalyses and model.

In good agreement with previous analyses from Dai (2006), Willett et al. (2008) show widespread increasing specific humidity across the globe from the homogenised gridded monthly mean anomaly product HadCRUH. There are some small isolated but coherent areas of drying over the more arid regions (Figure 2.30a). The globally averaged moistening trend from 1973–2003 is 0.07 g kg^{-1} per decade, with *very high confidence* and comparable with Dai (2006) 0.06 g kg^{-1} per decade for 1976–2004. Moistening is largest in the Tropics (Table 2.9) and the summer hemisphere over both land and ocean. Large uncertainty remains over the SH where data are sparse. Global specific humidity is sensitive to large scale phenomena such as ENSO (Figure 2.30b-e) and strongly correlated with land only surface temperature averages over the 23 Giorgi and Friancisco (2000) regions for the period 1973–2003 show mostly increases at or above Clausius-Clapeyron scaling (about 7% K^{-1}) with *very high confidence* (Willett et al., 2010).

[INSERT FIGURE 2.30 HERE]

Figure 2.30: a) Trends in surface specific humidity from HadCRUH over 1973–2003. Grid boxes with statistically significant trends at the 10% level are indicated by a +. b) Global anomalies in land surface specific humidity from HadCRUH, HadCRUHExt, (Dai, 2006), and ERA-interim (Simmons et al., 2010), c) As b) but for relative humidity.

Table 2.9: Large scale trends in surface humidity data sets.

Data Set, Reference, Source Data, Period of Record and Regional Delimitations	Specific Humidity (g kg^{-1} per decade)				Relative Humidity (% per decade)			
	Global	Northern Hemisphere	Tropics	Southern Hemisphere	Global	Northern Hemisphere	Tropics	Southern Hemisphere
Land								
(Dai, 2006)	---	---	---	---	0.05	0.12	---	–0.12

NCAR DS464.0 GTS weather station reports December 1975 to April 2005 Globe (60°S–75°N), N. Hem (0°N–75°N), S. Hem (60°S–0°S)								
HadCRUH, (Willett et al., 2008) NCDC ISD weather station reports January 1973 to December 2003 Globe (60°S–60°N), N. Hem (20°N–60°N), Tropics (20°S–20°N), S. Hem (60°S–20°S)	0.11	0.12	0.16	0.01	–0.03	0.07	–0.10	–0.34
Ocean								
(Dai, 2006) NCAR DS464.0 GTS marine ship reports and ICOADS data December 1975 to May 2005 (boundaries – as above)	---	---	---	---	–0.16	–0.11	---	–0.22
HadCRUH, (Willett et al., 2008) ICOADS v2.1 marine ship, buoy and platform data January 1973 to December 1997, NCEP GTS marine data January 1998 to December 2003 (boundaries - as above)	0.07	0.08	0.10	0.01	–0.10	–0.10	–0.11	–0.11
(Berry and Kent, 2009) ICOADS v2.4 marine ship data 1970 to 2006 Atlantic Trends only 40°S–70°N	0.13	---	---	---	---	---	---	---
Land and Ocean Combined								
(Dai, 2006) (as above combined) December 1975 to May 2005 (boundaries - as above)	0.06	0.08	---	0.02	–0.09	–0.02	---	–0.20
HadCRUH, (Willett et al., 2008) (as above combined) January 1973 to December 2003 (boundaries - as above)	0.07	0.08	0.10	0.02	–0.06	0.00	–0.10	–0.10

The extended series from ERA-interim in Figure 2.30 (Simmons et al., 2010) shows a flattening of the global land specific humidity series since 2000. While HadCRUH concluded negligible change in surface RH over land in 1973–2003, the more up to date 1989–2011 record from ERA-interim reveals an overall reduction in RH since 2000, compatible with the plateau in specific humidity. A 'quick-look' extension of HadCRUH to 2007 supports this (Simmons et al., 2010). This may be linked to the greater warming of the land surface relative to the ocean surface (Joshi et al., 2008).

The marine specific humidity (not shown), like that over land, shows widespread increases that correlate strongly with sea surface temperature. However, there is a marked decline in marine relative humidity around 1982. This is reported in Willett et al. (2008) where its origin is concluded to be a non-climatic data issue owing to a change in reporting practice for dewpoint temperature.

To conclude, it is *very likely* that surface humidity has increased across the globe since the 1970s. However, over recent years this has abated over land, coincident with greater warming over land relative to the oceans (Section 2.4). This has resulted in fairly widespread decreases in relative humidity over land. Whether this is part of a longer-term trend or merely a short lived feature remains to be seen.

2.5.6 Tropospheric Humidity

Tropospheric water vapour plays an important role in regulating the energy balance of the surface and top-of-atmosphere, provides a key feedback mechanism and is essential to the formation of clouds and precipitation. Observations from radiosonde and GPS measurements over land, and satellite measurements

over ocean indicate increases in tropospheric water vapour at near-global spatial scales which are consistent with the observed increase in atmospheric temperature over the last several decades.

2.5.6.1 Radiosonde

Radiosonde humidity data for the troposphere were used sparingly in AR4, noting a renewed appreciation for biases with the operational radiosonde data that had been highlighted by several major field campaigns and intercomparisons. Since AR4 there have been three distinct efforts to homogenize the tropospheric humidity records from operational radiosonde measurements (Dai et al., 2011; Durre et al., 2009; McCarthy et al., 2009) (Table 2.10). Each study takes a unique methodological approach to data selection and homogenization. Over the common period of record from 1973 onwards, the resulting estimates are in substantive agreement regarding specific humidity trends at the largest geographical scales. All remove an artificial temporal trend towards drying in the raw data and indicate a positive trend in free tropospheric specific humidity over the period of record. In each analysis, the rate of increase is concluded to be grossly consistent with the increase in equilibrium vapour pressure from the Clausius-Clapeyron relation (about 7% per degree Celsius increase in temperature). There is no evidence for a significant change in tropospheric relative humidity. McCarthy et al. (2009) show close agreement between their radiosonde product at the lowest levels and independent surface relative humidity data (Willett et al., 2008) both in low frequency and high frequency behaviour.

Table 2.10: Methodologically distinct aspects of the three approaches to homogenizing tropospheric humidity records from radiosondes.

Data Set	Region Considered	Time Resolution and Reporting Levels	Neighbours	First Guess	Automated	Variables Homogenized
(Durre et al., 2009)	NH	Monthly, mandatory and significant levels to 500 hPa	Pairwise homogenization	No	Yes	Column integrated water vapour
(McCarthy et al., 2009)	NH	Monthly, mandatory levels to 300 hPa	All neighbour average, iterative	Yes	Yes	Temperature, specific humidity, relative humidity
(Dai et al., 2011)	Globe	Observation resolution, mandatory levels to 100 hPa	None	Yes	Yes	Dew-point depression

2.5.6.2 GPS

Since the early 1990s, estimates of column integrated water vapour have been obtained from ground-based Global Position System (GPS) receivers. An international network started with about 100 stations in 1997 and has currently been expanded to over 500 (primarily land-based) stations. Several studies have compiled GPS water vapour data sets for climate studies (Jin et al., 2007); (Wang et al., 2007); (Wang and Zhang, 2008); (Wang and Zhang, 2009). Using such data, Mears et al. (2011) demonstrated general agreement of the interannual anomalies between ocean-based SSM/I and land-based GPS column integrated water vapour data. The interannual water vapour anomalies are closely tied to the atmospheric temperature changes in a manner consistent with that expected from the Clausius-Clapeyron relation. Jin et al. (2007) found an average column integrated water vapour trend of about 2 kg m^{-2} per decade during 1994–2006 for 150 (primarily land-based) stations over the globe, with positive trends at most of NH stations and negative trends in the SH. However, given the short length (about 10 years) of the GPS PW records, the estimated trends are very sensitive to the start and end years and the analyzed time period (see Box 2.2), and thus they should not be interpreted as long-term trends.

2.5.6.3 Satellite

AR4 reported positive decadal trends in lower and upper tropospheric water vapour based upon satellite observations for the period 1988–2004. Since AR4, there has been continued evidence for increases in lower tropospheric water vapour from microwave satellite measurements of column integrated water vapour (Santer et al., 2007); (Wentz et al., 2007) and globally from satellite measurements of spectrally-resolved reflected solar radiation (Mieruch et al., 2008). The interannual variability and longer-term trends in column-

integrated water vapour are closely tied to changes in SST at the global scale (Figure 2.31). Consistent with surface and radiosonde measurements, the rate of moistening at large spatial scales is close to that expected from the Clausius Clapeyron relation with invariant relative humidity. Satellite measurements also indicate that the globally-averaged upper tropospheric relative humidity has changed little over the period 1979–2010 while the troposphere has warmed, implying an increase in the mean water vapour mass in the upper troposphere (Shi and Bates, 2011).

[INSERT FIGURE 2.31 HERE]

Figure 2.31: Top**:** Global anomalies in column integrated water vapour averaged over ocean surfaces. Bottom: Trends (kg m^{-2} per decade) in column integrated water vapour from Special Sensor Microwave Imager, (Wentz et al., 2007) for the period 1988–2010. Grid boxes with statistically significant trends at the 10% level are indicated by a ♦.

Upper tropospheric relative humidity (UTH) in the tropics is strongly related to the convective activity and SST of the wet regimes(Chuang et al., 2010). Interannual variations in temperature and upper tropospheric water vapour from infrared satellite data are consistent with a constant RH behavior at large spatial scales (Gettelman and Fu, 2008); (Dessler et al., 2008); (Chung et al., 2010). On decadal time-scales, increased greenhouse gas concentrations reduce clear-sky OLR (Allan, 2009); (Chung and Soden, 2010), thereby influencing inferred relationships between moisture and temperature. Using Meteosat infrared radiances, (Brogniez et al., 2009) demonstrated that interannual variations in free tropospheric humidity over subtropical dry regions are heavily influenced by meridional mixing between the deep tropics and the extra tropics. Regionally, UTH changes in the tropics were shown to relate strongly to the movement of the ITCZ based upon microwave satellite data (Xavier et al., 2010). Shi and Bates (2011) found an increase in UTH over the equatorial tropics from 1979–2008. However there was no significant trend found on tropical-mean or global-mean averages, indicating that on these time and space scales the upper troposphere has seen little change in relative humidity over the past 30 years. While microwave satellite measurements have become increasingly relied upon for studies of UTH, the absence of a homogenized data set across multiple satellite platforms presents some difficulty in documenting coherent trends from these records (John et al., 2011).

Using NCEP reanalyses for the period 1973–2007, (Paltridge et al., 2009) found negative trends in specific humidity above 850 mb over both the tropics and southern midlatitudes, and above 600 mb in the NH midlatitudes. However, as noted in AR4, reanalysis products suffer from time dependent biases and have been shown to simulate unrealistic trends and variability over the ocean (John et al., 2009; Mears et al., 2007); (see also Box 2.3). As a result, different reanalysis products yield opposing trends in free tropospheric specific humidity (Chen et al., 2008). Furthermore, the main source of observations, radiosondes (Section 2.4.4.1) and infrared satellite measurements (Soden et al., 2005), indicate positive trends in tropospheric specific humidity. Consequently, reanalysis products are still considered to be unsuitable for the analysis of water vapour trends (Sherwood et al., 2009).

To summarize, while reanalysis products of water vapour remain unreliable for trend detection, radiosonde, GPS and satellite observations of tropospheric water vapour indicate positive trends at large spatial scales occurring at a rate that is generally consistent with the Clausius-Clapeyron relation and the observed increase in atmospheric temperature. Significant trends in tropospheric relative humidity at large spatial scales have not been observed. It is *very likely* that tropospheric specific humidity has increased since the 1970s.

2.5.7 Clouds

Clouds are important regulators of solar and terrestrial radiation and can provide potentially important feedbacks on changes in surface temperature.

2.5.7.1 Surface Observations

AR4 reported that surface-observed total cloud cover may have increased over many land areas since the middle of the 20th Century, including the USA, the former USSR, Western Europe, midlatitude Canada, and Australia. A few regions exhibited decreases, including China and central Europe. Trends were less globally consistent since the early 1970s, and regional reductions in cloud cover were reported for western Asia and Europe but increases over the USA.

Work done since AR4 has extended the preceding research, confirming many results but challenging others. In agreement with prior results, Milewska (2004) reported a significant increase in the frequency of mostly cloudy conditions at most stations in Canada from 1953 to 2002. Wibig (2008) found that total cloud cover over Poland decreased during 1971–2000 (compared to the period 1941–1970), with stratiform cloud types becoming less frequent and convective cloud types becoming more frequent. Xia (2010b) reported that total cloud cover declined over most of China since 1954 but then levelled off or slightly increased from the 1990s to 2005. Clear-sky frequency increased over China during the 1971–1996 time period (Endo and Yasunari, 2006). Duan and Wu (2006) documented a diurnal mean reduction in total cloud cover and a night time enhancement of low-level cloud cover over Tibet during 1961–2003, and they attributed part of the observed local warming to these cloud trends. (Warren et al., 2007) noted that the cloud cover decrease previously documented for China extended into neighbouring countries as well and was primarily attributable to a decrease in higher-level clouds. Jovanovic et al. (2011) found no significant changes in total cloud over Australia in a homogeneity-adjusted cloud data set since the mid 20th century.

Some new developments for surface-observed cloud cover over land since AR4 include the report of a decrease in total cloud cover of –1.8% per decade between 1971 and 1996 over South America (Warren et al., 2007). Warren et al. (2007) also found decreases in total cloud cover over Eurasia and Africa of –0.6% per decade and no trend for North America during 1971–1996. In general, low- and mid-level convective cloud types increased, stratiform cloud types decreased, and cirrus cloud cover declined over all continents (Warren et al., 2007).

Regional variability in surface-observed cloudiness over the ocean appeared more credible than zonal and global mean variations in AR4. Multidecadal changes in upper-level cloud cover and total cloud cover over particular areas of the tropical Indo-Pacific Ocean were consistent with island precipitation records and SST variability. This has been extended more recently by Deser et al. (2010b), who found that an eastward shift in tropical convection and total cloud cover from the western to central equatorial Pacific occurred over the 20th Century and attributed it to a long-term weakening of the Walker circulation. (Eastman et al., submitted) report that, after the removal of apparently spurious globally coherent variability, cloud cover decreased in all subtropical stratocumulus regions from 1954 to 2008.

2.5.7.2 Satellite Observations

Satellite cloud observations offer the advantage of much better spatial and temporal coverage compared to surface observations. However they require careful efforts to identify and correct for temporal discontinuities in the data sets associated with orbital drift, sensor degradation, and inter-satellite calibration differences.

AR4 noted that there were substantial uncertainties in decadal trends of cloud cover in all satellite data sets available at the time and concluded that there was no clear consensus regarding the decadal changes in total cloud cover. Since AR4 there has been continued effort to assess the quality of and develop improvements to multi-decadal cloud products from operational satellite platforms (Evan et al., 2007); (O'Dell et al., 2008); (Heidinger and Pavolonis, 2009) .

There are two primary satellite data sets which offer multi-decadal records of cloud cover: the International Satellite Cloud Climatology Project (ISCCP; Rossow and Schiffer (1999) and the Pathfinder Atmospheres Extended data set (PATMOS-x; Jacobowitz et al.(2003) both of which begin in the early 1980s. AR4 noted that there were discrepancies in global cloud cover trends between ISCCP and other satellite data products, notably a large downward trend of global cloudiness in ISCCP since the late 1980s, which is inconsistent with PATMOS-x and surface observations (Baringer et al., 2010). Recent work has confirmed the conclusion of AR4, that much of the downward trend is spurious and an artefact of changes in satellite viewing geometry (Evan et al., 2007).

Satellite observations of low level marine clouds suggest no long term trends in cloud liquid water path or optical properties (O'Dell et al., 2008); (Rausch et al., 2010). On regional scales, trends in cloud properties over China have been linked to changes in aerosol concentrations (Bennartz et al., 2011; Qian et al., 2009) (Norris et al., 2012).

To summarize, while there remains substantial ambiguity in surface observations of global-scale cloud variability and trends and what trends do exist are likely to be within the range of uncertainties of the surface observations. After correcting for artefacts, satellite observations of cloud cover reveal consistent patterns of change which indicate an expansion of subtropical dry zones and an increase in cloud height between the 1980s and 2000s.

2.5.8 Summary

Trends of components of the hydrological cycle are uncertain, as was also concluded in AR4. Large interannual variability, coupled with either short time series, or uneven spatial sampling, particularly early in the record (pre-1950), leads to uncertainty in trends in hydrological variables. Precipitation in the tropics appears to have increased over the last decade, reversing the drying trend that occurred from the mid-1970s to mid-1990s. Elsewhere, the mid-latitudes of the NH do show an overall increase in precipitation from 1900–2010. The high latitudes also show an increase, however there is much uncertainty in the results for the early 20th Century.

Studies using surface, homogeneity-adjusted radiosonde and satellite data indicate increases in surface and tropospheric water vapour since the 1970s at a rate consistent with that expected with the observed warming and the Clausius-Clapeyron relationship. Thus water vapour at the surface and through the troposphere has *very likely* been increasing since the 1970s. Clouds observed from the surface also continue to show increases over many land areas (e.g., North America, former USSR, parts of Europe and Australia), however other regions show declines (e.g., China and central Europe) and there does not appear to be a globally consistent trend. Satellite observations indicate changes in cloud cover which are consistent with an expansion of subtropical dry zones and an increase in cloud height between the 1980s and 2000s.

2.6 Changes in Extreme Events

AR4 highlighted the importance of understanding changes in extreme climatic events because of their disproportionate impact on society and ecosystems compared to changes in mean climate (see also WGII AR4). More recently a comprehensive assessment of observed changes in extreme events was undertaken by the IPCC Special Report on Managing the Risks of Extreme Events and Disasters to Advance Climate Change Adaptation (SREX) (Seneviratne et al., 2012b). SREX defined extreme weather and climate events as those that occur above (or below) a threshold value near the upper (or lower) ends (‘tails’) of the range of observed values of a given climate variable. Definitions of thresholds vary, but values with less than a 5% or 1% chance of occurrence during a specified reference period (generally 1961–1990) are often used. Absolute thresholds can also be used to identify extreme events, rather than relative thresholds based on the range of observed values of a variable.

Data availability, quality and consistency are of particular importance for the analysis of extreme events, since errors in long-term climate data are likely to appear ‘extreme’ and some variables are particularly sensitive to changing measurement practices over time. For example, the historical tropical cyclone records are known to be heterogeneous due to changing observing technology and reporting protocols (see Box 14.3). Additional heterogeneity is introduced when records from multiple ocean basins are combined to explore global trends, because data quality and reporting protocols vary substantially between regions (Knapp and Kruk, 2010). Similar problems have been discovered when analysing wind extremes, because of the sensitivity of measurements to changing instrumentation and observing practice (e.g., Smits et al., 2005; Wan et al., 2010).

Numerous regional studies indicate that changes observed in the frequency of extremes can be explained or inferred by shifts in the overall probability distribution of the climate variable (Ballester et al., 2010; Griffiths et al., 2005; Simolo et al., 2011). However, it should be noted that these studies refer to counts of threshold exceedance - frequency, duration - which closely follow mean changes. Departures from high percentiles/return periods (intensity, severity, magnitude) are highly sensitive to changes in the shape and scale parameters of the distribution (Clark et al., 2006; Della-Marta et al., 2007a; Della-Marta et al., 2007b; Fischer and Schar, 2010; Schar et al., 2004) and geographical location. In the following sections the conclusions from both AR4 and SREX are reviewed along with studies subsequent to those assessments.

[START BOX 2.4 HERE]

Box 2.4: Extremes Indices

As SREX highlighted, there there is no consistent definition of what constitutes a climate extreme in the scientific literature (Stephenson et al., 2008) and much of the available research is based on the use of so-called 'extreme indices' (Zhang et al., 2011). These indices can either be based on the probability of occurrence of given quantities or on absolute or percentage threshold exceedances but also include more complex definitions related to duration, intensity and persistence of extreme events. Box 2.4, Table 1 lists some of the common definitions for indices that are widely used in the scientific literature and for which near-global land-based data sets exist. Generally these data sets cover the post-1950 period but for regions such as Europe, North America, India and Australia much longer analyses are available. Note that the types of indices discussed here do not represent indices such as NINO3 representing strong positive and negative phases of the El Niño-Southern Oscillation (ENSO) (these are discussed in Section 2.7), nor do they include extremes such as 1 in 100 year events or extreme streamflow indices for which a large body of literature exists on regional scales within the hydrological community. Analyses of these rarer extremes are making their way into a growing body of literature which, for example, are investigating the use Extreme Value Theory (Coles, 2001) within the climate sciences (Brown et al., 2008; Zhang et al., 2011; Zwiers and Kharin, 1998).

Box 2.4, Table 1: Common definitions for extremes indices in the scientific literature.

Index	Definition
Cold days	The coldest daily maximum temperatures in a season/year or the percentage of days below a percentile threshold (usually 10%) or fixed threshold (dependent on region)
Warm days	The warmest daily maximum temperatures in a season/year or the percentage of days above a percentile threshold (usually 90%) or fixed threshold (dependent on region)
Cold nights (including frost)	The coldest daily minimum temperatures in a season/year or the percentage of days below a percentile threshold (usually 10%) or fixed threshold (dependent on region)
Warm nights	The warmest daily minimum temperatures in a season/year or the percentage of days above a percentile threshold (usually 90%) or fixed threshold (dependent on region)
Cold spells	Period of several consecutive low temperature days/nights using a fixed or percentile-based threshold
Warm spells	Period of several consecutive high temperature days/nights using a fixed or percentile-based threshold. Can be classified within just the summer season (heat wave) or can define any unusually warm period at any time of the year
Heavy precipitation	Measure of precipitation falling above a percentile threshold (commonly 95%) or fixed threshold (dependent on region) or can also relate to the contribution to annual total or wet-day precipitation falling from events above given threshold
Dryness	The maximum number of dry days (usually <1 mm) in a season/year; Palmer Drought Severity Index (PDSI); Standardised Precipitation Index (SPI); Standardised Precipitation Evapotranspiration Index (SPEI).

Typically extreme indices reflect more 'moderate' extremes, e.g., events occurring as often as 5% or 10% of the time. Typical indices include the number, percentage or fraction of cold/warm days/nights (days with maximum temperature (T_{max}) or minimum temperature (T_{min}) below or above the 10th percentile, or the 90th percentile, generally defined with respect to the 1961–1990 reference time period). Extreme indices are more generally defined for daily temperature and precipitation characteristics (Zhang et al., 2011) although research is developing on the analysis of sub-daily events but mostly only on regional scales (e.g., (G. et al., 2011; Jakob et al., 2011; Jones et al., 2010; Sen Roy, 2009; Shaw et al., 2011; Shiu et al., 2009). Indices rarely include other weather and climate variables, such as wind speed, humidity, or physical impacts and phenomena. Some examples are available in the literature for wind-based (Della-Marta et al., 2009) and pressure-based (Beniston, 2009) indices, for health-relevant indices combining temperature and relative humidity characteristics (e.g., Diffenbaugh et al., 2007; Fischer and Schar, 2010) and for a range of dryness indices (e.g., Palmer Drought Severity Index (PDSI) Palmer, 1965; Standardised Precipitation Index (SPI), Standardised Precipitation Evapotranspiration Index (SPEI) Vicente-Serrano et al., 2010a).

Advantages of using predefined extreme indices are that they may be easier to obtain than daily temperature and precipitation data, which are not always distributed by meteorological services. In addition they allow some comparability across observational and modelling studies and across regions and seasons and there has been much success in collaborative international efforts to monitor extremes in this way (Peterson and Manton (Donat et al., 2012a; Donat et al., 2012b; 2008; Zhang et al., 2011).

The choice of index may be influenced by the application. An absolute annual index may be most suitable for many impacts applications, whereas relative indices may be best for assessing changes in synoptic situations favourable for extreme temperatures. Hence the term 'heat wave' can mean very different things depending on the index formulation for the application for which it is required (Perkins and Alexander, 2012).

In addition to the complication of defining an index, the way in which indices are calculated (to create global averages for example) also adds an additional complication. This is due to the fact that different algorithms may be employed to create gridbox averages from station data, or that extremes indices may be calculated from gridded daily data or at station locations and then gridded. All of these factors add additional uncertainty to the calculation of an extreme. For example, the spatial patterns of trends in the hottest day of the year differ slightly between data sets although when globally averaged, trends are similar over the second half of the 20th Century (Box 2.4, Figure 1). Further discussion of the parametric and structural uncertainties in data sets is given in Box 2.1.

[**INSERT BOX 2.4, FIGURE 1 HERE**]

Box 2.4, Figure 1: Trends (°C per decade) in the warmest day of the year using different datasets for the period 1951–2010. The datasets are (a) HadEX2 (Donat et al., 2012a), (b) HadGHCND (Caesar et al., 2006) using data updated to 2010 (Donat et al., 2012b) , and (c) Globally averaged annual anomalies (thin solid lines) for each dataset with associated decadal variations (thick solid lines). Hatching on maps indicates gridboxes where trends are significant at 10% level. Annual anomalies are only calculated using gridboxes where both datasets have data and where 90% of data are available.

[END BOX 2.4 HERE]

2.6.1 Temperature Extremes

AR4 concluded that it was *very likely* that a large majority of global land areas had experienced decreases in indices of cold extremes, including frosts, and increases in indices of warm extremes, since the middle of the 20th Century, consistent with warming in global mean temperatures. In addition, globally averaged multi-day heat events had *likely* exhibited increases over a similar period. SREX updated information from AR4 and came to similar conclusions based on more recently available evidence and using the revised AR5 uncertainty guidance (Nicholls and Seneviratne, 2012). Further evidence since then indicates that the *level of confidence* that the majority of warm and cool extremes show warming remains *high*, particularly for minimum temperature extremes.

A large amount of evidence supports the conclusion that most global land areas analysed have experienced significant increases in warm nights and significant decreases in cold nights since about 1950 (Seneviratne et al., 2012b; Trenberth et al., 2007). Changes in the occurrence of cold and warm days also show warming, but generally less marked except in some regions where the El Niño-Southern Oscillation tends to dominate maximum temperature variability (e.g., Alexander et al., 2009; Kenyon and Hegerl, 2008). Different data sets using different gridding methods and/or input data indicate large coherent trends in temperature extremes globally, associated with warming (Figure 2.32). Trends over the common period when all data sets HadEX2 (Donat et al., 2012a), HadGHCND (Caesar et al., 2006) updated to 2010, and GHCNDEX (Donat et al., 2012b) have available data are shown in Table 2.11. Other data sets that have assessed these indices, but cover a shorter period, also agree very well over the period of overlapping data, e.g., HadEX (Alexander et al., 2006) and Duke (Morak et al., 2012; Morak et al., 2011).

Table 2.11: Trend estimates (days per decade) and 5 to 95% confidence intervals (Box 2.2) for global values of cold nights (TN10p), cold days (TX10p), warm nights (TN90p) and warm days (TX90p) over the period 1951–2010.

Data Set	TN10p	TX10p	TN90p	TX90p
HadEX2	–3.87 ± 0.56	–2.48 ± 0.64	4.47 ± 0.94	2.88 ± 1.22
HadGHCND	–4.52 ± 0.72	–3.26 ± 0.81	5.75 ± 1.33	4.16 ± 1.85
GHCNDEX	–3.88 ± 0.59	–2.55 ± 0.64	4.24 ± 0.94	2.94 ± 1.19

However, it is clear that some differences exist. These differences are most likely due to (i) the different input station data that are used to create each data set: HadGHCND and GHCNDEX use almost identical input data i.e., from the Global Historical Climatology Network-Daily (GHCND) data set (Durre et al., 2010; Menne et al., 2012) but different averaging methods, while HadEX2 primarily uses data from individual researchers or Meteororogical Services, and (ii) in one case the indices are calculated from a daily gridded temperature data set (HadGHCND) while in the other two cases indices are first calculated at the station level and then gridded. Comparison of these three data sets presents a measure of the structural uncertainty that exists when estimating trends in global temperature extremes (Box 2.1) while still in all cases indicating a robust warming trend over the latter part of the 20th Century.

Evidence suggests that the shift in the distribution of night-time temperatures is greater than daytime temperatures and that skewness changes are playing an important role in how extremes are affected (FAQ 2.2; Donat and Alexander, 2012). Indeed, all data sets examined (Duke, GHCNDEX, HadEX, HadEX2 and HadGHCND), indicate a faster increase in minimum temperature extremes than maximum temperature extremes. However this should not be confused with changes in diurnal temperature range (DTR) which are discussed in Section 2.4.1.3.

Regional studies covering central and eastern Europe (Bartholy and Pongracz, 2007; Kurbis et al., 2009), the Mediterranean (Efthymiadis et al., 2011), China and the Tibetan Plateau (You et al., 2010), Australia (Alexander and Arblaster, 2009), Africa and southwest Asia (Aguilar et al., 2009; Almazrouia et al.; Donat et al., 2012c; Kruger and Sekele, 2012; Rahimzadeh et al., 2009), North America (Peterson and Manton, 2008) and South America (de los Milagros Skansi et al., 2012; Marengo et al., 2010; Rusticucci, 2012), show significant increases in unusually warm nights and/or reductions in unusually cold nights. Some regions have experienced close to a doubling of the occurrence of warm and a halving of the occurrence of cold nights e.g., parts of the Asia-Pacific region (e.g., Choi et al., 2009), parts of Eurasia (e.g., Donat et al., 2012a; Donat et al., 2012b; Klein Tank et al., 2006). Changes in both local and global sea surface temperature patterns and large scale circulation patterns have been shown to be associated with regional changes in temperature extremes (Alexander et al., 2009; Barrucand et al., 2008; Li et al., 2012; Scaife et al., 2008a), particularly in regions around the Pacific Rim (Kenyon and Hegerl, 2008).

Record high temperatures now significantly outnumber record low temperatures compared to the mid-20th Century in USA (Meehl et al., 2009) and Australia (Trewin and Vermont, 2010) while in Europe warming has led to a substantial increase in record-breaking temperatures (Wergen and Krug, 2010). Statistically the number of record-breaking events increases approximately in proportion to the ratio of warming trend to short-term standard deviation (Rahmstorf and Coumou, 2011).

There are some exceptions to this large-scale warming of temperature extremes including central North America, eastern USA (e.g., Alexander et al., 2006; Kunkel et al., 2008; Peterson et al., 2008) and some parts of South America (e.g., Alexander et al., 2006; Rusticucci and Renom, 2008) which indicate changes consistent with cooling in these locations. However, these exceptions appear to be mostly associated with changes in maximum temperatures (Donat et al., 2012a).The so-called ‘warming hole’ in central North America and eastern USA, where temperatures have cooled relative to the significant warming elsewhere on the continent, has been ascribed to changes in the hydrological cycle, possibly linked to soil moisture and/or aerosol feedbacks (e.g., Pan et al., 2004; Portmann et al., 2009) or decadal variability linked with the Interdecadal Pacific Oscillation (Meehl et al., 2011).

[**INSERT FIGURE 2.32 HERE**]

Figure 2.32: Trends (days per decade) in the annual frequency of extreme temperatures, over the period 1951 to 2010, for: (a) cool nights (10th percentile), (b) cool days (10th percentile), (c) warm nights (90th percentile) and (d) warm days (90th percentile). Trends were calculated only for grid boxes that had at least 40 years of data during this period and where data ended no earlier than 2003. Hatching indicates gridboxes where trends are significant at the 10% level.

The data source for trend maps is HadEX2 (Donat et al., 2012a). Beside each map are the global annual time series of anomalies with respect to 1961 to 1990 (thin lines) along with decadal variations (thick lines) for three global datasets: HadEX2; HadGHCND (Caesar et al., 2006) and updated to 2010 and GHCNDEX (Donat et al., 2012b). Global averages are only calculated using gridboxes where all three datasets have at least 90% of data over the time period. Trends are significant at the 5% level for all the global indices shown.

AR4 found a widespread reduction in the occurrences of frosts in mid-latitude regions since the mid-20th Century. Recent work continues to provide strong evidence for widespread decreases in the number of frost days since about 1950 over those parts of the globe where frosts can be defined e.g., in Asia (Alexander et al., 2006; Donat et al., 2012a; Liu et al., 2006; Yang et al., 2011a; You et al., 2008) Europe (Alexander et al., 2006; Bartholy and Pongracz, 2007; Donat et al., 2012a; Scaife et al., 2008b); and large parts of North America (Alexander et al., 2006; Brown et al., 2010; Donat et al., 2012a). Globally, there is evidence of large-scale warming trends in the extremes of temperature, especially minimum temperature, since the beginning of the 20th Century (Donat et al., 2012a).

Since AR4 many studies have analysed local to regional changes in multi-day temperature extremes in more detail, specifically addressing different heat wave aspects such as frequency, intensity, duration and spatial extent (Box 2.4, FAQ 2.2). Several studies suggest that the increase in the temperature mean accounts for most of the changes in heat wave frequency and duration (Ballester et al., 2010; Barnett et al., 2006). However, heat wave intensity/amplitude is highly sensitive to changes in temperature variability and shape (Clark et al., 2006; Della-Marta et al., 2007a; Della-Marta et al., 2007b; Fischer and Schar, 2010; Schar et al., 2004) and heatwave definition also plays a role (Perkins and Alexander, 2012; Perkins et al., 2012).

Heat waves are often associated with quasi-stationary anticyclonic circulation anomalies that produce subsidence, light winds, clear skies, warm-air advection and prolonged hot conditions at the surface (Black and Sutton, 2007; Garcia-Herrera et al., 2010). Long-term changes in the persistence of anticyclonic summer circulation, which potentially have large effects on the duration of heat waves, are still relatively poorly understood (Section 2.7). Heat waves can also be amplified by pre-existing dry soil conditions in transitional climate zones (Ferranti and Viterbo, 2006; Fischer et al., 2007; Seneviratne et al., 2010) and the persistence of those soil-mositure anomalies (Lorenz et al., 2010). Dry soil-moisture conditions are either induced by precipitation deficits (Della-Marta et al., 2007b; Vautard et al., 2007a), or evapotranspiration excesses (Black and Sutton, 2007; Fischer et al., 2007), or a combination of both (Seneviratne et al., 2010). Higher evapotranspiration can be induced by early vegetation onset (Zaitchik et al., 2006), low cloudiness (Black and Sutton, 2007; Fischer et al., 2007), wind speed, advected air and other non-local feedbacks (Haarsma et al., 2009; Vautard et al., 2010; Vautard et al., 2007b). This amplification of soil moisture-temperature feedbacks is suggested to have partly enhanced the duration of extreme summer heat waves in southeastern Europe during the latter part of the 20th Century (Hirschi et al., 2011), with evidence emerging of a global signature in moisture-limited regions (Mueller and Seneviratne, 2012).

Regional studies have generally found statistically significant increasing trends in heat waves and decreasing trends in cold spells for example, over USA (Kunkel et al., 2008), China (Ding et al., 2010), Iran (Rahimzadeh et al., 2009), and Australia (Perkins and Alexander, 2012; Tryhorn and Risbey, 2006), primarily over the latter part of the 20th Century. However, over the USA, the decade of the 1930s has the most heat waves in the 1895 to 2005 time series and is also associated with extreme drought conditions (Kunkel et al., 2008). In Europe there is some suggestion that positive trends calculated in earlier studies may have been underestimated due to poor quality and/or consistency of data (e.g., Della-Marta et al. (2007a) over Western Europe; Kuglitsch et al. (2009; 2010) over the Mediterranean). Over Asia spatially consistent patterns of changes in warm spell duration were apparent over roughly the past five decades (Choi et al., 2009) with similar century-long trends identified in Hong Kong (Lee et al., 2011). For Africa as a whole there is insufficient evidence regarding changes in heat waves although parts of South Africa (Donat et al., 2012a; Kruger and Sekele, 2012) and North Africa (Donat et al., 2012a; Donat et al., 2012c) indicate some significant increases in heat wave duration.

In summary, analyses continue to support the AR4 and SREX conclusions that since 1950 it is *very likely* that the number of cold days and nights has decreased and the number of warm days and nights has increased overall on the global scale, i.e., for land areas with sufficient data. It is *likely* that such changes have also occurred at the continental scale in North America, Europe, and Australia. In addition, it is *likely* that the occurrence of frost days has decreased in regions where frosts can be defined. There is *medium confidence* of

a warming trend in daily temperature extremes in much of Asia, although *likely* increases in warm days and nights and decreases in cold days and nights have been observed in central Asia. There is *low* to *medium confidence* in historical trends in daily temperature extremes in Africa and South America as there is either insufficient data or trends vary across these regions. Globally, in many (but not all) regions with sufficient data, there is *medium confidence* that the length or number of warm spells, including heat waves, has increased since the middle of the 20th Century although there is *high confidence* that this is *likely* the case for large parts of Europe.

2.6.2 Hydrological Cycle

The hydrological cycle describes the continuous circulation of water between Earth's atmosphere and both surface and subsurface bodies of water. In Section 2.5 mean state changes in different aspects of the hydrological cycle are discussed. In this section we focus on the more extreme aspects of the cycle including extreme rainfall, severe local weather events like hail, flooding and droughts. Extreme events associated with tropical and extratropical storms are discussed in Sections 2.6.3 and 2.6.4 respectively.

2.6.2.1 Precipitation Extremes

AR4 concluded that it was *likely* that annual heavy precipitation events had disproportionately increased compared to mean changes between 1951 and 2003 over many mid-latitude regions, even where there had been a reduction in annual total precipitation. Rare precipitation (such as the highest annual daily precipitation total) events were likely to have increased over regions with sufficient data since the late 19th Century. SREX supported this view, as have subsequent analyses, although noting large spatial variability within and between regions (see Table 3.2 of Seneviratne et al. (2012b)).

Given the diverse climates across the globe it has been difficult to provide a universally valid definition of 'extreme precipitation'. In general, statistical tests indicate changes in precipitation extremes are consistent with a wetter climate, although with a less spatially coherent pattern of change than temperature change, in that large areas show both increasing and decreasing trends and a lower level of statistical significance than for temperature change (e.g., Alexander et al., 2006; Donat et al. 2012a; Donat et al. 2012b). Globally averaged trends in the wettest day of the year indicate more increases than would be expected by chance (Westra et al., 2012).

Figure 2.33a indicates areas of increasing and decreasing precipitation intensity in the HadEX2 dataset (Donat et al., 2012a) although with more areas showing significant increases but with little data coverage outside of the NH. Regional trends are varied but studies of North America and Central America indicate significant increases in either the frequency or intensity of heavy precipitation since about 1950 (Cavazos et al., 2008; Donat et al., 2012b; Gleason et al., 2008; Peterson et al., 2008) and over the whole of the 20th Century (Donat et al., 2012a; Pryor et al., 2009; Villarini et al., 2012). There are some exceptions e.g., no significant changes are observed in coastal zones in Mexico (Cavazos et al., 2008). In South America, there is *low confidence* of changes in heavy precipitation due to either insufficient eveidence or spatially varying trends (Dufek and Ambrizzi, 2008; Marengo et al., 2009; Marengo et al., 2010; Penalba and Robledo, 2010; Re and Barros, 2009) but the most recent integrative studies over the continent as a whole indicate heavy rain events are increasing in frequency and intensity particularly over Amazonia and South-east South America (de los Milagros Skansi et al., 2012; Donat et al., 2012a).

In Europe, over the past century increasing trends have be found in the winter extreme precipitation in many regions (Moberg et al., 2006); (Maraun et al., 2008); (Zolina et al., 2008), (Ntegeka and Willems, 2008); (Bartholy and Pongracz, 2007; Kysely, 2009) although with decreasing trends in some regions such as northern Italy (Pavan et al., 2008), Poland (Lupikasza, 2010) and some Mediterranean coastal sites (Toreti et al., 2010). The trend in summer precipitation extremes has been weak or not spatially coherent (Bartholy and Pongracz, 2007; Costa and Soares, 2009; Durao et al., 2010; Kysely, 2009; Maraun et al., 2008; Moberg et al., 2006; Pavan et al., 2008; Rodda et al., 2010; Zolina et al., 2008). Uncertainties are overall larger in southern Europe and the Mediterranean, where *confidence* in the trends *is low*.

In the Asia-Pacific region studies generally show mixed regional trends. Zhai et al. (2005) and (Wang and Zhou, 2005) found significant increases over the second half of the 20th Century in some regions but

significant decreases in other while other studies find no systematic changes over the region an a whole (Caesar et al., 2011; Choi et al., 2009). Studies have suggested significant trends in extreme precipitation at sub-regional scales during monsoon seasons over the Indian subcontinent (Krishnamurthy et al., 2009; Pattanaik and Rajeevan, 2010; Rajeevan et al., 2008; Sen Roy, 2009). In southern Australia and eastern New Zealand it is likely that there have been decreases in heavy precipitation events particularly in regions where mean precipitation has decreased (Alexander and Arblaster, 2009; Alexander et al., 2007; Gallant et al., 2007; Mullan et al., 2008). Several recent studies focused on Africa, in general, have not found significant trends in extreme precipitation (Aguilar et al., 2009; Donat et al., 2012c; Kruger, 2006; New et al., 2006; Seleshi and Camberlin, 2006) (see Chapter 14 for more on regional variations and trends).

The above studies generally use indices which reflect 'moderate' extremes e.g., events occurring as often as 5% or 10% of the time (Box 2.4). Only a few regions have sufficient data to assess trends in rarer precipitation events reliably, e.g., events occurring on average once in several decades. Using Extreme Value Theory, DeGaetano (2009) showed a 20% reduction in the return period for extreme precipitation events over large parts of the contiguous USA from 1950 to 2007. For Europe from 1951 to 2010 (Van den Besselaar et al., submitted) reported a median reduction in 5 to 20 year return periods of 18%, with a range between -4% and 59% depending on the subregion and season. This overall decrease in waiting times for rare extremes is qualitatively similar to the increase in moderate extremes for these regions reported above, and also consistent with earlier local results for the extreme tail of the distribution (Trenberth et al., 2007).

The above studies refer to daily precipitation extremes. The literature on sub-daily scales is too limited for a global assessment although we accept that analysis and framing of questions regarding sub-daily precipitation extremes is becoming more critical (Trenberth, 2011). Available regional studies have shown results that are more complex but mostly consistent with increases in sub-daily precipitation extremes linked to the 'Clausius-Clapeyron' relationship (G. et al., 2011; Haerter et al., 2010; Jones et al., 2010; Lenderink et al., 2011; Lenderink and Van Meijgaard, 2008; Utsumi et al., 2011) (see also Chapter 7).

2.6.2.2 Floods, Droughts and Severe Local Weather Events

AR4 concluded that there was not a general global trend in the incidence of floods (Kundzewicz et al., 2007) and SREX went further to suggest that there was low agreement and thus *low confidence* at the global scale regarding the magnitude or frequency of floods or even the sign of changes. AR4 reported that globally very dry areas had more than doubled in extent since 1970 but this conclusion was primarily based on the analysis of one study and one index (PDSI; Dai et al., 2004). Other analyses assessed in SREX have since come to light which highlight that observed global-scale trends in meteorological droughts still contain large uncertainties. Evidence for changes in small scale severe weather phenomena is limited.

AR5 WGII assess floods in regional detail. While the most evident flood trends appear to be in northern high latitudes, where observed warming trends have been largest, in some regions no evidence of a trend in extreme flooding has been found, e.g., over Russia based on daily river discharge (e.g., Shiklomanov et al., 2007). Other studies for Europe (Hannaford and Marsh, 2008; Petrow and Merz, 2009; Renard et al., 2008) and Asia (e.g., Delgado et al., 2010; Jiang et al., 2008) show evidence for upward, downward or no trend in the magnitude and frequency of floods, so that there is currently no clear and widespread evidence for observed changes in flooding (except for the earlier spring flow in snow-dominated regions (Seneviratne et al., 2012a)).

SREX provided a comprehensive assessment of changes in observed droughts (see Section 3.5.1 and Box 3.3 of SREX) and updated the conclusions provided by AR4. SREX considered three types of drought in their assessment: i) Meteorological drought (abnormal precipitation deficit usually relative to some 'normal' amount), ii) Agricultural drought (also soil-moisture drought – a soil moisture shortage during the growing season that affects agriculture or ecosystem functions); and iii) Hydrological drought (affecting surface (e.g., run-off) or subsurface water supply). The type of drought considered and the complexities in defining drought can substantially affect the conclusions regarding trends on a global scale (Nicholls and Seneviratne, 2012); see also Chapter 10).

AR4 concluded that droughts (as defined by PDSI, Dai et al. (2004)) had become more common, especially in the tropics and sub-tropics since about 1970. Based on evidence since AR4 (including studies by (Dai,

2011a; Dai, 2011b; Sheffield and Wood, 2008; Vicente-Serrano et al., 2010b), SREX stated that there were not enough direct observations of dryness to suggest *high confidence* in observed trends globally, although there was *medium confidence* that since the 1950s some regions of the world have experienced more intense and longer droughts. The differences between AR4 and SREX are primarily due to analyses post-AR4, differences in how both assessments considered drought and updated IPCC uncertainty guidance (Nicholls and Seneviratne, 2012).

Similarly to heatwaves (Section 2.6.1), droughts can be affected by land-atmosphere feedbacks and interactions. Because drought is a complex variable and can at best be incompletely represented by commonly used drought indices, discrepancies in the interpretation of changes can result (Seneviratne et al., 2012a). For example, Sheffield and Wood (2008) found decreasing trends in the duration, intensity and severity of drought globally by using a hydrological model forced with observations. Conversely, Dai (2011a; 2011b) found a general global increase in drought, although with substantial regional variation.

Because there are very few direct measurements of drought related variables, such as soil moisture (Robock et al., 2000), drought proxies (e.g., PDSI, SPI, SPEI) and hydrological drought proxies (e.g., Dai, 2011b; Vidal et al., 2010) are often used to assess drought conditions. Variable selection (e.g., precipitation, soil moisture, or streamflow) and time scale can strongly affect the ranking of drought events (Sheffield et al., 2009; Vidal et al., 2010). Analyses of these indirect indices come with substantial uncertainties. For example, PDSI may not be comparable across climate zones. A self-calibrating (sc-) PDSI can replace the fixed empirical constants in PDSI with values representative of the local climate (Wells et al., 2004). Using this measure van der Schrier et al. (2006) found no statistically significant soil moisture trends in Europe.

SREX indicated inconsistent trends in drought related variables across most other continents (see Table 3.2 of Seneviratne et al. (2012b)). For example, in North and Central America an overall slight decrease in dryness has been observed since 1950 (Figure 2.33b) although regional variability and the 1930s drought in the USA and Canadian Prairies dominate the signal (Aguilar et al., 2005; Alexander et al., 2006; Dai, 2011a; Dai, 2011b; Kunkel et al., 2008; Sheffield and Wood, 2008), while in Africa drought indices have generally increased (Figure 2.33b), the 1970s prolonged Sahel drought dominates the signal (Dai, 2011a; Dai, 2011b; Sheffield and Wood, 2008).

On the whole the annual maximum number of consecutive dry days appears to be declining in most regions since the 1950s (Figure 2.33b). Using a measure which combines both dry spell length and precipitation intensity Giorgi et al. (2011) indicate that 'hydroclimatic intensity' (Chapter 7) has increased over the latter part of the 20th Century in response to a warming climate. They show that positive trends are most marked in Europe, India, parts of South America and East Asia although trends appear to have decreased in Australia and northern South America (Figure 2.33c). Data availability, quality and length of record remain issues in drawing conclusions on a global scale, however.

[**INSERT FIGURE 2.33 HERE**]

Figure 2.33: (a) Trends (mm day^{-1} yr^{-1}) in daily precipitation intensity and (b) trends (days per year) in the frequency of the annual maximum number of consecutive dry days. Trends were calculated only for grid boxes that had at least 40 years of data during this period and where data ended no earlier than 2003. Hatching indicates gridboxes where trends are significant at the 10% level. The data source for trend maps is HadEX2 (Donat et al., 2012a). (c) Trends in hydroclimatic intensity (HY-INT: a multiplicative measure of length of dry spell and precipitation intensity) over the period 1976 to 2000 (from Giorgi et al. (2011)). An increase (decrease) in HY-INT reflects an increase (decrease) in the length of drought and /or extreme precipitation events.

Another extreme aspect of the hydrological cycle is severe local weather phenomena such as hail or thunder storms. These are not well observed in many parts of the world, since the density of surface meteorological observing stations required for detection is too coarse to measure all such events. Moreover, homogeneity of existing station series is questionable (Doswell et al., 2009; Verbout et al., 2006). Alternatively, measures of severe thunderstorms or hailstorms can be derived by assessing the environmental conditions that are favourable for their formation but this method is associated with high uncertainty (Seneviratne et al., 2012a). SREX highlighted studies such as Brooks and Dotzek (2008) who found significant variability but no clear trend in the past 50 years in severe thunderstorms in a region east of the Rocky Mountains in the United States, Cao (2008) who found an increasing frequency of severe hail events in Ontario, Canada during the period 1979–2002 and Kunz et al. (2009) who found that hail days significantly increased during the period

1974–2003 in southwest Germany. Hailpad studies from Italy (Eccel et al., 2012) and France (Berthet et al., 2011) suggest slight increases in larger hail sizes and a correlation between the fraction of precipitation falling as hail with average summer temperature. In China between 1961 and 2005, the number of hail days has been found to generally decrease, with the highest occurrence between 1960 and 1980 but with a sharp drop since the mid-1980s (CMA, 2007; Xie et al., 2008). However there is little consistency in hail size changes in different regions of China since 1980 (Xie et al., 2010).

In summary, analyses continue to support the AR4 and SREX conclusions that it is *likely* that there have been statistically significant increases in the number of heavy precipitation events (e.g., 95th percentile) in more regions than there has been statistically significant decreases, but there are strong regional and subregional variations in the trends. In particular, many regions present statistically non-significant or negative trends, and, where seasonal changes have been assessed, there are also variations between seasons (e.g., more consistent trends in winter than in summer in Europe). The overall most consistent trends towards heavier precipitation events are found in North America (*likely* increase over the continent). There continues to be a lack of evidence and thus *low confidence* regarding the sign of trend in the magnitude and/or frequency of floods on a global scale. The current assessment does not support the AR4 conclusions regarding global increasing trends in droughts but rather concludes that there is not enough evidence at present to suggest *high confidence* in observed trends in dryness due to lack of direct observations, some geographical inconsistencies in the trends, and some dependencies of inferred trends on the index choice. There is *low confidence* in observed trends in small-scale severe weather phenomena such as hail because of historical data inhomogeneities and inadequacies in monitoring systems.

2.6.3 Tropical Storms

AR4 concluded that it was *likely* that a trend had occurred in intense tropical cyclone activity since 1970 in some regions (IPCC, 2007b). In more detail it was stated that "there is observational evidence for an increase in intense tropical cyclone activity in the North Atlantic since about 1970, correlated with increases of tropical SSTs. There are also suggestions of increased intense tropical cyclone activity in some other regions where concerns over data quality are greater. Multi-decadal variability and the quality of the tropical cyclone records prior to routine satellite observations in about 1970 complicate the assessment of long-term trends in tropical cyclone activity. There is no clear trend in the annual numbers of tropical cyclones". Subsequent assessments, including SREX and more recent literature indicate that the AR4 assessment needs to be somewhat revised with respect to the confidence levels associated with observed trends.

Box 14.3 discusses changes in detail. In summary, current datasets indicate no significant observed trends in global tropical cyclone frequency and it remains uncertain whether any reported long-term increases in tropical cyclone frequency are robust, after accounting for past changes in observing capabilities (Knutson et al., 2010). Regional trends in tropical cyclone frequency have been identified in the North Atlantic, but on long time scales the fidelity of these trends is debated (Holland and Webster, 2007; Landsea, 2007; Landsea et al., 2006; Mann et al., 2007a) with different methods for estimating undercounts in the earlier part of the record providing mixed conclusions (Chang and Guo, 2007; Kunkel et al., 2008; Mann et al., 2007b; Vecchi and Knutson, 2008; Vecchi and Knutson, 2011b). Measures of land-falling tropical cyclone frequency are generally considered to be more reliable than counts of all storms which tend to be strongly influenced by those that are weak and/or short-lived. Callaghan and Power (2011) find a statistically significant decrease in Eastern Australia land-falling tropical cyclones since the late 19th century but evidence is limited on trends in other oceans on shorter timescales (Chan and Xu, 2009; Kubota and Chan, 2009; Lee and McPhaden, 2010; Mohapatra and Adhikary, 2011; Weinkle et al., 2012). Figure 2.34 summarises trends in the frequency of land-falling tropical cyclones in different ocean basins.

[**INSERT FIGURE 2.34 HERE**]

Figure 2.34: Normalized 5-year running means of the number of (a) adjusted land falling eastern Australian tropical cyclones (adapted from (Callaghan and Power, 2011) and updated to include 2010/2011 season) and (b) unadjusted land falling U.S. hurricanes (adapted from (Vecchi and Knutson, 2011a) and (c) land-falling typhoons in China. Vertical axis ticks represent one standard deviation, with all series normalized to unit standard deviation after a 5-year running mean was applied. The dashed lines are trends calculated using ordinary least squares regression.

Arguably, storm frequency is of limited usefulness if not considered in tandem with intensity and duration measures. Intensity measures in historical records are especially sensitive to changing technology and

improving methodology. However over the satellite era, increases in the intensity of the strongest storms in the Atlantic appear robust (Elsner et al., 2008; Kossin et al., 2007) but there is limited evidence for other regions and the globe. Time series of power dissipation, an aggregate compound of tropical cyclone frequency, duration, and intensity that measures total energy consumption by tropical cyclones, show upward trends in the North Atlantic and weaker upward trends in the western North Pacific over the past 25 years (Emanuel, 2007), but interpretation of longer-term trends is again constrained by data quality concerns.

Based on research subsequent to AR4, which further elucidated the scope of uncertainties in historical tropical cyclone data, more recent assessments (Knutson et al., 2010) do not conclude that it is *likely* that annual numbers of tropical storms, hurricanes and major hurricanes counts have increased over the past 100 years in the North Atlantic basin. Evidence however is robust for an increase in the most intense tropical cyclones since the 1970s in that region. This assessment does not revise the SREX conclusion of *low confidence* that any reported long-term increases in tropical cyclone activity are robust, after accounting for past changes in observing capabilities.

2.6.4 Extratropical Storms

AR4 noted a *likely* net increase in frequency/intensity of NH extreme extratropical cyclones and a poleward shift in storm tracks since the 1950s (Trenberth et al., 2007, Table 3.8). SREX further consolidated the AR4 assessment of poleward shifting storm tracks, but revised the assessment of the confidence levels associated with regional trends in the intensity of extreme extratropical cyclones.

There are inconsistencies among studies of extreme cyclones and work is required to consolidate findings for future assessments. Studies using reanalyses continue to support a northward and eastward shift in the Atlantic cyclone activity during the last 60 years with both more frequent and more intense wintertime cyclones in the high-latitude Atlantic (Raible et al., 2008; Schneidereit et al., 2007; Vilibic and Sepic, 2010) and fewer in the mid-latitude Atlantic (Raible et al., 2008; Wang et al., 2006b). Some studies show an increase in intensity and number of extreme Atlantic cyclones (Geng and Sugi, 2001; Lehmann et al., 2011; Paciorek et al., 2002) while others show opposite trends in eastern Pacific and North America (Gulev et al., 2001). Differences can be partly explained by sensitivities in identification schemes and/or different definitions for extreme cyclones (Leckebusch et al., 2006; Pinto et al., 2006).

In the North Pacific studies using reanalyses and in situ data for the last 50 years have noted an increase in the number and intensity of wintertime intense extratropical cyclone systems since the 1950s (Graham and Diaz, 2001; Raible et al., 2008; Simmonds and Keay, 2002) and cyclone activity (Zhang et al., 2004), but also in this region signs of some of the trends disagreed when different tracking algorithms or reanalysis products are used (Raible et al., 2008). A slight positive trend has been found in north Pacific extreme cyclones while others show opposite trends in the eastern Pacific and North America (Geng and Sugi, 2001; Gulev et al., 2001; Paciorek et al., 2002).

Over continental land areas most studies of severe storms or storminess have been performed for Europe where long running in situ pressure and wind observations exist. There are no clear trends over the past century or longer (Allan et al., 2009; Barring and Fortuniak, 2009; Hanna et al., 2008; Matulla et al., 2008) with substantial decadal and longer fluctuations but with some regional and seasonal trends (Wang et al. (2009c); Wang et al. (2011). Figure 2.35 shows some of these changes for boreal winter using geostrophic wind speeds indicating that decreasing trends outnumber increasing trends (Wang et al., 2011). Using the 20th Century Reanalysis (Compo et al., 2011), (Donat et al., 2011) however find significant increases in both the strength and frequency of wintertime storms for large parts of Europe but this is potentially an artefact of the reduction in data included in the reanalyses the further back in time it goes (Cornes and Jones, 2011a).

[**INSERT FIGURE 2.35 HERE**]

Figure 2.35: 99th percentiles of geostrophic wind speeds for winter. Triangles show regions where geostrophic wind speeds have been calculated from in situ surface pressure observations. Within each pressure triangle, Gaussian low-pass filtered curves and estimated linear trends of the 99th percentile of these geostrophic wind speeds for winter are shown. The ticks of the time (horizontal) axis range from 1875 to 2005, with an interval of 10 years. Disconnections in lines show periods of missing data. Red (blue) trend lines indicate upward (downward) trends of at least 5% significance. From Wang et al. (2011).

Robust conclusions about changes in extratropical cyclone activity in Asia will require further studies. SREX noted however that available studies using reanalyses indicate a decrease in extratropical cyclone activity (Zhang et al., 2004) and intensity (Wang et al., 2009d; Zhang et al., 2004) over the last 50 years has been reported for northern Eurasia (60°N–40°N) with a possible northward shift with increased cyclone frequency in the higher latitudes (50°N–45°N) and decrease in the lower latitudes (south of 45°N). The decrease at lower latitudes is also supported by a study of severe storms by Zou et al. (2006b) who used sub-daily in situ pressure data from a number of stations across China.

SREX also notes that, based on reanalyses, North American cyclone numbers have increased over the last 50 years, with no statistically significant change in cyclone intensity (Zhang et al., 2004). Hourly MSLP data from Canadian stations showed that winter cyclones have become significantly more frequent, longer lasting, and stronger in the lower Canadian Arctic over the last 50 years (1953–2002), but less frequent and weaker in the south, especially along the southeast and southwest Canadian coasts (Wang et al., 2006a). Further south, a tendency toward weaker low-pressure systems over the past few decades was found for U.S. east coast winter cyclones using reanalyses, but no statistically significant trends in the frequency of occurrence of systems (Hirsch et al., 2001).

In the SH, studies using in situ pressure observations indicate a significant decline in storminess since the mid-19th Century (Alexander and Power, 2009; Alexander et al., 2011), strengthening the evidence of a southward shift in storm tracks previously noted using reanalyses (Fyfe, 2003; Hope et al., 2006). Frederiksen and Frederiksen (2007) linked the reduction in cyclogenesis at 30°S and southward shift to a decrease in the vertical mean meridional temperature gradient. SREX notes some inconsistency among reanalysis products for the SH regarding trends in the frequency of intense extratropical cyclones (Pezza et al. (2007),(Lim and Simmonds, 2009) although studies tend to agree on a trend towards more intense systems. Links between extratropical cyclone activity and large scale variability are discussed in Section 2.7 and Chapter 14.

Recent studies that have examined trends in wind extremes from observations tend to point to declining trends in extremes in mid-latitudes (Pirazzoli and Tomasin, 2003; Pryor et al., 2007; Smits et al., 2005; Zhang et al., 2007b) and increasing trends in high latitudes (Hundecha et al., 2008; Lynch et al., 2004; Turner et al., 2005). Other recent studies have compared the trends from observations with reanalysis data and reported differing or even opposite trends in the reanalysis products (e.g., McVicar et al., 2008; Smits et al., 2005). On the other hand, declining trends reported by Xu et al. (2006b) over China were generally consistent with trends in NCEP reanalysis. The accuracy of trends extracted from reanalysis products (Box 2.3) however remains a source of debate since data assimilation methods can induce artificial trends (e.g., Bengtsson et al., 2004).

In summary, unlike in AR4, it is assessed here that there is *low confidence* of regional changes in the intensity of extreme extratropical cyclones. There is *low confidence* of a clear trend in storminess proxies over the last century due to inconsistencies between studies or lack of long-term data in some parts of the world (particularly in the SH). There is *low confidence* in trends in extreme winds due to quality and consistency issues with analysed data.

[START FAQ 2.2 HERE]

FAQ 2.2: Have there been any Changes in Climate Extremes?

There is strong evidence that statistically significant changes have occurred in temperature extremes—particularly those related to minimum temperature—associated with warming since the mid-20th Century. Heavy precipitation events show likely, but regionally dependent, increases. However, for other extremes, such as tropical cyclone frequency, we have generally low confidence that there have been discernable changes over the observed record.

From heat waves to cold snaps, droughts to flooding rains, recording and analysing climate extremes poses unique challenges, not just because of the intrinsically rare nature of these events, but because, they invariably happen in conjunction with disruptive conditions. Furthermore, there is no consistent definition in scientific literature of what constitutes an extreme climatic event, and this complicates global assessment.

While, in an absolute sense, an extreme climate event will vary from place to place—a hot day in the tropics, for instance, will be a different temperature to a hot day in the mid-latitudes—collaborative international efforts to monitor extremes have highlighted some significant global changes.

For example, studies using consistent definitions for cold (<10th percentile) and warm (>90th percentile) days and nights indicate changes associated with warming for most regions of the globe; a few exceptions being central and eastern North America, and southern South America but mostly only related to daytime temperatures. Those changes are generally most apparent in minimum temperature extremes. Limited data make it difficult to link these changes to increases in average temperatures, but FAQ 2.2, Figure 1 indicates that daily global temperature extremes have indeed changed: not only because average temperature has increased, but also because the 'shape' and 'spread' of both daytime and night-time temperature distributions has changed.

Warm spells or heat waves containing consecutive extremely hot days or nights have also been assessed, but there are fewer studies of heat wave characteristics than those that compare changes in merely warm days or nights. Most global land areas with available data have experienced more heat waves since the middle of the 20th century. One exception is the south-eastern United States, where heat wave frequency and duration measures generally show cooling. This has been associated with a so-called 'warming hole' in this region and is also linked with increases in extreme precipitation.

For regions such as Europe, where historical temperature reconstructions exist going back several hundreds of years, indications are that some have experienced a disproportionate number of extreme heat waves in recent decades. The historical evolution of the hottest summers in Europe suggests that the period between 2001 and 2010 stands substantially above any other decade since 1500.

[INSERT FAQ 2.2, FIGURE 1 HERE]

FAQ 2.2, Figure 1: Distribution of (a) daily minimum and (b) daily maximum temperature anomalies relative to a 1961–1990 climatology for two periods: 1951–1980 (blue) and 1981–2010 (red) using the HadGHCND data set. The vertical blue and red lines indicate the 10th (left-hand side) and 90th (right-hand side) percentiles for both periods.

Changes in extremes for other climate variables are generally less coherent than those observed for temperature, due to data limitations and inconsistencies between studies, regions and/or seasons. However, changes in precipitation extremes, for example, are consistent with a warmer climate. Analyses of land areas with sufficient data indicate increases in more extreme precipitation events in recent decades, but results are very regionally and seasonally dependent. For instance, increases in heavy precipitation are likely to have occurred in North America, Central America and Europe, but in other regions—such as southern Australia and western Asia—there is evidence of decreases. Likewise, drought studies do not agree on the sign of the global trend, with regional inconsistencies in trends also dependent on how droughts are defined.

Considering other extremes, such as tropical cyclones, the latest assessments show *low confidence* that any reported long-term increases in tropical cyclone activity are robust, after accounting for past changes in observing capabilities. There is some evidence, however, of an intensification of the most extreme storms, but records are currently very short.

Over periods of a century or more, evidence suggests slight decreases in the frequency of tropical cyclones making landfall in the North Atlantic and the South Pacific, once uncertainties in observing methods have been considered. Little evidence exists of any longer-term trend in other ocean basins. For extratropical cyclones, a likely poleward shift is evident in both hemispheres over the past 50 years, with further but *low confidence* evidence of a decrease in wind storm frequency at mid-latitudes. Several studies suggest an increase in intensity, but *confidence is low* due to data sampling issues.

FAQ 2.2, Figure 2 summarizes some of the observed changes in climate extremes, and associated levels of confidence regarding the sign of trends.

[INSERT FAQ 2.2, FIGURE 2 HERE]

FAQ 2.2, Figure 2: The likelihood and direction of trend in the frequency (or intensity) of various climate extremes since the middle of the 20th century. Where the trend goes both up and down, this implies that there is regional

variation in the sign of the trend, or that studies using different measures of dryness do not agree. Large regions that differ from the 'global' conclusion—either with respect to sign of, or confidence in, the trend—are also highlighted.

Overall, the most robust global changes in climate extremes are seen in measures of temperature, and to some extent, heat waves. Precipitation extremes also appear to be increasing, but there is large spatial inconsistency, and observed trends in droughts are still uncertain. There is limited evidence of changes in extremes associated with other climate variables.

[END FAQ 2.2 HERE]

2.7 Changes in Atmospheric Circulation and Patterns of Variability

Changes in atmospheric circulation and indices of climate variability, as expressed in Sea-Level Pressure (SLP), wind, Geopotential Height (GPH), and other variables such as cloud cover were assessed in AR4. Substantial multi-decadal variability was found in the large-scale atmospheric circulation over the Atlantic and the Pacific. A decrease was found in tropospheric GPH over high latitudes of both hemispheres and an increase over the mid-latitudes in boreal winter for the period 1979–2001. These changes were found to be associated with an intensification and poleward displacement of Atlantic and southern midlatitude jet streams and enhanced storm track activity in the NH from the 1960s to at least the 1990s. Changes in the North Atlantic Oscillation (NAO) and the Southern Annular Mode (SAM) towards their positive phases were observed, but it was noted that the NAO returned to its long-term mean state from the mid 1990s to the early 2000s.

The observational basis has changed since AR4. More and improved observational data sets (encompassing ground based, radiosonde, and satellite data) and reanalysis data sets (see Box 2.3) have been published. Uncertainties and inaccuracies in all data sets are better understood. Finally, the time elapsed since AR4 extends the period for trend calculation, in particular since several data sets start are considered most reliable after 1979, when satellite information became more widely available.

The studies since AR4 as assessed in this Section support the poleward movement of circulation features since the 1970s and the change in the SAM. At the same time, large decadal-to-multidecadal variability in atmospheric circulation is found that partially offsets previous trends in other circulation features such as the NAO or the Pacific Walker circulation.

This section assesses observational evidence for changes in atmospheric circulation in fields of SLP, GPH, and wind, in circulation features (such as the Hadley and Walker circulation, monsoons, or jet streams), as well as in circulation variability modes. Regional climate effects of the circulation changes are discussed in Chapter 14.

2.7.1 Sea Level Pressure

The spatial distribution of SLP represents the distribution of atmospheric mass, which is the surface imprint of the atmospheric circulation. Barometric measurements are made in weather stations or onboard ships. Fields are produced from the observations by interpolation or using data assimilation. One of the most widely used observational data sets is HadSLP2 (Allan and Ansell, 2006), which integrates 2228 historical global terrestrial stations with marine observations from the International Comprehensive Ocean-Atmosphere Data Set (ICOADS) on a 5° × 5°grid. Although the quality of SLP data is considered good, there are discrepancies between gridded SLP data sets in regions with sparse observations, e.g., over Antarctica (Jones and Lister, 2007).

AR4 concluded that SLP in December to February decreased between 1948 and 2005 in the Arctic, Antarctic and North Pacific. More recent studies using updated data for the period 1949–2009 (Gillett and Stott, 2009) also find decreases in SLP in the high latitudes of both hemispheres in all seasons and increasing SLP in the tropics and subtropics most of the year. However, due to decadal variability SLP trends are sensitive to the choice of the time period (see also Box 2.2). Seasonal trends in gridded SLP from 1979 to 2012 show decreasing trends in the tropical and subtropical Atlantic, Indian Ocean, and adjacent land regions as well as in boreal summer in northern Siberia and increasing trends over the Pacific and the Southern Ocean (see

Appendix 2.A). Trends in the equatorial Pacific zonal SLP gradient during the 20th Century (e.g., Power and Kociuba, 2011a; Power and Kociuba, 2011b; Vecchi et al., 2006) are discussed in Sect. 2.7.4.

The position and strength of semi-permanent pressure centres show no clear evidence for trends since 1951. However, prominent variability is found on decadal time scales (Figure 2.36). The Azores high and the Icelandic low in boreal winter, as captured by the high and low SLP contours, were both small in the 1960s and 1970s, large in the 1980s and 1990s, and again smaller in the 2000s. Favre and Gershunov (2006) find an eastward shift of the Aleutian low from the mid-1970s to 2001, which persisted during the 2000s (Figure 2.36). The Siberian High exhibits pronounced decadal-to-multidecadal variability (Huang et al., 2010; Panagiotopoulos et al., 2005). In boreal summer, the Atlantic and Pacific high-pressure systems extended more westward in the 1960s and 1970s than later. On interannual time scales, variations in pressure centres are related to modes of climate variability. Trends in the indices that capture the strength of these modes are reported in Section 2.7.9, their characteristics and impacts are discussed in Chapter 14.

[INSERT FIGURE 2.36 HERE]

Figure 2.36: Decadal averages of SLP from the 20th Century Reanalysis (20CR) for (left) November of previous year to April and (right) May to October shown by two selected contours. Topography above 2 km above sea level in 20CR is shaded in dark grey.

2.7.2 Surface Winds

Surface wind measurements over land and ocean are based on largely separate observing systems. Early marine observations were visual estimates made using the Beaufort scale. Anemometer measurements were introduced starting in the 1950s. All in situ observations are collected in ICOADS (currently version 2.5; Woodruff et al., 2011). Growth in ship size was responsible for an upward trend in the anemometer heights; uncorrected, it was causing a spurious increasing trend in wind speed estimates based on ICOADS data (Cardone et al., 1990; Gulev et al., 2007; Tokinaga and Xie, 2011a). In recent years, records of anemometer heights on many ships became available and were incorporated into ICOADS, v.2.5 (Kent et al., 2007), making corrections possible (Thomas et al., 2008) (Thomas et al., 2008). The interpolated, ICOADS-based data sets NOCS v.2.0 (1973-present) (Berry and Kent, 2011), and WASWind (1950-2010, Tokinaga and Xie (2011a) include such corrections, among other improvements.

Marine surface winds are also measured from space using various microwave range instruments: scatterometers and synthetic aperture radars measure wind vectors, while altimeters and passive radiometers measure wind speed only (Bourassa et al., 2010). The latter type provides the longest continuous record, starting in July 1987. Satellite-based interpolated marine surface wind data sets use objective anlysis methods to blend together data from different satellites and atmospheric reanalyses used either for wind directions as in Blended Sea Winds (BSW, Zhang et al., 2006), or as a background field as in Cross-Calibrated Multi-Platform winds (CCMP, Atlas et al., 2011) or OAFlux (Yu and Weller, 2007). CCMP uses additional dynamical constraints, *in situ* data and recently homogenized data set of SSM/I observations (Wentz et al., 2007), among other satellite sources.

Figure 2.37 compares 1988-2010 linear trends in surface wind speeds from interpolated data sets based on the satellite data, from interpolated and non-interpolated data sets based on the in situ data, and from atmospheric reanalyses. Kent et al. (2012) recently intercompared several of these data sets and found large differences. The differences in trend patterns in Figure 2.37 are large as well. Nevertheless, some statistically significant features are present in most data sets, including a pattern of positive and negative trend bands across the North Atlantic Ocean (see Section 2.7.6.2.) and positive trends along the west coast of North America.

Surface winds over land have been measured with anemometers on a global scale for decades, but until recently the data have been rarely used for trend analysis due to suspect quality. Century-long, homogenized instrumental records are rare (e.g., Usbeck et al., 2010). Winds near the surface can be derived from reanalysis products (see Box 2.3), but discrepancies are found when comparing trends therein with trends for land stations (McVicar et al., 2008; Smits et al., 2005). Because of shortcomings in the observations, SREX stated that *confidence* in wind trends *is low*. Further studies assessed here confirm this assessment.

Over land, a weakening of seasonal and annual as well as maximum winds is reported for many regions, including China (Guo et al., 2010; Xu et al., 2006b) and the Tibetan region (Zhang et al., 2007b) from the 1960s to the early 2000s, the Netherlands from 1962 to 2002 (Smits et al., 2005), much of the USA from 1973 to 2005 (Pryor et al., 2007), Australia from 1975 to 2006 (McVicar et al., 2008), and southern and western Canada from 1953 to 2006 (Wan et al., 2010). Increasing wind speeds were found at high latitudes in both hemispheres, namely in Alaska from 1921 to 2001 (Lynch et al., 2004), in parts of the Canadian Arctic from 1953 to 2006, and in coastal Antarctica over the second half of the 20th Century (Turner et al., 2005).

Vautard et al. (2010) analysed a global land surface wind data sets from 1979 to 2008 after quality screening. They found decreasing trends on the order of –0.1 m s^{-1} per decade over large portions of Northern Hemispheric land areas. They could only partly attribute the trends to changes in atmospheric circulation and suggested that increased surface roughness is mainly responsible. Wind speed trend pattern on the land inferred from their data (1988-2010, Figure 2.37) has many points with magnitudes much larger than those in the reanalysis products, which appear to systematically underestimate the variability of wind speed over land, as well as in coastal regions (Kent et al. 2012). Troccoli et al. (2012) found decreasing wind speeds over Australia, 1989-2006, at 2 m above ground but increasing wind speeds at 10 m, highlighting the sensitivity of trends in wind speed to changes in surface conditions.

[INSERT FIGURE 2.37 HERE]

Figure 2.37: Surface wind speed trends for 1988–2010. Shown in the top row are data sets based on the satellite wind observations: (a) Cross-Calibrated Multi-Platform wind product (CCMP, Atlas et al., 2011); (b) wind speed from the Objectively Analyzed Air-Sea Heat Fluxes data set, release 3 (OAFlux); (c) Blended Sea Winds (BSW, Zhang et al., 2006); in the middle row are data sets based on surface observations: (d) wind speed from the Surface Flux Data Set, v.2, from NOC, Southampton, U.K. (Berry and Kent, 2009); (e) Wave- and Anemometer-based Sea Surface Wind (WASWind, (Tokinaga and Xie, 2011a)); (f) Surface Winds on the Land (Vautard et al., 2010); and in the bottom row are surface wind speeds from atmospheric reanalyses: (g) ERA-Interim; (h) NCEP-NCAR, v.1 (NNR1); and (i) 20th Century Reanalysis (20CR, Compo et al., 2011). Wind speeds correspond to 10 m heights in all products. Land station winds (panel f) are also for 10 m (but ananometer height is not always reported) except for the Australian data where they correspond to 2 m height. To improve readability of plots, all data sets (including land station data) were averaged to the 4° × 4° uniform longitude-latitude grid. Linear trend slopes and their uncertainties were computed for the annually averaged timeseries of 4^{o}x4^{o} cells by the method described in Appendix 2.A For all data sets except land station data, an annual mean was considered available only if monthly means for no less than eight months were available in that calendar year. Trend values were computed only if no less that 70% of all years (17) had a values and no less than 20% of first and last 10% of the annual record were available as well (i.e., at least one year available out of the first three and the last three years each). Black plus signs (+) indicate areas where linear trends slopes are different from zero at 10% significance level.

2.7.3 Upper-Air Winds

In contrast to surface winds, which were discussed in previous assessment reports, upper air winds have received little attention. Radiosondes and pilot balloon observations are available from around the 1930s (Stickler et al., 2010). Temporal inhomogeneities in radiosonde wind records are less common, but also less studied, than those in radiosonde temperature records (Gruber and Haimberger, 2008). Upper air winds can also be derived from tracking clouds or water vapour in satellite imagery (Atmospheric Motion Vectors, Menzel, 2001), which serve as an input to reanalyses (Box 2.3).

In the past few years, interest in an accurate depiction of upper air winds has grown, since they are essential for estimating the state and changes of the general atmospheric circulation and for explaining changes in the surface winds (Vautard et al., 2010). In contrast to the wind slowing at the surface, no or much weaker trends were found for lower tropospheric winds from balloon data or reanalyses. Allen and Sherwood (2008) diagnosed significant positive zonal mean westerly wind trends in the northern extratropics in the upper troposphere and stratosphere and negative trends in the tropical upper troposphere for the period 1979–2005. The associated trend in wind shear has implications for upper tropical tropospheric temperature trends (see Section 2.4). Vautard et al. (2010) find increasing wind speed in rawinsonde observations in the lower and middle troposphere from 1979-2008 over Europe and North America and decreasing trends over Central and Eastern Asia. Systematic global trend analyses of radiosonde winds are lacking and the available regional studies do not allow conclusions on large-scale trends (specific features such as jet streams and storms are discussed in Sections 2.7.6 and 2.6, respectively).

2.7.4 Tropospheric Geopotential Height and Tropopause

Changes in GPH, which can be addressed using radiosonde data or reanalysis data (see Box 2.3), reflect SLP and temperature changes in the atmospheric levels below. The spatial gradients of the trend indicate changes in the upper-level circulation. AR4 concluded that over the NH between 1960 and 2000, boreal winter and annual means of tropospheric GPH decreased over high latitudes and increased over the mid-latitudes. Trends for 500 hPa GPH from 1979 to 2012 from the ERA-Interim reanalysis (see Appendix 2.A) show a significant decrease only at southern high latitudes in November to April, but significant positive GPH trends in the subtropics and northern high latitudes. The seasonality and spatial dependence of 500 hPa GPH trends over Antarctica was highlighted by Neff et al. (2008), based upon radiosonde data over the period 1957–2007.

Minimum temperatures near the tropical tropopause (and therefore tropical tropopause height) are important as they affect the water vapour input into the stratosphere. AR4 reported an increase in tropical tropopause height and a slight cooling of the tropical cold-point tropopause. Studies since AR4 confirm the increase in tropopause height (Wang et al., 2012a). For tropical tropopause temperatures, studies based on radiosonde data and reanalyses partly support a cooling between the 1990s and the early 2000s (Randel et al., 2006), but uncertainties in long-term trends of the tropical cold-point tropopause temperature from radiosonde are very large (Wang et al., 2012a) and confidence is therefore low.

2.7.5 Tropical Circulation

This section assesses trends and variability in the strength of the Hadley and Walker circulations, the monsoons, and the width of the tropical belt. Observational evidence is based on radiosonde and reanalyses data (see Box 2.3). Additionally, the tropical circulation imprints on other fields that are observed from space (e.g., total ozone, outgoing long-wave radiation). Changes in the tropical circulation are constrained by changes in the water cycle (Held and Soden, 2006; Schneider et al., 2010).

Changes in the monsoon systems are expressed in an altered circulation, moisture transport and convergence, and precipitation. Only few monsoon studies address circulation changes, while most work focuses on precipitation. AR4 found that rainfall in many monsoon systems exhibits decadal changes, but that data uncertainties restrict confidence in trends. SREX also attributed *low confidence* to observed trends in monsoons. The studies assessed here suggest a weakening of the East Asian summer monsoon (EASM), but only *medium confidence* is attributed to this trend, given the nature and quality of the evidence.

Several studies report a weakening of the monsoon circulation as well as a decrease of total monsoon rainfall or of the number of precipitation days over the past 40–50 years (Liu et al., 2011; Tianjun et al., 2008, see also SREX). Strongest evidence for a weakening monsoon circulation concerns the East Asian monsoon. A decrease is found in winter and annual wind speeds over China at the surface and in the lower troposphere based on observations and sounding data (Guo et al., 2010; Jiang et al., 2010; Vautard et al., 2010; Xu et al., 2010). The western Pacific subtropical high, which controls the water vapour supply for monsoon rainfall (Zhou and Yu, 2005), has extended westward and thus prevents the northward penetration of water vapour transport. In the upper level, the South Asian High has experienced a zonal expansion (Gong and Ho, 2002; Zhou et al., 2009b). The pronounced weakening tendency of the EASM in recent decades is unprecedented in the 20th Century (Zhou et al., 2009a). However, trends derived from wind observations as well as circulation trends from reanalysis data (see Box. 2.3) carry large uncertainties (see also Figure 2.37).

In AR4, large interannual variability of the Hadley and Walker circulation was highlighted, as well as the difficulty in addressing changes in these features in the light of discrepancies between data sets. The additional data sets that became available since AR4 confirm this view. The strengths of the northern Hadley circulation (Figure 2.38) in boreal winter and of the Pacific Walker circulation in boreal fall and winter are largely related to the El Niño/Southern Oscillation (see Box 2.5). This association dominates interannual variability and affects trends. Data sets disagree with respect to trends in the Hadley circulation (Figure 2.38). Two widely used reanalysis data sets, NNR and ERA-40, both have demonstrated shortcomings with respect to tropical circulation; hence their increases in the Hadley circulation strength since the 1970s might be artificial (Hu et al., 2011; Mitas and Clement, 2005; Song and Zhang, 2007; Stachnik and Schumacher,

2011). Additional reanalysis data sets (Bronnimann et al., 2009; Nguyen et al., 2012) as well as satellite humidity data (Sohn and Park, 2010) also suggest a strengthening from the mid 1970s to present, but the magnitude is strongly data set dependent. The *confidence* in trends in the strength of the Hadley circulation is therefore *low*.

[INSERT FIGURE 2.38 HERE]

Figure 2.38: Top: Indices of the strength of the northern Hadley circulation in December to March (Ψ_{max} is the maximum of the meridional mass stream function at 500 hPa between the equator and 40°N, updated from Broennimann et al. (2009)). Bottom: Indices of the strength of the Pacific Walker circulation in September to January ($\Delta\omega$ is the difference in the vertical velocity between [10°S to 10°N, 180°W to 100°W] and [10°S to 10°N, 100°E to 150°E] as in Oort and Yienger (1996), updated from Broennimann et al. (2009)), Δc is the difference in cloud cover between [6°N–12°S, 165°E–149°W] and [18°N–6°N, 165°E–149°W] as in Deser et al. (2010b), v_E is the effective wind index, updated from Sohn and Park (2010), u is the zonal wind at 10 m averaged in the region [10°S–10°N, 160°E–160°W], ΔSLP is the SLP difference between [5°S–5°N, 160°W–80°W] and [5°S–5°N, 80°E–160°E] as in Vecchi et al. (2006)). Time series based on ICOADS data are only shown from 1957 to 2009. All reanalysis data sets listed in Box 2.3 are used, if available until March 2012, except for the zonal wind at 10 m (20CR, ERA-Interim, ERA-40, NCEP2). Where more than one time series was available, anomalies from the 1979/1980 to 2001/2002 mean values of each series are shown.

Consistent changes in different observed variables suggest a weakening of the Pacific Walker circulation during much of the 20th Century that has been largely offset by a recent strengthening. A weakening is indicated by trends in the zonal SLP gradient across the equatorial Pacific (see also Sect. 2.7.1, Table 2.12) from 1861 to 1992 (Vecchi et al., 2006), or from 1901 to 2004 (Power and Kociuba, 2011b). Boreal spring and summer contribute most strongly to the centennial trend (Karnauskas et al., 2009); see also Nicholls (2008), as well as to the trend in the second half of the 20th Century (Tokinaga et al., 2012). For boreal fall and winter (Figure 2.39), no trend is found in the Pacific Walker circulation based on the vertical velocity at 500 hPa from reanalyses (Compo et al., 2011), equatorial Pacific 10 m zonal winds (Figure 2.39), or SLP in Darwin (Nicholls, 2008). However, as for the Hadley circulation, there are inconsistencies between ERA-40 and NNR (Chen et al., 2008). Deser et al. (2010b), based on marine air temperature and cloud cover over the Pacific, find a weakening of the Walker circulation during most of the 20th Century to be consistent with observations (see also Yu and Zwiers, 2010). Tokinaga et al. (2012) find robust evidence for a weakening of the Walker circulation (most notably over the Indian Ocean) from 1960 to 2008 based on observations of cloud cover, surface wind, and SLP. Since the 1980s or 1990s, however, trends in the Pacific Walker circulation have reversed (Figure 2.39). This is evident from changes in SLP (see equatorial SOI trends in Table 2.8, Box 2.5, Figure 1 and Appendix 2.A), vertical velocity (Compo et al., 2011), water vapour flux from satellite and reanalysis data (Sohn and Park, 2010), or sea level height (Merrifield, 2011).

Observed changes in several atmospheric parameters suggest that the width of the tropical belt has increased at least since 1979 (Forster et al., 2011; Hu et al., 2011; Seidel et al., 2008). Since AR4, wind, temperature, radiation, and ozone information from radiosondes, satellites, and reanalyses had been used to diagnose the tropical belt width and estimate their trends. Annual mean time series of the tropical belt width from various sources are shown in Figure 2.39.

[INSERT FIGURE 2.39 HERE]

Figure 2.39: Annually averaged tropical belt width (top) and tropical edge latitudes in each hemisphere (middle and bottom). The tropopause, Hadley cell, and jet stream metrics are based on reanalyses (see Box 2.3); outgoing longwave radiation and ozone metrics are based on satellite measurements. The ozone metric refers to equivalent latitude (Hudson, 2011; Hudson et al., 2006). Adapted and updated from Seidel et al. (2008) using data presented in Davis and Rosenlof (2011) and (Hudson, 2011; Hudson et al., 2006). Where multiple datasets are available for a particular metric, all are shown as light solid lines, with shading showing their range and a heavy solid line showing their median.

Since 1979 the region of low column ozone values typical of the tropics has expanded in the NH (Hudson, 2011; Hudson et al., 2006). Based on radiosonde observations and reanalyses, the region of the high tropical tropopause has expanded since 1979, and possibly since 1960 (Birner, 2010; Lucas et al., 2012; Seidel and Randel, 2007), although widening estimates from different reanalyses and using different methodologies show a range of magnitudes (Birner, 2010; Seidel and Randel, 2007).

Several lines of evidence indicate that climate features at the edges of the Hadley cell have also moved poleward since 1979. Subtropical jet metrics from reanalysis zonal winds (Archer and Caldeira, 2008a;

Archer and Caldeira, 2008b; Strong and Davis, 2007; Strong and Davis, 2008a) and layer-average satellite temperatures (Fu et al., 2006; Fu and Lin, 2011) also indicate widening, although 1979–2009 wind-based trends (Davis and Rosenlof, 2011) are not statistically significant. Changes in subtropical outgoing longwave radiation, a surrogate for high cloud, also suggest widening (Hu and Fu, 2007), but the methodology and results are disputed (Davis and Rosenlof, 2011). Precipitation patterns and subtropical high-pressure regions also indicate widening (Davis and Rosenlof, 2011; Hu and Fu, 2007; Hu et al., 2011; Kang et al., 2011; Zhou et al., 2011)

The qualitative consistency of these observed changes in independent data sets suggests a widening of the tropical belt between at least 1979 and 2005 (Seidel et al., 2008), and possibly longer. Widening estimates range between around 0° and 3° latitude per decade, and their uncertainties have been only partially explored (Birner, 2010; Davis and Rosenlof, 2011).

2.7.6 Jets, Storm Tracks and Weather Types

2.7.6.1 Midlatitude and Subtropical Jets

Subtropical and midlatitude jet streams are three-dimensional entities that vary meridionally and vertically. Jet stream winds can be determined from radiosonde measurements of GPH using quasi-geostrophic flow assumptions. Using reanalysis data sets, it is possible to track 3-dimensional jet variations by identifying a surface of maximum wind (SMW), although a high vertical resolution is required for identification of jets.

AR4 found a poleward displacement of Atlantic and southern polar front jet streams from the 1960s to at least the mid-1990s. Studies since AR4 confirm that in the Northern Hemisphere, the jet core has been migrating towards the pole since the 1970s, but trends in the jet speed are uncertain.

In NH summer, subtropical jets have significantly lowered in altitude over most of the tropics and subtropics from 1958 to 2004, particularly in the Eastern Hemisphere (Strong and Davis, 2006). Similar long-term trends in the SMW are not evident in boreal winter, where interannual jet variability is linked to monthly variations in the Arctic Oscillation or ENSO (Strong and Davis, 2008b).

Various analyses from different reanalysis data sets indicate that the jet streams (midlatitude and subtropical) have been moving poleward in most regions (in both hemispheres) over the last three decades (Archer and Caldeira, 2008b; Fu et al., 2009b; Fu et al., 2006; Strong and Davis, 2007). There is inconsistency with respect to speed trends based upon whether one uses an SMW-based or isobaric-based approach (Archer and Caldeira, 2008a; Archer and Caldeira, 2008b; Strong and Davis, 2007; Strong and Davis, 2008a). In general, jets have become more common (and jet speeds have increased) over Canada, the North Atlantic, and Europe (Barton and Ellis, 2009; Strong and Davis, 2007), trends that are coupled with regional increases in GPH gradients and circumpolar vortex contraction (Angell, 2006; Frauenfeld and Davis, 2003). From a climate dynamics perspective, these trends are driven by regional patterns of tropospheric and lower stratospheric warming or cooling and thus are coupled to large-scale circulation variability.

2.7.6.2 Storm Tracks and Frequency of Cyclones

Storm tracks are regions of enhanced synoptic activity due to the passage of cyclones. The main storm tracks stretch across the North Pacific, North Atlantic and Southern Oceans. They are defined by applying band pass filtering or cyclone tracking to daily or sub-daily SLP data (station data, gridded data, or reanalyses) or to upper level fields from reanalyses. Trends have been shown to be sensitive to the method (Raible et al., 2008).

In AR4 changes in storm tracks were assessed. A poleward shift of the northern hemispheric storm tracks was found. However, it was also noted that uncertainties are large and that NNR and ERA-40 disagree in important aspects. SREX also found a poleward shift of NH and SH storm tracks. Additional studies assessed here further support the poleward shift in the North Atlantic from the 1950s to the early 2000s.

For the North Atlantic, studies based on ERA40 (Schneidereit et al., 2007), SLP measurements from ships (Chang, 2007b), sea level time series (Vilibic and Sepic, 2010), and cloud analyses (Bender et al., 2012)

support a poleward shift and intensification of the cyclone tracks from the 1950s to the early 2000s, with more wintertime high-latitude cyclones (see also Cornes and Jones, 2011b; Sorteberg and Walsh, 2008) but fewer at mid-latitudes. This is consistent with changes in the NAO to which the Atlantic storm track is associated (Schneidereit et al., 2007). However, storminess derived from SLP station triangles in Europe from the 1870s to 2005 shows large decadal variations (Matulla et al., 2008; Wang et al., 2009c), and surface wind trends (see Figure 2.37) suggest an equatorward shift of the storm track over the 1988-2010 period. Storminess and extreme winds are further discussed in Section 2.6.

For the Pacific storm track, uncertainties are large, as studies based on reanalysis data and on SLP observations differ (Chang, 2007a). Knapp and Soule (2007) used station observations over the period 1900-2004 to infer that summertime major midlatitude cyclones over the Northern Rockies have become less frequent and occur later in the season, due to more frequent mid-tropospheric ridging upstream from the Northern Rockies.

Poleward shifts of the SH storm track and changes in storminess have been reported based on reanalysis data (e.g., Frederiksen and Frederiksen, 2007). Although a decrease in storminess in south eastern Australia based on records of SLP from 1865 to 2009 is consistent with this shift (Alexander and Power, 2009; Alexander et al., 2011), most work is based on reanalysis data which are of insufficient quality for analysing the SH storm tracks (see alsoTrenberth et al., 2005; Wang et al., 2006b).

2.7.6.3 Weather Types and Blocking

Changes in climate are associated with changes in weather. Changes in the frequency of weather types are of interest since weather extremes are often associated with specific weather types. For instance, persistent blocking of the westerly flow was essential in the development the 2010 heat wave in Russia (Dole et al., 2011) (see also Sections 9.5.2.2. and 14.2.11.). Synoptic classifications or statistical clustering (Philipp et al., 2007) are commonly used to classify the weather on a given day. Feature-based methods are also used (Croci-Maspoli et al., 2007b). All these methods require daily SLP or upper-level fields.

In AR4, weather types were not assessed as such, but an increase in blocking frequency in the Western Pacific and a decrease in North Atlantic were noted. Trends in synoptic weather types have been best analysed for Central Europe since the mid 20th Century, where several studies describe an increase in westerly or cyclonic weather types in winter but an increase of anticyclonic, drought-conducive weather types in summer (Philipp et al., 2007; Trnka et al., 2009; Werner et al., 2008). Using a feature-based approach, Croci-Maspoli et al. (2007b) found negative trends of blocking in winter over Greenland and in spring over the North Pacific during the period 1957–2001 (see also Kreienkamp et al., 2010). Long-lasting blocking is closely associated with modes of climate variability such as the NAO or the PNA (Croci-Maspoli et al., 2007a), which are discussed in Section 2.7.9. Häkkinen et al. (2011) found a relation between the frequency of wintertime blocking between Greenland and Western Europe and a warmer, more saline subpolar North Atlantic on decadal scales. For the Southern Hemisphere, Dong et al. (2008) found a decrease in number but increase in intensity of blocking days over the period 1948 to 1999.

2.7.7 Stratospheric Circulation

The stratosphere is coupled with the troposphere through fluxes of radiation, momentum, and mass. The most important characteristics of stratospheric circulation for climate and for trace gas distribution are the winter polar vortices and Sudden Stratospheric Warmings (rapid warmings of the middle stratosphere accompanied by a collapse of the Polar Vortex), the Quasi-Biennial Oscillation (an oscillation of equatorial zonal winds with a downward phase propagation), and the Brewer-Dobson circulation (BDC, the meridional overturning circulation transporting air upward in the tropics, poleward to the winter hemisphere, and downward at subpolar latitudes). Radiosonde observations, reanalysis data sets, and space-borne temperature or trace gas observations are used to address changes in the stratospheric circulation (see also Chapter 10), but all of these sources of information carry large trend uncertainties.

Changes in the polar vortices have been assessed in AR4. A significant decrease in lower-stratospheric GPH in summer over Antarctica since 1969 was found, whereas trends in the Northern Polar Vortex were considered uncertain due to its large variability. This assessment was further corroborated in Forster et al.

(2011) and in updated 100 hPa GPH trends from ERA-Interim reanalysis (see Appendix 2.A). There is *high confidence* that the Antarctic polar vortex has deepened at least since 1979. Cohen et al. (2009) reported an increase in the number of Arctic sudden stratospheric warmings during the last two decades. However, interannual variability in the Arctic Polar Vortex is large, uncertainties in the data products are high (Tegtmeier et al., 2008), and trends depend strongly on the time period analysed (Langematz and Kunze (2008).

The BDC is only indirectly observable via wave activity diagnostics (which represent the main driving mechanism of the BDC), via temperatures or via the distribution of trace gases, which may allow the determination of the 'age of air' (i.e., the time an air parcel has resided in the stratosphere after its entry from the troposphere). All of these methods are subject to considerable uncertainties, and they might shed light only on some aspects of the BDC. *Confidence* in trends in the BDC is therefore *low*. Randel et al. (2006), found a sudden decrease in lower stratospheric water vapour and ozone around 2001 that is consistent with an increase in the mean tropical upwelling, i.e., the tropical branch of the BDC (see also Lanzante, 2009; Rosenlof and Reid, 2008). On the other hand, Engel et al. (2009) found no statistically significant change in the age of air in the 24-35 km layer over the Northern Hemisphere from measurements of chemically inert trace gases from 1975–2005. However, this does not rule out trends in the lower stratospheric branch of the BDC (Bonisch et al., 2009; Ray et al., 2010).

[START BOX 2.5 HERE]

Box 2.5: Patterns and Indices of Climate Variability

Much of the spatial structure of climate variability can be described as a combination of 'preferred' patterns. The most prominent of these are known as *modes of climate variability* and impact weather and climate on many spatial and temporal scales (see Chapter 14). Individual climate modes historically have been identified through spatial *teleconnections*: correlations between regional climate variations at widely-separated, geographically-fixed spatial locations. An *index* describing temporal variations of the climate mode in question can be formed, e.g., by subtracting climate anomalies calculated from meteorological records at stations exhibiting the strongest anticorrelation (or adding stations with the positive correlations). By regressing climate records from other places on this index, one derives a spatial *climate pattern* characterizing this mode. Patterns of climate variability have also been derived using a variety of mathematical techniques such as principle component analysis (PCA). These patterns and their indices are useful both because they efficiently describe climate variability in terms of a few patterns and also because these patterns can provide clues about how the variablility is sustained (see Chapter 14, Box 14.1 for formal definitions of these terms).

Box 2.5, Table 1 lists some prominent modes of large-scale climate variability and indices used for defining them; changes in these indices are associated with large-scale climate variations on interannual and longer time scales. With some exceptions, indices shown have been (1) used by a variety of authors, (2) are defined relatively simply from raw or statistically analyzed observations of a *single* climate variable, which (3) has a history of *surface* observations, so that for most of these indices at least a century-long record is available for climate research.

[INSERT BOX 2.5, TABLE 1 HERE]

Box 2.5, Table 1: Established indices of climate variability with global or regional influence. Columns are: (1) name of a climate phenomenon, (2) name of the index, (3) index definition, (4) primary references, (5) comments, including when available, characterization of the index or its spatial pattern as a dominant variability mode.

Box 2.5, Figure 1 illustrates climate modes listed in Box 2.5, Table 1 by showing temporal variability of their indices. Most climate modes are illustrated by several indices, which often behave similarly to each other. Spatial patterns of sea surface temperature (SST) or mean sea level pressure (MSLP) associated with these climate modes are illustrated in Box 2.5, Figure 2. They can be interpreted as a change in the SST or MSLP field associated with one standard deviation change in the index.

[INSERT BOX 2.5, FIGURE 1 HERE]

Box 2.5, Figure 1: Some indices of climate variability, as defined in Table 1. Where 'HadISST1', 'HadSLP2r', or '20C RA' are indicated, the indices were computed from the SST or MSLP values of the former two data sets or from 500 or

850 hPa geopotential height fields from the 20th Century Reanalysis, version 2. A data set reference given in the title of each panel applies to all indices shown in that panel. 'CPC' indicates an index timeseries publicly available from the NOAA Climate Prediction Center. Where no data set is specified, a publicly available regularly updated version of an index from the authors of a primary reference given in Table 1 was used. (Citations are given in panel legends only when needed for unambiguous identification of a particular index definition from Table 1; their presence or absence does not mean that the index values obtained from the authors were or were not used here). All indices are shown as 12-month running means (r.m.) except when the temporal resolution is explicitly indicated (e.g., 'DJFM' for December-to-March averages) or smoothing level (e.g., 11-year LPF for a low-pass filter with half-power at 11 years).

[INSERT BOX 2.5, FIGURE 2 HERE]

Box 2.5, Figure 2: Spatial patterns of climate modes listed in Table 1. All patterns shown here are obtained by regression of either SST or MSLP fields on the standardized index of a climate mode. For each climate mode one of the indices shown in Figure 1 was used. SST and MSLP fields are from HadISST1 and HadSLP2r data sets (interpolated gridded products based on data sets of historical observations). All SST-based patterns are results of monthly regressions for the 1870–2010 period except for the PDO regression pattern, which was computed for 1900–2010. The MSLP-based patterns of NAO and PNA are regression coefficients of the DJFM means; PSA1 and PSA2 patterns are regressions of seasonal means; SAM pattern is from a monthly regression. All SLP-based patterns are results of the 1948–2010 regression, except for the PDO regression pattern which is from 1876–2010 regression. For each pattern the time series was linearly de-trended over the regression interval. All patterns are shown by color plots, except for PSA2, which is shown by white contours over the PSA1 color plot (contour steps are 0.5 hPa, zero contour is skipped, negative values are indicated by dash).

The difficulty of identifying a universally 'best' index for any particular climate mode is due to the fact that no simply defined indicator can achieve a perfect separation of the target phenomenon from all other effects occurring in the climate system. As a result, each index is affected by many climate phenomena whose relative contributions may change with the time period and the data set used. Limited length and quality of the observational record further compound this problem. Thus the choice of index is always application-specific.

[END BOX 2.5 HERE]

2.7.8 Changes in Indices of Climate Variability

Indices are used to measure the strength of modes of climate variability and to summarize large fractions of spatio-temporal variability using a single time series. Trends in indices are affected by the fact that records are relatively short, prone to error, and indices are subject to natural multidecadal variability. Moreover, some indices explicitly include a detrending of the entire record (e.g., Deser et al., 2010a).

Table 2.12 summarizes observed changes in some well-known indices of climate variability. Confidence intervals that do not cover zero indicate trend significance at 10%; however, the trends significant at 5% and 1% level are identified too and are discussed in particular here. Please refer to Chapter 14 for the discussion of main features and physical meaning of individual climate modes.

AR4 assessed patterns of atmospheric circulation variability in detail. Multidecadal variability was found in patterns referring to Pacific and Atlantic SSTs. The NAO and SAM were found to exhibit increasing trends (strengthened midlatitude westerlies) from the 1960s to 1990s, but the NAO has returned to its long-term mean state since then. After returning to its normal state in the last decade, the NAO index reached very low values in the winter of 2009/2010 (Osborn, 2011) and was below normal in the winter of 2010/2011 as well. As a result, with the exception of the PC-based NAO index, which still shows a 5%-significant positive trend from 1951 to present, other NAO or NAM indices do not show significant trends of either sign for the periods presented in Table 2.12. In contrast, the SAM has resumed its upward trend that was noted in AR4, peaking in a record high SAM index in austral winter 2010. Fogt et al. (2009) found a positive trend in the SAM index from 1957 to 2005, Visbeck (2009), in a station-based index, found an increase in recent decades (1970s to 2000s). The PC-based AAO index presented in Table 2.12 shows an increasing trend in the last 60 and 110 years with 1% level of significance.

The observed detrended multidecadal SST anomaly averaged over the North Atlantic Ocean area is often called Atlantic Multidecadal Oscillation Index (AMO, see Box 2.5, Table 1, Figure 1). The warming trend in the "revised" AMO index since 1979 is significant at 1% level (Table 2.12).

PDO, IPO, and NPI indices also show significant changes (positive for NPI and negative for PDO and IPO) since the 1980s that are consistent with the surface pressure changes discussed in Section 2.7.1. This change, and the teleconnection between the Equator and midlatitudes, is consistent with reversing trends in the Walker Circulation (Section 2.7.5), which was reported to have slowed down during much of the 20th Century but since the 1990s has sped up again. Since the beginning of the 20th Century, equatorial SOI does not show significant long-term trends, but has changed rapidly in the last 20 years (Table 2.12).

Bunge and Clarke (2009) found an increase in the NINO3.4 index since about the 1870s. NINO3.4 shows a century-scale warming trend significant at 5% level, if computed from the ERSSTv3b data set (see Section 2.2.2) but not if calculated from other data sets (Table 2.12). Furthermore, the sign (and significance) of the trend in east-west SST gradient across the Pacific remains ambiguous as well (Bunge and Clarke, 2009; Deser et al., 2010b; Karnauskas et al., 2009; Vecchi and Soden, 2007).

Table 2.12: Trends (standard deviation/decade) for selected indices listed in Box 2.5, Table 1. Except where DJFM averaging is noted, results are for the calendar year averages and are presented with their 5% to 95% confidence intervals. Trend values significant at 5% or 1% levels are italicized or underlined respectively. Index records where the source is not explicitly indicated were computed from either HadISST1 (for SST-based indices), or HadSLP2r (for MSLP-based indices), or the 20th Century Reanalysis fields of 500 hPa or 850 hPa geopotential height. CoA stands for 'Centers of Action' index definitions. Index standardization period is for 1948–2010 for Reanalysis-based indices, 1876–2010 for Troup and Darwin SOIs, 1900–2010 for PDO and NAO indices, and 1870–2010 for all other indices. Standardization was done on DJFM means for NAO and PNA, seasonal anomalies for PSA1,2, and monthly anomalies for all other indices.

Index Name	1901–2010	1951–2010	1979–2010
(–1)*SOI Troup, BOM records	0.019 ± 0.039	0.040 ± 0.103	–0.209 ± 0.251
SOI Darwin, BOM records	0.030 ± 0.037	0.095 ± 0.087	–0.100 ± 0.216
(–1)*EQSOI	0.015 ± 0.049	–0.040 ± 0.137	*–0.512* ± 0.321
NINO34	0.001 ± 0.043	0.030 ± 0.109	–0.121 ± 0.304
NINO34 (ERSSTv3b)	*0.071* ± 0.045	0.070 ± 0.107	–0.046 ± 0.285
NINO34 (COBE SST)	0.029 ± 0.042	0.026 ± 0.111	–0.114 ± 0.320
NINO4	0.033 ± 0.055	0.095 ± 0.149	–0.030 ± 0.414
EMI	–0.051 ± 0.062	–0.096 ± 0.202	–0.046 ± 0.653
TNI	–0.025 ± 0.053	–0.094 ± 0.175	–0.126 ± 0.608
PDO (Mantua et al., 1997)	–0.006 ± 0.072	0.160 ± 0.180	*–0.386* ± 0.308
(–1)*NPI	–0.023 ± 0.022	0.025 ± 0.045	*–0.143* ± 0.117
AMO revised	–0.035 ± 0.115	–0.066 ± 0.362	0.802 ± 0.305
NAO stations DJFM (Hurrell, 1995)	–0.010 ± 0.065	0.146 ± 0.159	–0.160 ± 0.409
NAO PC DJFM (Hurrell, 1995)	0.000 ± 0.063	*0.198* ± 0.157	–0.099 ± 0.442
NAM PC-based		0.081 ± 0.146	–0.094 ± 0.449
AAO PC-based		0.192 ± 0.047	0.139 ± 0.127
PNA DJFM, CoA		*0.151* ± 0.116	–0.080 ± 0.316
PSA CoA as in Karoly (1989)		–0.116 ± 0.058	*–0.243* ± 0.157
(–1)*PSA CoA as in Yuan and Li (2008)		*–0.081* ± 0.052	–0.138 ± 0.156
PSA1		0.019 ± 0.081	–0.091 ± 0.215
PSA2		0.140 ± 0.072	0.200 ± 0.188
ATL3	0.037 ± 0.044	*0.141* ± 0.092	*0.266* ± 0.205
AONM	*0.067* ± 0.053	*0.154* ± 0.116	0.427 ± 0.241
AMM	0.018 ± 0.059	–0.034 ± 0.159	0.295 ± 0.363
IOBM	*0.076* ± 0.054	0.331 ± 0.089	0.243 ± 0.229
DMI	0.029 ± 0.033	0.068 ± 0.095	0.176 ± 0.236
IODM	–0.017 ± 0.035	–0.042 ± 0.100	–0.104 ± 0.226

In addition to changes in the mean values of climate indices, changes in the modes of variability themselves are also possible. In particular, attempts to identify changes in the character of ENSO variability have received much attention but have been unable to demonstrate robust changes. Starting from the work of Trenberth and Stepaniak (2001), who proposed to characterize the evolution of ENSO events with the Trans-Niño Index (TNI), which is virtually uncorrelated with the standard ENSO index NINO3.4, other alternative ENSO indices have been introduced and proposals were made for classifying ENSO events according to the indices they primarily maximize. While a traditional, 'canonical' El Niño event type (Rasmusson and Carpenter, 1982) is viewed as the 'eastern Pacific' type, the alternative indices identify events that have central Pacific maxima and are called dateline El Niño (Larkin and Harrison, 2005), Modoki (Ashok et al., 2007), or Central Pacific El Niño (Kao and Yu, 2009). Takahashi et al. (2011) have recently represented many of the old and new ENSO indices as elements in a two-dimensional linear space spanned by two classical ENSO indices that summarize eastern and central Pacific SST anomalies: NINO1+2 and NINO4 (see Box 2.5, Table 1 for index definitions). None of Central and Western Pacific indices in Table 2.12 had shown trends even at 10% significance.

Table 2.12 also lists a significant positive PNA trend over the last 60 years and negative and positive trends in the first and second PSA modes respectively, throughout the 20th Century. The level of significance of trends in the PSA1 mode clearly depends on the index definition. Remaining indices with significant trends in Table 2.12 are tropical Atlantic and Indian Ocean regional modes. The increasing trend in ATL3 and AONM indices that represent Atlantic 'Niño' mode is due to the east-intensified warming in the Tropical Atlantic that causes the the weakening of the Atlantic equatorial cold tongue: this trend over the last 60 years has been recently identified and interpreted by Tokinaga and Xie (2011b). The Indian Ocean Basin Mode has a strong 1%-significant warming trend since the middle of the 20th Century. This phenomenon is well-known (Du and Xie, 2008) and its consequences for the regional climate is a subject of active research (Du et al., 2009; Xie et al., 2009).

2.7.9 Synthesis

New and improved data sets are available for addressing changes in the large-scale atmospheric circulation, but large variability on interannual to decadal time scales and remaining differences between data sets precludes robust conclusions on long-term changes in most cases. Some trend features that appeared from the 1950s or earlier to the 1990s (e.g., an increase in the NAO index or a weakening of the Pacific Walker circulation) have reversed in more recent periods so that confidence in long-term trends is low.

A few robust changes over the past several decades have been identified that were also described in AR4. It is *likely* that, in a zonal mean sense, circulation features have moved poleward (widening of the tropical belt, poleward shift of storm tracks and jet streams) since the 1970s. Trends in these features are consistent with each other and are based on many different data sets, variables, and approaches. It is *likely* that the SAM index has become more positive (the midlatitude wind maximum has shifted poleward) since the 1950s and that the Antarctic polar vortex has strengthened at least since 1979.

2.8 Consistency Across Observations

Comparing trends and variability across (independently measured) climate variables can help assess whether the observed changes are consistent. If the estimated changes are consistent with each other, this can enhance confidence in the observations and the overall assessment of change (see also FAQ 2.1). Observed inter-relationships among different variables described in this chapter include:

- Widespread decadal changes in surface solar radiation (dimming until the 1980s and subsequent brightening) are in line with observed changes in a variety of other related variables, such as sunshine duration and hydrological quantities. These changes also appear to be consistent with increasing and decreasing aerosol loadings;

- Globally averaged surface temperatures for land, sea surface and marine air all show significant warming trends, as do tropospheric observations from radiosondes and satellites;

- Changes in extremes of temperature are consistent with warming, showing decreases in cold extremes and increases in warm extremes;

- Land-based precipitation observations since 1900 are consistent with the most recent and comprehensive analyses of streamflow, in that, globally, neither show significant trends during the 20th Century;

- Over land, a strong negative correlation is observed between precipitation and surface temperature in summer and at low latitudes throughout the year, and areas that have become wetter, such as the eastern USA and Argentina, have not warmed as much as other land areas;

- Surface specific humidity has generally increased in close association with higher temperatures over both land and ocean. Upper-tropospheric water vapour has also increased and in turn, widespread observed increases in the fraction of heavy precipitation events (e.g., 95th percentile) are consistent with the increased water vapour amounts;

- Increasing zonal flow observed in the NH in the second half of the 20th Century brought milder maritime air into Europe and much of high-latitude Asia from the North Atlantic in winter, enhancing warming there. In recent decades, these trends have been largely offset and warming has slowed in these regions.

References

Abakumova, G.M., Gorbarenko, E.V., Nezval, E.I. and Shilovtseva, O.A., 2008. Fifty years of actinometrical measurements in Moscow. International Journal of Remote Sensing, **29**(9): 2629-2665.

Adam, J.C. and Lettenmaier, D.P., 2008. Application of new precipitation and reconstructed streamflow products to streamflow trend attribution in northern Eurasia. Journal of Climate, **21**(8): 1807-1828.

Adler, R.F., Huffman, G.J., Chang, A., Ferraro, R., Xie, P.P., Janowiak, J., Rudolf, B., Schneider, U., Curtis, S., Bolvin, D., Gruber, A., Susskind, J., Arkin, P. and Nelkin, E., 2003. The version-2 global precipitation climatology project (GPCP) monthly precipitation analysis (1979-present). Journal of Hydrometeorology, **4**(6): 1147-1167.

Aguilar, E., Barry, A.A., Brunet, M., Ekang, L., Fernandes, A., Massoukina, M., Mbah, J., Mhanda, A., do Nascimento, D.J., Peterson, T.C., Umba, O.T., Tomou, M. and Zhang, X., 2009. Changes in temperature and precipitation extremes in western central Africa, Guinea Conakry, and Zimbabwe, 1955-2006. Journal of Geophysical Research-Atmospheres, **114**.

Aguilar, E., Peterson, T.C., Obando, P.R., Frutos, R., Retana, J.A., Solera, M., Soley, J., Garcia, I.G., Araujo, R.M., Santos, A.R., Valle, V.E., Brunet, M., Aguilar, L., Alvarez, L., Bautista, M., Castanon, C., Herrera, L., Ruano, E., Sinay, J.J., Sanchez, E., Oviedo, G.I.H., Obed, F., Salgado, J.E., Vazquez, J.L., Baca, M., Gutierrez, M., Centella, C., Espinosa, J., Martinez, D., Olmedo, B., Espinoza, C.E.O., Nunez, R., Haylock, M., Benavides, H. and Mayorga, R., 2005. Changes in precipitation and temperature extremes in Central America and northern South America, 1961-2003. Journal of Geophysical Research-Atmospheres, **110**(D23).

Alexander, L.V. and Arblaster, J.M., 2009. Assessing trends in observed and modelled climate extremes over Australia in relation to future projections. Int. J. Climatology, **29**(3): 417-435.

Alexander, L.V., Hope, P., Collins, D., Trewin, B., Lynch, A. and Nicholls, N., 2007. Trends in Australia's climate means and extremes: a global context. Australian Meteorol. Mag., **56**(1): 1-18.

Alexander, L.V. and Power, S., 2009. Severe storms inferred from 150 years of sub-daily pressure observations along Victoria's "Shipwreck Coast". Australian Meteorological and Oceanographic Journal, **58**(2): 129-133.

Alexander, L.V., Uotila, P. and Nicholls, N., 2009. Influence of sea surface temperature variability on global temperature and precipitation extremes. Journal of Geophysical Research-Atmospheres, **114**.

Alexander, L.V., Wang, X.L.L., Wan, H. and Trewin, B., 2011. Significant decline in storminess over southeast Australia since the late 19th century. Australian Meteorological and Oceanographic Journal, **61**(1): 23-30.

Alexander, L.V., Zhang, X., Peterson, T.C., Caesar, J., Gleason, B., Tank, A., Haylock, M., Collins, D., Trewin, B., Rahimzadeh, F., Tagipour, A., Kumar, K.R., Revadekar, J., Griffiths, G., Vincent, L., Stephenson, D.B., Burn, J., Aguilar, E., Brunet, M., Taylor, M., New, M., Zhai, P., Rusticucci, M. and Vazquez-Aguirre, J.L., 2006. Global observed changes in daily climate extremes of temperature and precipitation. J. Geophys. Res.-Atmos., **111**(D5).

Allan, R. and Ansell, T., 2006. A new globally complete monthly historical gridded mean sea level pressure dataset (HadSLP2): 1850-2004. Journal of Climate, **19**(22): 5816-5842.

Allan, R., Brohan, P., Compo, G.P., Stone, R., Luterbacher, J. and Bronnimann, S., 2011. The International Atmospheric Circulation Reconstructions over the Earth (ACRE) Initiative. Bulletin of the American Meteorological Society.

Allan, R., Tett, S. and Alexander, L., 2009. Fluctuations in autumn-winter severe storms over the British Isles: 1920 to present. Int. J. Climatology, **29**(3): 357-371.

Allan, R.P., 2009. Examination of Relationships between Clear-Sky Longwave Radiation and Aspects of the Atmospheric Hydrological Cycle in Climate Models, Reanalyses, and Observations. Journal of Climate, **22**(11): 3127-3145.

Allan, R.P. and Slingo, A., 2002. Can current climate model forcings explain the spatial and temporal signatures of decadal OLR variations? Geophysical Research Letters, **29**(7): 1141.

Allan, R.P., Soden, B.J., John, V.O., Ingram, W. and Good, P., 2010. Current changes in tropical precipitation. Environmental Research Letters, **5**(2).

Allen, R.J. and Sherwood, S.C., 2007. Utility of radiosonde wind data in representing climatological variations of tropospheric temperature and baroclinicity in the western tropical Pacific. Journal of Climate, **20**(21): 5229-5243.

Allen, R.J. and Sherwood, S.C., 2008. Warming maximum in the tropical upper troposphere deduced from thermal winds. Nature Geoscience, **1**(6): 399-403.

Almazroui, M., Islam, M.N. and Jones, P.D., Submitted. Urbanization effects on the air temperature rise in Saudia Arabia, Geophysical Research Letters.

Almazrouia, M., Islama, M.N., Dambula, R. and Jones, P.D., Trends of temperature extremes in Saudi Arabia. International Journal of Climatology (submitted).

Alpert, P. and Kishcha, P., 2008. Quantification of the effect of urbanization on solar dimming. Geophysical Research Letters, **35**(8): L08801.

Alpert, P., Kishcha, P., Kaufman, Y.J. and Schwarzbard, R., 2005. Global dimming or local dimming?: Effect of urbanization on sunlight availability. Geophysical Research Letters, **32**(17): L17802.

Andreadis, K.M. and Lettenmaier, D.P., 2006. Trends in 20th century drought over the continental United States. Geophysical Research Letters, **33**(10).

Andronova, N., Penner, J.E. and Wong, T., 2009. Observed and modeled evolution of the tropical mean radiation budget at the top of the atmosphere since 1985. Journal of Geophysical Research-Atmospheres, **114**: -.

Angell, J.K., 2006. Changes in the 300-mb North Circumpolar Vortex, 1963-2001. Journal of Climate, **19**(12): 2984-2994.

Anthes, R.A., 2011. Exploring Earth's atmosphere with radio occultation: contributions to weather, climate and space weather. Atmospheric Measurement Techniques, **4**(6): 1077-1103.

Anthes, R.A., Bernhardt, P.A., Chen, Y., Cucurull, L., Dymond, K.F., Ector, D., Healy, S.B., Ho, S.P., Hunt, D.C., Kuo, Y.H., Liu, H., Manning, K., McCormick, C., Meehan, T.K., Randel, W.J., Rocken, C., Schreiner, W.S., Sokolovskiy, S.V., Syndergaard, S., Thompson, D.C., Trenberth, K.E., Wee, T.K., Yen, N.L. and Zeng, Z., 2008. The COSMOC/FORMOSAT-3 - Mission early results. Bulletin of the American Meteorological Society, **89**(3): 313-+.

Archer, C.L. and Caldeira, K., 2008a. Historical trends in the jet streams. Geophysical Research Letters, **35**(8).

Archer, C.L. and Caldeira, K., 2008b. Reply to comment by Courtenay Strong and Robert E. Davis on "Historical trends in the jet streams". Geophysical Research Letters, **35**(24).

Arndt, D.S., Baringer, M.O. and Johnson, M.R., 2010. STATE OF THE CLIMATE IN 2009. Bulletin of the American Meteorological Society, **91**(7): S1-+.

Arndt, D.S., Blunden, J. and Baringer, M.O., 2011. STATE OF THE CLIMATE IN 2010. Bulletin of the American Meteorological Society, **92**(6): S17-+.

Ashok, K., Behera, S.K., Rao, S.A., Weng, H.Y. and Yamagata, T., 2007. El Nino Modoki and its possible teleconnection. Journal of Geophysical Research-Oceans, **112**.

Asmi, A., Collaud Coen, M., J.A. Ogren, E. Andrews, P. Sheridan, A. Jefferson, E. Weingartner, U. Baltensperger, H. Lihavainen, N. Kivekas, E. Asmi, P.P. Aalto, M. Kulmala, A. Wiedensohler, W. Birmili, A. Hamed, C. O'Dowd, R. Weller, H. Flentje, A.M. Fjaeraa, M. Fiebig, N. Bukowiecki, G. Hallar, C.L. Myhre, Jennings, S.G. and P. Laj, 2012. Aerosol decadal trends (II): In-situ number concentrations at GAW and ACTRIS stations,. submitted to Atmospheric Chemistry and Physics.

Atlas, R., Hoffman, R., Ardizzone, J., Leidner, S., Jusem, J., Smith, D. and Gombos, D., 2011. A CROSS-CALIBRATED MULTIPLATFORM OCEAN SURFACE WIND VELOCITY PRODUCT FOR METEOROLOGICAL AND OCEANOGRAPHIC APPLICATIONS. Bulletin of the American Meteorological Society, **92**(2): 157-+.

Ballester, J., Giorgi, F. and Rodo, X., 2010. Changes in European temperature extremes can be predicted from changes in PDF central statistics. Climatic Change, **98**(1-2): 277-284.

Baringer, M.O., Arndt, D.S. and Johnson, M.R., 2010. STATE OF THE CLIMATE IN 2009. Bulletin of the American Meteorological Society, **91**(7): S1-+.

Barkstrom, B.R., 1984. The Earth Radiation Budget Experiment (Erbe). Bulletin of the American Meteorological Society, **65**(11): 1170-1185.

Barmpadimos, I., Keller, J., Oderbolz, D., Hueglin, C. and Prevot, A.S.H., 2012. One decade of parallel fine (PM2.5) and coarse (PM10-PM2.5) particulate matter measurements in Europe: trends and variability. Atmos. Chem. Phys., **12**(7): 3189-3203.

Barnes, N. and Jones, D., 2011. Clear Climate Code: Rewriting Legacy Science Software for Clarity. IEEE Software, **28**: 36-42.

Barnett, D.N., Brown, S.J., Murphy, J.M., Sexton, D.M.H. and Webb, M.J., 2006. Quantifying uncertainty in changes in extreme event frequency in response to doubled CO2 using a large ensemble of GCM simulations. Climate Dynamics, **26**(5): 489-511.

Barnston, A.G. and Livezey, R.E., 1987. Classification, seasonality and persistence of low-frequency atmospheric circulation patterns. Monthly Weather Review, **115**(6): 1083-1126.

Barring, L. and Fortuniak, K., 2009. Multi-indices analysis of southern Scandinavian storminess 1780-2005 and links to interdecadal variations in the NW Europe-North Sea region. International Journal of Climatology, **29**(3): 373-384.

Barrucand, M., Rusticucci, M. and Vargas, W., 2008. Temperature extremes in the south of South America in relation to Atlantic Ocean surface temperature and Southern Hemisphere circulation. Journal of Geophysical Research-Atmospheres, **113**(D20).

Bartholy, J. and Pongracz, R., 2007. Regional analysis of extreme temperature and precipitation indices for the Carpathian Basin from 1946 to 2001. Global and Planetary Change, **57**(1-2): 83-95.

Barton, N.P. and Ellis, A.W., 2009. Variability in wintertime position and strength of the North Pacific jet stream as represented by re-analysis data. International Journal of Climatology, **29**(6): 851-862.

Becker, A., Schneider, U., Meyer-Christoffer, A., Ziese, M., Mächel, H., Schamm, K., Finger, P., Stender, P. and Rudolf, B., 2012. A description of the global land-surface precipitation data products of the Global Precipitation Climatology Centre and their major use cases including centennial (trend) analysis from 1901-present. Earth System Science Data, **Submitted**.

Beig, G. and Singh, V., 2007. Trends in tropical tropospheric column ozone from satellite data and MOZART model. Geophys. Res. Lett., **34**(17): L17801.

Bell, G.D. and Halpert, M.S., 1998. Climate assessment for 1997. Bulletin of the American Meteorological Society, **79**(5): S1-S50.

Bender, F.A.M., Ramanathan, V. and Tselioudis, G., 2012. Changes in extratropical storm track cloudiness 1983-2008: observational support for a poleward shift. Climate Dynamics, **38**(9-10): 2037-2053.
Bengtsson, L., Hagemann, S. and Hodges, K.I., 2004. Can climate trends be calculated from reanalysis data? Journal of Geophysical Research-Atmospheres, **109**(D11).
Bengtsson, L. and Hodges, K.I., 2011. On the evaluation of temperature trends in the tropical troposphere. Climate Dynamics, **36**(3-4): 419-430.
Beniston, M., 2009. Decadal-scale changes in the tails of probability distribution functions of climate variables in Switzerland. International Journal of Climatology, **29**(10): 1362-1368.
Bennartz, R., Fan, J.W., Rausch, J., Leung, L.R. and Heidinger, A.K., 2011. Pollution from China increases cloud droplet number, suppresses rain over the East China Sea. Geophys. Res. Lett., **38**.
Berg, W., L'Ecuyer, T. and Haynes, J.M., 2010. The distribution of rainfall over oceans from spaceborne radars. (vol 49, pg 535, 2010). Journal of Applied Meteorology and Climatology, **49**(5): 1063-1063.
Berry, D. and Kent, E., 2011. Air-Sea fluxes from ICOADS: the construction of a new gridded dataset with uncertainty estimates. International Journal of Climatology, **31**(7): 987-1001.
Berry, D.I. and E.C. Kent, 2009: A New Air-Sea Interaction Gridded Dataset from ICOADS with Uncertainty Estimates. Bulletin of the American Meteorological Society, 90(5), 645-656 (DOI: 10.1175/2008BAMS2639.1).
Berry, D.I., Kent, E.C. and Taylor, P.K., 2004. An analytical model of heating errors in marine air temperatures from ships. Journal of Atmospheric and Oceanic Technology, **21**(8): 1198-1215.
Berthet, C., Dessens, J. and Sanchez, J., 2011. Regional and yearly variations of hail frequency and intensity in France. Atmospheric Research, **100**(4): 391-400.
Birner, T., 2010. Recent widening of the tropical belt from global tropopause statistics: Sensitivities. Journal of Geophysical Research-Atmospheres, **115**.
Bitz, C.M. and Fu, Q., 2008. Arctic warming aloft is data set dependent. Nature, **455**(7210): E3-E4.
Black, E. and Sutton, R., 2007. The influence of oceanic conditions on the hot European summer of 2003. Climate Dynamics, **28**(1): 53-66.
Blunden, J., Arndt, D.S. and Baringer, M.O., 2011. State of the Climate in 2010. Bulletin of the American Meteorological Society, **92**(6): S17-+.
Bohm, R., Jones, P.D., Hiebl, J., Frank, D., Brunetti, M. and Maugeri, M., 2010. The early instrumental warm-bias: a solution for long central European temperature series 1760-2007. Climatic Change, **101**(1-2): 41-67.
Bonisch, H., Engel, A., Curtius, J., Birner, T. and Hoor, P., 2009. Quantifying transport into the lowermost stratosphere using simultaneous in-situ measurements of SF6 and CO2. Atmospheric Chemistry and Physics, **9**(16): 5905-5919.
Bosilovich, M.G., Robertson, F.R. and Chen, J., 2011. Global Energy and Water Budgets in MERRA. J. Climate: in press.
Bottomley, M., Folland, C.K., Hsiung, J., Newell, R.E. and Parker, D.E., 1990. Global ocean surface temperature atlas "GOSTA", Meteorological Office, Bracknell, UK and Department of Earth, Atmospheric and Planetary Sciences, Massachusetts Institute of Technology, Cambridge, MA, USA.
Bourassa, M.A., Gille, S.T., Jackson, D.L., Roberts, J.B. and Wick, G.A., 2010. Ocean Winds and Turbulent Air-Sea Fluxes Inferred From Remote Sensing. Oceanography, **23**(4): 36-51.
Bousquet, P., 2011. Source attribution of the changes in atmospheric methane for 2006–2008. Atmos. Chem. Phys. Discuss., **10**: 27603-27630.
Brauer, M., Amann, M., Burnett, R.T., Cohen, A., Dentener, F., Ezzati, M., Henderson, S.B., Krzyzanowski, M., Martin, R.V., Van Dingenen, R., van Donkelaar, A. and Thurston, G.D., 2012. Exposure Assessment for Estimation of the Global Burden of Disease Attributable to Outdoor Air Pollution. Environmental Science & Technology, **46**(2): 652-660.
Brogniez, H., Roca, R. and Picon, L., 2009. Study of the Free Tropospheric Humidity Interannual Variability Using Meteosat Data and an Advection-Condensation Transport Model. Journal of Climate, **22**(24): 6773-6787.
Brohan, P., Allan, R., Freeman, J.E., Waple, A.M., Wheeler, D., Wilkinson, C. and Woodruff, S., 2009. MARINE OBSERVATIONS OF OLD WEATHER. Bulletin of the American Meteorological Society, **90**(2): 219-+.
Bronnimann, S., 2009. Early twentieth-century warming. Nature Geoscience, **2**(11): 735-736.
Bronnimann, S., Stickler, A., Griesser, T., Fischer, A.M., Grant, A., Ewen, T., Zhou, T.J., Schraner, M., Rozanov, E. and Peter, T., 2009. Variability of large-scale atmospheric circulation indices for the northern hemisphere during the past 100 years. Meteorologische Zeitschrift, **18**(4): 379-396.
Brooks, H.E. and Dotzek, N., 2008. The spatial distribution of severe convective storms and an analysis of their secular changes. In: H.F. Diaz and R.J. Murnane (Editors), Climate Extremes and Society. Cambridge University Press, Cambridge and New York, pp. 35-53.
Brown, R.D., 2000: Northern hemisphere snow cover variability and change, 1915-97. J. Clim., 13, 2339–2355.
Brown, P.J., Bradley, R.S. and Keimig, F.T., 2010. Changes in Extreme Climate Indices for the Northeastern United States, 1870-2005. Journal of Climate, **23**(24): 6555-6572.
Brown, S.J., Caesar, J. and Ferro, C.A.T., 2008. Global changes in extreme daily temperature since 1950. Journal of Geophysical Research-Atmospheres, **113**(D5).

Brownscombe, J.L., Nash, J., Vaughan, G. and Rogers, C.F., 1985. SOLAR TIDES IN THE MIDDLE ATMOSPHERE .1. DESCRIPTION OF SATELLITE-OBSERVATIONS AND COMPARISON WITH THEORETICAL CALCULATIONS AT EQUINOX. Quarterly Journal of the Royal Meteorological Society, **111**(469): 677-689.

Brunet, M., Asin, J., Sigro, J., Banon, M., Garcia, F., Aguilar, E., Palenzuela, J.E., Peterson, T.C. and Jones, P., 2011. The minimization of the screen bias from ancient Western Mediterranean air temperature records: an exploratory statistical analysis. International Journal of Climatology, **31**(12): 1879-1895.

Brunet, M. and Jones, P., 2011. Data rescue initiatives: bringing historical climate data into the 21st century. Climate Research, **47**(1-2): 29-40.

Bunge, L. and Clarke, A.J., 2009. A Verified Estimation of the El Nino Index Nino-3.4 since 1877. Journal of Climate, **22**(14): 3979-3992.

Burn, D.H. and Hesch, N.M., 2007. Trends in evaporation for the Canadian prairies. Journal of Hydrology, **336**(1-2): 61-73.

Butler, J., Montzka, S., Clarke, A., Lobert, J. and Elkins, J., 1998. Growth and distribution of halons in the atmosphere. Journal of Geophysical Research-Atmospheres, **103**(D1): 1503-1511.

Caesar, J., Alexander, L., Trewin, B., Tse-Ring, K., Sorany, L., Vuniyayawa, V., Keosavang, N., Shimana, A., Htay, M., Karmacharya, J., Jayasinghearachchi, D., Sakkamart, J., Soares, E., Hung, L., Thuong, L., Hue, C., Dung, N., Hung, P., Cuong, H., Cuong, N. and Sirabaha, S., 2011. Changes in temperature and precipitation extremes over the Indo-Pacific region from 1971 to 2005. International Journal of Climatology, **31**(6): 791-801.

Caesar, J., Alexander, L. and Vose, R., 2006. Large-scale changes in observed daily maximum and minimum temperatures: Creation and analysis of a new gridded data set. Journal of Geophysical Research-Atmospheres, **111**(D5).

Callaghan, J. and Power, S.B., 2011. Variability and decline in the number of severe tropical cyclones making land-fall over eastern Australia since the late nineteenth century. Climate Dynamics, **37**(3-4): 647-662.

Canada, 2012. Canadian Smog Science Assessment - Highlights and Key Messages., Environment Canada and Health Canada.

Cane, M.A., 1986. EL-NINO. Annual Review of Earth and Planetary Sciences, **14**: 43-70.

Cane, M.A., Zebiak, S.E. and Dolan, S.C., 1986. Experimental forecasts of El Nino. Nature, **321**(6073): 827-832.

Cao, Z.H., 2008. Severe hail frequency over Ontario, Canada: Recent trend and variability. Geophysical Research Letters, **35**(14).

Cardone, V.J., Greenwood, J.G. and Cane, M.A., 1990. ON TRENDS IN HISTORICAL MARINE WIND DATA. Journal of Climate, **3**(1): 113-127.

Carslaw, K.S., Boucher, O., Spracklen, D., Mann, G., Rae, J.G., Woodward, S. and Kumala, M., 2010. A review of natural aerosol interactions and feedbacks within the Earth System,. Atmospheric Chemistry and Physics, **10**: 1701-1737.

Casey, K.S., Brandon, T.B., Cornillon, P. and Evans, R., 2010. The Past, Present and Future of the AVHRR Pathfinder SST Program. In: V. Barale, J.F.R. Gower and L. Alberotanza (Editors), Oceanography from Space: Revisited. Springer.

Castellanos, P. and Boersma, K.F., 2012. Reductions in nitrogen oxides over Europe driven by environmental policy and economic recession. Sci. Rep., **2**.

CASTNET, 2010. Clean Air Status and Trends Network (CASTNET) 2008 Annual Report, US EPA.

Cavazos, T., Turrent, C. and Lettenmaier, D.P., 2008. Extreme precipitation trends associated with tropical cyclones in the core of the North American monsoon. Geophysical Research Letters, **35**(21).

Cermak, J., Wild, M., Knutti, R., Mishchenko, M.I. and Heidinger, A.K., 2010. Consistency of global satellite-derived aerosol and cloud data sets with recent brightening observations. Geophys. Res. Lett., **37**(21): L21704.

Chan, J.C.L. and Xu, M., 2009. Inter-annual and inter-decadal variations of landfalling tropical cyclones in East Asia. Part I: time series analysis. International Journal of Climatology, **29**(9): 1285-1293.

Chandler, R.E. and Scott, E.M., 2011. Statistical Methods for Trend Detection and Analysis in the Environmental Sciences. Wiley, Chichester.

Chang, E.K.M., 2007a. Assessing the increasing trend in Northern Hemisphere winter storm track activity using surface ship observations and a statistical storm track model. Journal of Climate, **20**(22): 5607-5628.

Chang, E.K.M., 2007b. Assessing the increasing trend in Northern Hemisphere winter storm track activity using surface ship observations and a statistical storm track model. Journal of Climate, **20**: 5607-5628.

Chang, E.K.M. and Guo, Y.J., 2007. Is the number of North Atlantic tropical cyclones significantly underestimated prior to the availability of satellite observations? Geophysical Research Letters, **34**(14).

Che, H.Z., Shi, G.Y., Zhang, X.Y., Arimoto, R., Zhao, J.Q., Xu, L., Wang, B. and Chen, Z.H., 2005. Analysis of 40 years of solar radiation data from China, 1961-2000. Geophysical Research Letters, **32**(6): L06803.

Chen, J.Y., Carlson, B.E. and Del Genio, A.D., 2002. Evidence for strengthening of the tropical general circulation in the 1990s. Science, **295**(5556): 838-841.

Chen, J.Y., Del Genio, A.D., Carlson, B.E. and Bosilovich, M.G., 2008. The spatiotemporal structure of twentieth-century climate variations in observations and reanalyses. Part I: Long-term trend. Journal of Climate, **21**(11): 2611-2633.

Chiacchio, M. and Wild, M., 2010. Influence of NAO and clouds on long-term seasonal variations of surface solar radiation in Europe. Journal of Geophysical Research-Atmospheres, **115**: D00d22.

Choi, G., Collins, D., Ren, G.Y., Trewin, B., Baldi, M., Fukuda, Y., Afzaal, M., Pianmana, T., Gomboluudev, P., Huong, P.T.T., Lias, N., Kwon, W.T., Boo, K.O., Cha, Y.M. and Zhou, Y.Q., 2009. Changes in means and extreme events of temperature and precipitation in the Asia-Pacific Network region, 1955-2007. International Journal of Climatology, **29**(13): 1906-1925.

Christy, J.R., Herman, B, Pielke, R., Klotzbach, P., McNider, R. T., Hnilo, J. J., Spencer, R. W., Chase, T., Douglass, D., 2010. What do observational datasets say about modeled tropospheric temperature trends since 1979?, Remote Sensing, pp. 2148-2169.

Christy, J.R. and Norris, W.B., 2006. Satellite and VIZ-radiosonde intercomparisons for diagnosis of nonclimatic influences. Journal of Atmospheric and Oceanic Technology, **23**(9): 1181-1194.

Christy, J.R. and Norris, W.B., 2009. Discontinuity Issues with Radiosonde and Satellite Temperatures in the Australian Region 1979-2006. Journal of Atmospheric and Oceanic Technology, **26**(3): 508-522.

Christy, J.R., Norris, W.B. and McNider, R.T., 2009. Surface Temperature Variations in East Africa and Possible Causes. Journal of Climate, **22**(12): 3342-3356.

Christy, J.R., Norris, W.B., Redmond, K. and Gallo, K.P., 2006. Methodology and results of calculating central california surface temperature trends: Evidence of human-induced climate change? Journal of Climate, **19**(4): 548-563.

Christy, J.R., Norris, W.B., Spencer, R.W. and Hnilo, J.J., 2007. Tropospheric temperature change since 1979 from tropical radiosonde and satellite measurements. Journal of Geophysical Research-Atmospheres, **112**(D6).

Christy, J.R., Parker, D.E., Brown, S.J., Macadam, I., Stendel, M. and Norris, W.B., 2001. Differential trends in tropical sea surface and atmospheric temperatures since 1979. Geophysical Research Letters, **28**(1): 183-186.

Christy, J.R. and Spencer, R.W., Submitted. Comment on "A bias in midtropospheric channel warm target factor on the NOAA-9 Microwave sounding Unit" by Po-Chedley and Fu, Journal of Atmospheric and Oceanic Technology.

Christy, J.R., Spencer, R.W. and Norris, W.B., 2011. The role of remote sensing in monitoring global bulk tropospheric temperatures. International Journal of Remote Sensing, **32**(3): 671-685.

Christy, J.R., Spencer, R.W., Norris, W.B., Braswell, W.D. and Parker, D.E., 2003. Error estimates of version 5.0 of MSU-AMSU bulk atmospheric temperatures. Journal of Atmospheric and Oceanic Technology, **20**(5): 613-629.

Chuang, H., Huang, X. and Minschwaner, K., 2010. Interannual variations of tropical upper tropospheric humidity and tropical rainy-region SST: Comparisons between models, reanalyses, and observations. Journal of Geophysical Research-Atmospheres, **115**: -.

Chung, E.S. and Soden, B.J., 2010. Investigating the Influence of Carbon Dioxide and the Stratosphere on the Long-Term Tropospheric Temperature Monitoring from HIRS. Journal of Applied Meteorology and Climatology, **49**(9): 1927-1937.

Chung, E.S., Yeomans, D. and Soden, B.J., 2010. An assessment of climate feedback processes using satellite observations of clear-sky OLR. Geophysical Research Letters, **37**.

Church, J.A., and N.J. White, 2011: Sea-Level Rise from the Late 19th to the Early 21st Century. Surveys in Geophysics 32(4-5), 585-602, DOI: 10.1007/s10712-011-9119-1 http://www.cmar.csiro.au/sealevel/sl_data_cmar.html

Church, J.A., and N.J. White, 2006: A 20th century acceleration in global sea-level rise. Geophys. Res. Lett., 33, L01602, doi:10.1029/2005GL024826.

Clain, G., Baray, J.L., Delmas, R., Diab, R., Leclair de Bellevue, J., Keckhut, P., Posny, F., Metzger, J.M. and Cammas, J.P., 2009. Tropospheric ozone climatology at two Southern Hemisphere tropical/subtropical sites, (Reunion Island and Irene, South Africa) from ozonesondes, LIDAR, and in situ aircraft measurements. Atmos. Chem. Phys., **9**(5): 1723-1734.

Clark, R.T., Brown, S.J. and Murphy, J.M., 2006. Modeling northern hemisphere summer heat extreme changes and their uncertainties using a physics ensemble of climate sensitivity experiments. Journal of Climate, **19**(17): 4418-4435.

Clement, A.C. and Soden, B., 2005. The sensitivity of the tropical-mean radiation budget. Journal of Climate, **18**(16): 3189-3203.

CMA, 2007. Atlas of China disastrous weather and climate, Chinese Meteorological Administration.

Cogley J.G. (2009): Geodetic and direct mass-balance measurements: comparison and joint analysis. Annals of Glaciology 50(50) 96-100.

Cohen, J., Barlow, M. and Saito, K., 2009. Decadal Fluctuations in Planetary Wave Forcing Modulate Global Warming in Late Boreal Winter. Journal of Climate, **22**(16): 4418-4426.

Cohn, T.A. and Lins, H.F., 2005. Nature's style: Naturally trendy. Geophysical Research Letters, **32**(23).

Coles, S., 2001. An Introduction to Statistical Modeling of Extreme Values. Springer-Verlag, Heidelberg, 208 pp.

Collaud Coen, M., Andrew, E., Asmi, A., Baltensperger, U., Bukowiecki, N., Day, D., Fiebig, M., Fjaera, A.M., Flentje, H., Hyvarinen, A., Jefferson, A., Jennings, S.G., Kouvarikis, G., Lihavainen, H., Lund Myhre, C., Malm, W.C., Mihalopoulos, N., Molenar, J.V., O'Dowd, C.O., Ogren, J., Schichtel, B.A., Sheridan, P., Virkkula, A., Weingartner, E., Weller, R. and Weingartner, E., 2012. Aerosol decadal trends (I): In-situ optical measurements at GAW and IMPROVE stations. submitted to ACP.

Comiso, J. 1999, updated 2008. Bootstrap Sea Ice Concentrations from NIMBUS-7 SMMR and DMSP SSM/I, 1979-2007. Boulder, Colorado USA: National Snow and Ice Data Center. Digital media. http://nsidc.org/data/nsidc-0079.html

Compo, G.P., Whitaker, J.S., Sardeshmukh, P.D., Matsui, N., Allan, R.J., Yin, X., Gleason, B.E., Vose, R.S., Rutledge, G., Bessemoulin, P., Brönnimann, S., Brunet, M., Crouthamel, R.I., Grant, A.N., Groisman, P.Y., Jones, P.D., Kruk, M., Kruger, A.C., Marshall, G.J., Maugeri, M., Mok, H.Y., Nordli, Ø., Ross, T.F., Trigo, R.M., Wang, X.L., Woodruff, S.D. and Worley, S.J., 2011. The Twentieth Century Reanalysis Project. Q. J. Roy. Meteorol. Soc., **137**: 1-28.

Cooper, O.R., 2012. Long-term ozone trends at rural ozone monitoring sites across the United States, 1990-2010, . manuscript submitted to J. Geophys. Res.

Cornes, R.C. and Jones, P.D., 2011a. An examination of storm activity in the northeast Atlantic region over the 1851-2003 period using the EMULATE gridded MSLP data series. Journal of Geophysical Research-Atmospheres, **116**.

Cornes, R.C. and Jones, P.D., 2011b. An examination of storm activity in the northeast Atlantic region over the 1851-2003 period using the EMULATE gridded MSLP data series. J. Geophys. Res.-Atmos., **116**.

Costa, A.C. and Soares, A., 2009. Trends in extreme precipitation indices derived from a daily rainfall database for the South of Portugal. International Journal of Climatology, **29**(13): 1956-1975.

Croci-Maspoli, M., Schwierz, C. and Davies, H.C., 2007a. Atmospheric blocking: space-time links to the NAO and PNA. Climate Dynamics, **29**: 713-725.

Croci-Maspoli, M., Schwierz, C. and Davies, H.C., 2007b. A multifaceted climatology of atmospheric blocking and its recent linear trend. Journal of Climate, **20**(4): 633-649.

Cunnold, D., Weiss, R., Prinn, R., Hartley, D., Simmonds, P., Fraser, P., Miller, B., Alyea, F. and Porter, L., 1997. GAGE/AGAGE measurements indicating reductions in global emissions of CCl3F and CCl2F2 in 1992-1994. Journal of Geophysical Research-Atmospheres, **102**(D1): 1259-1269.

Cutforth, H.W. and Judiesch, D., 2007. Long-term changes to incoming solar energy on the Canadian Prairie. Agricultural and Forest Meteorology, **145**(3-4): 167-175.

Dai, A., 2006. Recent climatology, variability, and trends in global surface humidity. Journal of Climate, **19**(15): 3589-3606.

Dai, A., 2011a. Characteristics and trends in various forms of the Palmer Drought Severity Index during 1900-2008. Journal of Geophysical Research-Atmospheres, **116**.

Dai, A., Qian, T.T., Trenberth, K.E. and Milliman, J.D., 2009. Changes in Continental Freshwater Discharge from 1948 to 2004. Journal of Climate, **22**(10): 2773-2792.

Dai, A., Trenberth, K.E. and Qian, T.T., 2004. A global dataset of Palmer Drought Severity Index for 1870-2002: Relationship with soil moisture and effects of surface warming. Journal of Hydrometeorology, **5**(6): 1117-1130.

Dai, A.G., 2011b. Drought under global warming: a review. Wiley Interdisciplinary Reviews-Climate Change, **2**(1): 45-65.

Dai, A.G., Wang, J.H., Thorne, P.W., Parker, D.E., Haimberger, L. and Wang, X.L.L., 2011. A New Approach to Homogenize Daily Radiosonde Humidity Data. Journal of Climate, **24**(4): 965-991.

Das, L., Annan, J.D., Hargreaves, J.C. and Emori, S., 2011. Centennial scale warming over Japan: are the rural stations really rural? Atmospheric Science Letters.

Davidson, E., 2009. The contribution of manure and fertilizer nitrogen to atmospheric nitrous oxide since 1860. Nature Geoscience, **2**(9): 659-662.

Davis, S.M. and Rosenlof, K.H., 2011. A multi-diagnostic intercomparison of tropical width time series using reanalyses and satellite observations. J. Climate: doi: http://dx.doi.org/10.1175/JCLI-D-11-00127.1.

De Laat, A.T.J. and Maurellis, A.N., 2006. Evidence for influence of anthropogenic surface processes on lower tropospheric and surface temperature trends. International Journal of Climatology, **26**(7): 897-913.

de los Milagros Skansi, M., Brunet, M. and al., e., 2012. Warming and wetting signals emerging from an analysis of changes in climate extreme indices over South America. Submitted to Global and Planetary change.

de Meij, A., Pozzer, A. and Lelieveld, J., 2012. Trend analysis in aerosol optical depths and pollutant emission estimates between 2000 and 2009. Atmospheric Environment, **51**: 75-85.

Dee, D.P., Uppala, S.M., Simmons, A.J., Berrisford, P., Poli, P., Kobayashi, S., Andrae, U., Balmaseda, M.A., Balsamo, G., Bauer, P., Bechtold, P., Beljaars, A.C.M., van de Berg, L., Bidlot, J., Bormann, N., Delsol, C., Dragani, R., Fuentes, M., Geer, A.J., Haimberger, L., Healy, S.B., Hersbach, H., Holm, E.V., Isaksen, L., Kallberg, P., Kohler, M., Matricardi, M., McNally, A.P., Monge-Sanz, B.M., Morcrette, J.J., Park, B.K., Peubey, C., de Rosnay, P., Tavolato, C., Thepaut, J.N. and Vitart, F., 2011. The ERA-Interim reanalysis: configuration and performance of the data assimilation system. Quarterly Journal of the Royal Meteorological Society, **137**(656): 553-597.

Deeds, D., Vollmer, M., Kulongoski, J., Miller, B., Muhle, J., Harth, C., Izbicki, J., Hilton, D. and Weiss, R., 2008. Evidence for crustal degassing of CF4 and SF6 in Mojave Desert groundwaters. Geochimica Et Cosmochimica Acta: 999-1013.

DeGaetano, A.T., 2009. Time-Dependent Changes in Extreme-Precipitation Return-Period Amounts in the Continental United States. Journal of Applied Meteorology and Climatology, **48**(10): 2086-2099.

Delgado, J.M., Apel, H. and Merz, B., 2010. Flood trends and variability in the Mekong river. Hydrology and Earth System Sciences, **14**(3): 407-418.

Della-Marta, P.M., Haylock, M.R., Luterbacher, J. and Wanner, H., 2007a. Doubled length of western European summer heat waves since 1880. Journal of Geophysical Research-Atmospheres, **112**(D15).

Della-Marta, P.M., Luterbacher, J., von Weissenfluh, H., Xoplaki, E., Brunet, M. and Wanner, H., 2007b. Summer heat waves over western Europe 1880-2003, their relationship to large-scale forcings and predictability. Climate Dynamics, **29**(2-3): 251-275.

Della-Marta, P.M., Mathis, H., Frei, C., Liniger, M.A., Kleinn, J. and Appenzeller, C., 2009. The return period of wind storms over Europe. International Journal of Climatology, **29**(3): 437-459.

Deser, C., Alexander, M.A., Xie, S.P. and Phillips, A.S., 2010a. Sea Surface Temperature Variability: Patterns and Mechanisms. Annual Review of Marine Science, **2**: 115-143.

Deser, C., Phillips, A.S. and Alexander, M.A., 2010b. Twentieth century tropical sea surface temperature trends revisited. Geophysical Research Letters, **37**.

Dessler, A.E., Zhang, Z. and Yang, P., 2008. Water-vapor climate feedback inferred from climate fluctuations, 2003-2008. Geophysical Research Letters, **35**(20).

Diffenbaugh, N.S., Pal, J.S., Giorgi, F. and Gao, X.J., 2007. Heat stress intensification in the Mediterranean climate change hotspot. Geophysical Research Letters, **34**(11).

Ding, A.J., Wang, T., Thouret, V., Cammas, J.P. and NÃ©dÃ©lec, P., 2008. Tropospheric ozone climatology over Beijing: analysis of aircraft data from the MOZAIC program. Atmos. Chem. Phys., **8**(1): 1-13.

Ding, T., Qian, W.H. and Yan, Z.W., 2010. Changes in hot days and heat waves in China during 1961-2007. International Journal of Climatology, **30**(10): 1452-1462.

Ding, Y.H., Ren, G.Y., Zhao, Z.C., Xu, Y., Luo, Y., Li, Q.P. and Zhang, J., 2007. Detection, causes and projection of climate change over China: An overview of recent progress. Advances in Atmospheric Sciences, **24**(6): 954-971.

Dlugokencky, E., Bruhwiler, L., White, J., Emmons, L., Novelli, P., Montzka, S., Masarie, K., Lang, P., Crotwell, A., Miller, J. and Gatti, L., 2009. Observational constraints on recent increases in the atmospheric CH4 burden. Geophysical Research Letters: -.

Dlugokencky, E., Myers, R., Lang, P., Masarie, K., Crotwell, A., Thoning, K., Hall, B., Elkins, J. and Steele, L., 2005. Conversion of NOAA atmospheric dry air CH4 mole fractions to a gravimetrically prepared standard scale. Journal of Geophysical Research-Atmospheres, **110**(D18).

Dlugokencky, E., Nisbet, E., Fisher, R. and Lowry, D., 2011. Global atmospheric methane: budget, changes and dangers. Philosophical Transactions of the Royal Society a-Mathematical Physical and Engineering Sciences, **369**(1943): 2058-2072.

Dole, R., Hoerling, M., Perlwitz, J., Eischeid, J., Pegion, P., Zhang, T., Quan, X.W., Xu, T.Y. and Murray, D., 2011. Was there a basis for anticipating the 2010 Russian heat wave? Geophysical Research Letters, **38**.

Domingues C.M., J.A. Church, N.J. White, P.J. Gleckler, S.E. Wijffels, P.M. Barker and J.R. Dunn, 2008. Improved estimates of upper-ocean warming and multi-decadal sea-level rise, Nature 453 1090-1093, doi:10.1038/nature07080 http://www.cmar.csiro.au/sealevel/sl_data_cmar.html

Donat, M.G., Alexander, L., Yang, H., Durre, I., Vose, R., Dunn, R., Willett, K., Aguilar, E., Brunet, M., Caesar, J., Hewitson, B., Tank, A.K., Kruger, A., Marengo, J., Peterson, T., Renom, M., Rojas, C.O., Rusticucci, M., Salinger, J., Sekele, S., Srivastava, A., Trewin, B., Villarroel, C., Vincent, L., Zhai, P., Zhang, X. and Kitching, S., 2012a. Updated analyses of temperature and precipitation extreme indices since the beginning of the twentieth century: The HadEX2 dataset. submitted to JGR-Atmospheres.

Donat, M.G. and Alexander, L.V., 2012. The shifting probability distribution of global daytime and night-time temperatures. *Geophysical Research Letters*, Accepted 13th Jun 2012.

Donat, M.G., Alexander, L.V., Yang, H., Durre, I., Vose, R. and Caesar, J., 2012b. Global land-based datasets for monitoring climatic extremes. *Bulletin of the American Meteorological Society*, submitted 18th July 2012.

Donat, M.G., Peterson, T. and al., e., 2012c. Changes of extreme temperature and precipitation in the Arab region: long-term trends and variability related to ENSO and NAO. Submitted to International Journal of Climatology.

Donat, M.G., Renggli, D., Wild, S., Alexander, L.V., Leckebusch, G.C. and Ulbrich, U., 2011. Reanalysis suggests long-term upward trends in European storminess since 1871. Geophysical Research Letters, **38**.

Dong, L., Vogelsang, T.J. and Colucci, S.J., 2008. Interdecadal trend and ENSO-related interannual variability in Southern Hemisphere blocking. Journal of Climate, **21**(12): 3068-3077.

Donlon, C., Robinson, I., Casey, K.S., Vazquez-Cuervo, J., Armstrong, E., Arino, O., Gentemann, C., May, D., LeBorgne, P., Piolle, J., Barton, I., Beggs, H., Poulter, D.J.S., Merchant, C.J., Bingham, A., Heinz, S., Harris, A., Wick, G., Emery, B., Minnett, P., Evans, R., Llewellyn-Jones, D., Mutlow, C., Reynolds, R.W., Kawamura, H. and Rayner, N., 2007. The global ocean data assimilation experiment high-resolution sea surface temperature pilot project. Bulletin of the American Meteorological Society, **88**(8): 1197-1213.

Doswell, C., Brooks, H. and Dotzek, N., 2009. On the implementation of the enhanced Fujita scale in the USA. Atmospheric Research, **93**(1-3): 554-563.

Douglass, A., Fioletov, V.E.C.L.A., S. Godin-Beekmann, R. Müller, R. Stolarski, A. Webb, A. Arola, J. Burkholder, J. Burrows, M. Chipperfield, J. V. Canossa, R. Cordero, C, D., P. den Outer, S. Diaz, L. Flynn, M. Hegglin, J. Herman, P. Huck, S. Janjai, I. Janosi, J. Krzyscin, Y. Liu, J. Logan, R. McKenzie, K. Matthes, N. J. Muthama, I. Petropavlovskikh, M. Pitts, S. Ramachandran, M. Rex, R. Salawitch, B.-M. Sinnhuber, J. Staehelin, S. Strahan, K. Tourpali and C. Vigouroux, 2011. W MO/UNEP Scientific Assessment of Ozone Depletion: 2010, Chapter 2 Stratospheric Ozone and Surface Ultraviolet Radiation World Meteorological Organisation, Geneva.

Douglass, A., Stolarski, R., Schoeberl, M., Jackman, C., Gupta, M., NeW man, P., Nielsen, J. and Fleming, E., 2008. Relationship of loss, mean age of air and the distribution of CFCs to stratospheric circulation and implications for atmospheric lifetimes. Journal of Geophysical Research-Atmospheres: -.

Du, Y. and Xie, S., 2008. Role of atmospheric adjustments in the tropical Indian Ocean warming during the 20th century in climate models. Geophysical Research Letters, **35**(8): -.

Du, Y., Xie, S., Huang, G. and Hu, K., 2009. Role of Air-Sea Interaction in the Long Persistence of El Nino-Induced North Indian Ocean Warming. Journal of Climate, **22**(8): 2023-2038.

Duan, A.M. and Wu, G.X., 2006. Change of cloud amount and the climate warming on the Tibetan Plateau. Geophysical Research Letters, **33**(22).

Dufek, A.S. and Ambrizzi, T., 2008. Precipitation variability in Sao Paulo State, Brazil. Theoretical and Applied Climatology, **93**(3-4): 167-178.

Durao, R.M., Pereira, M.J., Costa, A.C., Delgado, J., del Barrio, G. and Soares, A., 2010. Spatial-temporal dynamics of precipitation extremes in southern Portugal: a geostatistical assessment study. International Journal of Climatology, **30**(10): 1526-1537.

Durre, I., Menne, M.J., Gleason, B.E., Houston, T.G. and Vose, R.S., 2010. Comprehensive Automated Quality Assurance of Daily Surface Observations. Journal of Applied Meteorology and Climatology, **49**(8): 1615-1633.

Durre, I., Williams, C.N., Yin, X.G. and Vose, R.S., 2009. Radiosonde-based trends in precipitable water over the Northern Hemisphere: An update. Journal of Geophysical Research-Atmospheres, **114**.

Dutton, E.G., and Bodhaine, B.A., 2001. Solar irradiance anomalies caused by clear-sky transmission variations above Mauna Loa: 1958-99. Journal of Climate, **14**(15): 3255-3262.

Dutton, E.G., Nelson, D.W., Stone, R.S., Longenecker, D., Carbaugh, G., Harris, J.M. and Wendell, J., 2006. Decadal variations in surface solar irradiance as observed in a globally remote network. Journal of Geophysical Research-Atmospheres, **111**(D19): D19101.

EANET, 2011. EANET Data Report on the Acid Deposition in the East Asian Region 2009.

Easterling, D. and Wehner, M., 2009. Is the climate warming or cooling? Geophysical Research Letters: -.

Eastman, R., Warren, S.G. and Hahn, C.J., submitted. Variations in cloud cover and cloud types over the ocean from surface observations, 1954-2008. J. Climate.

Eccel, E., Cau, P., Riemann-Campe, K. and Biasioli, F., 2012. Quantitative hail monitoring in an alpine area: 35-year climatology and links with atmospheric variables. International Journal of Climatology, **32**(4): 503-517.

Efthymiadis, D., Goodess, C.M. and Jones, P.D., 2011. Trends in Mediterranean gridded temperature extremes and large-scale circulation influences. Natural Hazards and Earth System Sciences, **11**(8): 2199-2214.

Efthymiadis, D.A. and Jones, P.D., 2010. Assessment of Maximum Possible Urbanization Influences on Land Temperature Data by Comparison of Land and Marine Data around Coasts. Atmosphere, **1**: 51-61.

Elkins, J.W. and Dutton, G.S., 2011. Nitrous oxide and sulfur hexaflouride. *Bulletin of the American Meteorological Society*, **92**(6): 2.

Ellis, T.D., L'Ecuyer, T., Haynes, J.M. and Stephens, G.L., 2009. How often does it rain over the global oceans? The perspective from CloudSat. Geophysical Research Letters, **36**.

Elsner, J.B., Kossin, J.P. and Jagger, T.H., 2008. The increasing intensity of the strongest tropical cyclones. Nature, **455**(7209): 92-95.

Emanuel, K., 2007. Environmental factors affecting tropical cyclone power dissipation. Journal of Climate, **20**: 5497-5509.

Embury, O. and Merchant, C.J., 2011. Reprocessing for Climate of Sea Surface Temperature from the Along-Track Scanning Radiometers: A New Retrieval Scheme. Remote Sensing Environment.

Embury, O., Merchant, C.J. and Corlett, G.K., 2011. A reprocessing for Climate of Sea Surface Temperature from the Along-Track Scanning Radiometers: Preliminary validation, accounting for skin and diurnal variability. Remote Sensing Environment.

EMEP, 2010. EMEP Status report 4/2010, Transboundary Particulate Matter in Europe.

EMEP, 2011. Transboundary particulate matter in Europe, Status Report 4/2011.

Emery, W.J., Baldwin, D.J., Schlussel, P. and Reynolds, R.W., 2001. Accuracy of in situ sea surface temperatures used to calibrate infrared satellite measurements. Journal of Geophysical Research-Oceans, **106**(C2): 2387-2405.

Endo, N. and Yasunari, T., 2006. Changes in low cloudiness over China between 1971 and 1996. Journal of Climate, **19**(7): 1204-1213.

Enfield, D.B., Mestas-Nunez, A.M. and Trimble, P.J., 2001. The Atlantic multidecadal oscillation and its relation to rainfall and river flows in the continental US. Geophysical Research Letters, **28**(10): 2077-2080.

Engel, A., Mobius, T., Bonisch, H., Schmidt, U., Heinz, R., Levin, I., Atlas, E., Aoki, S., Nakazawa, T., Sugawara, S., Moore, F., Hurst, D., Elkins, J., Schauffler, S., Andrews, A. and Boering, K., 2009. Age of stratospheric air unchanged within uncertainties over the past 30 years. Nature Geoscience, **2**(1): 28-31.

Etheridge, D., Steele, L., Francey, R. and Langenfelds, R., 1998. Atmospheric methane between 1000 AD and present: Evidence of anthropogenic emissions and climatic variability. Journal of Geophysical Research-Atmospheres: 15979-15993.

Etheridge, D.M., Steele, L.P., Langenfelds, R.L., Francey, R.J., Barnola, J.M. and Morgan, V.I., 1996. Natural and anthropogenic changes in atmospheric CO2 over the last 1000 years from air in Antarctic ice and firn. Journal of Geophysical Research-Atmospheres: 4115-4128.

Evan, A.T., Heidinger, A.K. and Vimont, D.J., 2007. Arguments against a physical long-term trend in global ISCCP cloud amounts. Geophysical Research Letters, **34**(4): L04701.

Evans, W.F.J. and Puckrin, E., 1995. An observation of the greenhouse radiation associated with carbon monoxide. Geophys. Res. Lett., **22**(8): 925-928.

Fall, S., Niyogi, D., Gluhovsky, A., Pielke, R.A., Kalnay, E. and Rochon, G., 2010. Impacts of land use land cover on temperature trends over the continental United States: assessment using the North American Regional Reanalysis. International Journal of Climatology, **30**(13): 1980-1993.

Fall, S., Watts, A., Nielsen-Gammon, J., Jones, E., Niyogi, D., Christy, J.R. and Pielke, R.A., 2011. Analysis of the impacts of station exposure on the US Historical Climatology Network temperatures and temperature trends. Journal of Geophysical Research-Atmospheres, **116**.

Favre, A. and Gershunov, A., 2006. Extra-tropical cyclonic/anticyclonic activity in North-Eastern Pacific and air temperature extremes in Western North America. Climate Dynamics, **26**(6): 617-629.

Feng, S. and Hu, Q., 2007. Changes in winter snowfall/precipitation ratio in the contiguous United States. Journal of Geophysical Research-Atmospheres, **112**(D15).

Ferguson, C.R. and Villarini, G., 2012. Detecting inhomogeneities in the Twentieth Century Reanalysis over the central United States. Journal of Geophysical Research-Atmospheres, **117**.

Ferguson, C.R. and Villarini, G., Submitted. Suitability of the Twentieth Century Reanalysis for climate change assessment, Climate Dynamics.

Ferranti, L. and Viterbo, P., 2006. The European summer of 2003: Sensitivity to soil water initial conditions. Journal of Climate: 3659-3680.

Ferretti, D., Miller, J., White, J., Etheridge, D., Lassey, K., Lowe, D., Meure, C., Dreier, M., Trudinger, C., van Ommen, T. and Langenfelds, R., 2005. Unexpected changes to the global methane budget over the past 2000 years. Science: 1714-1717.

Fetterer, F., K. Knowles, W. Meier, and M. Savoie. 2002, updated 2009. Sea Ice Index. Boulder, Colorado USA: National Snow and Ice Data Center. Digital media.
http://nsidc.org/data/docs/noaa/g02135_seaice_index/index.html
ftp://sidads.colorado.edu/DATASETS/NOAA/G02135/Sep/

Fischer, E.M. and Schar, C., 2010. Consistent geographical patterns of changes in high-impact European heatwaves. Nature Geoscience, **3**(6): 398-403.

Fischer, E.M., Seneviratne, S.I., Vidale, P.L., Luthi, D. and Schar, C., 2007. Soil moisture - Atmosphere interactions during the 2003 European summer heat wave. Journal of Climate, **20**(20): 5081-5099.

Foelsche, U., Pirscher, B., Borsche, M., Kirchengast, G. and Wickert, J., 2009. Assessing the Climate Monitoring Utility of Radio Occultation Data: From CHAMP to FORMOSAT-3/COSMIC. Terrestrial Atmospheric and Oceanic Sciences, **20**(1): 155-170.

Fogt, R.L., Perlwitz, J., Monaghan, A.J., Bromwich, D.H., Jones, J.M. and Marshall, G.J., 2009. Historical SAM Variability. Part II: Twentieth-Century Variability and Trends from Reconstructions, Observations, and the IPCC AR4 Models. Journal of Climate, **22**(20): 5346-5365.

Folland, C.K., Knight, J., Linderholm, H.W., Fereday, D., Ineson, S. and Hurrell, J.W., 2009. The Summer North Atlantic Oscillation: Past, Present, and Future. Journal of Climate, **22**(5): 1082-1103.

Folland, C.K. and Parker, D.E., 1995. CORRECTION OF INSTRUMENTAL BIASES IN HISTORICAL SEA-SURFACE TEMPERATURE DATA. Quarterly Journal of the Royal Meteorological Society, **121**(522): 319-367.

Folland, C.K., Parker, D.E., Colman, A. and R., W., 1999. Large scale modes of ocean surface temperature since the late nineteenth century. In: A. Navarra (Editor), Beyond El Nino: Decadal and Interdecadal Climate Variability. Springer-Verlag, Berlin, pp. 73-102.

Forster, P.M., Thompson, D.W.J., Baldwin, M.P., Chipperfield, M.P., Dameris, M., Haigh, J.D., Karoly, D.J., Kushner, P.J., Randel, W.J., Rosenlof, K.H., Seidel, D.J., Solomon, S., Beig, G., Braesicke, P., Butchart, N., Gillett, N.P., Grise, K.M., Marsh, D.R., McLandress, C., Rao, T.N., Son, S.-W., Stenchikov, G.L. and Yoden, S., 2011. Stratospheric changes and climate, Chapter 4 in Scientific Assessment of Ozone Depletion: 2010, World Meteorological Organization, Geneva.

Fortems-Cheiney, A., Chevallier, F., Pison, I., Bousquet, P., Szopa, S., Deeter, M.N. and Clerbaux, C., 2011. Ten years of CO emissions as seen from Measurements of Pollution in the Troposphere (MOPITT). J. Geophys. Res., **116**(D5): D05304.

Fraser, P., Cunnold, D., Alyea, F., Weiss, R., Prinn, R., Simmonds, P., Miller, B. and Langenfelds, R., 1996. Lifetime and emission estimates of 1,1,2-trichlorotrifluorethane (CFC-113) from daily global background observations June 1982 June 1994. Journal of Geophysical Research-Atmospheres, **101**(D7): 12585-12599.

Frauenfeld, O.W. and Davis, R.E., 2003. Northern Hemisphere circumpolar vortex trends and climate change implications. Journal of Geophysical Research-Atmospheres, **108**(D14).

Frederiksen, J.S. and Frederiksen, C.S., 2007. Interdecadal changes in southern hemisphere winter storm track modes. Tellus Series a-Dynamic Meteorology and Oceanography, **59**(5): 599-617.

Free, M. and Seidel, D.J., 2007. Comments on "biases in stratospheric and tropospheric temperature trends derived from historical radiosonde data". Journal of Climate, **20**(14): 3704-3709.

Free, M., Seidel, D.J., Angell, J.K., Lanzante, J., Durre, I. and Peterson, T.C., 2005. Radiosonde Atmospheric Temperature Products for Assessing Climate (RATPAC): A new data set of large-area anomaly time series. Journal of Geophysical Research-Atmospheres, **110**(D22).

Fu, G.B., Charles, S.P. and Yu, J.J., 2009a. A critical overview of pan evaporation trends over the last 50 years. Climatic Change, **97**(1-2): 193-214.

Fu, G.B., Charles, S.P., Yu, J.J. and Liu, C.M., 2009b. Decadal Climatic Variability, Trends, and Future Scenarios for the North China Plain. Journal of Climate, **22**(8): 2111-2123.

Fu, Q., Johanson, C.M., Wallace, J.M. and Reichler, T., 2006. Enhanced mid-latitude tropospheric warming in satellite measurements. Science, **312**(5777): 1179-1179.

Fu, Q., Johanson, C.M., Warren, S.G. and Seidel, D.J., 2004. Contribution of stratospheric cooling to satellite-inferred tropospheric temperature trends. Nature, **429**(6987): 55-58.

Fu, Q. and Lin, P., 2011. Poleward shift of subtropical jets inferred from satellite-observed lower stratospheric temperatures. J. Climate, **24**: 5597-5603.

Fueglistaler, S. and Haynes, P.H., 2005. Control of interannual and longer-term variability of stratospheric water vapor. Journal of Geophysical Research-Atmospheres, **110**(D24).

Fujibe, F., 2009. Detection of urban warming in recent temperature trends in Japan. International Journal of Climatology, **29**(12): 1811-1822.

Fujiwara, M., Vomel, H., Hasebe, F., Shiotani, M., Ogino, S.Y., Iwasaki, S., Nishi, N., Shibata, T., Shimizu, K., Nishimoto, E., Canossa, J.M.V., Selkirk, H.B. and Oltmans, S.J., 2010. Seasonal to decadal variations of water vapor in the tropical lower stratosphere observed with balloon-borne cryogenic frost point hygrometers. Journal of Geophysical Research-Atmospheres, **115**.

Fyfe, J.C., 2003. Extratropical southern hemisphere cyclones: Harbingers of climate change? Journal of Climate, **16**(17): 2802-2805.

G., L., Y., M.H., C., L.T. and al., e., 2011. Scaling and trends of hourly precipitation extremes in two different climate zones - Hong Kong and the Netherlands. HYDROLOGY AND EARTH SYSTEM SCIENCES, **15**(9): 3033-3041.

Gallant, A.J.E., Hennessy, K.J. and Risbey, J., 2007. Trends in rainfall indices for six Australian regions: 1910-2005. Australian Meteor. Mag., **56**(4): 223-239.

Garcia-Herrera, R., Diaz, J., Trigo, R.M., Luterbacher, J. and Fischer, E.M., 2010. A Review of the European Summer Heat Wave of 2003. Critical Reviews in Environmental Science and Technology, **40**(4): 267-306.

Geng, Q.Z. and Sugi, M., 2001. Variability of the North Atlantic cyclone activity in winter analyzed from NCEP-NCAR reanalysis data. Journal of Climate, **14**(18): 3863-3873.

Gentemann, C., Wentz, F., Mears, C. and Smith, D., 2004. In situ validation of Tropical Rainfall Measuring Mission microwave sea surface temperatures. Journal of Geophysical Research-Oceans, **109**(C4).

Gettelman, A. and Fu, Q., 2008. Observed and simulated upper-tropospheric water vapor feedback. Journal of Climate, **21**(13): 3282-3289.

Gilgen, H., Roesch, A., Wild, M. and Ohmura, A., 2009. Decadal changes in shortwave irradiance at the surface in the period from 1960 to 2000 estimated from Global Energy Balance Archive Data. Journal of Geophysical Research-Atmospheres, **114**: D00d08.

Gillett, N.P. and Stott, P.A., 2009. Attribution of anthropogenic influence on seasonal sea level pressure. Geophysical Research Letters, **36**.

Giorgi, F. and Francisco, R., 2000. Evaluating uncertainties in the prediction of regional climate change. Geophysical Research Letters, **27**(9): 1295-1298.

Giorgi, F., Im, E.S., Coppola, E., Diffenbaugh, N.S., Gao, X.J., Mariotti, L. and Shi, Y., 2011. Higher Hydroclimatic Intensity with Global Warming. Journal of Climate, **24**(20): 5309-5324.

Gleason, K.L., Lawrimore, J.H., Levinson, D.H., Karl, T.R. and Karoly, D.J., 2008. A revised US Climate Extremes Index. Journal of Climate, **21**(10): 2124-2137.

Gong, D.Y. and Ho, C.H., 2002. The Siberian High and climate change over middle to high latitude Asia. Theor. Appl. Climatology, **72**(1-2): 1-9.

Gong, D.Y. and Wang, S.W., 1999. Definition of Antarctic Oscillation Index. Geophysical Research Letters, **26**(4): 459-462.

Gornitz V, Lebedeff S. 1987. Global sea-level changes during the past century. In Sea-level Fluctuation and Coastal Evolution, Nummedal D, Pilkey OH, Howard JD (eds). The Society for Sedimentary Geology: Tulsa, Oklahoma; 3–16, (SEPM Special Publication No.41).(1987)

Gouretski V. and F. Reseghetti 2010. On depth and temperature biases in bathythermograph data: development of a new correction scheme based on the analysis of global ocean data. Deep Sea Res. **57**, 812-833.

Gouretski, V., Kennedy, J., Boyer, T. and Kohl, A., Submitted. Consistent nesr-surface ocean warming since 1900 in two largely independent observing networks, Geophysical Research Letters.

Graham, N.E. and Diaz, H.F., 2001. Evidence for intensification of North Pacific winter cyclones since 1948. Bulletin of the American Meteorological Society, **82**(9): 1869-1893.

Grant, A.N., Bronnimann, S. and Haimberger, L., 2008. Recent Arctic warming vertical structure contested. Nature, **455**(7210): E2-E3.

Grant Foster and Stefan, R., 2011. Global temperature evolution 1979–2010. Environmental Research Letters, **6**(4): 044022.

Graversen, R.G., Mauritsen, T., Tjernstrom, M., Kallen, E. and Svensson, G., 2008. Vertical structure of recent Arctic warming. Nature, **451**(7174): 53-U4.

Greally, B., Manning, A., Reimann, S., McCulloch, A., Huang, J., Dunse, B., Simmonds, P., Prinn, R., Fraser, P., Cunnold, D., O'Doherty, S., Porter, L., Stemmler, K., Vollmer, M., Lunder, C., Schmidbauer, N., Hermansen, O., Arduini, J., Salameh, P., Krummel, P., Wang, R., Folini, D., Weiss, R., Maione, M., Nickless, G., Stordal, F. and Derwent, R., 2007. Observations of 1,1-difluoroethane (HFC-152a) at AGAGE and SOGE monitoring stations in 1994-2004 and derived global and regional emission estimates. Journal of Geophysical Research-Atmospheres, **112**(D6): -.

Griffiths, G.M., Chambers, L.E., Haylock, M.R., Manton, M.J., Nicholls, N., Baek, H.J., Choi, Y., Della-Marta, P.M., Gosai, A., Iga, N., Lata, R., Laurent, V., Maitrepierre, L., Nakamigawa, H., Ouprasitwong, N., Solofa, D., Tahani, L., Thuy, D.T., Tibig, L., Trewin, B., Vediapan, K. and Zhai, P., 2005. Change in mean temperature as a predictor of extreme temperature change in the Asia-Pacific region. Int. J. Climatology, **25**(10): 1301-1330.

Grody, N.C., Vinnikov, K.Y., Goldberg, M.D., Sullivan, J.T. and Tarpley, J.D., 2004. Calibration of multisatellite observations for climatic studies: Microwave Sounding Unit (MSU). Journal of Geophysical Research-Atmospheres, **109**(D24).

Groisman, P., Knight, R., Karl, T.R., Easterling, D., Sun, B.M. and Lawrimore, J., 2004. Contemporary Changes of the Hydrological Cycle over the Contiguous United States: Trends Derived from In Situ Observations. Journal of Hydrometeorology, **5**(1): 64-85.

Gruber, C. and Haimberger, L., 2008. On the homogeneity of radiosonde wind time series. Meteorologische Zeitschrift, **17**(5): 631-643.

Gulev, S., Jung, T. and Ruprecht, E., 2007. Estimation of the impact of sampling errors in the VOS observations on air-sea fluxes. Part II: Impact on trends and interannual variability. Journal of Climate, **20**(2): 302-315.

Gulev, S.K., Zolina, O. and Grigoriev, S., 2001. Extratropical cyclone variability in the Northern Hemisphere winter from the NCEP/NCAR reanalysis data. Climate Dynamics, **17**(10): 795-809.

Guo, H., Xu, M. and Hub, Q., 2010. Changes in near-surface wind speed in China: 1969–2005. Int. J. Climatol.

Haarsma, R., Selten, F., Hurk, B., Hazeleger, W. and Wang, X., 2009. Drier Mediterranean soils due to greenhouse warming bring easterly winds over summertime central Europe. Geophysical Research Letters, **36**.

Haerter, J., Berg, P. and Hagemann, S., 2010. Heavy rain intensity distributions on varying time scales and at different temperatures. Journal of Geophysical Research-Atmospheres, **115**.

Haimberger, L., 2004. Checking the temporal homogeneity of radiosonde data in the Alpine region using ERA-40 analysis feedback data. Meteorologische Zeitschrift, **13**(2): 123-129.

Haimberger, L., 2007. Homogenization of radiosonde temperature time series using innovation statistics. Journal of Climate, **20**(7): 1377-1403.

Haimberger, L., Tavolato, C. and Sperka, S., 2008. Toward elimination of the warm bias in historic radiosonde temperature records - Some new results from a comprehensive intercomparison of upper-air data. Journal of Climate, **21**(18): 4587-4606.

Haimberger, L., Tavolato, C. and Sperka, S., 2012. Homogenization of the global radiosonde temperature dataset through combined comparison with reanalysis background series and neighboring stations. Journal of Climate.

Hajj, G.A., Ao, C.O., Iijima, B.A., Kuang, D., Kursinski, E.R., Mannucci, A.J., Meehan, T.K., Romans, L.J., Juarez, M.D. and Yunck, T.P., 2004. CHAMP and SAC-C atmospheric occultation results and intercomparisons. Journal of Geophysical Research-Atmospheres, **109**(D6).

Häkkinen, S., Rhines, P.B. and Worthen, D.L., 2011. Atmospheric Blocking and Atlantic Multidecadal Ocean variability. Science, **334**: 655-659.

Hall, B., Dutton, G. and Elkins, J., 2007. The NOAA nitrous oxide standard scale for atmospheric observations. Journal of Geophysical Research-Atmospheres, **112**(D9).

Hall, B., Dutton, G., Mondeel, D., Nance, J., Rigby, M., Butler, J., Moore, F., Hurst, D. and Elkins, J., 2011. Improving measurements of SF6 for the study of atmospheric transport and emissions. Atmospheric Measurement Techniques, **4**(11): 2441-2451.

Han, Y.M., Cao, J.J., Yan, B.Z., Kenna, T.C., Jin, Z.D., Cheng, Y., Chow, J.C. and An, Z.S., 2011. Comparison of Elemental Carbon in Lake Sediments Measured by Three Different Methods and 150-Year Pollution History in Eastern China. Environmental Science & Technology, **45**(12): 5287-5293.

Hand, J.L., S.A. Copeland, D.E. Day, A.M. Dillner, H. Indresand, W.C. Malm, C.E. McDade, C.T.Moore, J., M. L. Pitchford , B.A. Schichtel and Watson, J.G., 2011a. IMPROVE, Spatial and Seasonal Patterns and Temporal Variability of Haze and its Constituents in the United States.

Hand, J.L., S.A. Copeland, D.E. Day, A.M. Dillner, H. Indresand, W.C. Malm, C.E. McDade, C.T.Moore, J., M. L. Pitchford , B.A. Schichtel and Watson, J.G., 2011b. IMPROVE, Spatial and Seasonal Patterns and Temporal Variability of Haze and its Constituents in the United States,.

Hand, J.L., S.A. Copeland, D.E. Day, A.M. Dillner, H. Indresand, W.C. Malm, C.E. McDade, C.T.Moore, J., M. L. Pitchford , B.A. Schichtel and Watson, J.G., 2011c. IMPROVE, Spatial and Seasonal Patterns and Temporal Variability of Haze and its Constituents in the United States,.

Hanna, E., Cappelen, J., Allan, R., Jonsson, T., Le Blancq, F., Lillington, T. and Hickey, K., 2008. New Insights into North European and North Atlantic Surface Pressure Variability, Storminess, and Related Climatic Change since 1830. Journal of Climate, **21**(24): 6739-6766.

Hannaford, J. and Marsh, T., 2008. High-flow and flood trends in a network of undisturbed catchments in the UK. International Journal of Climatology, **28**(10): 1325-1338.

Hansen, J., R. Ruedy, M. Sato, and K. Lo, 2010: Global surface temperature change, Rev. Geophys., 48, RG4004, doi:10.1029/2010RG000345. Gridded data from: ftp://data.giss.nasa.gov/pub/gistemp/download_v3/

Hansen, J., Sato, M., Kharecha, P. and von Schuckmann, K., 2011. Earth's energy imbalance and implications. Atmospheric Chemistry and Physics, **11**(24): 13421-13449.

Harris, I., Jones, P.D., Osborn, T.J. and Lister, D.H., 2012. Updated high-resolution grids of monthly climatic observations - the CRU TS 3.1 Dataset. International Journal of Climatology, **Submitted**.

Hatzianastassiou, N., Matsoukas, C., Fotiadi, A., Pavlakis, K.G., Drakakis, E., Hatzidimitriou, D. and Vardavas, I., 2005. Global distribution of Earth's surface shortwave radiation budget. Atmospheric Chemistry and Physics, **5**: 2847-2867.

Hatzianastassiou, N., Papadimas, C.D., Matsoukas, C., Pavlakis, K., Fotiadi, A., Wild, M. and Vardavas, I., 2012. Recent regional surface solar radiation dimming and brightening patterns: inter-hemispherical asymmetry and a dimming in the Southern Hemisphere. Atmospheric Science Letters, **13**(1): 43-48.

Hausfather, Z., Menne, M.J., Williams, C.N., Masters, T., Broberg, R. and Jones, D., Submitted. Quantifying the Effect of Urbanization on U.S. Historical Climatology Network Temperature Records, Journal of Geophysical Research.

Haynes, J.M., L'Ecuyer, T.S., Stephens, G.L., Miller, S.D., Mitrescu, C., Wood, N.B. and Tanelli, S., 2009. Rainfall retrieval over the ocean with spaceborne W-band radar. Journal of Geophysical Research-Atmospheres, **114**.

He, W.Y., Ho, S.P., Chen, H.B., Zhou, X.J., Hunt, D. and Kuo, Y.H., 2009. Assessment of radiosonde temperature measurements in the upper troposphere and lower stratosphere using COSMIC radio occultation data. Geophysical Research Letters, **36**.

Heidinger, A.K. and Pavolonis, M.J., 2009. Gazing at Cirrus Clouds for 25 Years through a Split Window. Part I: Methodology. Journal of Applied Meteorology and Climatology, **48**(6): 1100-1116.

Held, I.M. and Soden, B.J., 2006. Robust responses of the hydrological cycle to global warming. Journal of Climate, **19**(21): 5686-5699.

Helmig, D., Oltmans, S.J., Carlson, D., Lamarque, J.-F., Jones, A., Labuschagne, C., Anlauf, K. and Hayden, K., 2007. A review of surface ozone in the polar regions. Atmospheric Environment, , **41,**: 5138–5161.

Hess, P.G. and Zbinden, R., 2011. Stratospheric impact on tropospheric ozone variability and trends: 1990–2009. Atmos. Chem. Phys. Discuss., **11**(8): 22719-22770.

Hidy, G.M. and Pennell, G.T., 2010. Multipollutant Air Quality Management: 2010 Critical Review. J. Air & Waste Management Assocciation, **60,** DOI:10.3155/1047-3289.60.6.645: 645–674.

Hinkelman, L.M., Stackhouse, P.W., Wielicki, B.A., Zhang, T.P. and Wilson, S.R., 2009. Surface insolation trends from satellite and ground measurements: Comparisons and challenges. Journal of Geophysical Research-Atmospheres, **114**: D00d20.

Hirdman, D., Burkhart, J.F., Sodemann, H., Eckhardt, S., Jefferson, A., Quinn, P.K., Sharma, S., Strom, J. and Stohl, A., 2010. Long-term trends of black carbon and sulphate aerosol in the Arctic: changes in atmospheric transport and source region emissions. Atmos. Chem. Phys., **10**(19): 9351-9368.

Hirsch, M.E., DeGaetano, A.T. and Colucci, S.J., 2001. An East Coast winter storm climatology. Journal of Climate, **14**(5): 882-899.

Hirschi, M., Seneviratne, S.I., Alexandrov, V., Boberg, F., Boroneant, C., Christensen, O.B., Formayer, H., Orlowsky, B. and Stepanek, P., 2011. Observational evidence for soil-moisture impact on hot extremes in southeastern Europe. Nature Geoscience, **4**(1): 17-21.

Ho, S.-P., Hunt, D., Steiner, A.K., Mannucci, A.J., Kirchengast, G., Gleisner, H., Heise, S., von Engeln, A., Marquardt, C., Sokolovskiy, S., Schreiner, W., Scherllin-Pirscher, B., Ao, C., Wickert, J., Syndergaard, S., Lauritsenn, K.B., Leroy, S., Kursinski, E.R., Kuo, Y.-H., Foelsche, U., Schmidt, T. and Gorbunov, M., Submitted. Reproducibility of GPS Radio Occultation Data for Climate Monitoring: Profile-to-Profile Inter-comparison of CHAMP Climate Records 2002 to 2008 from Six Data Centers, Journal of Geophysical Research.

Ho, S.P., Goldberg, M., Kuo, Y.H., Zou, C.Z. and Schreiner, W., 2009a. Calibration of Temperature in the Lower Stratosphere from Microwave Measurements Using COSMIC Radio Occultation Data: Preliminary Results. Terrestrial Atmospheric and Oceanic Sciences, **20**(1): 87-100.

Ho, S.P., He, W. and Kuo, Y.H., 2009b. Construction of Consistent Temperature Records in the Lower Stratosphere Using Global Positioning System Radio Occultation Data and Microwave Sounding Measurements. New Horizons in Occultation Research - Studies in Atmosphere and Climate, 207-217 pp.

Ho, S.P., Kirchengast, G., Leroy, S., Wickert, J., Mannucci, A.J., Steiner, A., Hunt, D., Schreiner, W., Sokolovskiy, S., Ao, C., Borsche, M., von Engeln, A., Foelsche, U., Heise, S., Iijima, B., Kuo, Y.H., Kursinski, R., Pirscher, B., Ringer, M., Rocken, C. and Schmidt, T., 2009c. Estimating the uncertainty of using GPS radio occultation data for climate monitoring: Intercomparison of CHAMP refractivity climate records from 2002 to 2006 from different data centers. Journal of Geophysical Research-Atmospheres, **114**.

Ho, S.P., Kuo, Y.H., Zeng, Z. and Peterson, T.C., 2007. A comparison of lower stratosphere temperature from microwave measurements with CHAMP GPS RO data. Geophysical Research Letters, **34**(15).
Holben, B.N., Eck, T.F., Slutsker, I., Tanré, D., Buis, J.P., Setzer, A., Vermote, E., Reagan, J.A., Kaufman, Y.J., Nakajima, T., Lavenu, F., Jankowiak, I. and Smirnov, A., 1998. AERONET--A Federated Instrument Network and Data Archive for Aerosol Characterization. Remote Sensing of Environment, **66**(1): 1-16.
Holgate, S.J., and P.L. Woodworth, 2004: Evidence for enhanced coastal sea level rise during the 1990s. Geophys. Res. Lett., 31, L07305, doi:10.1029/2004GL019626.
Holland, G.J. and Webster, P.J., 2007. Heightened tropical cyclone activity in the North Atlantic: natural variability or climate trend? Philosophical Transactions of the Royal Society a-Mathematical Physical and Engineering Sciences, **365**(1860): 2695-2716.
Hope, P.K., Drosdowsky, W. and Nicholls, N., 2006. Shifts in the synoptic systems influencing southwest Western Australia. Climate Dynamics, **26**(7-8): 751-764.
Hsu, N.C., Gautam, R., Sayer, A.M., Bettenhausen, C., Li, C., Jeong, M.J., Tsay, S.C. and Holben, B.N., 2012. Global and regional trends of aerosol optical depth over land and ocean using SeaWiFS measurements from 1997 to 2010. Atmos. Chem. Phys. Discuss., **12**(3): 8465-8501.
Hu, Y. and Fu, Q., 2007. Observed poleward expansion of the Hadley circulation since 1979. Atmospheric Chemistry and Physics, **7**: 5229-5236.
Hu, Y.C., Dong, W.J. and He, Y., 2010. Impact of land surface forcings on mean and extreme temperature in eastern China. Journal of Geophysical Research-Atmospheres, **115**: 11.
Hu, Y.Y., Zhou, C. and Liu, J.P., 2011. Observational evidence for the poleward expansion of the Hadley circulation. Adv. Atmos. Sci., **28**: 33-44.
Huang, J., Golombek, A., Prinn, R., Weiss, R., Fraser, P., Simmonds, P., Dlugokencky, E., Hall, B., Elkins, J., Steele, P., Langenfelds, R., Krummel, P., Dutton, G. and Porter, L., 2008. Estimation of regional emissions of nitrous oxide from 1997 to 2005 using multinetwork measurements, a chemical transport model, and an inverse method. Journal of Geophysical Research-Atmospheres: -.
Huang, W.-R., Wang, S.-Y. and Chan, J.C.L., 2010. Discrepancies between global reanalyses and observations in the interdecadal variations of Southeast Asian cold surge. Int. J. Climatol.
Hudson, R.D., 2011. Measurements of the movement of the jet streams at mid-latitudes, in the Northern and Southern Hemispheres, 1979 to 2010. Atmos. Chem. Physics, **11**: 31067-31090.
Hudson, R.D., Andrade, M.F., Follette, M.B. and Frolov, A.D., 2006. The total ozone field separated into meteorological regimes - Part II: Northern Hemisphere mid-latitude total ozone trends. Atmospheric Chemistry and Physics, **6**: 5183-5191.
Hundecha, Y., St-Hilaire, A., Ouarda, T., El Adlouni, S. and Gachon, P., 2008. A Nonstationary Extreme Value Analysis for the Assessment of Changes in Extreme Annual Wind Speed over the Gulf of St. Lawrence, Canada. Journal of Applied Meteorology and Climatology, **47**(11): 2745-2759.
Hurrell, J.W., 1995a. DECADAL TRENDS IN THE NORTH-ATLANTIC OSCILLATION - REGIONAL TEMPERATURES AND PRECIPITATION. Science, **269**(5224): 676-679.
Hurrell, J.W., 1995b. Decadal trends in the North Atlantic Oscillation: Regional temperatures and precipitation. Science, **269**(5224): 676-679.
Hurst, D., 2011. Stratospheric water vapor trends over Boulder, Colorado: Analysis of the 30 year Boulder record. J. Geophys. Res., **116**.
Idso, S.B. and Brazel, A.J., 1984. RISING ATMOSPHERIC CARBON-DIOXIDE CONCENTRATIONS MAY INCREASE STREAMFLOW. Nature, **312**(5989): 51-53.
IPCC, 2007a. Climate Change 2007: The Physical Science Basis. Contribution of Working Group I to the Fourth Assessment Report of the Intergovernmental Panel on Climate Change (IPCC). Cambridge University Press, Cambridge, United Kingdom and New York, NY, USA, 996 pp pp.
IPCC, 2007b. Summary for Policymakers, In: Climate Change 2007: The Physical Science Basis. Contribution of Working Group I to the Fourth Assessment Report of the Intergovernmental Panel on Climate Change. Cambridge University Press, Cambridge, United Kingdom and New York, NY, USA.
Ishii, M., A. Shouji, S. Sugimoto, T. Matsumoto 2005: Objective analysis of SST and marine meteorological variables for the 20th Century using ICOADS and the Kobe Collection. Int. J. Climatol., 25, 865–879. http://ghrsst.nodc.noaa.gov/intercomp.html
Ishii, M. and M. Kimoto, 2009: Reevaluation of Historical Ocean Heat Content Variations with Time-varying XBT and MBT depth bias corrections. J. Oceanogr., 65, 287-299.
Ishijima, K., Sugawara, S., Kawamura, K., Hashida, G., Morimoto, S., Murayama, S., Aoki, S. and Nakazawa, T., 2007. Temporal variations of the atmospheric nitrous oxide concentration and its delta N-15 and delta O-18 for the latter half of the 20th century reconstructed from firn air analyses. Journal of Geophysical Research-Atmospheres: -.
Ivy, D., Arnold, T., Harth, C., Steele, L., Muhle, J., Rigby, M., Salameh, P., Leist, M., Krummel, P., Fraser, P., Weiss, R. and Prinn, R., 2012. Atmospheric histories and growth trends of C4F10, C5F12, C6F14, C7F16 and C8F18. Atmospheric Chemistry and Physics, **12**(9): 4313-4325.
Jacob, D.J., Logan, J.A. and P., M.P., 1999. Effect of rising Asian emissions on surface ozone in the United States. . Geophys. Res. Lett., **26**(2): 175–2178, doi:10.1029/1999GL900450.

Jacobowitz, H., Stowe, L.L., Ohring, G., Heidinger, A., Knapp, K. and Nalli, N.R., 2003. The advanced very high resolution radiometer Pathfinder Atmosphere (PATMOS) climate dataset - A resource for climate research. Bulletin of the American Meteorological Society, **84**(6): 785-+.

Jaffe, D. and Ray, J., 2007. Increase in surface ozone at rural sites in the western US. Atmospheric Environment, **41**(26): 5452-5463.

Jain, S.K. and Kumar, V., 2012. Trend analysis of rainfall and temperature data for India. Current Science, **102**(1): 37-49.

Jakob, D., Karoly, D. and Seed, A., 2011. Non-stationarity in daily and sub-daily intense rainfall - Part 2: Regional assessment for sites in south-east Australia. Natural Hazards and Earth System Sciences, **11**(8): 2273-2284.

Jevrejeva S, Grinsted A, Moore JC, Holgate SJ. 2006. Nonlinear trends and multiyear cycles in sea level records. Journal of Geophysical Research 111: C09012, DOI: 10.1029/2005JC003229.

Jhajharia, D., Shrivastava, S., Sarkar, D. and Sarkar, S., 2009. Temporal characteristics of pan evaporation trends under humid conditions of northeast India. Agricultural and Forest Meteorology, **336**: 61-73.

Jiang, T., Kundzewicz, Z.W. and Su, B., 2008. Changes in monthly precipitation and flood hazard in the Yangtze River Basin, China. International Journal of Climatology, **28**(11): 1471-1481.

Jiang, X., Ku, W., Shia, R., Li, Q., Elkins, J., Prinn, R. and Yung, Y., 2007. Seasonal cycle of N2O: Analysis of data. Global Biogeochemical Cycles: -.

Jiang, Y., Luo, Y., Zhao, Z.C. and Tao, S.W., 2010. Changes in wind speed over China during 1956-2004. Theoretical and Applied Climatology, **99**(3-4): 421-430.

Jin, S.G., Park, J.U., Cho, J.H. and Park, P.H., 2007. Seasonal variability of GPS-derived zenith tropospheric delay (1994-2006) and climate implications. Journal of Geophysical Research-Atmospheres, **112**(D9).

John, V.O., Allan, R.P. and Soden, B.J., 2009. How robust are observed and simulated precipitation responses to tropical ocean warming? Geophysical Research Letters, **36**.

John, V.O., Holl, G., Allan, R.P., Buehler, S.A., Parker, D.E. and Soden, B.J., 2011. Clear-sky biases in satellite infrared estimates of upper tropospheric humidity and its trends. Journal of Geophysical Research-Atmospheres, **116**.

Johnson, G.C., Lyman, J.M., Willis, J.K., Levitus, S., Boyer, T., Antonov, J. and Good, S.A., 2011. [Global Oceans] Ocean heat content [in "State of the Climate in 2010"]. Bull. Amer. Meteor. Soc., pp. S161–S163.

Jones, P.D., Jonsson, T. and Wheeler, D., 1997. Extension to the North Atlantic Oscillation using early instrumental pressure observations from Gibraltar and south-west Iceland. International Journal of Climatology, **17**(13): 1433-1450.

Jones, P.D. and Lister, D.H., 2007. Intercomparison of four different Southern Hemisphere sea level pressure datasets. Geophysical Research Letters, **34**(10).

Jones, P.D. and Lister, D.H., 2009. The urban heat island in Central London and urban-related warming trends in Central London since 1900. Weather, **64**(12): 323-327.

Jones, P.D., Lister, D.H. and Li, Q., 2008. Urbanization effects in large-scale temperature records, with an emphasis on China. Journal of Geophysical Research-Atmospheres, **113**(D16).

Jones, P.D., Lister, D.H., Osborn, T.J., Harpham, C., Salmon, M. and Morice, C.P., 2012a. Hemispheric and large-scale land-surface air temperature variations: An extensive revision and an update to 2010. Journal of Geophysical Research-Atmospheres, **117**: 29.

Jones, P.D., Lister, D.H., Osborn, T.J., Harpham, C., Salmon, M. and Morice, C.P., 2012b. Hemispheric and large-scale land-surface air temperature variations: An extensive revision and an update to 2010. Journal of Geophysical Research-Atmospheres, **117**.

Jones, R., Westra, S. and Sharma, A., 2010. Observed relationships between extreme sub-daily precipitation, surface temperature, and relative humidity. Geophysical Research Letters, **37**.

Joshi, M.M., Gregory, J.M., Webb, M.J., Sexton, D.M.H. and Johns, T.C., 2008. Mechanisms for the land/sea warming contrast exhibited by simulations of climate change. Climate Dynamics, **30**(5): 455-465.

Jovanovic, B., Collins, D., Braganza, K., Jakob, D. and Jones, D.A., 2011. A high-quality monthly total cloud amount dataset for Australia. Climatic Change, **108**(3).

Jung, M., Reichstein, M., Ciais, P., Seneviratne, S.I., Sheffield, J., Goulden, M.L., Bonan, G., Cescatti, A., Chen, J.Q., de Jeu, R., Dolman, A.J., Eugster, W., Gerten, D., Gianelle, D., Gobron, N., Heinke, J., Kimball, J., Law, B.E., Montagnani, L., Mu, Q.Z., Mueller, B., Oleson, K., Papale, D., Richardson, A.D., Roupsard, O., Running, S., Tomelleri, E., Viovy, N., Weber, U., Williams, C., Wood, E., Zaehle, S. and Zhang, K., 2010. Recent decline in the global land evapotranspiration trend due to limited moisture supply. Nature, **467**(7318): 951-954.

Kanamitsu, M., Ebisuzaki, W., Woollen, J., Yang, S.K., Hnilo, J.J., Fiorino, M. and Potter, G.L., 2002. NCEP-DOE AMIP-II reanalysis (R-2). Bulletin of the American Meteorological Society, **83**(11): 1631-1643.

Kang, S.M., Polvani, L.M., Fyfe, J.C. and Sigmond, M., 2011. Impact of Polar Ozone Depletion on Subtropical Precipitation. Science, **332**(6032): 951-954.

Kao, H.Y. and Yu, J.Y., 2009. Contrasting Eastern-Pacific and Central-Pacific Types of ENSO. Journal of Climate, **22**(3): 615-632.

Kaplan, A., M. Cane, Y. Kushnir, A. Clement, M. Blumenthal, and B. Rajagopalan, 1998. Analyses of global sea surface temperature 1856-1991, Journal of Geophysical Research, 103, 18,567-18,589. http://granger.ldeo.columbia.edu/expert/%28/nasa/alexeyk/AR5/KAPLAN_EXT_glav.cdf%29readfile/.ssta/

Karnauskas, K.B., Seager, R., Kaplan, A., Kushnir, Y. and Cane, M.A., 2009. Observed Strengthening of the Zonal Sea Surface Temperature Gradient across the Equatorial Pacific Ocean. Journal of Climate, **22**(16): 4316-4321.
Karnieli, A., Derimian, Y., Indoitu, R., Panov, N., Levy, R.C., Remer, L.A., Maenhaut, W. and Holben, B.N., 2009. Temporal trend in anthropogenic sulfur aerosol transport from central and eastern Europe to Israel. Journal of Geophysical Research-Atmospheres, **114**: D00d19.
KAROLY, D., 1989. SOUTHERN-HEMISPHERE CIRCULATION FEATURES ASSOCIATED WITH ELNINO - SOUTHERN OSCILLATION EVENTS. Journal of Climate, **2**(11): 1239-1252.
Kaskaoutis, D.G., P, S.R., Gautam, R., Sharma, M., Kosmopoulos, P.G. and Tripathi, S.N., 2012. Variability and trends of aerosol properties over Kanpur, northern India using AERONET data (2001-10). Environmental Research Letters, **7**(2): 024003.
Kato, S., Rose, F.G., Sun-Mack, S., Miller, W.F., Chen, Y., Rutan, D.A., Stephens, G.L., Loeb, N.G., Minnis, P., Wielicki, B.A., Winker, D.M., Charlock, T.P., Stackhouse, P.W., Xu, K.M. and Collins, W.D., 2011. Improvements of top-of-atmosphere and surface irradiance computations with CALIPSO-, CloudSat-, and MODIS-derived cloud and aerosol properties. Journal of Geophysical Research-Atmospheres, **116**(D19209): doi:10.1029/2011JD016050.
Kawai, Y. and Wada, A., 2007. Diurnal sea surface temperature variation and its impact on the atmosphere and ocean: A review. Journal of Oceanography, **63**(5): 721-744.
KEELING, C., ADAMS, J. and EKDAHL, C., 1976a. ATMOSPHERIC CARBON-DIOXIDE VARIATIONS AT SOUTH POLE. Tellus, **28**(6): 553-564.
Keeling, C., Bacastow, R., Bainbridge, A., Ekdahl, C., Guenther, P., Waterman, L. and Chin, J., 1976b. Atmospheric Carbon-Dioxide Variations at Mauna-Loa Observatory, Hawaii. Tellus, **28**(6): 538-551.
Keeling, C.D., Bacastow, R. B., Bainbridge, A. E., Ekdahl, C. A., Guenther, P. R., Waterman, L. S., 1976. Atmospheric carbon dioxide variations at Mauna Loa Observatory, Hawaii, Tellus, pp. 538-551.
Keller, C., Brunner, D., Henne, S., Vollmer, M., O'Doherty, S. and Reimann, S., 2011. Evidence for under-reported western European emissions of the potent greenhouse gas HFC-23. Geophysical Research Letters, **38**.
Kennedy, J.J., Brohan, P. and Tett, S.F.B., 2007. A global climatology of the diurnal variations in sea-surface temperature and implications for MSU temperature trends. Geophysical Research Letters, **34**(5).
Kennedy, J.J., Rayner, N.A. and Smith, R.O., 2011a. Using AATSR data to assess the quality of in situ sea surface temperature observations for climate studies. Remote Sensing Environ., **in press**.
Kennedy, J.J., Rayner, N.A., Smith, R.O., Saunby, M. and Parker, D.E., 2011b. Reassessing biases and other uncertainties in sea surface temperature observations since 1850, part 1: Measurement and sampling uncertainties. J. Geophys. Res., **116**.
Kennedy, J.J., Rayner, N.A., Smith, R.O., Saunby, M. and Parker, D.E., 2011c. Reassessing biases and other uncertainties in sea surface temperature observations since 1850, part 2: Biases and homogenization. J. Geophys. Res., **116**. http://www.metoffice.gov.uk/hadobs/hadsst3/data/download.html http://www.metoffice.gov.uk/hadobs/hadsst3/data/TS_all_realisations.zip
Kent, E.C. and Berry, D.I., 2005. Quantifying random measurement errors in voluntary observing ships' meteorological observations. International Journal of Climatology, **25**(7): 843-856.
Kent, E.C. and Berry, D.I., 2008. Assessment of the Marine Observing System (ASMOS): Final Report, Southampton.
Kent, E.C. and Challenor, P.G., 2006. Toward estimating climatic trends in SST. Part II: Random errors. Journal of Atmospheric and Oceanic Technology, **23**(3): 476-486.
Kent, E.C., Challenor, P.G. and Taylor, P.K., 1999. A statistical determination of the random observational errors present in voluntary observing ships meteorological reports. Journal of Atmospheric and Oceanic Technology, **16**(7): 905-914.
Kent, E.C., Kennedy, J.J., Berry, D.I. and Smith, R.O., 2010. Effects of instrumentation changes on sea surface temperature measured in situ. Wiley Interdisciplinary Reviews: Climate Change, **1**(5): 718-728.
Kent, E.C., Rayner, N.A., Berry, D.I., Saunby, M., Moat, B.I., Kennedy, J.J. and Parker, D.E., Submitted. Global analysis of night marine air temperature and its uncertainty since 1880, the HadNMAT2 Dataset, Journal of Geophysical Research.
Kent, E.C., Woodruff, S.D. and Berry, D.I., 2007. Metadata from W MO publication no. 47 and an assessment of voluntary observing ship observation heights in ICOADS. Journal of Atmospheric and Oceanic Technology, **24**(2): 214-234.
Kenyon, J. and Hegerl, G.C., 2008. Influence of modes of climate variability on global temperature extremes. Journal of Climate, **21**(15): 3872-3889.
Kiehl, J.T. and Trenberth, K.E., 1997. Earth's annual global mean energy budget. Bulletin of the American Meteorological Society, **78**(2): 197-208.
Kim, D.-H., Sohn, B.-J., Nakajima, T., Takamura, T., Takemura, T., Choi, B.-C. and Yoon, S.-C., 2004. Aerosol optical properties over east Asia determined from ground-based sky radiation measurements. J. Geophys. Res., **109**(D2): D02209.
Kim, D.Y. and Ramanathan, V., 2008. Solar radiation budget and radiative forcing due to aerosols and clouds. Journal of Geophysical Research-Atmospheres, **113**(D2).

Kim, J., Li, S., Kim, K., Stohl, A., Muhle, J., Kim, S., Park, M., Kang, D., Lee, G., Harth, C., Salameh, P. and Weiss, R., 2010. Regional atmospheric emissions determined from measurements at Jeju Island, Korea: Halogenated compounds from China. Geophysical Research Letters, **37**.

Kistler, R., Kalnay, E., Collins, W., Saha, S., White, G., Woollen, J., Chelliah, M., Ebisuzaki, W., Kanamitsu, M., Kousky, V., van den Dool, H., Jenne, R. and Fiorino, M., 2001. The NCEP-NCAR 50-year reanalysis: Monthly means CD-ROM and documentation. Bulletin of the American Meteorological Society, **82**(2): 247-267.

Klein Tank, A.M.G., Peterson, T.C., Quadir, D.A., Dorji, S., Zou, X., Tang, H., Santhosh, K., Joshi, U.R., Jaswal, A.K., Kolli, R.K., Sikder, A.B., Deshpande, N.R., Revadekar, J.V., Yeleuova, K., Vandasheva, S., Faleyeva, M., Gomboluudev, P., Budhathoki, K.P., Hussain, A., Afzaal, M., Chandrapala, L., Anvar, H., Amanmurad, D., Asanova, V.S., Jones, P.D., New, M.G. and Spektorman, T., 2006. Changes in daily temperature and precipitation extremes in central and south Asia. Journal of Geophysical Research-Atmospheres, **111**(D16).

Knapp, K.R. and Kruk, M.C., 2010. Quantifying Interagency Differences in Tropical Cyclone Best-Track Wind Speed Estimates. Monthly Weather Review, **138**(4): 1459-1473.

Knapp, P.A. and Soule, P.T., 2007. Trends in midlatitude cyclone frequency and occurrence during fire season in the Northern Rockies: 1900-2004. Geophysical Research Letters, **34**(20).

Knowles, N., Dettinger, M.D. and Cayan, D.R., 2006. Trends in snowfall versus rainfall in the Western United States. Journal of Climate, **19**(18): 4545-4559.

Knutson, T.R., McBride, J.L., Chan, J., Emanuel, K., Holland, G., Landsea, C., Held, I., Kossin, J.P., Srivastava, A.K. and Sugi, M., 2010. Tropical cyclones and climate change. Nature Geoscience, **3**(3): 157-163.

Kobayashi, S., Matricardi, M., Dee, D. and Uppala, S., 2009. Toward a consistent reanalysis of the upper stratosphere based on radiance measurements from SSU and AMSU-A. Quarterly Journal of the Royal Meteorological Society, **135**(645): 2086-2099.

Kopp, G. and Lawrence, G., 2005. The Total Irradiance Monitor (TIM): Instrument design. Solar Physics, **230**(1-2): 91-109.

Kopp, G., Lawrence, G. and Rottman, G., 2005. The Total Irradiance Monitor (TIM): Science results. Solar Physics, **230**(1-2): 129-139.

Kopp, G. and Lean, J.L., 2011. A new, lower value of total solar irradiance: Evidence and climate significance. Geophysical Research Letters, **38**.

Kossin, J.P., Knapp, K.R., Vimont, D.J., Murnane, R.J. and Harper, B.A., 2007. A globally consistent reanalysis of hurricane variability and trends. Geophysical Research Letters, **34**(4).

Kreienkamp, F., Spekat, A. and Enke, W., 2010. Stationarity of atmospheric waves and blocking over Europe-based on a reanalysis dataset and two climate scenarios. Theoretical and Applied Climatology, **102**(1-2): 205-212.

Krishna Moorthy, K., Babu, S.S., Satheesh, S.K., Lal, S., Sarin, M.M. and Ramachandran, S., 2009. Climate implications of atmospheric aerosols and trace gases: Indian Scenario, Climate Sense, World Meteorological Organisation, Tudor Rose, UK.

Krishna Moorthy, K., Suresh Babu, S., Manoy, M.R. and Satheesh, S.K., 2012. Buildup of Aerosols over the Asian Monsoon Regime. submitted.

Krishnamurthy, C.K.B., Lall, U. and Kwon, H.H., 2009. Changing Frequency and Intensity of Rainfall Extremes over India from 1951 to 2003. Journal of Climate, **22**(18): 4737-4746.

Kruger, A. and Sekele, S., 2012. Trends in extreme temperature indices in South Africa: 1962–2009. International Journal of Climatology.

Kruger, A.C., 2006. Observed trends in daily precipitation indices in South Africa: 1910-2004. International Journal of Climatology, **26**(15): 2275-2285.

Kubota, H. and Chan, J.C.L., 2009. Interdecadal variability of tropical cyclone landfall in the Philippines from 1902 to 2005. Geophysical Research Letters, **36**.

Kudo, R., Uchiyama, A., Yamazaki, A., Sakami, T. and Ijima, O., 2011. Decadal changes in aerosol optical thickness and single scattering albedo estimated from ground-based broadband radiometers: A case study in Japan. J. Geophys. Res., **116**(D3): D03207.

Kuglitsch, F.G., Toreti, A., Xoplaki, E., Della-Marta, P.M., Luterbacher, J. and Wanner, H., 2009. Homogenization of daily maximum temperature series in the Mediterranean. Journal of Geophysical Research-Atmospheres, **114**.

Kuglitsch, F.G., Toreti, A., Xoplaki, E., Della-Marta, P.M., Zerefos, C.S., Turkes, M. and Luterbacher, J., 2010. Heat wave changes in the eastern Mediterranean since 1960. Geophysical Research Letters, **37**.

Kumari, B.P. and Goswami, B.N., 2010. Seminal role of clouds on solar dimming over the Indian monsoon region. Geophysical Research Letters, **37**: -.

Kumari, B.P., Londhe, A.L., Daniel, S. and Jadhav, D.B., 2007. Observational evidence of solar dimming: Offsetting surface warming over India. Geophysical Research Letters, **34**(21): L21810.

Kundzewicz, Z.W., Mata, L.J., Arnell, N.W., Döll, P., Kabat, P., Jiménez, B., Miller, K.A., Oki, T., Sen, Z. and Shiklomanov, I.A., 2007. Freshwater resources and their management, Climate Change 2007: Impacts, Adaptation and Vulnerability. Contribution of Working Group II to the Fourth Assessment Report of the Intergovernmental Panel on Climate Change. Cambridge University Press, Cambridge, United Kingdom and New York, NY, USA.

Kunkel, K.E., Bromirski, P.D., Brooks, H.E., Cavazos, T., Douglas, A.V., Easterling, D.R., Emanual, K.A., Groisman, P.Y., Holland, G.J., Knutson, T.R., Kossin, J.P., Komar, P.D., Levinson, D.H. and Smith, R.L., 2008. Observed

Changes in Weather and Climate Extremes. In: T.R. Karl, G.A. Meehl, D.M. Christopher, S.J. Hassol, A.M. Waple and W.L. Murray (Editors), Weather and Climate Extremes in a Changing Climate. Regions of Focus: North America, Hawaii, Caribbean, and U.S. Pacific Islands. A Report by the U.S. Climate Change Science Program and the Subcommittee on Global Change Research, Washington, DC., pp. 222.

Kunkel, K.E., Palecki, M.A., Ensor, L., Easterling, D., Hubbard, K.G., Robinson, D. and Redmond, K., 2009. Trends in Twentieth-Century US Extreme Snowfall Seasons. Journal of Climate, **22**(23): 6204-6216.

Kunz, M., Sander, J. and Kottmeier, C., 2009. Recent trends of thunderstorm and hailstorm frequency and their relation to atmospheric characteristics in southwest Germany. International Journal of Climatology, **29**(15): 2283-2297.

Kuo, Y.H., Schreiner, W.S., Wang, J., Rossiter, D.L. and Zhang, Y., 2005. Comparison of GPS radio occultation soundings with radiosondes. Geophysical Research Letters, **32**(5).

Kuo, Y.H., Wee, T.K., Sokolovskiy, S., Rocken, C., Schreiner, W., Hunt, D. and Anthes, R.A., 2004. Inversion and error estimation of GPS radio occultation data. Journal of the Meteorological Society of Japan, **82**(1B): 507-531.

Kurbis, K., Mudelsee, M., Tetzlaff, G. and Brazdil, R., 2009. Trends in extremes of temperature, dew point, and precipitation from long instrumental series from central Europe. Theoretical and Applied Climatology, **98**(1-2): 187-195.

Kvalevag, M.M. and Myhre, G., 2007. Human impact on direct and diffuse solar radiation during the industrial era. Journal of Climate, **20**(19): 4874-4883.

Kysely, J., 2009. Trends in heavy precipitation in the Czech Republic over 1961-2005. International Journal of Climatology, **29**(12): 1745-1758.

L'Ecuyer, T.S., Wood, N.B., Haladay, T., Stephens, G.L. and Stackhouse, P.W., 2008. Impact of clouds on atmospheric heating based on the R04 CloudSat fluxes and heating rates data set. Journal of Geophysical Research-Atmospheres, **113**: 15.

Labat, D., Godderis, Y., Probst, J.L. and Guyot, J.L., 2004. Evidence for global runoff increase related to climate warming. Advances in Water Resources, **27**(6): 631-642.

Ladstadter, F., Steiner, A.K., Foelsche, U., Haimberger, L., Tavolato, C. and Kirchneb=ngast, G., 2011. An assessment of differences in lower stratospheric temperature records from (A)MSU, radiosondes and GPS radio occultation. Atmospheric Measurement Techniques, **4**: 1965-1977.

Landsea, C.W., 2007. Counting Atlantic tropical cyclones back to 1900. EOS Transactions (AGU), **88**(18): 197-202.

Landsea, C.W., Harper, B.A., Hoarau, K. and Knaff, J.A., 2006. Can we detect trends in extreme tropical cyclones? Science, **313**(5786): 452-454.

Langematz, U. and Kunze, M., 2008. Dynamical changes in the Arctic and Antarctic stratosphere during spring. In: S. Brönnimann, J. Luterbacher, T. Ewen, H.F. Diaz, R.S. Stolarski and U. Neu (Editors), Climate Variability and Extremes during the Past 100 Years. Advances in Global Change Research, pp. 293-301.

Lanzante, J.R., 2009. Comment on "Trends in the temperature and water vapor content of the tropical lower stratosphere: Sea surface connection" by Karen H. Rosenlof and George C. Reid. Journal of Geophysical Research-Atmospheres, **114**.

Larkin, N.K. and Harrison, D.E., 2005. On the definition of El Nino and associated seasonal average US weather anomalies. Geophysical Research Letters, **32**(13).

Laube, J., Martinerie, P., Witrant, E., Blunier, T., Schwander, J., Brenninkmeijer, C., Schuck, T., Bolder, M., Rockmann, T., van der Veen, C., Bonisch, H., Engel, A., Mills, G., Newland, M., Oram, D., Reeves, C. and Sturges, W., 2010. Accelerating growth of HFC-227ea (1,1,1,2,3,3,3-heptafluoropropane) in the atmosphere. Atmospheric Chemistry and Physics, **10**(13): 5903-5910.

Lawrimore, J.H., Menne, M.J., Gleason, B.E., Williams, C.N., Wuertz, D.B., Vose, R.S. and Rennie, J., 2011a. An overview of the Global Historical Climatology Network monthly mean temperature data set, version 3. Journal of Geophysical Research-Atmospheres, **116**.

Lawrimore, J.H., Menne, M.J., Gleason, B.E., Williams, C.N., Wuertz, D.B., Vose, R.S. and Rennie, J., 2011b. An overview of the Global Historical Climatology Network monthly mean temperature data set, version 3. Journal of Geophysical Research-Atmospheres, **116**(D19121): doi:10.1029/2011jd016187.

Leakey, A.D.B., Uribelarrea, M., Ainsworth, E.A., Naidu, S.L., Rogers, A., Ort, D.R. and Long, S.P., 2006. Photosynthesis, productivity, and yield of maize are not affected by open-air elevation of CO2 concentration in the absence of drought. Plant Physiology, **140**(2): 779-790.

Leckebusch, G.C., Koffi, B., Ulbrich, U., Pinto, J.G., Spangehl, T. and Zacharias, S., 2006. Analysis of frequency and intensity of European winter storm events from a multi-model perspective, at synoptic and regional scales. Climate Research, **31**(1): 59-74.

Lee, H.T., Gruber, A., Ellingson, R.G. and Laszlo, I., 2007. Development of the HIRS outgoing longwave radiation climate dataset. Journal of Atmospheric and Oceanic Technology, **24**(12): 2029-2047.

Lee, H.T., Heidinger, A., Gruber, A. and Ellingson, R.G., 2004. The HIRS outgoing longwave radiation product from hybrid polar and geosynchronous satellite observations. Climate Change Processes in the Stratosphere, Earth-Atmosphere-Ocean Systems, and Oceanographic Processes from Satellite Data, **33**(7): 1120-1124.

Lee, T. and McPhaden, M.J., 2010. Increasing intensity of El Nino in the central-equatorial Pacific. Geophysical Research Letters, **37**.

Lee, T.C., Chan, H.S., Ginn, E.W.L. and Wong, M.C., 2011. Long-Term Trends in Extreme Temperatures in Hong Kong and Southern China. Adv. Atmos. Sci., **28**(1): 147-157.

Lefohn, A.S., Shadwick, D. and Oltmans, S.J., 2010. Characterizing changes in surface ozone levels in metropolitan and rural areas in the United States for 1980-2008 and 1994-2008. Atmos. Environ., **44**: 5199-5210.
Lehmann, A., Getzlaff, K. and Harlass, J., 2011. Detailed assessment of climate variability in the Baltic Sea area for the period 1958 to 2009. Climate Research, **46**(2): 185-196.
Lelieveld, J., van Aardenne, J., Fischer, H., de Reus, M., Williams, J. and Winkler, P., 2004. Increasing Ozone over the Atlantic Ocean. Science, **304**(5676): 1483-1487.
Lenderink, G., Mok, H.Y., Lee, T.C. and al., e., 2011. Scaling and trends of hourly precipitation extremes in two different climate zones - Hong Kong and the Netherlands. HYDROLOGY AND EARTH SYSTEM SCIENCES, **15**(9): 3033-3041.
Lenderink, G. and Van Meijgaard, E., 2008. Increase in hourly precipitation extremes beyond expectations from temperature changes. Nature Geoscience, **1**(8): 511-514.
Leuliette, E.W., R.S. Nerem, and G.T. Mitchum, 2004: Calibration of TOPEX/Poseidon and Jason altimeter data to construct a continuous record of mean sea level change. Mar. Geodesy, 27(1–2), 79–94.
Levin, I., Naegler, T., Heinz, R., Osusko, D., Cuevas, E., Engel, A., Ilmberger, J., Langenfelds, R., Neininger, B., Von Rohden, C., Steele, L., Weller, R., Worthy, D. and Zimov, S., 2010. The global SF6 source inferred from long-term high precision atmospheric measurements and its comparison with emission inventories. Atmospheric Chemistry and Physics: 2655-2662.
Levitus S., J. I. Antonov, T. P. Boyer, R. A. Locarnini, H. E. Garcia, and A. V. Mishonov, 2009. Global ocean heat content 1955–2008 in light of recently revealed instrumentation problems GRL, 36, L07608, doi:10.1029/2008GL037155.
http://www.nodc.noaa.gov/OC5/3M_HEAT_CONTENT/ftp://ftp.nodc.noaa.gov/pub/data.nodc/woa/DATA_ANALYSIS/3M_HEAT_CONTENT/DATA/basin/yearly/h22-w0-700m.dat
Li, Q., Zhang, H., Liu, X., Chen, J., Li, W. and Jones, P., 2009. A Mainland China Homogenized Historical Temperature Dataset of 1951–2004. Bulletin of the American Meteorological Society, **90**(8): 1062-1065.
Li, Z., He, Y., Wang, P., Theakstone, W., An, W., Wang, X., Lu, A., Zhang, W. and Cao, W., 2012. Changes of daily climate extremes in southwestern China during 1961-2008. Global and Planetary Change, **80-81**: 255-272.
Liang, F. and Xia, X.A., 2005. Long-term trends in solar radiation and the associated climatic factors over China for 1961-2000. Annales Geophysicae, **23**(7): 2425-2432.
Liepert, B.G., 2002. Observed reductions of surface solar radiation at sites in the United States and worldwide from 1961 to 1990. Geophysical Research Letters, **29**(10): 4.
Liley, J.B., 2009. New Zealand dimming and brightening. Journal of Geophysical Research-Atmospheres, **114**: D00d10.
Lim, E.P. and Simmonds, I., 2009. Effect of tropospheric temperature change on the zonal mean circulation and SH winter extratropical cyclones. Climate Dynamics, **33**(1): 19-32.
Lin, Y.K., Lin, T.H. and S.C., C., 2010. The changes in different ozone metrics and their implications following precursor reductions over northern Taiwan from 1994 to 2007. Environmental Monitoring and Assessment, **169** 143–157.
Liu, B.H., Xu, M. and Henderson, M., 2011. Where have all the showers gone? Regional declines in light precipitation events in China, 1960-2000. Int. J. Climatology, **31**(8): 1177-1191.
Liu, B.H., Xu, M., Henderson, M. and Gong, W.G., 2004a. A spatial analysis of pan evaporation trends in China, 1955-2000. Journal of Geophysical Research-Atmospheres, **109**(D15): D15102.
Liu, B.H., Xu, M., Henderson, M., Qi, Y. and Li, Y.Q., 2004b. Taking China's temperature: Daily range, warming trends, and regional variations, 1955-2000. Journal of Climate, **17**(22): 4453-4462.
Liu, Q.H. and Weng, F.Z., 2009. Recent Stratospheric Temperature Observed from Satellite Measurements. Sola, **5**: 53-56.
Liu, X., Yin, Z.-Y., Shao, X. and Qin, N., 2006. Temporal trends and variability of daily maximum and minimum, extreme temperature events, and growing season length over the eastern and central Tibetan Plateau during 1961-2003. Journal of Geophysical Research-Atmospheres, **111**(D19).
Loeb, N.G., Lyman, J.M., Johnson, G.C., Allan, R.P., Doelling, D.R., Wong, T., Soden, B.J. and Stephens, G., 2012. Observed changes in top-of-the-atmosphere radiation and upper-ocean heating consistent within uncertainty. Nature Geoscience, **5**: 110-113.
Loeb, N.G., Wielicki, B.A., Doelling, D.R., Smith, G.L., Keyes, D.F., Kato, S., Manalo-Smith, N. and Wong, T., 2009. Toward Optimal Closure of the Earth's Top-of-Atmosphere Radiation Budget. Journal of Climate, **22**(3): 748-766.
Logan, J.A., Staehelin, J., Megretskaia, I.A., Cammas, J.P., Thouret, V., Claude, H., De Backer, H., Hueglin, C., Scheel, H.E., Stubi, R., Froehlich, M. and Derwent, D., 2012. Changes in Ozone over Europe since 1990: analysis of ozone measurements from sondes, regular Aircraft (MOZAIC), and alpine surface sites. Journal Geophysical Research, in press, http://www.agu.org/pubs/crossref/pip/2011JD016952.shtml.
Long, C.N., Dutton, E.G., Augustine, J.A., Wiscombe, W., Wild, M., McFarlane, S.A. and Flynn, C.J., 2009. Significant decadal brightening of downwelling shortwave in the continental United States. Journal of Geophysical Research-Atmospheres, **114**: D00d06.
Lorenz, R., Jaeger, E.B. and Seneviratne, S.I., 2010. Persistence of heat waves and its link to soil moisture memory. Geophysical Research Letters, **37**.

Lucas, C., Nguyen, H. and Timbal, B., 2012. An Observational Analysis of Southern Hemisphere Tropical Expansion. Journal of Geohysical Research, **submitted**.
Lugina, K.M., P.Ya. Groisman, K.Ya. Vinnikov, V.V. Koknaeva, and N.A. Speranskaya 2005: Monthly surface air temperature time series area-averaged over the 30-degree latitudinal belts of the globe, 1881-2004. In: Trends: A Compendium of Data on Global Change. Carbon Dioxide Information Analysis Center, Oak Ridge National Laboratory, US Department of Energy, Oak Ridge, TN, http://cdiac.esd.ornl.gov/trends/temp/lugina/lugina.html
Lupikasza, E., 2010. Spatial and temporal variability of extreme precipitation in Poland in the period 1951-2006. International Journal of Climatology, **30**(7): 991-1007.
Lyman, J.M. and G.C. Johnson, 2008: Estimating annual global upper ocean heat content anomalies despite irregular in situ ocean sampling. J. Clim. 21 5629-5641.
Lynch, A.H., Curry, J.A., Brunner, R.D. and Maslanik, J.A., 2004. Toward an integrated assessment of the impacts of extreme wind events on Barrow, Alaska. Bulletin of the American Meteorological Society, **85**(2): 209-+.
Mahowald, N., Kloster, S., Engelstaedter, S., M., J. K.,, Mukhopadhyay, S., McConnell, Albani, S., Doney, S., Bhattacharya, A., Curran, M., Flanner, M., Hoffman, F., Lawrence, D., Lindsay, K., Mayewski, P., Neff, J., Rothenberg, D., Thomas, E., Thornton, P. and Zender, C., 2010. Observed 20th century desert dust variability: impact on climate and biogeochemistry. Atmospheric Chemistry and Physics, **10**: 10875-10893.
Makowski, K., Jaeger, E.B., Chiacchio, M., Wild, M., Ewen, T. and Ohmura, A., 2009. On the relationship between diurnal temperature range and surface solar radiation in Europe. Journal of Geophysical Research-Atmospheres, **114**: D00d07.
Mann, M.E., 2011. On long range dependence in global surface temperature series. Climatic Change, **107**(3-4): 267-276.
Mann, M.E., Emanual, K.A., Holland, G.J. and Webster, P.J., 2007a. Atlantic tropical cyclones revisited. Eos Transactions (AGU), **88**: 349-350.
Mann, M.E., Sabbatelli, T.A. and Neu, U., 2007b. Evidence for a modest undercount bias in early historical Atlantic tropical cyclone counts. Geophysical Research Letters, **34**(L22707).
Manney, G.L., Santee, M.L., Rex, M., Livesey, N.J., Pitts, M.C., Veefkind, P., Nash, E.R., Wohltmann, I., Lehmann, R., Froidevaux, L., Poole, L.R., Schoeberl, M.R., Haffner, D.P., Davies, J., Dorokhov, V., Gernandt, H., Johnson, B., Kivi, R., Kyro, E., Larsen, N., Levelt, P.F., Makshtas, A., McElroy, C.T., Nakajima, H., Parrondo, M.C., Tarasick, D.W., von der Gathen, P., Walker, K.A. and Zinoviev, N.S., 2011. Unprecedented Arctic ozone loss in 2011. Nature, **478**(7370): 469-475.
Mantua, N.J., Hare, S.R., Zhang, Y., Wallace, J.M. and Francis, R.C., 1997. A Pacific interdecadal climate oscillation with impacts on salmon production. Bulletin of the American Meteorological Society, **78**(6): 1069-1079.
Maraun, D., Osborn, T.J. and Gillett, N.P., 2008. United Kingdom daily precipitation intensity: improved early data, error estimates and an update from 2000 to 2006. International Journal of Climatology, **28**(6): 833-842.
Marengo, J.A., Jones, R., Alves, L.M. and Valverde, M.C., 2009. Future change of temperature and precipitation extremes in South America as derived from the PRECIS regional climate modeling system. International Journal of Climatology, **29**(15): 2241-2255.
Marengo, J.A., Rusticucci, M., Penalba, O. and Renom, M., 2010. An intercomparison of observed and simulated extreme rainfall and temperature events during the last half of the twentieth century: part 2: historical trends. Climatic Change, **98**(3-4): 509-529.
Marshall, G.J., 2003. Trends in the southern annular mode from observations and reanalyses. Journal of Climate, **16**(24): 4134-4143.
Martinerie, P., Nourtier-Mazauric, E., Barnola, J., Sturges, W., Worton, D., Atlas, E., Gohar, L., Shine, K. and Brasseur, G., 2009. Long-lived halocarbon trends and budgets from atmospheric chemistry modelling constrained with measurements in polar firn. Atmospheric Chemistry and Physics: 3911-3934.
Matulla, C., Schoner, W., Alexandersson, H., von Storch, H. and Wang, X.L., 2008. European storminess: late nineteenth century to present. Climate Dynamics, **31**(2-3): 125-130.
McCarthy, M.P., Thorne, P.W. and Titchner, H.A., 2009. An Analysis of Tropospheric Humidity Trends from Radiosondes. Journal of Climate, **22**(22): 5820-5838.
McCarthy, M.P., Titchner, H.A., Thorne, P.W., Tett, S.F.B., Haimberger, L. and Parker, D.E., 2008. Assessing bias and uncertainty in the HadAT-adjusted radiosonde climate record. Journal of Climate, **21**(4): 817-832.
McKitrick, R., 2010. Atmospheric Circulations Do Not Explain the Temperature-Industrialization Correlation, Statistics, Politics, and Policy.
McKitrick, R., Submitted. Encompassing tests of socioeconomic signals in surface climate data, Climatic Change.
McKitrick, R., McIntyre, S. and Herman, C., 2010. Panel and multivariate methods for tests of trend equivalence in climate data series. Atmospheric Science Letters, **11**(4): 270-277.
McKitrick, R. and Michaels, P.J., 2004. A test of corrections for extraneous signals in gridded surface temperature data. Climate Research, **26**(2): 159-173.
McKitrick, R. and Nierenberg, N., 2010. Socioeconomic patterns in climate data. Journal of Economic and Social Measurement, **35**(3): 149-175.
McKitrick, R.R. and Michaels, P.J., 2007. Quantifying the influence of anthropogenic surface processes and inhomogeneities on gridded global climate data. Journal of Geophysical Research-Atmospheres, **112**(D24).

McNider, R.T., Steeneveld, G.J., Holtslag, A.A.M., Pielke, R.A., Sr., Mackaro, S., Pour-Biazar, A., Walters, J., Nair, U. and Christy, J., 2012. Response and sensitivity of the nocturnal boundary layer over land to added longwave radiative forcing. J. Geophys. Res., **117**(D14): D14106.

McVicar, T.R., Van Niel, T.G., Li, L.T., Roderick, M.L., Rayner, D.P., Ricciardulli, L. and Donohue, R.J., 2008. Wind speed climatology and trends for Australia, 1975-2006: Capturing the stilling phenomenon and comparison with near-surface reanalysis output. Geophysical Research Letters, **35**(20).

Mears, C.A., Forest, C.E., Spencer, R.W., Vose, R.S. and Reynolds, R.W., 2006. What is ourunderstanding of the contribution made by observational or methodological uncertainties to the previously reported vertical differences in temperature trends? In: T.R. Karl, S.J. Hassol, C.D. Miller and W.L. Murray (Editors), Temperature Trends in the Lower Tmosphere: Steps for Understanding and Reconciling Differences, Washington DC.

Mears, C.A., Santer, B.D., Wentz, F.J., Taylor, K.E. and Wehner, M.F., 2007. Relationship between temperature and precipitable water changes over tropical oceans. Geophysical Research Letters, **34**(24).

Mears, C.A. and Wentz, F.J., 2009a. Construction of the Remote Sensing Systems V3.2 Atmospheric Temperature Records from the MSU and AMSU Microwave Sounders. Journal of Atmospheric and Oceanic Technology, **26**(6): 1040-1056.

Mears, C.A. and Wentz, F.J., 2009b. Construction of the RSS V3.2 Lower-Tropospheric Temperature Dataset from the MSU and AMSU Microwave Sounders. Journal of Atmospheric and Oceanic Technology, **26**(8): 1493-1509.

Mears, C.A., Wentz, F.J., Thorne, P. and Bernie, D., 2011. Assessing uncertainty in estimates of atmospheric temperature changes from MSU and AMSU using a Monte-Carlo estimation technique. Journal of Geophysical Research-Atmospheres, **116**.

Mears, C.A., Wentz, F.J. and Thorne, P.W., Submitted. Assessing the value of Microwave Sounding Unit-radiosonde comparisons in ascertaining errors in climate data records of tropospheric temperatures, Journal of Geophysical Research.

Mears, C.A., Wentz, F. J., Thorne, P., Bernie, D., 2011. Assessing uncertainty in estimates of atmospheric temperature changes from MSU and AMSU using a monte-carlo estimation technique, Journal of Geophysical Research.

Meehl, G.A., Arblaster, J.M. and Branstator, G., 2011. Understanding the U.S. east-west differential of heat extremes in terms of record temperatures and the warming hole. Journal of Climate: submitted.

Meehl, G.A., Tebaldi, C., Walton, G., Easterling, D. and McDaniel, L., 2009. Relative increase of record high maximum temperatures compared to record low minimum temperatures in the U. S. Geophysical Research Letters, **36**.

Menne, M.J., Durre, I., Gleason, B.G., Houston, T.G. and Vose, R.S., 2012. An overview of the Global Historical Climatology Network-Daily database. Journal of Atmospheric and Oceanic Technology, **29**: 897-910.

Menne, M.J. and Williams, C.N., 2009. Homogenization of Temperature Series via Pairwise Comparisons. Journal of Climate, **22**(7): 1700-1717.

Menne, M.J., Williams, C.N. and Palecki, M.A., 2010. On the reliability of the US surface temperature record. Journal of Geophysical Research-Atmospheres, **115**.

Menzel, W.P., 2001. Cloud tracking with satellite imagery: From the pioneering work of Ted Fujita to the present. Bulletin of the American Meteorological Society, **82**(1): 33-47.

Merchant, C.J., Embury, O., Rayner, N.A., Berry, D.I., Corlett, G.K., Lean, K., Veal, K.L., Kent, E.C., Llevellyn-Jones, D.T., Remedios, J.J. and Sounders, R., Submitted. A twenty-year independent record of sea surface temperaturefor climate from Alon Track Scnning Radiometer.

Merrifield, M.A., 2011. A Shift in Western Tropical Pacific Sea Level Trends during the 1990s. Journal of Climate, **24**(15): 4126-4138.

Mieruch, S., Noel, S., Bovensmann, H. and Burrows, J.P., 2008. Analysis of global water vapour trends from satellite measurements in the visible spectral range. Atmospheric Chemistry and Physics, **8**(3): 491-504.

Milewska, E.J., 2004. Baseline cloudiness trends in Canada 1953-2002. Atmosphere-Ocean, **42**(4): 267-280.

Miller, B., Rigby, M., Kuijpers, L., Krummel, P., Steele, L., Leist, M., Fraser, P., McCulloch, A., Harth, C., Salameh, P., Muhle, J., Weiss, R., Prinn, R., Wang, R., O'Doherty, S., Greally, B. and Simmonds, P., 2010. HFC-23 (CHF3) emission trend response to HCFC-22 (CHClF2) production and recent HFC-23 emission abatement measures. Atmospheric Chemistry and Physics: 7875-7890.

Miller, B., Weiss, R., Salameh, P., Tanhua, T., Greally, B., Muhle, J. and Simmonds, P., 2008. Medusa: A sample preconcentration and GC/MS detector system for in situ measurements of atmospheric trace halocarbons, hydrocarbons, and sulfur compounds. Analytical Chemistry: 1536-1545.

Milliman, J.D., Farnsworth, K.L., Jones, P.D., Xu, K.H. and Smith, L.C., 2008. Climatic and anthropogenic factors affecting river discharge to the global ocean, 1951-2000. Global and Planetary Change, **62**(3-4): 187-194.

Mills, T.C., 2010. 'Skinning a cat': alternative models of representing temperature trends. Climatic Change, **101**(3-4): 415-426.

Milz, M., von Clarmann, T., Fischer, H., Glatthor, N., Grabowski, U., Höpfner, M., Kellmann, S., Kiefer, M., Linden, A., Mengistu Tsidu, G., Steck, T., Stiller, G.P., Funke, B., López-Puertas, M. and Koukouli, M.E., 2005. Water vapor distributions measured with the Michelson Interferometer for Passive Atmospheric Sounding on board Envisat (MIPAS/Envisat). J. Geophys. Res., **110**(D24): D24307.

Ministery of Environment and Forest, G.o.I., 2009. State of Environmnet Report, India- 2009, Ministery of Environment and Forest, New Delhi.

Mishchenko, M.I., Geogdzhayev, I.V., Rossow, W.B., Cairns, B., Carlson, B.E., Lacis, A.A., Liu, L. and Travis, L.D., 2007a. Long-Term Satellite Record Reveals Likely Recent Aerosol Trend. Science, **315**(5818): 1543-1543.

Mishchenko, M.I., Geogdzhayev, I.V., Rossow, W.B., Cairns, B., Carlson, B.E., Lacis, A.w.A., Liu, L. and Travis, L.D., 2007b. Long-Term Satellite Record Reveals Likely Recent Aerosol Trend. Science, **315**(5818): 1543-1543.

Mitas, C.M. and Clement, A., 2005. Has the Hadley cell been strengthening in recent decades? Geophysical Research Letters, **32**(3).

Mo, K. and Paegle, J., 2001. The Pacific-South American modes and their downstream effects. International Journal of Climatology, **21**(10): 1211-1229.

Mo, T., 2009. A study of the NOAA-15 AMSU-A brightness temperatures from 1998 through 2007. Journal of Geophysical Research-Atmospheres, **114**.

Moberg, A., Jones, P.D., Lister, D., Walther, A., Brunet, M., Jacobeit, J., Alexander, L.V., Della-Marta, P.M., Luterbacher, J., Yiou, P., Chen, D.L., Tank, A., Saladie, O., Sigro, J., Aguilar, E., Alexandersson, H., Almarza, C., Auer, I., Barriendos, M., Begert, M., Bergstrom, H., Bohm, R., Butler, C.J., Caesar, J., Drebs, A., Founda, D., Gerstengarbe, F.W., Micela, G., Maugeri, M., Osterle, H., Pandzic, K., Petrakis, M., Srnec, L., Tolasz, R., Tuomenvirta, H., Werner, P.C., Linderholm, H., Philipp, A., Wanner, H. and Xoplaki, E., 2006. Indices for daily temperature and precipitation extremes in Europe analyzed for the period 1901-2000. Journal of Geophysical Research-Atmospheres, **111**(D22).

Mohapatra, M. and Adhikary, S., 2011. Modulation of cyclonic disturbances over the north Indian Ocean by Madden - Julian oscillation. Mausam, **62**(3): 375-390.

Monaghan, A.J. and Bromwich, D.H., 2008. Advances describing recent Antarctic climate variability. Bull. Amer. Meteorol. Soc., **89**(9): 1295-1306.

Montzka, S., Hall, B. and Elkins, J., 2009. Accelerated increases observed for hydrochlorofluorocarbons since 2004 in the global atmosphere. Geophysical Research Letters: -.

Montzka, S., Krol, M., Dlugokencky, E., Hall, B., Jockel, P. and Lelieveld, J., 2011a. Small Interannual Variability of Global Atmospheric Hydroxyl. Science: -.

Montzka, S., Kuijpers, L., Battle, M., Aydin, M., Verhulst, K., Saltzman, E. and Fahey, D., 2010. Recent increases in global HFC-23 emissions. Geophysical Research Letters: -.

Montzka, S., Myers, R., Butler, J., Elkins, J. and Cummings, S., 1993. Global Tropospheric Distribution and Calibration Scale of HCFC-22. Geophysical Research Letters, **20**(8): 703-706.

Montzka, S., Myers, R., Butler, J., Elkins, J., Lock, L., Clarke, A. and Goldstein, A., 1996. Observations of HFC-134a in the remote troposphere. Geophysical Research Letters, **23**(2): 169-172.

Montzka, S.A., Reimann, S., Engel, A., Krüger, K., O'Doherty, S., Sturges, W.T., Blake, D., Dorf, M., Fraser, P., Froidevaux, L., Jucks, K., Kreher, K., Kurylo, M.J., Mellouki, A., Miller, J., Nielsen, O.-J., Orkin, V.L., Prinn, R.G., Rhew, R., Santee, M.L., Stohl, A. and Verdonik, D., 2011b. Ozone-depleting substances (ODSs) and related chemicals, Chapter 1 in Scientific Assessment of Ozone Depletion: 2010, Global Ozone Research and Monitoring Project—Report No. 52, 516 pp., World Meteorological Organization, Geneva, Switzerland, 2011.

Moorthy, K.K., Satheesh, S.K., Suresh Babu, S. and Dutt, C.B.S., 2008. Integrated campaign for aerosols, gases and radiation budget (ICARB): An overview. . J. Earth Syst. Sci., **117**: 243–262.

Morak, S., Hegerl, G. and Christidis, N., 2012. Detectable changes in the frequency of temperature extremes. Journal of Climate (accepted).

Morak, S., Hegerl, G.C. and Kenyon, J., 2011. Detectable regional changes in the number of warm nights. Geophysical Research Letters, **38**: 5.

Morice, C.P., Kennedy, J.J., Rayner, N.A. and Jones, P.D., 2012. Quantifying uncertainties in global and regional temperature change using an ensemble of observational estimates: The HadCRUT4 data set. Journal of Geophysical Research-Atmospheres, **117**, D08101, 22, doi:10.1029/2011JD017187 http://www.metoffice.gov.uk/hadobs/hadcrut4/data/download.html

Mueller, B. and Seneviratne, S., 2012. Hot days induced by precipitation deficits at the global scale. *Proceedings of the National Academy of Sciences*.

Mueller, B., Seneviratne, S.I., Jimenez, C., Corti, T., Hirschi, M., Balsamo, G., Ciais, P., Dirmeyer, P., Fisher, J.B., Guo, Z., Jung, M., Maignan, F., McCabe, M.F., Reichle, R., Reichstein, M., Rodell, M., Sheffield, J., Teuling, A.J., Wang, K., Wood, E.F. and Zhang, Y., 2011. Evaluation of global observations-based evapotranspiration datasets and IPCC AR4 simulations. Geophysical Research Letters, **38**.

Muhle, J., Ganesan, A., Miller, B., Salameh, P., Harth, C., Greally, B., Rigby, M., Porter, L., Steele, L., Trudinger, C., Krummel, P., O'Doherty, S., Fraser, P., Simmonds, P., Prinn, R. and Weiss, R., 2010. Perfluorocarbons in the global atmosphere: tetrafluoromethane, hexafluoroethane, and octafluoropropane. Atmospheric Chemistry and Physics: 5145-5164.

Muhle, J., Huang, J., Weiss, R., Prinn, R., Miller, B., Salameh, P., Harth, C., Fraser, P., Porter, L., Greally, B., O'Doherty, S. and Simmonds, P., 2009a. Sulfuryl fluoride in the global atmosphere. Journal of Geophysical Research-Atmospheres: -.

Muhle, J., Huang, J., Weiss, R., Prinn, R., Miller, B., Salameh, P., Harth, C., Fraser, P., Porter, L., Greally, B., O'Doherty, S., Simmonds, P., Krummel, P. and Steele, L., 2009b. Sulfuryl fluoride in the global atmosphere (vol 114, D05306, 2009). Journal of Geophysical Research-Atmospheres: -.

Mullan, B., Wratt, D., Dean, S., Hollis, M., Allan, S., Williams, T. and Kenny, G., 2008. *Climate Change Effects and Impacts Assessment: A Guidance Manual for Local Government in New Zealand*. Ministry for the Environment, Wellington, New Zealand, 149 pp.

Muller, R.A., Curry, J., Groom, D., Jacobsen, R., Perlmutter, S., Rhode, R., Rosenfeld, A., Wickham, C. and Wurtele, J., submitted. Earth Atmospheric Land Surface Temperature and Station Quality in the United States. Journal of Geophysical Research-Atmospheres: submitted.

Murphy, D.M., Chow, J.C., Leibensperger, E.M., Malm, W.C., Pitchford, M., Schichtel, B.A., Watson, J.G. and White, W.H., 2011. Decreases in elemental carbon and fine particle mass in the United States. Atmos. Chem. Phys., **11**(10): 4679-4686.

Nan, S. and Li, J.P., 2003. The relationship between the summer precipitation in the Yangtze River valley and the boreal spring Southern Hemisphere annular mode. Geophysical Research Letters, **30**(24).

Nash, J. and Edge, P.R., 1989. Temperature changes in the stratosphere and lower mesosphere 197-1988 inferred from TOVS radiance observations, Advances in Space Research, pp. 333-341.

Neff, W., Perlwitz, J. and Hoerling, M., 2008. Observational evidence for asymmetric changes in tropospheric heights over Antarctica on decadal time scales. Geophysical Research Letters, **35**(18).

Nerem, R. S., D. Chambers, C. Choe, and G. T. Mitchum. "Estimating Mean Sea Level Change from the TOPEX and Jason Altimeter Missions." Marine Geodesy 33, no. 1 supp 1 (2010): 435. http://sealevel.colorado.edu/files/2012_rel2/sl_ns_global.txt

Nevison, C., Dlugokencky, E., Dutton, G., Elkins, J., Fraser, P., Hall, B., Krummel, P., Langenfelds, R., O'Doherty, S., Prinn, R., Steele, L. and Weiss, R., 2011. Exploring causes of interannual variability in the seasonal cycles of tropospheric nitrous oxide. Atmospheric Chemistry and Physics, **11**(8): 3713-3730.

New, M., Hewitson, B., Stephenson, D.B., Tsiga, A., Kruger, A., Manhique, A., Gomez, B., Coelho, C.A.S., Masisi, D.N., Kululanga, E., Mbambalala, E., Adesina, F., Saleh, H., Kanyanga, J., Adosi, J., Bulane, L., Fortunata, L., Mdoka, M.L. and Lajoie, R., 2006. Evidence of trends in daily climate extremes over southern and west Africa. Journal of Geophysical Research-Atmospheres, **111**(D14).

Nguyen, H., Timbal, B., Smith, I., Evans, A. and Lucas, C., 2012. The Hadley Circulation in Reanalyses: climatology, variability and change. Journal of Climate, **submitted**.

Nicholls, N., 2008. Recent trends in the seasonal and temporal behaviour of the El Nino-Southern Oscillation. Geophysical Research Letters, **35**(19).

Nicholls, N. and Seneviratne, S., 2012. Comparing IPCC Assessments: How do the AR4 and SREX assessments of changes in extremes differ? Submitted to Climatic Change 19th July 2012.

Nisbet, E. and Weiss, R., 2010. Top-Down Versus Bottom-Up. Science: 1241-1243.

Norris, J.R., Evan, A.T., Allen, R.J., Zelinka, M.D., O'Dell, C. and Klein, S.A., 2012. Evidence for Climate Change in the Satellite Cloud Record. Science, **Submitted**.

Norris, J.R. and Wild, M., 2007. Trends in aerosol radiative effects over Europe inferred from observed cloud cover, solar "dimming" and solar "brightening". Journal of Geophysical Research-Atmospheres, **112**(D8).

Norris, J.R. and Wild, M., 2009. Trends in aerosol radiative effects over China and Japan inferred from observed cloud cover, solar dimming, and solar brightening. Journal of Geophysical Research-Atmospheres, **114**: D00d15.

Ntegeka, V. and Willems, P., 2008. Trends and multidecadal oscillations in rainfall extremes, based on a more than 100-year time series of 10 min rainfall intensities at Uccle, Belgium. Water Resources Research, **44**(7).

O'Carroll, A.G., Eyre, J.R. and Saunders, R.W., 2008. Three-way error analysis between AATSR, AMSR-E, and in situ sea surface temperature observations. Journal of Atmospheric and Oceanic Technology, **25**(7): 1197-1207.

O'Dell, C.W., Wentz, F.J. and Bennartz, R., 2008. Cloud liquid water path from satellite-based passive microwave observations: A new climatology over the global oceans. Journal of Climate, **21**(8): 1721-1739.

O'Doherty, S., Cunnold, D., Manning, A., Miller, B., Wang, R., Krummel, P., Fraser, P., Simmonds, P., McCulloch, A., Weiss, R., Salameh, P., Porter, L., Prinn, R., Huang, J., Sturrock, G., Ryall, D., Derwent, R. and Montzka, S., 2004. Rapid growth of hydrofluorocarbon 134a and hydrochlorofluorocarbons 141b, 142b, and 22 from Advanced Global Atmospheric Gases Experiment (AGAGE) observations at Cape Grim, Tasmania, and Mace Head, Ireland. Journal of Geophysical Research-Atmospheres, **109**(D6).

O'Doherty, S., Cunnold, D., Miller, B., Muhle, J., McCulloch, A., Simmonds, P., Manning, A., Reimann, S., Vollmer, M., Greally, B., Prinn, R., Fraser, P., Steele, L., Krummel, P., Dunse, B., Porter, L., Lunder, C., Schmidbauer, N., Hermansen, O., Salameh, P., Harth, C., Wang, R. and Weiss, R., 2009. Global and regional emissions of HFC-125 (CHF2CF3) from in situ and air archive atmospheric observations at AGAGE and SOGE observatories. Journal of Geophysical Research-Atmospheres: -.

O'Donnell, R., Lewis, N., McIntyre, S. and Condon, J., 2011. Improved Methods for PCA-Based Reconstructions: Case Study Using the Steig et al. (2009) Antarctic Temperature Reconstruction. J. Climate, **24**(8): 2099-2115.

Ohmura, A., 2009. Observed decadal variations in surface solar radiation and their causes. Journal of Geophysical Research-Atmospheres, **114**: D00d05.

Ohmura, A., Dutton, E.G., Forgan, B., Frohlich, C., Gilgen, H., Hegner, H., Heimo, A., Konig-Langlo, G., McArthur, B., Muller, G., Philipona, R., Pinker, R., Whitlock, C.H., Dehne, K. and Wild, M., 1998. Baseline Surface

Radiation Network (BSRN/WCRP): New precision radiometry for climate research. Bulletin of the American Meteorological Society, **79**(10): 2115-2136.
Ohvril, H., Teral, H., Neiman, L., Kannel, M., Uustare, M., Tee, M., Russak, V., Okulov, O., Joeveer, A., Kallis, A., Ohvril, T., Terez, E.I., Terez, G.A., Gushchin, G.K., Abakumova, G.M., Gorbarenko, E.V., Tsvetkov, A.V. and Laulainen, N., 2009. Global dimming and brightening versus atmospheric column transparency, Europe, 1906-2007. Journal of Geophysical Research-Atmospheres, **114**: D00d12.
Oltmans, S.J., Lefohn, A.S., Harris, J.M., Galbally, I., Scheel, H.E., Bodeker, G., Brunke, E., Claude, H., Tarasick, D., Johnson, B.J., Simmonds, P., Shadwick, D., Anlauf, K., Hayden, K., Schmidlin, F., Fujimoto, T., Akagi, K., Meyer, C., Nichol, S., Davies, J., Redondas, A. and Cuevas, E., 2006. Long-term changes in tropospheric ozone. Atmospheric Environment, **40**(17): 3156-3173.
Onogi, K., Tslttsui, J., Koide, H., Sakamoto, M., Kobayashi, S., Hatsushika, H., Matsumoto, T., Yamazaki, N., Kaalhori, H., Takahashi, K., Kadokura, S., Wada, K., Kato, K., Oyama, R., Ose, T., Mannoji, N. and Taira, R., 2007. The JRA-25 reanalysis. Journal of the Meteorological Society of Japan, **85**(3): 369-432.
Oort, A.H. and Yienger, J.J., 1996. Observed interannual variability in the Hadley circulation and its connection to ENSO. Journal of Climate, **9**(11): 2751-2767.
Oram, D., Mani, F., Laube, J., Newland, M., Reeves, C., Sturges, W., Penkett, S., Brenninkmeijer, C., Rockmann, T. and Fraser, P., 2012. Long-term tropospheric trend of octafluorocyclobutane (c-C4F8 or PFC-318). Atmospheric Chemistry and Physics, **12**(1): 261-269.
Osborn, T.J., 2011. Winter 2009/2010 temperatures and a record breaking North Atlantic Oscillation index. Weather, **66**: 19-21.
Paciorek, C.J., Risbey, J.S., Ventura, V. and Rosen, R.D., 2002. Multiple indices of Northern Hemisphere cyclone activity, winters 1949-99. Journal of Climate, **15**(13): 1573-1590.
Palmer, M., J. Antonov, P. Barker, N. Bindoff, T. Boyer, M. Carson, C. Domingues, C., S. Gille, P. Gleckler, S. Good, V. Gouretski, S. Guinehut, K. Haines, D. E. Harrison, M. Ishii, G. Johnson, S. Levitus, S. Lozier, J. Lyman., A. Meijers, K. von Schuckmann, D. Smith, S. Wijffels and J. Willis, 2010: "Future observations for monitoring global ocean heat content", in Proceedings of the "OceanObs'09: Sustained Ocean Observations and Information for Society" Conference (Vol. 2), Venice, Italy, 21-25 September 2009, Hall, J., Harrison D.E. and Stammer, D., Eds., ESA Publication WPP-306, 2010.
Palmer M. D., K. Haines, S. F. B. Tett and T. J. Ansell (2007), "Isolating the signal of ocean global warming", Geophys. Res. Lett., 34, L23610, doi:10.1029/2007GL031712.
Palmer, W.C., 1965. Meteorological drought, Washington DC.
Paltridge, G., Arking, A. and Pook, M., 2009. Trends in middle- and upper-level tropospheric humidity from NCEP reanalysis data. Theoretical and Applied Climatology, **98**(3-4): 351-359.
Pan, Z.T., Arritt, R.W., Takle, E.S., Gutowski, W.J., Anderson, C.J. and Segal, M., 2004. Altered hydrologic feedback in a warming climate introduces a "warming hole". Geophysical Research Letters, **31**(17).
Panagiotopoulos, F., Shahgedanova, M., Hannachi, A. and Stephenson, D.B., 2005. Observed trends and teleconnections of the Siberian high: A recently declining center of action. Journal of Climate, **18**(9): 1411-1422.
Parker, D., Folland, C., Scaife, A., Knight, J., Colman, A., Baines, P. and Dong, B., 2007. Decadal to multidecadal variability and the climate change background. Journal of Geophysical Research-Atmospheres, **112**(D18): -.
Parker, D.E., 2006. A demonstration that large-scale warming is not urban. Journal of Climate, **19**(12): 2882-2895.
Parker, D.E., 2010. Urban heat island effects on estimates of observed climate change. Wiley Interdisciplinary Reviews-Climate Change, **1**(1): 123-133.
Parker, D.E., 2011. Recent land surface air temperature trends assessed using the 20th Century Reanalysis. Journal of Geophysical Research - Atmospheres, **116**: D20125.
Parker, D.E., Jones, P., Peterson, T.C. and Kennedy, J., 2009. Comment on "Unresolved issues with the assessment of multidecadal global land surface temperature trends" by Roger A. Pielke Sr. et al. Journal of Geophysical Research-Atmospheres, **114**.
Parrish, D.D., Law, K.S., Staehelin, J., Derwent, R., Cooper, O.R., Tanimoto, H., Volz-Thomas, A., Gilge, S., Scheel, H.E., Steinbacher, M. and Chan, E., 2012. Long-term changes in lower tropospheric baseline ozone concentrations at northern mid-latitudes. Atmos. Chem. Phys. Discuss., **12**(6): 13881-13931.
Pattanaik, D.R. and Rajeevan, M., 2010. Variability of extreme rainfall events over India during southwest monsoon season. Meteorological Applications, **17**(1): 88-104.
Pavan, V., Tomozeiu, R., Cacciamani, C. and Di Lorenzo, M., 2008. Daily precipitation observations over Emilia-Romagna: mean values and extremes. International Journal of Climatology, **28**(15): 2065-2079.
Penalba, O.C. and Robledo, F.A., 2010. Spatial and temporal variability of the frequency of extreme daily rainfall regime in the La Plata Basin during the 20th century. Climatic Change, **98**(3-4): 531-550.
Perkins, S. and Alexander, L., 2012. On the Measurement of Heat Waves. Journal of Climate, **submitted June 2012**.
Perkins, S., Alexander, L. and Nairn, J., 2012. Increasing Intensity and Frequency of Observed Global Heat Waves. Geophysical Research Letters (submitted).
Peterson, T.C., Baringer, M.O., Thorne, P.W., Menne, M.J., Kennedy, J.J., Christy, J., Seidel, D., Mears, C., Haimberger, L., Wang, J., Zhang, L., Levinson, D.H., Hilburn, K.A., Kruk, M.C., Robinson, D.A., Foster, M.J., Ackerman, S.A., Bennartz, R., Heidinger, A.K., Maddux, B.C., Rossow, W.B., Macdonald, A.M., Fekete, B.M., Bowling, L.C., Lammers, R.B., Lawford, R., Allan, R., Wong, T., Stackhouse, P.W., Kratz, D.P., Wilber, A.C.,

Schnell, R.C., Dlugokencky, E.J., Montzka, S.A., Elkins, J.W., Dutton, G.S., Haywood, J., Bellouin, N., Jones, A., Weber, M., Pelto, M.S., Belward, A.S., Bartholome, E., Achard, F., Brink, A.B., Gobron, N., Levy, J.M., Xue, Y., Reynolds, R.W., Johnson, G.C., Lyman, J.M., Willis, J.K., Levitus, S., Boyer, T., Antonov, J., Schmid, C., Goni, G.J., Yu, L., Weller, R.A., Knaff, J.A., Lumpkin, R., Goni, G., Dohan, K., Meinen, C.S., Kanzow, T.O., Cunningham, S.A., Johns, W.E., Beal, L.M., Hirschi, J.J.M., Rayner, D., Longworth, H.R., Bryden, H.L., Marotzke, J., Merrifield, M.A., Nerem, R.S., Mitchum, G.T., Miller, L., Leuliette, E., Gill, S., Feely, R.A., Sabine, C.L., Wanninkhof, R., Takahashi, T., Behrenfeld, M.J., Siegel, D.A., O'Malley, R.T., Maritorena, S., Dickson, A.G., Diamond, H.J., L'Heureux, M., Bell, G., Halpert, M., Bell, G.D., Blake, E., Goldenberg, S.B., Kimberlain, T., Landsea, C.W., Pasch, R., Schemm, J., Weyman, J., Camargo, S.J., Gleason, K.L., Salinger, M.J., Trewin, B., Watkins, A.B., Luo, J.J., Richter-Menge, J., Overland, J., Wang, M., Walsh, J., Perovich, D.K., Meier, W., Nghiem, S.V., Walker, D.A., Bhatt, U.S., Raynolds, M.K., Comiso, J.E., Epstein, H.E., Jia, G.J., Romanovsky, V., Oberman, N., Drozdov, D., Malkova, G., Kholodov, A., Marchenko, S., Derksen, C., Brown, R., Wang, L., Sharp, M., Wolken, G., Box, J.E., Bai, L.S., Benson, R., Bhattacharya, I., Bromwich, D.H., Cappelen, J., Decker, D., DiGirolamo, N., Fettweis, X., Hall, D., Hanna, E., Mote, T., Tedesco, M., van de Wal, R., van den Broeke, M., Fogt, R.L., Scambos, T.A., Barreira, S., Colwell, S., Turner, J., Liu, H., Massom, R.A., Reid, P., Stammerjohn, S., NeW man, P.A., Vincent, L.A., Stephens, S.E., Heim, R.R., Fenimore, C., Shulski, M., Ballard, R.A., Davydova-Belitskaya, V., Romero-Cruz, F., Fonseca, C., Perez, R., Lapinel, B., Cutie, V., Gonzales, I., Boudet, D., Hernandez, M., Stephenson, T.S., Taylor, M.A., Spence, J.M., Rossi, S., Cupo, J.P., Martinez, R., Pabon, D., Leon, G., Jaimes, E., Quintero, A., Mascarenhas, A., Marengo, J.A., Baez, J., Ronchail, J., Aceituno, P., Bidegain, M., Quintana, J., Skansi, M., Rusticucci, M., Kabidi, K., Sayouri, A., Sebbari, R., Attaher, S., Khalil, A., Medany, M., Njau, L.N., Bell, M.A., Thiaw, W.M., Osman-Elasha, B., Oludhe, C., Ogallo, L., Mhanda, A., Mutasa, W.Z.C., Gamedze, M.S., Kruger, A., McBride, C., Obregon, A., Bissolli, P., Parker, D.E., Trigo, R.M., Barriopedro, D., Bulygina, O.N., Korshunova, N.N., Razuvaev, V.N., Guo, Y., Sakai, Y., Zhao, S., Wang, X., Lee, H., Rajeevan, M., Revadekar, J., Rogers, M., Khoshkam, M., Rahimzadeh, F., Trewin, B.C., McGree, S., Guard, C. and Lander, M.A., 2009. State of the Climate in 2008. Bulletin of the American Meteorological Society, **90**(8): S13-+.

Peterson, T.C. and Manton, M.J., 2008. Monitoring changes in climate extremes - A tale of international collaboration. Bulletin of the American Meteorological Society, **89**(9): 1266-1271.

Peterson, T.C., Willett, K.M. and Thorne, P.W., 2011. Observed changes in surface atmospheric energy over land. Geophysical Research Letters, **38**.

Peterson, T.C., Zhang, X.B., Brunet-India, M. and Vazquez-Aguirre, J.L., 2008. Changes in North American extremes derived from daily weather data. Journal of Geophysical Research-Atmospheres, **113**(D7).

Petrow, T. and Merz, B., 2009. Trends in flood magnitude, frequency and seasonality in Germany in the period 1951-2002. Journal of Hydrology, **371**(1-4): 129-141.

Pezza, A.B., Simmonds, I. and Renwick, J.A., 2007. Southern Hemisphere cyclones and anticyclones: Recent trends and links with decadal variability in the Pacific Ocean. International Journal of Climatology, **27**(11): 1403-1419.

Philipona, R., Behrens, K. and Ruckstuhl, C., 2009. How declining aerosols and rising greenhouse gases forced rapid warming in Europe since the 1980s. Geophysical Research Letters, **36**: L02806.

Philipona, R., Durr, B., Marty, C., Ohmura, A. and Wild, M., 2004. Radiative forcing - measured at Earth's surface - corroborate the increasing greenhouse effect. Geophysical Research Letters, **31**(3): L03202.

Philipp, A., Della-Marta, P.M., Jacobeit, J., Fereday, D.R., Jones, P.D., Moberg, A. and Wanner, H., 2007. Long-term variability of daily North Atlantic-European pressure patterns since 1850 classified by simulated annealing clustering. Journal of Climate, **20**(16): 4065-4095.

Piao, S., Ciais, P. and al., e., 2010. The impacts of climate change on water resources and agriculture in China. Nature, **467**: 43-51.

Pielke, R.A. and Matsui, T., 2005. Should light wind and windy nights have the same temperature trends at individual levels even if the boundary layer averaged heat content change is the same? Geophysical Research Letters, **32**(21).

Pielke, R.A., Sr., Davey, C.A., Niyogi, D., Fall, S., Steinweg-Woods, J., Hubbard, K., Lin, X., Cai, M., Lim, Y.-K., Li, H., Nielsen-Gammon, J., Gallo, K., Hale, R., Mahmood, R., Foster, S., McNider, R.T. and Blanken, P., 2007. Unresolved issues with the assessment of multidecadal global land surface temperature trends. Journal of Geophysical Research-Atmospheres, **112**(D24).

Pinker, R.T., Zhang, B. and Dutton, E.G., 2005. Do satellites detect trends in surface solar radiation? Science, **308**(5723): 850-854.

Pinto, J.G., Spangehl, T., Ulbrich, U. and Speth, P., 2006. Assessment of winter cyclone activity in a transient ECHAM4-OPYC3 GHG experiment. Meteorologische Zeitschrift, **15**(3): 279-291.

Pirazzoli, P.A. and Tomasin, A., 2003. Recent near-surface wind changes in the central Mediterranean and Adriatic areas. International Journal of Climatology, **23**(8): 963-973.

Po-Chedley, S. and Fu, Q., 2012. A Bias in the Midtropospheric Channel Warm Target Factor on the NOAA-9 Microwave Sounding Unit. Journal of Atmospheric and Oceanic Technology, **29**(5): 646-652.

Portmann, R.W., Solomon, S. and Hegerl, G.C., 2009. Linkages between climate change, extreme temperature and precipitation across the United States. Proceedings of the National Academy of Sciences, **106**(18): 7324-7329.

Power, S., Casey, T., Folland, C., Colman, A. and Mehta, V., 1999. Inter-decadal modulation of the impact of ENSO on Australia. Climate Dynamics, **15**(5): 319-324.
Power, S.B. and Kociuba, G., 2011a. The impact of global warming on the Southern Oscillation Index. Clim. Dynamics, **37**(9-10): 1745-1754.
Power, S.B. and Kociuba, G., 2011b. What Caused the Observed Twentieth-Century Weakening of the Walker Circulation? J. Climate, **24**(24): 6501-6514.
Pozzoli, L., Janssens-Maenhout, G., Diehl, T., Bey, I., Schultz, M.G., Feichter, J., Vignati, E. and Dentener, F., 2011. Reanalysis of tropospheric sulfate aerosol and ozone for the period 1980-2005 using the aerosol-chemistry-climate model ECHAM5-HAMMOZ. Atmospheric Chemistry and Physics, **11**: 9563-9594.
Prata, F., 2008. The climatological record of clear-sky longwave radiation at the Earth's surface: evidence for water vapour feedback? International Journal of Remote Sensing, **29**(17-18): 5247-5263.
Prather, M. and Hsu, J., 2008. NF3, the greenhouse gas missing from Kyoto. Geophysical Research Letters: -.
Prinn, R., Cunnold, D., Rasmussen, R., Simmonds, P., Alyea, F., Crawford, A., Fraser, P. and Rosen, R., 1990. Atmospheric Emissions and Trends of Nitrous Oxide Deduced From 10 Years of ALE-GAGE Data. J. Geophys. Res., **95**(D11): 18,369-18,385.
Prinn, R., Huang, J., Weiss, R., Cunnold, D., Fraser, P., Simmonds, P., McCulloch, A., Harth, C., Reimann, S., Salameh, P., O'Doherty, S., Wang, R., Porter, L., Miller, B. and Krummel, P., 2005. Evidence for variability of atmospheric hydroxyl radicals over the past quarter century. Geophysical Research Letters: -.
Prinn, R., Weiss, R., Fraser, P., Simmonds, P., Cunnold, D., Alyea, F., O'Doherty, S., Salameh, P., Miller, B., Huang, J., Wang, R., Hartley, D., Harth, C., Steele, L., Sturrock, G., Midgley, P. and McCulloch, A., 2000. A history of chemically and radiatively important gases in air deduced from ALE/GAGE/AGAGE. Journal of Geophysical Research-Atmospheres, **105**(D14): 17751-17792.
Pryor, S.C., Barthelmie, R.J. and Riley, E.S., 2007. Historical evolution of wind climates in the USA - art. no. 012065. In: M.O.L. Hansen and K.S. Hansen (Editors), Science of Making Torque from Wind. Journal of Physics Conference Series, pp. 12065-12065.
Pryor, S.C., Howe, J.A. and Kunkel, K.E., 2009. How spatially coherent and statistically robust are temporal changes in extreme precipitation in the contiguous USA? International Journal of Climatology, **29**(1): 31-45.
Qian, Y., Gong, D.Y., Fan, J.W., Leung, L.R., Bennartz, R., Chen, D.L. and Wang, W.G., 2009. Heavy pollution suppresses light rain in China: Observations and modeling. J. Geophys. Res.-Atmos., **114**.
Qian, Y., Kaiser, D.P., Leung, L.R. and Xu, M., 2006. More frequent cloud-free sky and less surface solar radiation in China from 1955 to 2000. Geophysical Research Letters, **33**(1): L01812.
QingXiang, L., WenJie, D., Wei, L., Xiaorong, G., Jones, P., Kennedy, J. and Parker, D., 2010. Assessment of the uncertainties in temperature change in China during the last century, Chinese Science Bulletin, pp. 1974-1982.
Qu, W.J., Arimoto, R., Zhang, X.Y., Zhao, C.H., Wang, Y.Q., Sheng, L.F. and Fu, G., 2010. Spatial distribution and interannual variation of surface PM10 concentrations over eighty-six Chinese cities. Atmos. Chem. Phys., **10**(12): 5641-5662.
Quan, J., Zhang, Q., He, H., Liu, J., Huang, M. and Jin, H., 2011. Analysis of the formation of fog and haze in North China Plain (NCP). Atmos. Chem. Phys., **11**(15): 8205-8214.
Quinn, P.K., Bates, T.S., Schulz, K. and Shaw, G.E., 2009. Decadal trends in aerosol chemical composition at Barrow, Alaska: 1976-2008. Atmos. Chem. Phys., **9**(22): 8883-8888.
Rahimzadeh, F., Asgari, A. and Fattahi, E., 2009. Variability of extreme temperature and precipitation in Iran during recent decades. International Journal of Climatology, **29**(3): 329-343.
Rahmstorf, S. and Coumou, D., 2011. Increase of extreme events in a warming world. Proceedings of the National Academy of Sciences of the United States of America, **108**(44): 17905-17909.
Raible, C.C., Della-Marta, P.M., Schwierz, C., Wernli, H. and Blender, R., 2008. Northern hemisphere extratropical cyclones: A comparison of detection and tracking methods and different reanalyses. Monthly Weather Review, **136**(3): 880-897.
Raichijk, C., 2011. Observed trends in sunshine duration over South America. Int. J. Climatol.: DOI: 10.1002/joc.2296.
Rajeevan, M., Bhate, J. and Jaswal, A.K., 2008. Analysis of variability and trends of extreme rainfall events over India using 104 years of gridded daily rainfall data. Geophysical Research Letters, **35**(18).
Ramanathan, V., Crutzen, P.J., Kiehl, J.T. and Rosenfeld, D., 2001. Atmosphere - Aerosols, climate, and the hydrological cycle. Science, **294**(5549): 2119-2124.
Randall, R.M. and Herman, B.M., 2008. Using limited time period trends as a means to determine attribution of discrepancies in microwave sounding unit-derived tropospheric temperature time series. Journal of Geophysical Research-Atmospheres, **113**(D5).
Randel, W., J., 2010. **Variability and trends in stratospheric temperature and water vapor**. In: S. Polvani, and Waugh (Editor), *The Stratosphere: Dynamics, Transport and Chemistry*. American Geophysical Union, pp. 123-135.
Randel, W.J., Shine, K.P., Austin, J., Barnett, J., Claud, C., Gillett, N.P., Keckhut, P., Langematz, U., Lin, R., Long, C., Mears, C., Miller, A., Nash, J., Seidel, D.J., Thompson, D.W.J., Wu, F. and Yoden, S., 2009. An update of observed stratospheric temperature trends. Journal of Geophysical Research-Atmospheres, **114**.

Randel, W.J., Wu, F., Vomel, H., Nedoluha, G.E. and Forster, P., 2006. Decreases in stratospheric water vapor after 2001: Links to changes in the tropical tropopause and the Brewer-Dobson circulation. Journal of Geophysical Research-Atmospheres, **111**(D12).

Rasmusson, E.M. and Carpenter, T.H., 1982. Variations in Tropical Sea Surface Temperature and Surface Wind Fields Associated with the Southern Oscillation/El Niño. Monthly Weather Review, **110**(5): 354-384.

Rasmusson, E.M. and Wallace, J.M., 1983. Meteorological aspects of the El Nino - Southern Oscillation. Science, **222**(4629): 1195-1202.

Rausch, J., Heidinger, A. and Bennartz, R., 2010. Regional assessment of microphysical properties of marine boundary layer cloud using the PATMOS-x dataset. Journal of Geophysical Research-Atmospheres, **115**.

Ray, E.A., Moore, F.L., Rosenlof, K.H., Davis, S.M., Boenisch, H., Morgenstern, O., Smale, D., Rozanov, E., Hegglin, M., Pitari, G., Mancini, E., Braesicke, P., Butchart, N., Hardiman, S., Li, F., Shibata, K. and Plummer, D.A., 2010. Evidence for changes in stratospheric transport and mixing over the past three decades based on multiple data sets and tropical leaky pipe analysis. Journal of Geophysical Research-Atmospheres, **115**.

Rayner, D.P., 2007. Wind run changes: The dominant factor affecting pan evaporation trends in Australia. Journal of Climate, **20**(14): 3379-3394.

Rayner, N.A., Brohan, P., Parker, D.E., Folland, C.K., Kennedy, J.J., Vanicek, M., Ansell, T.J. and Tett, S.F.B., 2006. Improved analyses of changes and uncertainties in sea surface temperature measured in situ sice the mid-nineteenth century: The HadSST2 dataset. Journal of Climate, **19**(3): 446-469. http://hadobs.metoffice.com/hadsst2/diagnostics/global/nh+sh/annual

Rayner, N.A., Parker, D.E., Horton, E.B., Folland, C.K., Alexander, L.V., Rowell, D.P., Kent, E.C. and Kaplan, A., 2003. Global analyses of sea surface temperature, sea ice, and night marine air temperature since the late nineteenth century. Journal of Geophysical Research-Atmospheres, **108**(D14).

Re, M. and Barros, V.R., 2009. Extreme rainfalls in SE South America. Climatic Change, **96**(1-2): 119-136.

Read, W.G., Lambert, A., Bacmeister, J., Cofield, R.E., Christensen, L.E., Cuddy, D.T., Daffer, W.H., Drouin, B.J., Fetzer, E., Froidevaux, L., Fuller, R., Herman, R., Jarnot, R.F., Jiang, J.H., Jiang, Y.B., Kelly, K., Knosp, B.W., Kovalenko, L.J., Livesey, N.J., Liu, H.C., Manney, G.L., Pickett, H.M., Pumphrey, H.C., Rosenlof, K.H., Sabounchi, X., Santee, M.L., Schwartz, M.J., Snyder, W.V., Stek, P.C., Su, H., Takacs, L.L., Thurstans, R.P., Vomel, H., Wagner, P.A., Waters, J.W., Webster, C.R., Weinstock, E.M. and Wu, D.L., 2007. Aura Microwave Limb Sounder upper tropospheric and lower stratospheric H2O and relative humidity with respect to ice validation. Journal of Geophysical Research-Atmospheres, **112**(D24).

Ren, G.Y., Zhou, Y.Q., Chu, Z.Y., Zhou, J.X., Zhang, A.Y., Guo, J. and Liu, X.F., 2008. Urbanization effects on observed surface air temperature trends in north China. Journal of Climate, **21**(6): 1333-1348.

Renard, B., Lang, M., Bois, P., Dupeyrat, A., Mestre, O., Niel, H., Sauquet, E., Prudhomme, C., Parey, S., Paquet, E., Neppel, L. and Gailhard, J., 2008. Regional methods for trend detection: Assessing field significance and regional consistency. Water Resources Research, **44**(8).

Reynolds R.W., T. M. Smith. Improved global sea surface temperature analyses.. J. Climate 7, 1994

Reynolds, R., Rayner, N., Smith, T., Stokes, D. and Wang, W., 2002a. An improved in situ and satellite SST analysis for climate. Journal of Climate, **15**(13): 1609-1625.

Reynolds, R.W., Gentemann, C.L. and Corlett, G.K., 2010. Evaluation of AATSR and TMI Satellite SST Data. Journal of Climate, **23**(1): 152-165.

Reynolds, R.W., Rayner, N.A., Smith, T.M., Stokes, D.C., Wang, W. and Ams, A.M.S., 2002b. An improved in situ and satellite SST analysis. 13th Symposium on Global Change and Climate Variations, 146-148 pp.

Richter, A., J. P. Burrows, H. Nüß, C. Granier and Niemeier, U., 2005. Increase in tropospheric nitrogen dioxide over China observed from space. Nature, **437,**(doi:10.1038/nature04092): 129-132, d.

Rienecker, M.M., Suarez, M.J., Gelaro, R., Todling, R., Bacmeister, J., Liu, E., Bosilovich, M.G., Schubert, S.D., Takacs, L., Kim, G.-K., Bloom, S., Chen, J., Collins, D., Conaty, A., da Silva, A., Gu, W., Joiner, J., Koster, R.D., Lucchesi, R., Molod, A., Owens, T., Pawson, S., Pegion, P., Redder, C. R., Reichle, R., Robertson, F. R., Ruddick, A. G., Sienkiewicz, M., Woollen, J., 2011. MERRA: NASA's Modern-Era Retrospective Analysis for Research and Applications. J. Climate, **in press**.

Rigby, M., Muhle, J., Miller, B., Prinn, R., Krummel, P., Steele, L., Fraser, P., Salameh, P., Harth, C., Weiss, R., Greally, B., O'Doherty, S., Simmonds, P., Vollmer, M., Reimann, S., Kim, J., Kim, K., Wang, H., Olivier, J., Dlugokencky, E., Dutton, G., Hall, B. and Elkins, J., 2010. History of atmospheric SF6 from 1973 to 2008. Atmospheric Chemistry and Physics: 10305-10320.

Rigby, M., Prinn, R., Fraser, P., Simmonds, P., Langenfelds, R., Huang, J., Cunnold, D., Steele, L., Krummel, P., Weiss, R., O'Doherty, S., Salameh, P., Wang, H., Harth, C., Muhle, J. and Porter, L., 2008. Renewed growth of atmospheric methane. Geophysical Research Letters: -.

Riihimaki, L.D., Vignola, F.E. and Long, C.N., 2009. Analyzing the contribution of aerosols to an observed increase in direct normal irradiance in Oregon. Journal of Geophysical Research-Atmospheres, **114**: D00d02.

Robinson, D.A. and A. Frei. 2000: Seasonal variability of northern hemisphere snow extent using visible satellite data. Professional Geographer , 51, 307-314.

Robock, A., Mu, M.Q., Vinnikov, K., Trofimova, I.V. and Adamenko, T.I., 2005. Forty-five years of observed soil moisture in the Ukraine: No summer desiccation (yet). Geophys. Res. Lett., **32**(3).

Robock, A., Vinnikov, K.Y., Srinivasan, G., Entin, J.K., Hollinger, S.E., Speranskaya, N.A., Liu, S.X. and Namkhai, A., 2000. The Global Soil Moisture Data Bank. Bulletin of the American Meteorological Society, **81**(6): 1281-1299.

Rodda, J.C., Little, M.A., Rodda, H.J.E. and McSharry, P.E., 2010. A comparative study of the magnitude, frequency and distribution of intense rainfall in the United Kingdom. International Journal of Climatology, **30**(12): 1776-1783.

Roderick, M.L. and Farquhar, G.D., 2002. The cause of decreased pan evaporation over the past 50 years. Science, **298**(5597): 1410-1411.

Roderick, M.L., Rotstayn, L.D., Farquhar, G.D. and Hobbins, M.T., 2007. On the attribution of changing pan evaporation. Geophysical Research Letters, **34**(17).

Rohde, R., Curry, J., Groom, D., Jacobsen, R., Muller, R.A., Perlmutter, S., Rosenfeld, A., Wickham, C. and Wurtele, J., submitted. Berkeley Earth Temperature Averaging Process. Journal of Geophysical Reseach: submitted.

Rohs, S., Schiller, C., Riese, M., Engel, A., Schmidt, U., Wetter, T., Levin, I., Nakazawa, T. and Aoki, S., 2006. Long-term changes of methane and hydrogen in the stratosphere in the period 1978-2003 and their impact on the abundance of stratospheric water vapor. Journal of Geophysical Research-Atmospheres, **111**(D14).

Rosenlof, K.H. and Reid, G.C., 2008. Trends in the temperature and water vapor content of the tropical lower stratosphere: Sea surface connection. Journal of Geophysical Research-Atmospheres, **113**(D6).

Rossow, W.B. and Schiffer, R.A., 1999. Advances in understanding clouds from ISCCP. Bulletin of the American Meteorological Society, **80**(11): 2261-2287.

Ruckstuhl, C., Philipona, R., Behrens, K., Coen, M.C., Durr, B., Heimo, A., Matzler, C., Nyeki, S., Ohmura, A., Vuilleumier, L., Weller, M., Wehrli, C. and Zelenka, A., 2008. Aerosol and cloud effects on solar brightening and the recent rapid warming. Geophysical Research Letters, **35**(12): L12708.

Ruddiman, W., 2003. The anthropogenic greenhouse era began thousands of years ago. Climatic Change: 261-293.

Ruddiman, W., 2007. The early anthropogenic hypothesis: Challenges and responses. Reviews of Geophysics: -.

Russak, V., 2009. Changes in solar radiation and their influence on temperature trend in Estonia (1955-2007). Journal of Geophysical Research-Atmospheres, **114**: D00d01.

RUSSELL, J., GORDLEY, L., PARK, J., DRAYSON, S., HESKETH, W., CICERONE, R., TUCK, A., FREDERICK, J., HARRIES, J. and CRUTZEN, P., 1993. THE HALOGEN OCCULTATION EXPERIMENT. Journal of Geophysical Research-Atmospheres, **98**(D6): 10777-10797.

Rusticucci, M., 2012. Observed and simulated variability of extreme temperature events over South America. Atmospheric Research, **106**(2012): 1–17.

Rusticucci, M. and Renom, M., 2008. Variability and trends in indices of quality-controlled daily temperature extremes in Uruguay. International Journal of Climatology, **28**(8): 1083-1095.

Saha, S., Moorthi, S., Pan, H.L., Wu, X.R., Wang, J.D., Nadiga, S., Tripp, P., Kistler, R., Woollen, J., Behringer, D., Liu, H.X., Stokes, D., Grumbine, R., Gayno, G., Wang, J., Hou, Y.T., Chuang, H.Y., Juang, H.M.H., Sela, J., Iredell, M., Treadon, R., Kleist, D., Van Delst, P., Keyser, D., Derber, J., Ek, M., Meng, J., Wei, H.L., Yang, R.Q., Lord, S., Van den Dool, H., Kumar, A., Wang, W.Q., Long, C., Chelliah, M., Xue, Y., Huang, B.Y., Schemm, J.K., Ebisuzaki, W., Lin, R., Xie, P.P., Chen, M.Y., Zhou, S.T., Higgins, W., Zou, C.Z., Liu, Q.H., Chen, Y., Han, Y., Cucurull, L., Reynolds, R.W., Rutledge, G. and Goldberg, M., 2010. THE NCEP CLIMATE FORECAST SYSTEM REANALYSIS. Bulletin of the American Meteorological Society, **91**(8): 1015-1057.

Saikawa, E., Rigby, M., Prinn, R.J., Montzka, S.A., Miller, B.R., Kuijpers, L.J.M., Fraser, P.J.B., Vollmer, M.K., Saito, T., Yokouchi, Y., Harth, C.M., Mühle, J., Weiss, R.F., Salameh, P.K., Kim, J., Li, S., Park, S., Kim, K.-R., Young, D., O'Doherty, S., Simmonds, P.G., McCulloch, A., Krummel, P.B., Steele, L.P., Lunder, C., Hermansen, O., Maione, M., Arduini, J., Yao, B., Zhou, L.X., Wang, H.J., Elkins, J.W. and Hall, B., 2012. Global and regional emissions estimates for HCFC-22. Atmos. Chem. Phys. Discuss., **12**: 18423-18285.

Saito, T., Yokouchi, Y., Stohl, A., Taguchi, S. and Mukai, H., 2010. Large Emissions of Perfluorocarbons in East Asia Deduced from Continuous Atmospheric Measurements. Environmental Science & Technology, **44**(11): 4089-4095.

Saji, N.H., Goswami, B.N., Vinayachandran, P.N. and Yamagata, T., 1999. A dipole mode in the tropical Indian Ocean. Nature, **401**(6751): 360-363.

Sakamoto, M. and Christy, J.R., 2009. The Influences of TOVS Radiance Assimilation on Temperature and Moisture Tendencies in JRA-25 and ERA-40. Journal of Atmospheric and Oceanic Technology, **26**(8): 1435-1455.

Sanchez-Lorenzo, A., Calbo, J., Brunetti, M. and Deser, C., 2009. Dimming/brightening over the Iberian Peninsula: Trends in sunshine duration and cloud cover and their relations with atmospheric circulation. Journal of Geophysical Research-Atmospheres, **114**: D00d09.

Sanchez-Lorenzo, A., Calbo, J. and Martin-Vide, J., 2008. Spatial and Temporal Trends in Sunshine Duration over Western Europe (1938-2004). Journal of Climate, **21**(22): 6089-6098.

Sanchez-Lorenzo, A. and Wild, M., 2012. Decadal variations in estimated surface solar radiation over Switzerland since the late 19th century. Atmospheric Chemistry and Physics Discussion, **12**: 10815-10843.

Santer, B., Thorne, P., Haimberger, L., Taylor, K., Wigley, T., Lanzante, J., Solomon, S., Free, M., Gleckler, P., Jones, P., Karl, T., Klein, S., Mears, C., Nychka, D., Schmidt, G., Sherwood, S. and Wentz, F., 2008. Consistency of modelled and observed temperature trends in the tropical troposphere. International Journal of Climatology, **28**(13): 1703-1722.

Santer, B.D., Mears, C., Wentz, F.J., Taylor, K.E., Gleckler, P.J., Wigley, T.M.L., Barnett, T.P., Boyle, J.S., Bruggemann, W., Gillett, N.P., Klein, S.A., Meehl, G.A., Nozawa, T., Pierce, D.W., Stott, P.A., Washington, W.M. and Wehner, M.F., 2007. Identification of human-induced changes in atmospheric moisture content. Proceedings of the National Academy of Sciences of the United States of America, **104**: 15248-15253.

Santer, B.D., Mears, C.A., Doutriaux, C., Caldwell, P.M., Gleckler, P.J., Wigley, T.M.L., Solomon, S., Gillett, N., Ivanova, D.P., Karl, T.R., Lanzante, J.R., Meehl, G.A., Stott, P.A., Taylor, K.E., Thorne, P., Wehner, M.F. and Wentz, F.J., 2011. Separating Signal and Noise in Atmospheric Temperature Changes: The Importance of Timescale. Journal of Geophysical Research.

Scaife, A., Folland, C., Alexander, L., Moberg, A. and Knight, J., 2008a. European climate extremes and the North Atlantic Oscillation. Journal of Climate, **21**(1): 72-83.

Scaife, A.A., Folland, C.K., Alexander, L.V., Moberg, A. and Knight, J.R., 2008b. European climate extremes and the North Atlantic Oscillation. Journal of Climate, **21**(1): 72-83.

Schar, C., Vidale, P.L., Luthi, D., Frei, C., Haberli, C., Liniger, M.A. and Appenzeller, C., 2004. The role of increasing temperature variability in European summer heatwaves. Nature, **427**(6972): 332-336.

Scherer, M., Vomel, H., Fueglistaler, S., Oltmans, S.J. and Staehelin, J., 2008. Trends and variability of midlatitude stratospheric water vapour deduced from the re-evaluated Boulder balloon series and HALOE. Atmospheric Chemistry and Physics, **8**(5): 1391-1402.

Scherrer, S.C. and Appenzeller, C., 2006. Swiss Alpine snow pack variability: major patterns and links to local climate and large-scale flow. Climate Res., **32**(3): 187-199.

Schiller, C., Grooss, J.U., Konopka, P., Plager, F., Silva dos Santos, F.H. and Spelten, N., 2009. Hydration and dehydration at the tropical tropopause. Atmos. Chem. Phys., **9**(24): 9647-9660.

Schmidt, G.A., 2009. Spurious correlations between recent warming and indices of local economic activity. International Journal of Climatology, **29**(14): 2041-2048.

Schnadt Poberaj, C., Staehelin, J., Brunner, D., Thouret, V., De Backer, H. and StÃ¼bi, R., 2009. Long-term changes in UT/LS ozone between the late 1970s and the 1990s deduced from the GASP and MOZAIC aircraft programs and from ozonesondes. Atmos. Chem. Phys. Discuss., **9**(1): 2435-2499.

Schneider, T., O'Gorman, P.A. and Levine, X.J., 2010. Water vapour and the dynamics of climate changes. Reviews of Geophysics, pp. RG3001.

Schneidereit, A., Blender, R., Fraedrich, K. and Lunkeit, F., 2007. Icelandic climate and north Atlantic cyclones in ERA-40 reanalyses. Meteorologische Zeitschrift, **16**(1): 17-23.

Schwartz, R.D., 2005. Global dimming: Clear-sky atmospheric transmission from astronomical extinction measurements. Journal of Geophysical Research-Atmospheres, **110**(D14).

Scinocca, J.F., Stephenson, D.B., Bailey, T.C. and Austin, J., 2010. Estimates of past and future ozone trends from multimodel simulations using a flexible smoothing spline methodology. Journal of Geophysical Research-Atmospheres, **115**.

Seidel, D.J., Fu, Q., Randel, W.J. and Reichler, T.J., 2008. Widening of the tropical belt in a changing climate. Nature Geoscience, **1**(1): 21-24.

Seidel, D.J., Gillett, N.P., Lanzante, J.R., Shine, K.P. and Thorne, P.W., 2011. Stratospheric temperature trends: our evolving understanding. Wiley Interdisciplinary Reviews-Climate Change, **2**(4): 592-616.

Seidel, D.J., Gillett, N. P., Lanzante, J. R., Shine, K. P., Thorne, P. W., 2011. Stratospheric temperature trends: Our evolving understanding, WIRES: Climate Change.

Seidel, D.J. and Lanzante, J.R., 2004. An assessment of three alternatives to linear trends for characterizing global atmospheric temperature changes. Journal of Geophysical Research-Atmospheres, **109**(D14).

Seidel, D.J. and Randel, W.J., 2007. Recent widening of the tropical belt: Evidence from tropopause observations. Journal of Geophysical Research-Atmospheres, **112**(D20).

Seleshi, Y. and Camberlin, P., 2006. Recent changes in dry spell and extreme rainfall events in Ethiopia. Theoretical and Applied Climatology, **83**(1-4): 181-191.

SEN, P., 1968. ESTIMATES OF REGRESSION COEFFICIENT BASED ON KENDALLS TAU. Journal of the American Statistical Association, **63**(324): 1379-&.

Sen Roy, S., 2009. A spatial analysis of extreme hourly precipitation patterns in India. International Journal of Climatology, **29**(3): 345-355.

Sen Roy, S. and Balling, R.C., 2005. Analysis of trends in maximum and minimum temperature, diurnal temperature range, and cloud cover over India. Geophysical Research Letters, **32**(12).

Seneviratne, S.I., Corti, T., Davin, E.L., Hirschi, M., Jaeger, E.B., Lehner, I., Orlowsky, B. and Teuling, A.J., 2010. Investigating soil moisture-climate interactions in a changing climate: A review. Earth-Science Reviews, **99**(3-4): 125-161.

Seneviratne, S.I., Nicholls, N., Easterling, D., Goodess, C.M., Kanae, S., Kossin, J., Luo, Y., Marengo, J., McInnes, K., Rahimi, M., Reichstein, M., Sorteberg, A., Vera, C. and Zhang, X., 2012a. Changes in Climate Extremes and their Impacts on the Natural Physical Environment.

Seneviratne, S.I., Nicholls, N., Easterling, D., Goodess, C.M., Kanae, S., Kossin, J., Luo, Y., Marengo, J., McInnes, K., Rahimi, M., Reichstein, M., Sorteberg, A., Vera, C. and Zhang, X., 2012b. Changes in Climate Extremes and their Impacts on the Natural Physical Environment, IPCC, Geneva.

Serquet, G., Marty, C., Dulex, J.P. and Rebetez, M., 2011. Seasonal trends and temperature dependence of the snowfall/precipitation-day ratio in Switzerland. Geophysical Research Letters, **38**.
Sharma, S., Andrews, E., Barrie, L.A., Ogren, J.A. and Lavoué, D., 2006. Variations and sources of the equivalent black carbon in the high Arctic revealed by long-term observations at Alert and Barrow: 1989-2003. J. Geophys. Res., **111**(D14): D14208.
Shaw, S.B., Royem, A.A. and Riha, S.J., 2011. The Relationship between Extreme Hourly Precipitation and Surface Temperature in Different Hydroclimatic Regions of the United States. JOURNAL OF HYDROMETEOROLOGY, **12**(2): 319-325.
Sheffield, J., Andreadis, K., Wood, E. and Lettenmaier, D., 2009. Global and Continental Drought in the Second Half of the Twentieth Century: Severity-Area-Duration Analysis and Temporal Variability of Large-Scale Events. Journal of Climate, **22**(8): 1962-1981.
Sheffield, J. and Wood, E.F., 2007. Characteristics of global and regional drought, 1950-2000: Analysis of soil moisture data from off-line simulation of the terrestrial hydrologic cycle. Journal of Geophysical Research-Atmospheres, **112**(D17).
Sheffield, J. and Wood, E.F., 2008. Global trends and variability in soil moisture and drought characteristics, 1950-2000, from observation-driven Simulations of the terrestrial hydrologic cycle. Journal of Climate, **21**(3): 432-458.
Shekar, M., Chand, H., Kumar, S., Srinivasan, K. and Ganju, A., 2010. Climate change studies in the western Himalaya. Annals of Glaciology, **51**.
Sherwood, S.C., 2007. Simultaneous detection of climate change and observing biases in a network with incomplete sampling. Journal of Climate, **20**(15): 4047-4062.
Sherwood, S.C., Meyer, C.L., Allen, R.J. and Titchner, H.A., 2008. Robust Tropospheric Warming Revealed by Iteratively Homogenized Radiosonde Data. Journal of Climate, **21**(20): 5336-5350.
Sherwood, S.C., Titchner, H.A., Thorne, P.W. and McCarthy, M.P., 2009. How do we tell which estimates of past climate change are correct. International Journal of Climatology, **29**(10): 1520-1523.
Shi, G.Y., Hayasaka, T., Ohmura, A., Chen, Z.H., Wang, B., Zhao, J.Q., Che, H.Z. and Xu, L., 2008. Data quality assessment and the long-term trend of ground solar radiation in China. Journal of Applied Meteorology and Climatology, **47**(4): 1006-1016.
Shi, L. and Bates, J.J., 2011. Three decades of intersatellite-calibrated High-Resolution Infrared Radiation Sounder upper tropospheric water vapor. J. Geophys. Res.-Atmos., **116**.
Shiklomanov, A.I., Lammers, R.B., Rawlins, M.A., Smith, L.C. and Pavelsky, T.M., 2007. Temporal and spatial variations in maximum river discharge from a new Russian data set. Journal of Geophysical Research-Biogeosciences, **112**(G4).
Shiklomanov, I.A., Georgievskii, V.Y., Babkin, V.I. and Balonishnikova, Z.A., 2010. Research Problems of Formation and Estimation of Water Resources and Water Availability Changes of the Russian Federation. Russian Meteorology and Hydrology, **35**(1): 13-19.
Shine, K.P., Barnett, J.J. and Randel, W.J., 2008. Temperature trends derived from Stratospheric Sounding Unit radiances: The effect of increasing CO2 on the weighting function. Geophysical Research Letters, **35**(2).
Shiu, C.J., Liu, S.C. and Chen, J.P., 2009. Diurnally Asymmetric Trends of Temperature, Humidity, and Precipitation in Taiwan. Journal of Climate, **22**(21): 5635-5649.
Sickles, J.E., II and Shadwick, D.S., 2007a. Changes in air quality and atmospheric deposition in the eastern United States: 1990-2004. J. Geophys. Res., **112**(D17): D17301.
Sickles, J.E., II and Shadwick, D.S., 2007b. Seasonal and regional air quality and atmospheric deposition in the eastern United States. J. Geophys. Res., **112**(D17): D17302.
Simmonds, I. and Keay, K., 2002. Surface fluxes of momentum and mechanical energy over the North Pacific and North Atlantic Oceans. Meteorology and Atmospheric Physics, **80**(1-4): 1-18.
Simmonds, P., Cunnold, D., Weiss, R., Miller, B., Prinn, R., Fraser, P., McCulloch, A., Alyea, F. and O'Doherty, S., 1998. Global trends and emission estimates of CCl4 from in situ background observations from July 1978 to June 1996 (vol 103, pg 16017, 1998). Journal of Geophysical Research-Atmospheres, **103**(D23): 31331-31331.
Simmons, A.J., Willett, K.M., Jones, P.D., Thorne, P.W. and Dee, D.P., 2010. Low-frequency variations in surface atmospheric humidity, temperature, and precipitation: Inferences from reanalyses and monthly gridded observational data sets. Journal of Geophysical Research-Atmospheres, **115**.
Simolo, C., Brunetti, M., Maugeri, M. and Nanni, T., 2011. Evolution of extreme temperatures in a warming climate. Geophysical Research Letters, **38**: 6.
Smith, L.C., Pavelsky, T., MacDonald, G., Shiklomanov, I.A. and Lammers, R., 2007. Rising minimum daily flows in northern Eurasian rivers suggest a growing influence of groundwater in the high-latitude water cycle. Journal of Geophysical Research.
Smith, T.M., Arkin, P.A., Sapiano, M.R.P. and Chang, C.Y., 2010. Merged Statistical Analyses of Historical Monthly Precipitation Anomalies Beginning 1900. Journal of Climate, **23**(21): 5755-5770.
Smith, T.M. and Reynolds, R.W., 2002. Bias corrections for historical sea surface temperatures based on marine air temperatures. Journal of Climate, **15**(1): 73-87.
Smith, T.M., Reynolds, R.W., Peterson, T.C. and Lawrimore, J., 2008. Improvements to NOAA's historical merged land-ocean surface temperature analysis (1880-2006). J. Climate, **21**(10): 2283-2296. Land temperatures:

ftp://ftp.ncdc.noaa.gov/pub/data/anomalies/monthly.land.90S.90N.df_1901-2000mean.dat Sea-surface temperatures: ftp://ftp.ncdc.noaa.gov/pub/data/mlost/operational/products/aravg.mon.ocean.90S.90N.asc

Smits, A., Tank, A. and Konnen, G.P., 2005. Trends in storminess over the Netherlands, 1962-2002. International Journal of Climatology, **25**(10): 1331-1344.

Soden, B.J., Jackson, D.L., Ramaswamy, V., Schwarzkopf, M.D. and Huang, X.L., 2005. The radiative signature of upper tropospheric moistening. Science, **310**(5749): 841-844.

Sohn, B.J. and Park, S.C., 2010. Strengthened tropical circulations in past three decades inferred from water vapor transport. Journal of Geophysical Research-Atmospheres, **115**.

Solomon, S., Rosenlof, K., Portmann, R., Daniel, J., Davis, S., Sanford, T. and Plattner, G., 2010. Contributions of Stratospheric Water Vapor to Decadal Changes in the Rate of Global Warming. Science: 1219-1223.

Song, H. and Zhang, M.H., 2007. Changes of the boreal winter Hadley circulation in the NCEP-NCAR and ECMWF reanalyses: A comparative study. Journal of Climate, **20**(20): 5191-5200.

Sorteberg, A. and Walsh, J.E., 2008. Seasonal cyclone variability at 70 degrees N and its impact on moisture transport into the Arctic. Tellus Series a-Dynamic Meteorology and Oceanography, **60**(3): 570-586.

Spencer, R.W. and Christy, J.R., 1992. PRECISION AND RADIOSONDE VALIDATION OF SATELLITE GRIDPOINT TEMPERATURE ANOMALIES .2. A TROPOSPHERIC RETRIEVAL AND TRENDS DURING 1979-90. Journal of Climate, **5**(8): 858-866.

St. Jacques, J.-M. and Sauchyn, D., 2009. Increasing winter baseflow and mean annual streamflow from possible permafrost thawing in the Northwest Territories, Canada. Geophys. Res. Lett., **36**.

Stachnik, J.P. and Schumacher, C., 2011. A comparison of the Hadley circulation in modern reanalyses. J. Geophys. Res.-Atmos., **116**.

Stahl, K., Hisdal, H., Hannaford, J., Tallaksen, L.M., Van Lanen, H.A.J., Sauquet, E., Demuth, S., Fendekova, M. and Jordar, J., 2010. Streamflow trends in Europe: evidence from a dataset of near-natural catchments. Hydrology and Earth System Sciences Discussions, **14**: 2367-2382.

Stahl, K. and Tallaksen, L.M., 2012. Filling the white space on maps of European runoff trends: estimates from a multi-model ensemble. Hydrology and Earth System Sciences Discussions, **9**: 2005-2032.

Stanhill, G. and Cohen, S., 2001. Global dimming: a review of the evidence for a widespread and significant reduction in global radiation with discussion of its probable causes and possible agricultural consequences. Agricultural and Forest Meteorology, **107**(4): 255-278.

Steeneveld, G.J., Holtslag, A.A.M., McNider, R.T. and Pielke, R.A., 2011. Screen level temperature increase due to higher atmospheric carbon dioxide in calm and windy nights revisited. Journal of Geophysical Research-Atmospheres, **116**.

Steig, E.J., Schneider, D.P., Rutherford, S.D., Mann, M.E., Comiso, J.C. and Shindell, D.T., 2009. Warming of the Antarctic ice-sheet surface since the 1957 International Geophysical Year. Nature, **460**(7256): 766-766.

Stemmler, K., Folini, D., Ubl, S., Vollmer, M., Reimann, S., Doherty, S., Greally, B., Simmonds, P. and Manning, A., 2007. European emissions of HFC-365mfc, a chlorine-free substitute for the foam blowing agents HCFC-141b and CFC-11. Environmental Science & Technology, **41**(4): 1145-1151.

Stephens, G.L., Li, J.L., Wild, M., C.A., C., Loeb, N., Kato, S., L'Ecuyer, T., Stackhouse, P.W. and Andrews, T., in press. The energy balance of the Earth's climate system.

Stephens, G.L., Wild, M., Stackhouse, P.W., L'Ecuyer, T., Kato, S. and Henderson, D.S., 2012. The Global Character of the Flux of Downward Longwave Radiation. Journal of Climate, **25**(7): 2329-2340.

Stephenson, D.B., Diaz, H.F. and Murnane, R.J., 2008. Definition, diagnosis and origin of extreme weather and climate events. In: R.J. Murnane and H.F. Diaz (Editors), Climate Extremes and Society. Cambridge University Press, Cambridge and New York, pp. 11-23.

Stephenson, D.B., Pavan, V., Collins, M., Junge, M.M., Quadrelli, R. and Participating, C.M.G., 2006. North Atlantic Oscillation response to transient greenhouse gas forcing and the impact on European winter climate: a CMIP2 multi-model assessment. Climate Dynamics, **27**(4).

Stern, D.I., 2006. Reversal of the trend in global anthropogenic sulfur emissions. Global Environmental Change-Human and Policy Dimensions, **16**(2): 207-220.

Stickler, A., Grant, A.N., Ewen, T., Ross, T.F., Vose, R.S., Comeaux, J., Bessemoulin, P., Jylha, K., Adam, W.K., Jeannet, P., Nagumy, A., Sterin, A.M., Allan, R., Compo, G.P., Griesser, T. and Bronnimann, S., 2010. THE COMPREHENSIVE HISTORICAL UPPER-AIR NETWORK. Bulletin of the American Meteorological Society, **91**(6): 741-+.

Stjern, C.W., Kristjansson, J.E. and Hansen, A.W., 2009. Global dimming and global brightening - an analysis of surface radiation and cloud cover data in northern Europe. International Journal of Climatology, **29**(5): 643-653.

Stohl, A., Kim, J., Li, S., O'Doherty, S., Muhle, J., Salameh, P., Saito, T., Vollmer, M., Wan, D., Weiss, R., Yao, B., Yokouchi, Y. and Zhou, L., 2010. Hydrochlorofluorocarbon and hydrofluorocarbon emissions in East Asia determined by inverse modeling. Atmospheric Chemistry and Physics: 3545-3560.

Stohl, A., Seibert, P., Arduini, J., Eckhardt, S., Fraser, P., Greally, B., Lunder, C., Maione, M., Muhle, J., O'Doherty, S., Prinn, R., Reimann, S., Saito, T., Schmidbauer, N., Simmonds, P., Vollmer, M., Weiss, R. and Yokouchi, Y., 2009. An analytical inversion method for determining regional and global emissions of greenhouse gases: Sensitivity studies and application to halocarbons. Atmospheric Chemistry and Physics: 1597-1620.

Streets, D.G., Wu, Y. and Chin, M., 2006. Two-decadal aerosol trends as a likely explanation of the global dimming/brightening transition. Geophysical Research Letters, **33**(15): L15806.
Streets, D.G., Yan, F., Chin, M., Diehl, T., Mahowald, N., Schultz, M., Wild, M., Wu, Y. and Yu, C., 2009. Anthropogenic and natural contributions to regional trends in aerosol optical depth, 1980-2006. Journal of Geophysical Research-Atmospheres, **114**.
Strong, C. and Davis, R.E., 2006. Temperature-related trends in the vertical position of the summer upper tropospheric surface of maximum wind over the Northern Hemisphere. International Journal of Climatology, **26**(14): 1977-1997.
Strong, C. and Davis, R.E., 2007. Winter jet stream trends over the Northern Hemisphere. Quarterly Journal of the Royal Meteorological Society, **133**(629): 2109-2115.
Strong, C. and Davis, R.E., 2008a. Comment on "Historical trends in the jet streams" by Cristina L. Archer and Ken Caldeira. Geophysical Research Letters: L24806 (2 pp.).
Strong, C. and Davis, R.E., 2008b. Variability in the position and strength of winter jet stream cores related to northern hemisphere teleconnections. Journal of Climate, **21**(3): 584-592.
Sun, B.M., Reale, A., Seidel, D.J. and Hunt, D.C., 2010. Comparing radiosonde and COSMIC atmospheric profile data to quantify differences among radiosonde types and the effects of imperfect collocation on comparison statistics. Journal of Geophysical Research-Atmospheres, **115**.
Syakila, A. and Kroeze, C., 2011. The global nitrous oxide budget revisited. Greenhouse Gas Measurement and Management, **1**(1): 17-26.
Takahashi, K., Montecinos, A., Goubanova, K. and Dewitte, B., 2011. ENSO regimes: Reinterpreting the canonical and Modoki El Nino. Geophysical Research Letters, **38**: -.
Takeuchi, Y., Endo, Y. and Murakami, S., 2008. High correlation between winter precipitation and air temperature in heavy-snowfall areas in Japan. Annals of Glaciology, **49**: 7-10.
Tang, G., Ding, Y., Wang, S., Ren, G., Liu, H. and Zhang, L., 2010. Comparative analysis of China surface air temperature series for the past 100 years, Advances in climate change research, pp. 11-19.
Tang, W.J., Yang, K., Qin, J., Cheng, C.C.K. and He, J., 2011. Solar radiation trend across China in recent decades: a revisit with quality-controlled data. Atmospheric Chemistry and Physics, **11**(1): 393-406.
Tans, P., 2009. An Accounting of the Observed Increase in Oceanic and Atmospheric CO2 and an Outlook for the Future. Oceanography: 26-35.
Tarasova, O.A., Senik, I.A., Sosonkin, M.G., Cui, J., Staehelin, J. and PrÃ©vÃ´t, A.S.H., 2009. Surface ozone at the Caucasian site Kislovodsk High Mountain Station and the Swiss Alpine site Jungfraujoch: data analysis and trends (1990â€“2006). Atmos. Chem. Phys., **9**(12): 4157-4175.
Tegtmeier, S., Kruger, K., Wohltmann, I., Schoellhammer, K. and Rex, M., 2008. Variations of the residual circulation in the Northern Hemispheric winter. Journal of Geophysical Research-Atmospheres, **113**(D16).
Teuling, A.J., Hirschi, M., Ohmura, A., Wild, M., Reichstein, M., Ciais, P., Buchmann, N., Ammann, C., Montagnani, L., Richardson, A.D., Wohlfahrt, G. and Seneviratne, S.I., 2009. A regional perspective on trends in continental evaporation. Geophysical Research Letters, **36**: L02404.
Thomas, B., Kent, E., Swail, V. and Berry, D., 2008. Trends in ship wind speeds adjusted for observation method and height. International Journal of Climatology, **28**(6): 747-763.
Thomas, G.E., Poulsen, C.A., Siddans, R., Sayer, A.M., Carboni, E., Marsh, S.H., Dean, S.M., Grainger, R.G. and Lawrence, B.N., 2010. Validation of the GRAPE single view aerosol retrieval for ATSR-2 and insights into the long term global AOD trend over the ocean. Atmos. Chem. Phys., **10**(10): 4849-4866.
Thompson, D.W.J., Kennedy, J.J., Wallace, J.M. and Jones, P.D., 2008. A large discontinuity in the mid-twentieth century in observed global-mean surface temperature. Nature, **453**(7195): 646-U5.
Thompson, D.W.J. and Wallace, J.M., 1998. The Arctic Oscillation signature in the wintertime geopotential height and temperature fields. Geophysical Research Letters, **25**(9): 1297-1300.
Thompson, D.W.J. and Wallace, J.M., 2000. Annular modes in the extratropical circulation. Part I: Month-to-month variability. Journal of Climate, **13**(5): 1000-1016.
Thompson, T.A., et al., 2004. Halocarbons and Other Atmospheric Trace Species, NOAA CMDL, Boulder, CO.
Thorne, P.W., 2008. Arctic tropospheric warming amplification? Nature, **455**(7210): E1-E2.
Thorne, P.W., Brohan, P., Titchner, H.A., McCarthy, M.P., Sherwood, S.C., Peterson, T.C., Haimberger, L., Parker, D.E., Tett, S.F.B., Santer, B.D., Fereday, D.R. and Kennedy, J.J., 2011a. A quantification of uncertainties in historical tropical tropospheric temperature trends from radiosondes. Journal of Geophysical Research-Atmospheres, **116**.
Thorne, P.W., Parker, D.E., Tett, S.F.B., Jones, P.D., McCarthy, M., Coleman, H. and Brohan, P., 2005. Revisiting radiosonde upper air temperatures from 1958 to 2002. Journal of Geophysical Research-Atmospheres, **110**(D18105), doi:10.1029/2004JD005753.
Thorne, P.W. and Vose, R.S., 2010. REANALYSES SUITABLE FOR CHARACTERIZING LONG-TERM TRENDS Are They Really Achievable? Bulletin of the American Meteorological Society, **91**(3): 353-+.
Thorne, P.W., Willett, K.M., Allan, R.J., Bojinski, S., Christy, J.R., Fox, N., Gilbert, S., Jolliffe, I., Kennedy, J.J., Kent, E., Klein Tank, A., Lawrimore, J., Parker, D.E., Rayner, N., Simmons, A., Song, L., Stott, P.A. and Trewin, B., 2011b. Guiding the Creation of a Comprehensive Surface Temperature Resource for 21st Century Climate Science. Bulletin of the American Meteorological Society.

Tianjun, Z., Lixia, Z. and Hongmei, L., 2008. Changes in global land monsoon area and total rainfall accumulation over the last half century. Geophysical Research Letters: L16707 (6 pp.).
Tietavainen, H., Tuomenvirta, H. and Venalainen, A., 2010. Annual and seasonal mean temperatures in Finland during the last 160 years based on gridded temperature data. International Journal of Climatology, **30**(15): 2247-2256.
Tokinaga, H. and Xie, S.-P., 2011a. Wave and anemometer-based sea surface wind (WASWind) for climate change analysis (in press). J. Clim.
Tokinaga, H. and Xie, S.P., 2011b. Weakening of the equatorial Atlantic cold tongue over the past six decades. Nature Geosci.
Tokinaga, H., Xie, S.P., Timmermann, A., McGregor, S., Ogata, T., Kubota, H. and Okumura, Y.M., 2012. Regional Patterns of Tropical Indo-Pacific Climate Change: Evidence of the Walker Circulation Weakening. J. Climate, **25**(5): 1689-1710.
Toreti, A., Xoplaki, E., Maraun, D., Kuglitsch, F.G., Wanner, H. and Luterbacher, J., 2010. Characterisation of extreme winter precipitation in Mediterranean coastal sites and associated anomalous atmospheric circulation patterns. Natural Hazards and Earth System Sciences, **10**(5): 1037-1050.
Torseth, K., Aas, W., Breivik, K., Fjaeraa, A.M., Fiebig, M., Hjellbrekke, A.G., Lund Myhre, C., Solberg, S. and Yttri, K.E., 2012. Introduction to the European Monitoring and Evaluation Programme (EMEP) and observed atmospheric composition change during 1972-2009. Atmos. Chem. Phys. Discuss., **12**(1): 1733-1820.
Trenberth, K., 2011. Changes in precipitation with climate change. Climate Research, **47**(1-2): 123-138.
Trenberth, K.E., 1984. Signal versus noise in the Southern Oscillation. Monthly Weather Review, **112**(2): 326-332.
Trenberth, K.E., 1997. The definition of El Nino. Bulletin of the American Meteorological Society, **78**(12): 2771-2777.
Trenberth, K.E. and Fasullo, J.T., 2010. Climate Change Tracking Earth's Energy. Science, **328**(5976): 316-317.
Trenberth, K.E. and Fasullo, J.T., 2012. Tracking Earth's Energy: From El Nio to Global Warming. Surveys in Geophysics, **33**(3-4): 413-426.
Trenberth, K.E., Fasullo, J.T. and Kiehl, J., 2009. Earth's Global Energy Budget. Bulletin of the American Meteorological Society, **90**(3): 311.
Trenberth, K.E., Fasullo, J.T. and Mackaro, J., 2011. Atmospheric Moisture Transports from Ocean to Land and Global Energy Flows in Reanalyses. Journal of Climate, **24**(18): 4907-4924.
Trenberth, K.E. and Hoar, T.J., 1996. The 1990-1995 El Nino Southern Oscillation event: Longest on record. Geophysical Research Letters, **23**(1): 57-60.
Trenberth, K.E. and Hurrell, J.W., 1994. Decadal atmosphere-ocean variations in the Pacific. Climate Dynamics, **9**(6): 303-319.
Trenberth, K.E., Jones, P.D., Ambenje, P., Bojariu, R., Easterling, D., Klein Tank, A., Parker, D., Rahimzadeh, F., Renwick, J.A., Rusticucci, M., Soden, B. and Zhai, P., 2007. Observations: Surface and Atmospheric Climate Change, Climate Change 2007: The Physical Science Basis. Contribution of Working Group I to the Fourth Assessment Report of the Intergovernmental Panel on Climate Change. Cambridge University Press, Cambridge, United Kingdom and New York, NY, USA.
Trenberth, K.E. and Shea, D.J., 2006. Atlantic hurricanes and natural variability in 2005. Geophysical Research Letters, **33**(12).
Trenberth, K.E. and Stepaniak, D.P., 2001. Indices of El Nino evolution. Journal of Climate, **14**(8): 1697-1701.
Trenberth, K.E., Stepaniak, D.P. and Smith, L., 2005. Interannual variability of patterns of atmospheric mass distribution. J. Climate, **18**(15): 2812-2825.
Trewin, B., 2012. A daily homogenized temperature data set for Australia. International Journal of Climatology: n/a-n/a.
Trewin, B. and Vermont, H., 2010. Changes in the frequency of record temperatures in Australia, 1957-2009. Australian Meteorological and Oceanographic Journal, **60**(2): 113-119.
Trnka, M., Kysely, J., Mozny, M. and Dubrovsky, M., 2009. Changes in Central-European soil-moisture availability and circulation patterns in 1881-2005. International Journal of Climatology, **29**(5): 655-672.
Troccoli, A., Muller, K., Coppin, P., Davy, R., Russell, C. and Hirsch, A.L., 2012. Long-Term Wind Speed Trends over Australia. J. Climate, **25**(1): 170-183.
Troup, A.J., 1965. Southern Oscillation. Quarterly Journal of the Royal Meteorological Society, **91**(390): 490-&.
Trupin AS,Wahr JM. 1992. Spectroscopic analysis of global tide gauge sea level data. Geophysical Journal International 108: 1–15.
Tryhorn, L. and Risbey, J., 2006. On the distribution of heat waves over the Australian region. Australian Meteorological Magazine, **55**(3): 169-182.
Turner, J., Colwell, S.R., Marshall, G.J., Lachlan-Cope, T.A., Carleton, A.M., Jones, P.D., Lagun, V., Reid, P.A. and Iagovkina, S., 2005. Antarctic climate change during the last 50 years. International Journal of Climatology, **25**(3): 279-294.
Uppala, S.M., Kallberg, P.W., Simmons, A.J., Andrae, U., Bechtold, V.D., Fiorino, M., Gibson, J.K., Haseler, J., Hernandez, A., Kelly, G.A., Li, X., Onogi, K., Saarinen, S., Sokka, N., Allan, R.P., Andersson, E., Arpe, K., Balmaseda, M.A., Beljaars, A.C.M., Van De Berg, L., Bidlot, J., Bormann, N., Caires, S., Chevallier, F., Dethof, A., Dragosavac, M., Fisher, M., Fuentes, M., Hagemann, S., Holm, E., Hoskins, B.J., Isaksen, L., Janssen, P., Jenne, R., McNally, A.P., Mahfouf, J.F., Morcrette, J.J., Rayner, N.A., Saunders, R.W., Simon, P., Sterl, A.,

Trenberth, K.E., Untch, A., Vasiljevic, D., Viterbo, P. and Woollen, J., 2005. The ERA-40 re-analysis. Quarterly Journal of the Royal Meteorological Society, **131**(612): 2961-3012.
Usbeck, T., Wohlgemuth, T., Pfister, C., Volz, R., Beniston, M. and Dobbertin, M., 2010. Wind speed measurements and forest damage in Canton Zurich (Central Europe) from 1891 to winter 2007. International Journal of Climatology, **30**(3): 347-358.
Utsumi, N., Seto, S., Kanae, S., Maeda, E. and Oki, T., 2011. Does higher surface temperature intensify extreme precipitation? Geophysical Research Letters, **38**.
Van den Besselaar, E.J.M., Klein Tank, A.M.G. and Buishand, T.A., submitted. Trends in European precipitation extremes. Int. J. Climatol.
van der Schrier, G., Briffa, K.R., Jones, P.D. and Osborn, T.J., 2006. Summer moisture variability across Europe. Journal of Climate, **19**(12): 2818-2834.
van der Schrier, G., van Ulden, A. and van Oldenborgh, G.J., 2011. The construction of a Central Netherlands temperature. Climate of the Past, **7**(2): 527-542.
van Heerwaarden, C.C., de Arellano, J.V.G. and Teuling, A.J., 2010. Land-atmosphere coupling explains the link between pan evaporation and actual evapotranspiration trends in a changing climate. Geophysical Research Letters, **37**.
van Ommen, T.D. and Morgan, V., 2010. Snowfall increase in coastal East Antarctica linked with southwest Western Australian drought. Nature Geoscience, **3**(4): 267-272.
Vautard, R., Cattiaux, J., Yiou, P., The paut, J.N. and Ciais, P., 2010. Northern Hemisphere atmospheric stilling partly attributed to an increase in surface roughness. Nature Geoscience: 756-61.
Vautard, R., Yiou, P., D'Andrea, F., de Noblet, N., Viovy, N., Cassou, C., Polcher, J., Ciais, P., Kageyama, M. and Fan, Y., 2007a. Summertime European heat and drought waves induced by wintertime Mediterranean rainfall deficit. Geophysical Research Letters, **34**(7).
Vautard, R., Yiou, P., D'Andrea, F., Noblet, N.d., Viovy, N., Cassou, C., Polcher, J., Ciais, P., Kageyama, M. and Fan, Y., 2007b. Summertime European heat and drought waves induced by wintertime Mediterranean rainfall deficit. Geophys. Res. Lett., **34**(L07711).
Vautard, R., Yiou, P. and van Oldenborgh, G.J., 2009. Decline of fog, mist and haze in Europe over the past 30 years. Nature Geoscience, **2**(2): 115-119.
Vecchi, G.A. and Knutson, T.R., 2008. On estimates of historical north Atlantic tropical cyclone activity. Journal of Climate, **21**(14): 3580-3600.
Vecchi, G.A. and Knutson, T.R., 2011a. Estimating Annual Numbers of Atlantic Hurricanes Missing from the HURDAT Database (1878-1965) Using Ship Track Density. Journal of Climate, **24**(6): 1736-1746.
Vecchi, G.A. and Knutson, T.R., 2011b. Estimating Annual Numbers of Atlantic Hurricanes Missing from the HURDAT Database (1878-1965) Using Ship Track Density. J. Climate, **24**(6): 1736-1746.
Vecchi, G.A. and Soden, B.J., 2007. Global warming and the weakening of the tropical circulation. Journal of Climate, **20**(17): 4316-4340.
Vecchi, G.A., Soden, B.J., Wittenberg, A.T., Held, I.M., Leetmaa, A. and Harrison, M.J., 2006. Weakening of tropical Pacific atmospheric circulation due to anthropogenic forcing. Nature, **441**(7089): 73-76.
Velders, G., Andersen, S., Daniel, J., Fahey, D. and McFarland, M., 2007. The importance of the Montreal Protocol in protecting climate. Proceedings of the National Academy of Sciences of the United States of America: 4814-4819.
Velders, G., Fahey, D., Daniel, J., McFarland, M. and Andersen, S., 2009. The large contribution of projected HFC emissions to future climate forcing. Proceedings of the National Academy of Sciences of the United States of America: 10949-10954.
Venema, V.K., Mestre, O., Aguilar, E., Auer, I., Guijarro, A., Domonkos, P., Vertacnik, G., Szentimery, T., Stepanek, P., Zahradnicek, P., Viarre, J., Muller-Westermeier, G., Lakatos, M., Williams, C.N., Menne, M., Lindau, R., Rasol, D., Rustemeier, E., Kolokythas, K., Marinova, T., Andresen, L., Acquuaotta, F., Fratianni, S., Cheval, S., Klancar, M., Brunetti, M., Gruber, C., Prohom Duran, M., Likso, T., Esteban, P. and Brandsma, T., 2011. Benchmarking monthly homogenization algorithms. Climates of the Past Discussion, **7**: 2655-2718.
Verbout, S., Brooks, H., Leslie, L. and Schultz, D., 2006. Evolution of the US tornado database: 1954-2003. Weather and Forecasting, **21**(1): 86-93.
Vicente-Serrano, S.M., Begueria, S. and Lopez-Moreno, J.I., 2010a. A Multiscalar Drought Index Sensitive to Global Warming: The Standardized Precipitation Evapotranspiration Index. Journal of Climate, **23**(7): 1696-1718.
Vicente-Serrano, S.M., Begueria, S., Lopez-Moreno, J.I., Angulo, M. and El Kenawy, A., 2010b. A New Global 0.5 degrees Gridded Dataset (1901-2006) of a Multiscalar Drought Index: Comparison with Current Drought Index Datasets Based on the Palmer Drought Severity Index. Journal of Hydrometeorology, **11**(4): 1033-1043.
Vidal, J., Martin, E., Franchisteguy, L., Habets, F., Soubeyroux, J., Blanchard, M. and Baillon, M., 2010. Multilevel and multiscale drought reanalysis over France with the Safran-Isba-Modcou hydrometeorological suite. Hydrology and Earth System Sciences, **14**(3): 459-478.
Vignati, E., Karl, M., Krol, M., Wilson, J., Stier, P. and Cavalli, F., 2010. Sources of uncertainties in modelling black carbon at the global scale. Atmos. Chem. Phys., **10**(6): 2595-2611.
Vilibic, I. and Sepic, J., 2010. Long-term variability and trends of sea level storminess and extremes in European Seas. Global and Planetary Change, **71**(1-2): 1-12.

Villarini, G., Smith, J. and Vecchi, G., 2012. Changing frequency of heavy rainfall over the central United States. Journal of Climate, **in press**.

Vincent, L.A., Wang, X.L., Milewska, E.J., Wan, H., Yang, F. and Swail, V., Submitted. A Second Generation of Homogenized Canadian Monthly Surface Air Temperature for Climate Trend Analysis, Journal of Geophysical Research.

Visbeck, M., 2009. A Station-Based Southern Annular Mode Index from 1884 to 2005. Journal of Climate, **22**(4): 940-950.

Vollmer, M., Miller, B., Rigby, M., Reimann, S., Muhle, J., Krummel, P., O'Doherty, S., Kim, J., Rhee, T., Weiss, R., Fraser, P., Simmonds, P., Salameh, P., Harth, C., Wang, R., Steele, L., Young, D., Lunder, C., Hermansen, O., Ivy, D., Arnold, T., Schmidbauer, N., Kim, K., Greally, B., Hill, M., Leist, M., Wenger, A. and Prinn, R., 2011. Atmospheric histories and global emissions of the anthropogenic hydrofluorocarbons HFC-365mfc, HFC-245fa, HFC-227ea, and HFC-236fa. Journal of Geophysical Research-Atmospheres, **116**.

Vollmer, M., Reimann, S., Folini, D., Porter, L. and Steele, L., 2006. First appearance and rapid growth of anthropogenic HFC-245fa (CHF2CH2CF3) in the atmosphere. Geophysical Research Letters, **33**(20): -.

Vomel, H., Barnes, J.E., Forno, R.N., Fujiwara, M., Hasebe, F., Iwasaki, S., Kivi, R., Komala, N., Kyro, E., Leblanc, T., Morel, B., Ogino, S.Y., Read, W.G., Ryan, S.C., Saraspriya, S., Selkirk, H., Shiotani, M., Canossa, J.V. and Whiteman, D.N., 2007a. Validation of Aura Microwave Limb Sounder water vapor by balloon-borne Cryogenic Frost point Hygrometer measurements. Journal of Geophysical Research-Atmospheres, **112**(D24).

Vomel, H., David, D.E. and Smith, K., 2007b. Accuracy of tropospheric and stratospheric water vapor measurements by the cryogenic frost point hygrometer: Instrumental details and observations. Journal of Geophysical Research-Atmospheres, **112**(D8).

von Clarmann, T., Haepfner, M., Kellmann, S., Linden, A., Chauhan, S., Funke, B., Grabowski, U., Glatthor, N., Kiefer, M., Schieferdecker, T., Stiller, G.P. and Versick, S., 2009. Retrieval of temperature, H2O, O3, HNO3, CH4, N2O, ClONO2 and ClO from MIPAS reduced resolution nominal mode limb emission measurements. Atmos. Meas. Tech., **2**(1): 159-175.

Von Storch, H., 1999. Misuses of Statistical Analysis in Climate Research. In: H. Von Storch and A. Navarra (Editors), Analysis of Climate Variability: Applications of Statistical Techniques. Springer-Verlag, Heidelberg, pp. 11-26.

von Storch, H. and Zwiers, F.W., 1999. Statistical Analysis in Climate Research. Cambridge University Press, Cambridge, 484 pp.

Vose, R.S., Applequist, S., Menne, M.J., Williams, C.N., Jr. and Thorne, P., 2012a. An intercomparison of temperature trends in the US Historical Climatology Network and recent atmospheric reanalyses. Geophysical Research Letters, **39**.

Vose, R.S., Arndt, D., Banzon, V.F., Easterling, D.R., Gleason, B., Huang, B., Kearns, E., Lawrimore, J.H., Menne, M.J., Peterson, T.C., Reynolds, R.W., Smith, T.M., Williams, C.N. and Wuertz, D.L., 2012b. NOAA's Merged Land-Ocean Surface Temperature Analysis. Bulletin of the American Meteorological Society.

Vose, R.S., Arndt, D., Banzon, V.F., Easterling, D.R., Gleason, B., Huang, B., Kearns, E., Lawrimore, J.H., Menne, M.J., Peterson, T.C., Reynolds, R.W., Smith, T.M., Williams, C.N. and Wuertz, D.L., Submitted. NOAA's Merged Land-Ocean Surface Temperature Analysis. Bulletin of the American Meteorological Society.

Vose, R.S., Easterling, D.R. and Gleason, B., 2005a. Maximum and minimum temperature trends for the globe: An update through 2004. Geophysical Research Letters, **32**(23).

Vose, R.S., Oak Ridge National Laboratory. Environmental Sciences Division., U.S. Global Change Research Program, United States. Dept. of Energy. Office of Health and Environmental Research., Carbon Dioxide Information Analysis Center (U.S.) and Martin Marietta Energy Systems Inc., 1992. The Global historical climatology network : long-term monthly temperature, precipitation, sea level pressure, and station pressure data. Environmental Sciences Division publication ;. Carbon Dioxide Information Analysis Center Available to the public from N.T.I.S., Oak Ridge, Tenn., 1 v. (various pagings) pp.

Vose, R.S., Wuertz, D., Peterson, T.C. and Jones, P.D., 2005b. An intercomparison of trends in surface air temperature analyses at the global, hemispheric, and grid-box scale. Geophysical Research Letters, **32**(18).

Wahba, G., 1990. *Spline models for observational data*. SIAM, Philadelphia.

Wallace, J.M. and Gutzler, D.S., 1981. Teleconnections in the geopotential height field during the Northern Hemisphere winter. Monthly Weather Review, **109**(4): 784-812.

Wan, H., Wang, X.L. and Swail, V.R., 2010. Homogenization and Trend Analysis of Canadian Near-Surface Wind Speeds. Journal of Climate, **23**(5): 1209-1225.

Wan, H., Zhang, X., Zwiers, F., Emori, S. and Shiogama, H., 2012. Effect of data coverage on the estimation of mean and variability of precipitation at global and regional scales. Journal of Geophysical Research, **Submitted.**

Wang, B. and Shi, G., 2010. Long term trends of atmospheric absorbing and scattering optical depths over China region estimated from the routine observation data of surface solar irradiances. Geophys. Res., **2010**(115, D00K28, doi:10.1029/2009JD013239).

Wang, J.H. and Zhang, L.Y., 2008. Systematic errors in global radiosonde precipitable water data from comparisons with ground-based GPS measurements. Journal of Climate, **21**(10): 2218-2238.

Wang, J.H. and Zhang, L.Y., 2009. Climate applications of a global, 2-hourly atmospheric precipitable water dataset derived from IGS tropospheric products. Journal of Geodesy, **83**(3-4): 209-217.

Wang, J.H., Zhang, L.Y., Dai, A., Van Hove, T. and Van Baelen, J., 2007. A near-global, 2-hourly data set of atmospheric precipitable water from ground-based GPS measurements. Journal of Geophysical Research-Atmospheres, **112**(D11).

Wang, J.S., Seidel, D.J. and Free, M., 2012a. How well do we know recent climate trends at the tropical tropopause? J. Geophys. Res.-Atmos., **117**.

Wang, K., Dickinson, R.E., Wild, M. and Liang, S., 2012. Atmospheric impacts on climatic variability of surface incident solar radiation. Atmos. Che,. Phys. Discuss., **12**, 14009-14042.

Wang, K., Ye, H., Chen, F., Xiong, Y.Z. and Wang, C.P., 2012b. Urbanization Effect on the Diurnal Temperature Range: Different Roles under Solar Dimming and Brightening. Journal of Climate, **25**(3): 1022-1027.

Wang, K.C., Dickinson, R.E. and Liang, S.L., 2009a. Clear Sky Visibility Has Decreased over Land Globally from 1973 to 2007. Science, **323**(5920): 1468-1470.

Wang, K.C., Dickinson, R.E., Wild, M. and Liang, S.L., 2010. Evidence for decadal variation in global terrestrial evapotranspiration between 1982 and 2002: 2. Results. Journal of Geophysical Research-Atmospheres, **115**.

Wang, K.C. and Liang, S.L., 2009. Global atmospheric downward longwave radiation over land surface under all-sky conditions from 1973 to 2008. Journal of Geophysical Research-Atmospheres, **114**: -.

Wang, L.K., Zou, C.Z. and Qian, H.F., 2012c. Construction of Stratospheric Temperature Data Records from Stratospheric Sounding Units. Journal of Climate, **25**(8): 2931-2946.

Wang, T., Wei, X.L., Ding, A.J., Poon, C.N., Lam, K.S., Li, Y.S., Chan, L.Y. and Anson, M., 2009b. Increasing surface ozone concentrations in the background atmosphere of Southern China, 1994–2007. Atmos. Chem. Phys., **9**(16): 6217-6227.

Wang, X., Wan, H. and Swail, V., 2006a. Observed changes in cyclone activity in Canada and their relationships to major circulation regimes. Journal of Climate, **19**(6): 896-915.

Wang, X., Wan, H., Zwiers, F., Swail, V., Compo, G., Allan, R., Vose, R., Jourdain, S. and Yin, X., 2011. Trends and low-frequency variability of storminess over western Europe, 1878–2007. Climate Dynamics: 1-17.

Wang, X.L.L. and Swail, V.R., 2001. Changes of extreme wave heights in Northern Hemisphere oceans and related atmospheric circulation regimes. Journal of Climate, **14**(10): 2204-2221.

Wang, X.L.L., Swail, V.R. and Zwiers, F.W., 2006b. Climatology and changes of extratropical cyclone activity: Comparison of ERA-40 with NCEP-NCAR reanalysis for 1958-2001. Journal of Climate, **19**(13): 3145-3166.

Wang, X.L.L., Zwiers, F.W., Swail, V.R. and Feng, Y., 2009c. Trends and variability of storminess in the Northeast Atlantic region, 1874-2007. Climate Dynamics, **33**(7-8): 1179-1195.

Wang, X.M., Zhai, P.M. and Wang, C.C., 2009d. Variations in extratropical cyclone activity in northern East Asia. Advances in Atmospheric Sciences, **26**(3): 471-479.

Wang, Y. and Zhou, L., 2005. Observed trends in extreme precipitation events in China during 1961-2001 and the associated changes in large-scale circulation. Geophysical Research Letters, **32**(9).

Warren, S.G., Eastman, R.M. and Hahn, C.J., 2007. A survey of changes in cloud cover and cloud types over land from surface observations, 1971-96. Journal of Climate, **20**(4): 717-738.

Weber, M., Steinbrecht, W., Long, C., Fioletov, V.E., Frith, S.H., Stolarski, R. and NeW man, P.A., 2012. State of the Climate in 2012; Stratospheric Ozone. Bull. Am. Met. Soc., **submitted**.

Weinkle, J., Maue, R. and Pielke, R., 2012. Historical Global Tropical Cyclone Landfalls. Journal of Climate, **25**(13): 4729-4735.

Weinstock, E.M., Smith, J.B., Sayres, D.S., Pittman, J.V., Spackman, J.R., Hintsa, E.J., Hanisco, T.F., Moyer, E.J., St Clair, J.M., Sargent, M.R. and Anderson, J.G., 2009. Validation of the Harvard Lyman-alpha in situ water vapor instrument: Implications for the mechanisms that control stratospheric water vapor. Journal of Geophysical Research-Atmospheres, **114**.

Weiss, R., Muhle, J., Salameh, P. and Harth, C., 2008. Nitrogen trifluoride in the global atmosphere. Geophysical Research Letters: -.

Wells, N., Goddard, S. and Hayes, M.J., 2004. A self-calibrating Palmer Drought Severity Index. Journal of Climate, **17**(12): 2335-2351.

Wentz, F., Gentemann, C., Smith, D. and Chelton, D., 2000. Satellite measurements of sea surface temperature through clouds. Science, **288**(5467): 847-850.

Wentz, F.J., Ricciardulli, L., Hilburn, K. and Mears, C., 2007. How much more rain will global warming bring? Science, **317**(5835): 233-235.

Wergen, G. and Krug, J., 2010. Record-breaking temperatures reveal a warming climate. Epl, **92**(3).

Werner, P.C., Gerstengarbe, F.W. and Wechsung, F., 2008. Grosswetterlagen and precipitation trends in the Elbe river catchment. Meteorologische Zeitschrift, **17**(1): 61-66.

Westra, S., Alexander, L. and Zwiers, F., 2012. Global increasing trends in annual maximum daily precipitation. Journal of Climate: submitted.

WGMS 2009: Glacier Mass Balance Bulletin No. 10 (2006-2007). W. Haeberli, I. Gärtner-Roer, M. Hoelzle, F. Paul, M. Zemp (eds.), (World Glacier Monitoring Service, Zurich, Switzerland, 2010). http://www.geo.unizh.ch/wgms/gmbb.html http://www.geo.unizh.ch/wgms/mbb/sum08.html

Wibig, J., 2008. Cloudiness variations in Lodz in the second half of the 20th century. International Journal of Climatology, **28**(4): 479-491.

Wickham, C., Curry, J., Groom, D., Jacobsen, R., Muller, R., Perlmutter, S., Rhode, R., Rosenfeld, A. and Wurtele, J., submitted. Influence of Urban Heating on the Global Temperature Land average Using Rural Sites Identified from MODIS Classifications. Journal of Geophysical Research: Submitted.

Wielicki, B.A., Barkstrom, B.R., Harrison, E.F., Lee, R.B., Smith, G.L. and Cooper, J.E., 1996. Clouds and the earth's radiant energy system (CERES): An earth observing system experiment. Bulletin of the American Meteorological Society, **77**(5): 853-868.

Wilby, R.L., Jones, P.D. and Lister, D.H., 2011. Decadal variations in the nocturnal heat island of London. Weather, **66**(3): 59-64.

Wild, M., 2008. Short-wave and long-wave surface radiation budgets in GCMs: a review based on the IPCC-AR4/CMIP3 models. Tellus Series a-Dynamic Meteorology and Oceanography, **60**(5): 932-945.

Wild, M., 2009. Global dimming and brightening: A review. Journal of Geophysical Research-Atmospheres, **114**.

Wild, M., 2012. Enlightening global dimming and brightening. Bulletin of the American Meteorological Society, **93**(1): 27-37.

Wild, M., Folini, D., Schär, C., Loeb, N., Dutton, E.G., and König-Langlo, G., submitted. The global energy balance from a surface perspective: an assessment based on direct observations and CMIP5 climate models.

Wild, M., Gilgen, H., Roesch, A., Ohmura, A., Long, C.N., Dutton, E.G., Forgan, B., Kallis, A., Russak, V. and Tsvetkov, A., 2005. From dimming to brightening: Decadal changes in solar radiation at Earth's surface. Science, **308**(5723): 847-850.

Wild, M., Grieser, J. and Schaer, C., 2008. Combined surface solar brightening and increasing greenhouse effect support recent intensification of the global land-based hydrological cycle. Geophysical Research Letters, **35**(17): L17706.

Wild, M. and Liepert, B., 2010. The Earth radiation balance as driver of the global hydrological cycle. Environmental Research Letters, **5**(2).

Wild, M., Ohmura, A., Gilgen, H., Morcrette, J.J. and Slingo, A., 2001. Evaluation of downward longwave radiation in general circulation models. Journal of Climate, **14**(15): 3227-3239.

Wild, M., Ohmura, A., Gilgen, H., Roeckner, E., Giorgetta, M. and Morcrette, J.J., 1998. The disposition of radiative energy in the global climate system: GCM-calculated versus observational estimates. Climate Dynamics, **14**(12): 853-869.

Wild, M., Ohmura, A., Gilgen, H. and Rosenfeld, D., 2004. On the consistency of trends in radiation and temperature records and implications for the global hydrological cycle. Geophysical Research Letters, **31**(11): L11201.

Wild, M., Ohmura, A. and Makowski, K., 2007. Impact of global dimming and brightening on global warming. Geophysical Research Letters, **34**(4): L04702.

Wild, M., Truessel, B., Ohmura, A., Long, C.N., Konig-Langlo, G., Dutton, E.G., and Tsvetkov, A., 2009. Global dimming and brightening: An update beyond 2000. Journal of Geophysical Research-Atmospheres, **114**: D00d13.

Wilks, D.S., 2006. Statistical Methods in the Atmospheric Sciences. Elsevier, Amsterdam, 627 pp.

Willett, K.M., Jones, P.D., Gillett, N.P. and Thorne, P.W., 2008. Recent Changes in Surface Humidity: Development of the HadCRUH Dataset. Journal of Climate, **21**(20): 5364-5383. http://hadobs.metoffice.com/hadcruh/

Willett, K.M., Jones, P.D., Thorne, P.W. and Gillett, N.P., 2010. A comparison of large scale changes in surface humidity over land in observations and CMIP3 general circulation models. Environmental Research Letters, **5**(2).

Williams, C.N., Menne, M.J. and Thorne, P.W., 2012. Benchmarking the performance of pairwise homogenization of surface temperatures in the United States. Journal of Geophysical Research-Atmospheres, **117**.

Willis, J.K., D. Roemmich and B. Cornuelle (2004). Interannual variability in upper ocean heat content, temperature, and thermosteric expansion on global scales, J. Geophys. Res., 109, C12036, doi:10.1029/2003JC002260.

Willson, R.C. and Mordvinov, A.V., 2003. Secular total solar irradiance trend during solar cycles 21-23. Geophysical Research Letters, **30**(5).

W MO, 2011. Scientific Assessment of Ozone Depletion: 2010, Global Ozone Research and Monitoring Project–Report No. 52, Geneva, Switzerland.

Wong, T., Wielicki, B.A., Lee, R.B., ., Smith, G.L., Bush, K.A. and Willis, J.K., 2006. Reexamination of the observed decadal variability of the earth radiation budget using altitude-corrected ERBE/ERBS nonscanner WFOV data. Journal of Climate, **19**(16): 4028-4040.

Wood, S.N., 2006. *Generalized Additive Models: An Introduction with R*. CRC/Chapman & Hall.

Woodruff, S.D., Worley, S.J., Lubker, S.J., Freeman, Z.J., J. E., Berry, D.I., Brohan, P., Kent, E.C., Reynolds, R.W., Smith, S.R. and Wilkinson, C., 2011. ICOADS Release 2.5: Extensions and Enhancements to the Surface Marine Meteorological Archive. Int. J. Climatol., **31**: 951-967.

Woodworth P.L., White N.J., Jevrejeva S., Holgate S.J., Church J.A. and Gehrels W.R. (2008): Evidence for the accelerations of sea level on multi-decade and century timescales. International Journal of Climatology, 29(6), 777 – 789 doi:10.1002/joc.1771

Worden, H.M., Deeter, M.N., Frankenberg, C., George, M., Nichitiu, F., Worden, J., Aben, I., BoW man, K.W., Clerbaux, C., Coheur, P.F., de Laat, A.T.J., Detweiler, R., Drummond, J.R., Edwards, D.P., Gille, J.C., Hurtmans, D., Luo, M., Martínez-Alonso, S., Massie, S., Pfister, G. and Warner, J.X., 2012a. Decadal Record of Satellite Carbon Monoxide Observations. Atmos. Chem. Phys.: submitted.

Worden, H.M., Deeter, M.N., Frankenberg, C., George, M., Nichitiu, F., Worden, J., I.Aben, BoW man, K.W., Clerbaux, C., Coheur, P.F., Laat, A.T.J.d., Detweiler, R., Drummond, J.R., Edwards, D.P., Gille, J.C., Hurtmans, D., Luo, M., Martínez-Alonso, S., Massie, S., Pfister, G. and Warner, J.X., 2012b. Decadal Record of Satellite Carbon Monoxide Observations. Atmos. Chem. Phys.: submitted.

Worley, S.J., S.D. Woodruff, R.W. Reynolds, S.J. Lubker, and N. Lott, 2005: ICOADS Release 2.1 data and products. Int. J. Climatol. (CLIMAR-II Special Issue), 25, 823-842 (DOI: 10.1002/joc.1166). http://ghrsst.nodc.noaa.gov/intercomp.html

Worton, D., Sturges, W., Gohar, L., Shine, K., Martinerie, P., Oram, D., Humphrey, S., Begley, P., Gunn, L., Barnola, J., Schwander, J. and Mulvaney, R., 2007. Atmospheric trends and radiative forcings of CF4 and C2F6 inferred from firn air. Environmental Science & Technology: 2184-2189.

Wu, Z., Huang, N.E., Wallace, J.M., Smoliak, B.V. and Chen, X., 2011. On the time-varying trend in global-mean surface temperature. Climate Dynamics, **37**(3-4): 759-773.

Xavier, P.K., John, V.O., Buehler, S.A., Ajayamohan, R.S. and Sijikumar, S., 2010. Variability of Indian summer monsoon in a new upper tropospheric humidity data set. Geophysical Research Letters, **37**.

Xia, X., 2010a. A closer looking at dimming and brightening in China during 1961-2005. Annales Geophysicae, **28**(5): 1121-1132.

Xia, X.G., 2010b. Spatiotemporal changes in sunshine duration and cloud amount as well as their relationship in China during 1954-2005. Journal of Geophysical Research-Atmospheres, **115**.

Xie, B., Zhang, Q. and Wang, Y., 2010. Observed Characteristics of Hail Size in Four Regions in China during 1980-2005. Journal of Climate, **23**(18): 4973-4982.

Xie, B.G., Zhang, Q.H. and Wang, Y.Q., 2008. Trends in hail in China during 1960-2005. Geophysical Research Letters, **35**(13).

Xie, S., Hu, K., Hafner, J., Tokinaga, H., Du, Y., Huang, G. and Sampe, T., 2009. Indian Ocean Capacitor Effect on Indo-Western Pacific Climate during the Summer following El Nino. Journal of Climate, **22**(3): 730-747.

Xu, C.Y., Gong, L.B., Tong, J. and Chen, D.L., 2006a. Decreasing reference evapotranspiration in a warming climate - A case of Changjiang (Yangtze) River catchment during 1970-2000. Advances in Atmospheric Sciences, **23**(4): 513-520.

Xu, K.H., Milliman, J.D. and Xu, H., 2010. Temporal trend of precipitation and runoff in major Chinese Rivers since 1951. Global and Planetary Change, **73**(3-4): 219-232.

Xu, M., Chang, C.P., Fu, C.B., Qi, Y., Robock, A., Robinson, D. and Zhang, H.M., 2006b. Steady decline of east Asian monsoon winds, 1969-2000: Evidence from direct ground measurements of wind speed. Journal of Geophysical Research-Atmospheres, **111**(D24).

Yang, J., Liu, Q., Xie, S.-P., Liu, Z. and Wu, L., 2007. Impact of the Indian Ocean SST basin mode on the Asian summer monsoon. Geophysical Research Letters, **34**(2).

Yang, T., Wang, X.Y., Zhao, C.Y., Chen, X., Yu, Z.B., Shao, Q.X., Xu, C.Y., Xia, J. and Wang, W.G., 2011a. Changes of climate extremes in a typical arid zone: Observations and multimodel ensemble projections. Journal of Geophysical Research-Atmospheres, **116**.

Yang, X.C., Hou, Y.L. and Chen, B.D., 2011b. Observed surface warming induced by urbanization in east China. Journal of Geophysical Research-Atmospheres, **116**: 12.

Yokouchi, Y., Taguchi, S., Saito, T., Tohjima, Y., Tanimoto, H. and Mukai, H., 2006. High frequency measurements of HFCs at a remote site in east Asia and their implications for Chinese emissions. Geophysical Research Letters, **33**(21).

Yoon, J., von Hoyningen-Huene, W., Kokhanovsky, A.A., Vountas, M. and Burrows, J.P., 2012. Trend analysis of aerosol optical thickness and Angstrom exponent derived from the global AERONET spectral observations. Atmos. Meas. Tech., **5**(6): 1271-1299.

You, Q., Kang, S., Aguilar, E., Pepin, N., Flügel, W.A., Yan, Y., Xu, Y., Zhang, Y. and Huang, J., 2010. Changes in daily climate extremes in China and their connection to the large scale atmospheric circulation during 1961-2003. Climate Dynamics.

You, Q.L., Kang, S.C., Aguilar, E. and Yan, Y.P., 2008. Changes in daily climate extremes in the eastern and central Tibetan Plateau during 1961-2005. Journal of Geophysical Research-Atmospheres, **113**(D7).

Yu, B. and Zwiers, F.W., 2010. Changes in equatorial atmospheric zonal circulations in recent decades. Geophysical Research Letters, **37**.

Yu, L. and Weller, R., 2007. Objectively analyzed air-sea heat fluxes for the global ice-free oceans (1981-2005). Bulletin of the American Meteorological Society, **88**(4): 527-+.

Yuan, X. and Li, C., 2008. Climate modes in southern high latitudes and their impacts on Antarctic sea ice. Journal of Geophysical Research-Oceans, **113**(C6): -.

Yurganov, L., McMillan, W., Grechko, E. and Dzhola, A., 2010. Analysis of global and regional CO burdens measured from space between 2000 and 2009 and validated by ground-based solar tracking spectrometers. Atmos. Chem. Phys., **10**(8): 3479-3494.

Zaitchik, B.F., Macalady, A.K., Bonneau, L.R. and Smith, R.B., 2006. Europe's 2003 heat wave: A satellite view of impacts and land-atmosphere feedbacks. International Journal of Climatology, **26**(6): 743-769.

Zebiak, S.E., 1993. Air-sea interaction in the equatorial Atlantic region. Journal of Climate, **6**(8): 1567-1568.

Zerefos, C.S., Eleftheratos, K., Meleti, C., Kazadzis, S., Romanou, A., Ichoku, C., Tselioudis, G. and Bais, A., 2009. Solar dimming and brightening over Thessaloniki, Greece, and Beijing, China. Tellus Series B-Chemical and Physical Meteorology, **61**(4): 657-665.

Zhai, P.M., Zhang, X.B., Wan, H. and Pan, X.H., 2005. Trends in total precipitation and frequency of daily precipitation extremes over China. Journal of Climate, **18**(7): 1096-1108.

Zhang, H., Bates, J. and Reynolds, R., 2006. Assessment of composite global sampling: Sea srface wind speed. Geophysical Research Letters, **33**(17): -.

Zhang, J. and Reid, J.S., 2010. A decadal regional and global trend analysis of the aerosol optical depth using a data-assimilation grade over-water MODIS and Level 2 MISR aerosol products. Atmos. Chem. Phys., **10**(22): 10949-10963.

Zhang, X., Alexander, L., Hegerl, G.C., Jones, P., Tank, A.K., Peterson, T.C., Trewin, B. and Zwiers, F.W., 2011. Indices for monitoring changes in extremes based on daily temperature and precipitation data. Wiley Interdisciplinary Reviews: Climate Change: n/a-n/a.

Zhang, X. and Zwiers, F., 2004. Comment on "Applicability of prewhitening to eliminate the influence of serial correlation on the Mann-Kendall test" by Sheng Yue and Chun Yuan Wang. Water Resources Research, **40**(3): -.

Zhang, X., Zwiers, F.W., Hegerl, G.C., Lambert, F.H., Gillett, N.P., Solomon, S., Stott, P.A. and Nozawa, T., 2007a. Detection of human influence on twentieth-century precipitation trends. Nature, **448**(7152): 461-U4.

Zhang, X.D., Walsh, J.E., Zhang, J., Bhatt, U.S. and Ikeda, M., 2004. Climatology and interannual variability of arctic cyclone activity: 1948-2002. Journal of Climate, **17**(12): 2300-2317.

Zhang, X.Y., Wang, Y.Q., Niu, T., Zhang, X.C., Gong, S.L., Zhang, Y.M. and Sun, J.Y., 2012. Atmospheric aerosol compositions in China: spatial/temporal variability, chemical signature, regional haze distribution and comparisons with global aerosols. Atmos. Chem. Phys., **12**(2): 779-799.

Zhang, Y., Wallace, J.M. and Battisti, D.S., 1997. ENSO-like interdecadal variability: 1900-93. Journal of Climate, **10**(5): 1004-1020.

Zhang, Y.Q., Liu, C.M., Tang, Y.H. and Yang, Y.H., 2007b. Trends in pan evaporation and reference and actual evapotranspiration across the Tibetan Plateau. Journal of Geophysical Research-Atmospheres, **112**(D12).

Zhao, C. and Tans, P., 2006. Estimating uncertainty of the W MO mole fraction scale for carbon dioxide in air. Journal of Geophysical Research-Atmospheres, **111**(D8).

Zhen, L. and Zhong-Wei, Y., 2009. Homogenized daily mean.maximum/minimum temperature series for China from 1960-2008, Atmospheric and Oceanic Science Letters, pp. 237-243.

Zhou, T.J., Gong, D.Y., Li, J. and Li, B., 2009a. Detecting and understanding the multi-decadal variability of the East Asian Summer Monsoon - Recent progress and state of affairs. Meteorologische Zeitschrift, **18**(4): 455-467.

Zhou, T.J. and Yu, R.C., 2005. Atmospheric water vapor transport associated with typical anomalous summer rainfall patterns in China. J. Geophy. Res.-Atmos., **110**(D8).

Zhou, T.J., Yu, R.C., Zhang, J., Drange, H., Cassou, C., Deser, C., Hodson, D.L.R., Sanchez-Gomez, E., Li, J., Keenlyside, N., Xin, X.G. and Okumura, Y., 2009b. Why the Western Pacific Subtropical High Has Extended Westward since the Late 1970s. Journal of Climate, **22**(8): 2199-2215.

Zhou, Y.P., Xu, K.M., Sud, Y.C. and Betts, A.K., 2011. Recent trends of the tropical hydrological cycle inferred from Global Precipitation Climatology Project and International Satellite Cloud Climatology Project data. Journal of Geophysical Research-Atmospheres, **116**.

Ziemke, J.R., Chandra, S. and Bhartia, P.K., 2005. A 25-year data record of atmospheric ozone in the Pacific from Total Ozone Mapping Spectrometer (TOMS) cloud slicing: Implications for ozone trends in the stratosphere and troposphere. J. Geophys. Res., **110**(D15): D15105.

Ziemke, J.R., Chandra, S., Labow, G.J., Bhartia, P.K., Froidevaux, L. and Witte, J.C., 2011. A global climatology of tropospheric and stratospheric ozone derived from Aura OMI and MLS measurements. Atmos. Chem. Phys., **11**(17): 9237-9251.

Zolina, O., Simmer, C., Kapala, A., Bachner, S., Gulev, S. and Maechel, H., 2008. Seasonally dependent changes of precipitation extremes over Germany since 1950 from a very dense observational network. Journal of Geophysical Research-Atmospheres, **113**(D6).

Zou, C.-Z. and Wang, W., 2011a. Inter-Satellite Calibration of AMSU-A Observations for Weather and Climate Applications. Journal of Geophysical Research.

Zou, C.Z., Gao, M. and Goldberg, M.D., 2009. Error Structure and Atmospheric Temperature Trends in Observations from the Microwave Sounding Unit. Journal of Climate, **22**(7): 1661-1681.

Zou, C.Z., Goldberg, M.D., Cheng, Z.H., Grody, N.C., Sullivan, J.T., Cao, C.Y. and Tarpley, D., 2006a. Recalibration of microwave sounding unit for climate studies using simultaneous nadir overpasses. Journal of Geophysical Research-Atmospheres, **111**(D19).

Zou, C.Z. and Wang, W.H., 2010. Stability of the MSU-Derived Atmospheric Temperature Trend. Journal of Atmospheric and Oceanic Technology, **27**(11): 1960-1971.

Zou, C.Z. and Wang, W.H., 2011b. Intersatellite calibration of AMSU-A observations for weather and climate applications. Journal of Geophysical Research-Atmospheres, **116**.

Zou, X., Alexander, L.V., Parker, D. and Caesar, J., 2006b. Variations in severe storms over China. Geophysical Research Letters, **33**(17).

Zwiers, F.W. and Kharin, V.V., 1998. Changes in the extremes of the climate simulated by CCC GCM2 under CO2 doubling. Journal of Climate, **11**(9): 2200-2222.

Appendix 2.A: Supplementary Material

2.A.1 Introduction

2.A.2 Changes in Atmospheric Composition

2.A.2.1 Long-Lived Greenhouse Gases

Appendix Table 2.A.1 contains the full list of species compiled for Chapter 8 to use for radiative forcing calculations. Following are discussions of additional species not discussed in Section 2.2.1 of the main text.

HFCs:
New measurements of several HFCs have been reported since AR4: HFC-365mfc (Stemmler et al., 2007), HFC-245fa (Vollmer et al., 2006), HFC-227ea (Laube et al., 2010), and HFC-236fa (Vollmer et al., 2011). Observation-based estimates of emissions show a mix of poor to good agreement with bottom-up inventories (Vollmer et al., 2011). Atmospheric abundances of these 4 minor HFCs were <2 ppt in 2011, but their atmospheric burdens are increasing rapidly, with relative increases >8% yr^{-1}.

PFCs:
Atmospheric measurements of high molecular weight PFCs have also been reported, including fully fluorine-substituted alkanes (C_3-C_8) (Ivy et al., 2012; Saito et al., 2010); and octafluorocyclobutane (c-C_4F_8) (Oram et al., 2012; Saito et al., 2010). All are currently <2 ppt, except when pollution events are observed at the air sampling sites.

NF_3 and SO_2F_2:
Since AR4, atmospheric observations of two new species that are not covered by the Kyoto Protocol were reported: NF_3 and SO_2F_2. Prather and Hsu (2008) reported the potential importance of NF_3 for radiative forcing. It is a substitute for PFCs as a plasma source in the semiconductor industry, has a lifetime of 500 year, and a GWP100 = 17,500 (W MO, 2011) (GWPs are described in Chapter 8). Weiss et al. (2008) determined 0.45 ppt for its global annual mean mole fraction in 2008, growing from almost zero in 1978. In 2011, NF_3 was 0.60 ppt, increasing by 0.30 ppt since 2005. Initial bottom-up inventories underestimated its emissions; based on the atmospheric observations, NF_3 emissions were 0.62 Gg in 2008. SO_2F_2 replaces CH_3Br as a fumigant. Its GWP100 ≈ 4740, is comparable to CFC-11. A new estimate of its lifetime, 36 ± 11 year (Muhle et al., 2009a), is significantly longer than previous estimates. Its global annual mean mole fraction in 2011 was 1.71 ppt and it increased by 0.36 ppt from 2005 to 2011.

Halons:
Atmospheric abundances of halons, except for halon-1301, have been decreasing. All have relatively small atmospheric abundances, ≤5 ppt, and are unlikely to accumulate to levels that can significantly affect radiative forcing either directly or indirectly through destruction of stratospheric O_3, if current emission projections are followed (W MO, 2011).

Table 2.A.1: Global annual mean mole fractions for LLGHGs for use in calculating radiative forcing in Chapter 8, indication if significant natural source exists, references to the data used to calculate global means, and summary of standard scales used.

Species	2011 Global Annual Mean (ppt)[a]	Relative Diff[b]	Data Source[c]	Natural Source	References	Scale
CO_2 (ppm)	390.46	negligible	NOAA SIO		(Zhao and Tans, 2006);(Keeling et al., 1976b)	N07; 08A
CH_4 (ppb)	1803.15	negligible		Yes	(Rigby et al., 2008);(Dlugokencky et al., 2005)	TU; N04
N_2O (ppb)	324.15	0.1%		Yes	(Prinn et al., 1990);(Hall et al., 2007)	S98; N06A
C_2F_6	4.16		AGAGE		(Muhle et al., 2010);	S07
C_3F_8	0.55		AGAGE		(Muhle et al., 2010);	S07
CCl_4	85.7	-1.7%			(Simmonds et al., 1998);(Thompson, 2004)[e]	S05; N08

CF_4	79.0		AGAGE	Yes	(Muhle et al., 2010);	S05
CFC-11	237.7	-0.7%			(Cunnold et al., 1997);(Thompson, 2004)[e]	S05; N92
CFC-113	74.3	-0.1%			(Fraser et al., 1996);(Miller et al., 2008);(Thompson, 2004)[e]	S05; N03
CFC-115	8.37		AGAGE		(Miller et al., 2008)	S05; N08
CFC-12	528.4	0.4%			(Cunnold et al., 1997);(Thompson, 2004)[e]	S05; N08
CH_2Cl_2	25.9	-18.7%			(Thompson, 2004)[e]	UB98
CH_3Br	7.11	1.7%		Yes	(Thompson, 2004)[e]	S05; N03
CH_3CCl_3	6.31	-0.1%			(Prinn et al., 2005);(Thompson, 2004)[e];(Montzka et al., 2011a)	S05; N03
CH_3Cl	534.1	-1.6%		Yes	(Miller et al., 2008; Thompson, 2004)[e]	S98; N03
$CHCl_3$	7.41		AGAGE[d]	Yes	(Miller et al., 2008; Prinn et al., 2000)	S05; N03
H-1211	4.07	2.2%			(Miller et al., 2008);(Thompson, 2004)[e]	S05; N06
H-1301	3.23	2.8%			(Miller et al., 2008);(Thompson, 2004)[e]	S05; N06
H-2402	0.45		NOAA		(Butler et al., 1998)	N92
HCFC-141b	21.4	0.3%			(O'Doherty et al., 2004);(Miller et al., 2008);(Thompson, 2004);(Montzka et al., 2009)	S05; N94
HCFC-142b	21.1	1.9%			(O'Doherty et al., 2004);(Miller et al., 2008);(Thompson, 2004);(Montzka et al., 2009)	S05; N94
HCFC-22	213.0	0.4%			(O'Doherty et al., 2004);(Miller et al., 2008);(Montzka et al., 1993)	S05; N06
HFC-125	9.58		AGAGE[d]		(O'Doherty et al., 2009)	UB98; N08
HFC-134a	62.5	-0.3%			(O'Doherty et al., 2004);(Miller et al., 2008);(Montzka et al., 1996)	S05; N00
HFC-143a	12.0		AGAGE[d]		(Miller et al., 2008)	S07; N08
HFC-152a	6.42		AGAGE		(Greally et al., 2007);(Miller et al., 2008)	S05
HFC-227ea	0.65		AGAGE[d]		(Laube et al., 2010);(Vollmer et al., 2011)	E05; N11
HFC-23	24.0		AGAGE[d]		(Miller et al., 2010)	S07; N08
HFC-236fa	0.08		AGAGE		(Vollmer et al., 2011)	E09
HFC-245fa	1.24		AGAGE		(Vollmer et al., 2006)	E05
HFC-32	4.92		AGAGE[d]		(Miller et al., 2008)	S07; N08
HFC-365mfc	0.58		AGAGE[d]		(Vollmer et al., 2011);(Stemmler et al., 2007)	E03; N11
SF_6	7.28	-0.6%			(Rigby et al., 2010);(Hall et al., 2011)	S05; N06
SO_2F_2	1.71		AGAGE		(Muhle et al., 2009b)	S07
NF_3	0.6		AGAGE		(Weiss et al., 2008)	Sp

Notes:
(a) Global surface annual mean dry-air mole fraction.
(b) Relative difference between AGAGE and NOAA 2011 global annual mean values (AGAGE – NOAA)/average).
(c) Source of data. Blank space indicated NOAA + AGAGE.
(d) Value listed from AGAGE data only, but NOAA maintains a scale and has unpublished data.
(e) Updated information about NOAA standard scales available at:
http://www.esrl.noaa.gov/gmd/ccl/summary_table.html. Scale: Standard gas scales used to calibrate instrument response. AGAGE/SIO: TU = Tohoku University CH_4 scale; SXX = Scripps Institution of Oceanography (SIO) trace gas scale developed in year [XX] (e.g., S98 = SIO-98); Sp = SIO-provisional; UB98 = Bristol University scale developed in 1998; EXX = Empa-20XX; E09 = Empa-2009-p (provisional); 08A = Scripps Institution of Oceanography 08A CO_2 standard scale. NOAA: NXX = NOAA scale developed in year [XX].

2.A.2.2 Short-Lived Greenhouse Gases

Table 2.A.2: Overview of O_3 trends reported in the literature, using data sets with at least 10 years of measurements.

Measurement Region	Site or Seasonal Information	Trend (ppb yr^{-1} or % yr^{-1})[a]	Period	Reference	Remarks
Europe					
Alpine high elevation surface sites, 3.0 – 3.6 km above sea level	A composite of Zugspitze, Jungfraujoch and Sonnblick	**0.87 ± 0.13** **0.33 ± 0.10** **-0.16 ± 0.14**	1978-1989 1990-1999 2000-2009	(Logan et al., 2012)	Unfiltered data, although data from Jan.-May, 1982 at Zugspitze were dropped. Quadratic fit to seasonal time series for 1978-2009.
Surface, rural central Europe	Hohenpeissenberg	**0.46 ± 0.11** (winter) **0.39 ± 0.13** (spring) **0.35 ± 0.19** (summer) **0.19 ± 0.10** (autumn)	1971-2000	(Parrish et al., 2012)	Filtered to remove very local contamination. Linear regression of seasonal averages through 2000, after which ozone began to decrease (2000-2010).
Surface, west coast of Ireland	Mace Head	**0.88 ± 0.31** (winter) **0.72 ± 0.34** (spring) **0.35 ± 0.30** (summer) **0.38 ± 0.37** (autumn)	1989-2000	(Parrish et al., 2012)	Filtered to represent baseline transport conditions. Linear regression of seasonal averages through 2000, after which ozone has levelled off or begun to decrease (2000-2010).
Surface, rural northern German coast	Arkona-Zingst	**0.26 ± 0.05** (winter) **0.43 ± 0.06** (spring) **0.36 ± 0.07** (summer) **0.20 ± 0.04** (autumn)	1956-2010	(Parrish et al., 2012)	Unfiltered data. Linear regression of seasonal averages. Trends based on 1956-2000 are similar to 1956-2010.
Surface, alpine valley	Arosa	**0.53 ± 0.08** (winter) **0.57 ± 0.08** (spring) **0.55 ± 0.08** (summer) **0.46 ± 0.07** (autumn)	1950-2000	(Parrish et al., 2012)	Unfiltered data. Linear regression of seasonal averages through 2000, after which ozone began to decrease (2000-2010). No measurements were made from the late 1950s through 1988.
Surface, rural elevated site in south eastern Europe	Kislovodsk High Mountain Station	**-0.48 ± 0.13** (winter) **-0.69 ± 0.14** (spring) **-0.80 ±0.14**(summer) **-0.48 ±0.20** (autumn)	1991-2006	(Tarasova et al., 2009)	Unfiltered data. Linear regression of seasonal averages.
Arctic Europe mid-troposphere, 500 hPa	Composite of ozonesondes from Ny Alesund, Scoresbysund and Sodankyla	**0.36 ± 0.23**	1990-2006	(Hess and Zbinden, 2011)	Unfiltered data. Linear regression of 12-month running mean of monthly ozone deviations.
Central Europe lower free troposphere, 2.6-3.8 km above sea level	MOZAIC MOZAIC Hohenpeissenberg Payerne	0.15 ± 0.15 **-0.21 ± 0.20** **-0.20 ± 0.16** **-0.25 ± 0.17**	1995-2008 1998-2008 1998-2008 1998-2008	(Logan et al., 2012)	Unfiltered data, see box above. Trends at alpine sites for 1998-2008 show similar rates.
Central Europe mid-free troposphere, 5-6.1 km above sea level	MOZAIC MOZAIC Hohenpeissenberg	**0.33 ± 0.21** -0.08 ± 0.30 -0.1 ± 0.17	1995-2008 1998-2008 1998-2008	(Logan et al., 2012)	Unfiltered data. Linear regression, with annual trend calculated from four seasonal

	Payerne	**-0.43 ± 0.19**	1998-2008		trends; trends and annual cycle fit to monthly means. MOZAIC is a composite of aircraft flights to 5 European airports. Others are sonde stations.
North America					
Eastern USA, rural surface sites	Winter, 36 sites Spring, 40 sites Summer, 41 sites	0.12 (**44%, 0%**) -0.03 (**5%, 8%**) -0.45 (**0%, 66%**)	1990-2010	(Cooper, 2012)	Mid-day data only. Linear regression of seasonal medians at a site. The reported trend is the average of the individual trends in the region. Values in parentheses indicate the percent of sites with statistically significant positive or negative trends, respectively.
Western USA, rural surface sites	Winter, 11 sites Spring, 12 sites Summer, 12 sites	0.12 (**36%, 0%**) 0.19 (**50%, 0%**) 0.10 (**17%, 8%**)	1990-2010	(Cooper, 2012)	See box above.
USA west coast, marine boundary layer, composite of several sites	Winter Spring Summer Autumn	**0.37 ± 0.14** **0.41 ± 0.11** **0.23 ± 0.11** 0.09 ± 0.11	1985-2010	(Parrish et al., 2012)	Filtered for baseline transport conditions. Linear regression of seasonal averages.
High latitudes, surface	Denali, central Alaska	0.08	1987-2004	(Jaffe and Ray, 2007)	Mid-day data only. Annual trend from a linear regression of deseasonalized monthly mean concentrations.
Arctic, surface	Barrow, Alaska	0.04 ± 0.06	1974-2010	(analysis conducted for IPCC AR5)	Unfiltered data. Linear regression of annual averages, using method of (Parrish et al., 2012), and updated from the measurements in (Oltmans et al., 2006)
Arctic, surface	Alert, Nunavut, Canada	**0.87 ± 0.50 % yr^{-1}**	1992-2004	(Oltmans et al., 2006)	See box above.
Western North America free troposphere (3-8 km)	A springtime composite of lidar, ozonesonde and aircraft measurements.	**0.52 ± 0.20** **0.41 ± 0.27**	1984-2011 1995-2011	(Cooper, 2012)	Unfiltered data. Linear regression based on median values of all available measurements in the 3-8 km range during April-May.
Eastern USA free troposphere, 500 hPa	Annual composite of ozonesonde and MOZAIC profiles.	0.24 ± 0.26	1995-2005	(Hess and Zbinden, 2011)	Unfiltered data. Linear regression of annually averaged values for years when both ozonesonde and MOZAIC profiles were available.
Eastern Canada, Goose Bay ozonesonde profiles	Surface – 850 hPa 850-700 hPa 700-500 hPa 500-300 hPa	**-0.7 ± 0.4 % yr^{-1}** **-0.8 ± 0.3 % yr^{-1}** **-0.9 ± 0.2 % yr^{-1}** -0.5 ± 0.6 % yr^{-1}	1980-2004	(Oltmans et al., 2006)	Annual trend is determined from an autoregressive model that incorporates explanatory variables and a cubic polynomial fit. Reported values were read from their Figure 10.
Central Canada, Churchill ozonesonde profiles	Surface – 850 hPa 850-700 hPa 700-500 hPa 500-300 hPa	-0.2 ± 0.3 % yr^{-1} -0.1 ± 0.3 % yr^{-1} -0.1 ± 0.3 % yr^{-1} 0.3 ± 0.5 % yr^{-1}	1980-2004	(Oltmans et al., 2006)	See box above.
Western Canada, Edmonton ozonesonde	Surface – 850 hPa 850-700 hPa	0.3 ± 0.5 % yr^{-1} **0.4 ± 0.2 % yr^{-1}**	1980-2004	(Oltmans et al.,	See box above.

profiles	700-500 hPa 500-300 hPa	0.2 ± 0.2 % yr^{-1} 0.0 ± 0.4 % yr^{-1}		2006)	
Asia					
Surface, Mt. Happo, Japan, 1.85 km above sea level	Winter Spring Summer Autumn	**1.18 ± 0.27** **1.31 ± 0.28** **1.21 ± 0.41** **0.73 ± 0.32**	1991-2007	(Parrish et al., 2012)	Unfiltered data. Linear regression of seasonal averages.
Japanese marine boundary layer	Winter Spring Summer Autumn	0.29 ± 0.48 **0.62 ± 0.55** **0.59 ± 0.56** **0.52 ± 0.50**	1998-2009	(Parrish et al., 2012)	Unfiltered data. Linear regression of seasonal averages.
Beijing boundary layer	Annual Summer afternoons	**~1** **~3**	1997-2004	(Ding et al., 2008)	The rate of change was derived from a comparison of mean MOZAIC aircraft profiles during the periods 1995-1999 and 2000-2005.
Taiwan, surface,	YangMing mountain site in north of the country.	**0.54 ± 0.2**1 (annual)	1994-2007	(Lin et al., 2010)	Unfiltered data. Linear regression of annual means, using data from all times of day.
Taiwan, surface	Composite of 3 coastal sites	**0.52 ± 0.10** (annual)	1994-2007	(Lin et al., 2010)	Unfiltered data. Linear regression of annual means, using data from all times of day.
Taiwan, surface	Composite of 12 urban sites in the north of the country.	**0.75 ± 0.07** (annual)	1994-2007	(Lin et al., 2010)	Unfiltered data. Linear regression of annual means, using data from all times of day.
Taiwan, surface	Composite of 4 sites in the south of the country	~1.5 (annual)	1997-2006	(Lin et al., 2010)	Unfiltered data. Linear regression using monthly means. The reported trend was inferred from the regression line in Figure 2, and significance at the 95% confidence limit was not specified.
Hong Kong, surface	Hok Tsui coastal site on southern tip of Hong Kong Island, often upwind of the urban area.	**0.58** (annual)	1994-2007	(Wang et al., 2009b)	Unfiltered data. Linear regression of monthly means, using all months and all times of day.
Northern Japan, Sapporo ozonesonde profiles	Surface – 850 hPa 850-700 hPa 700-500 hPa 500-300 hPa	**0.7 ± 0.4 % yr^{-1}** **0.6 ± 0.3 % yr^{-1}** **0.5 ± 0.2 % yr^{-1}** 0.4 ± 0.5 % yr^{-1}	1970-2004	(Oltmans et al., 2006)	Annual trend is determined from an autoregressive model that incorporates explanatory variables and a cubic polynomial fit. Reported values were read from Figure 9.
Central Japan, Tsukuba ozonesonde profiles	Surface – 850 hPa 850-700 hPa 700-500 hPa 500-300 hPa	0.4 ± 0.4 % yr^{-1} **0.5 ± 0.3 % yr^{-1}** -0.2 ± 0.3 % yr^{-1} 0.3 ± 0.3 % yr^{-1}	1970-2004	(Oltmans et al., 2006)	See box above.
Central Japan, Kagoshima ozonesonde profiles	Surface – 850 hPa 850-700 hPa 700-500 hPa 500-300 hPa	**0.6 ± 0.5 % yr^{-1}** **0.6 ± 0.4 % yr^{-1}** 0.4 ± 0.4 % yr^{-1} 0.3 ± 0.4 % yr^{-1}	1970-2004	(Oltmans et al., 2006)	See box above.
Southern Japan, Naha ozonesonde profiles	Surface – 850 hPa 850-700 hPa	-0.5 ± 0.9 % yr^{-1} -0.8 ± 0.8 % yr^{-1}	1990-2004	(Oltmans et al.,	See box above.

	700-500 hPa 500-300 hPa	**0.7 ± 0.6 % yr^{-1}** 0.7 ± 0.7 % yr^{-1}		2006)	
South Asia, Tropospheric column ozone as measured by satellites	A broad region including much of India, southeast Asia and Indonesia	**0.3-0.7 % yr^{-1}**	1979-2005	(Beig and Singh, 2007)	The decadal trend was calculated using a multifunctional regression model. Here the trend is converted to percent yr^{-1}.
Northern Hemisphere Tropics					
Mauna Loa, Hawaii	3.4 km above sea level	**0.14 ± 0.07**	1974-2010	(analysis conducted for IPCC AR5)	Unfiltered data. Linear regression of annual averages, using method of (Parrish et al., 2012), and updated from the measurements in (Oltmans et al., 2006)
Northern Hemisphere Atlantic Ocean					
Marine boundary layer, eastern North Atlantic Ocean	40°-60° N 20°-40° N 0°-20° N	0.05 **0.51** **0.42**	1977-2002	(Lelieveld et al., 2004)	Unfiltered measurements from ships traversing the indicated regions. The 95% confidence limits were not reported, although statistical significance was.
Marine boundary layer, western North Atlantic Ocean	Bermuda	**0.31 ± 0.25** (winter) 0.27 ± 0.29 (spring) **0.30 ± 0.16** (summer) 0.05 ± 0.33 (autumn)	1989-2010	(Parrish et al., 2012)	Unfiltered data. Linear regression of seasonal averages. There is a data gap of 5 years in the middle of the record.
Northern Hemisphere Upper Troposphere		Seasons with significant increase in ozone			
Western USA Northeast USA Atlantic Ocean Europe Middle East Northern India South China Northern Japan Southern Japan		None **Winter, spring** **Winter** **Spring** **Spring, summer** **Spring, summer** **Summer** **Summer, autumn** **All seasons**	Ozone change between 1975-1979 and 1994-2001	(Schnadt Poberaj et al., 2009)	Ozone changes were calculated for various regions of the northern hemisphere that were sampled by the NASA GASP aircraft program in the 1970s and by the European MOZAIC program in the 1990s.
Southern Hemisphere					
Tropical South Pacific Ocean, marine boundary layer	Samoa	-0.01 ± 0.03	1976-2009	(analysis conducted for IPCC AR5)	Unfiltered data. Linear regression of annual averages, using method of (Parrish et al., 2012). This trend is an update to the measurements discussed in Oltmans et al., 2006.
Marine boundary layer, western South Atlantic Ocean	40°-60° S 20°-40° S 0°-20° S	**0.17** **0.24** 0.12	1977-2002	(Lelieveld et al., 2004)	See box above.
Marine boundary layer, eastern South Atlantic Ocean	20°-40° S 0°-20° S	**0.68** **0.37**	1977-2002	(Lelieveld et al., 2004)	See box above
Mid-latitude marine boundary layer	Cape Point, South Africa	0.01 ± 0.09	1997-2010	(analysis conducted for IPCC	Unfiltered data. Linear regression of annual averages, using method of (Parrish et al.,

				AR5)	2012). This trend is an update to the measurements discussed in Oltmans et al., 2006.
Mid-latitude marine boundary layer	Cape Grim, Tasmania, Australia	**0.06 ± 0.02**	1982-2010	(analysis conducted for IPCC AR5)	See box above
Antarctica, Ekström ice shelf, 10 km from the ocean	Neumayer	0.13 ± 0.16	1995-2005	(Helmig et al., 2007)	Unfiltered data. Linear regression based on annual median values.
Antarctica, 2.8 km above sea level	South Pole	0.00 ± 0.06	1975-2010	(analysis conducted for IPCC AR5)	Unfiltered data. Linear regression of annual averages, using method of (Parrish et al., 2012), and updated from the measurements in (Oltmans et al., 2006)
Ozonesonde profiles, La Reunion Island in the tropical Indian Ocean	2-4 km a.s.l 4-10 km a.s.l. 10-16 km a.s.l.	0.01 ± 0.69 % yr^{-1} 0.44 ± 0.58 % yr^{-1} **1.23 ± 0.58 % yr^{-1}**	1992-2008	(Clain et al., 2009)	Unfiltered ozonesonde measurements. Linear regression of all available year-round measurements.
Ozonesonde profiles, Irene in subtropical South Africa	2-4 km a.s.l 4-10 km a.s.l. 10-16 km a.s.l.	**1.44 ± 0.40 % yr^{-1}** **0.40 ± 0.33 % yr^{-1}** 0.19 ± 0.35 % yr^{-1}	1990-2008	(Clain et al., 2009)	Unfiltered ozonesonde measurements. Linear regression of all available year-round measurements. No data for 1994-1997.
Ozonesonde profiles, Lauder, New Zealand	Surface – 850 hPa 850-700 hPa 700-500 hPa 500-300 hPa	**0.7 ± 0.4 % yr^{-1}** **0.5 ± 0.3 % yr^{-1}** 0.2 ± 0.3 % yr^{-1} -0.1± 0.4 % yr^{-1}	1986-2003	(Oltmans et al., 2006)	Annual trend is determined from an autoregressive model that incorporates explanatory variables and a cubic polynomial fit. Reported values were read from Figure 19.

Notes:
(a) Trends are based on annual data unless seasons are specified, and reported in units of ppb yr^{-1}, with the 95% confidence limits, unless indicated differently. Trends that are statistically significant at the 95% confidence level are shown in bold.

2.A.2.3 Aerosols

Comprehensive, long-term, and high quality observations of aerosols have been initiated mainly after 2000, and are currently only available at a few locations and regions. The monitoring and observations of aerosols are still to a large degree uncoordinated on continental and global scale, despite the crucial importance of aerosols as short-lived climate forcers. A few long-term background measurements of aerosol properties are performed within the framework of the W MO GAW (Global Atmosphere Watch) program; however the data coverage is low. An overview and critical evaluation of worldwide, quality assured, aerosol trend measurements presently does not exist. For studies of aerosol-climate interactions, it is crucial that the sites are representative for regional/rural conditions, with low influence of local pollution and that the measurements are harmonised among sites and networks, and provided as homogeneous time series.

Regional air pollution networks in Europe and North America are the most reliable source of information on long-term surface aerosol trends in these parts of the world.

In Europe, the EMEP network provides regionally representative measurements of aerosol composition since the 1980s; these measurements are described in annual reports, and they are available via www.emep.int. (Torseth et al., 2012) provide an overview of results from 2-3 decades of EMEP measurements, as discussed in Section 2.2.3.

In North America, the U.S. Clean Air Status and Trends Network (CASTNET) and the Canadian Air and Precipitation Monitoring Network (CAPMoN) provide regionally-representative long term measurements of

major ions in aerosols, including sulfate, i.e., (Hidy and Pennell, 2010); these networks do not report PM2.5. The U.S. Interagency Monitoring of Protected Visual Environments (IMPROVE) Network has measured PM2.5 and PM10 mass, total aerosol composition, and visibility at ca. 60 regional stations since 1989 (Hand et al., 2011c). Canadian CAPMoN network results are summarized in (Canada, 2012).

In Asia, the Acid Deposition Network East Asia (EANET, 2011) has measured particulate matter and deposition since 2001, but thus far no trend studies have been published. In China, CAWNET and CARSNET recently started systematic aerosol observation, e.g., (Zhang et al., 2012), however only few years of data are available. An analysis of population weighted PM2.5 measurements reported in (Brauer et al., 2012) showed that China has the worlds highest average PM2.5 (55 μg m^{-3}); more than twice the global average, indicating a strong influence of pollutant emissions. In China (Qu et al., 2010) reconstruct urban PM10 time trends (2000-2006) from reported Air pollution indices in 86 Chinese cities. Their analysis suggests that median aerosol concentration declined from 108 to 95 μg m^{-3} in 16 Northern cities and increased slightly from 52 to 60 μg m^{-3} values in 12 southern cities. Quan et al (2011) report strong declines commencing in the 1970s in visibility in the Eastern provinces of China, and continuing in the 2000s. They link these reduced visibility levels to the emission changes and high PM levels.
In some other Asian regions long-term measurements from individual research groups or small networks are becoming available, but it is often difficult to assess the significance of these measurements for larger regions.

In India, the Central Pollution Control Board (CPCB), Government of India, is executing a nation-wide programme of ambient air quality monitoring known as the National Air Quality Monitoring Programme (NAMP). The network consists of 342 monitoring stations covering 127 cities/towns in 26 States and 4 Union Territories. The State of Environment Report (Ministery of Environment and Forest, 2009) reported annual average levels of respirable particulate matter (approximately PM10) in residential areas of major cities ranging from 120-160 μg m^{-3} (Delhi), 80-120 μg m^{-3} (Mumbai), 30-90 μg m^{-3} (Chennai), and 120-140 μg m^{-3} (Kolkata); in these cities' trends are mostly stable or increasing for 2000-2007. No details on the robustness of trends are given, and the validity of these trends for rural regions not reported.

Surface based remote sensing of aerosol, as discussed in Section 2.2.3.1, is mainly based on results from the global AERONET network (Holben et al., 1998). However, coverage of AERONET over several regions is poor. Since AR4 several other regional networks were established such as ARFINET covering India (Moorthy et al., 2008); AEROCAN over Canada (http://www.aerocanonline.com/), and SKYNET over Japan (Kim et al., 2004), not included in our analysis.

2.A.2.3.1 North American sulphate trends

In Section 2.2.3.2 overall declines of SO_4^{2-} from the IMPROVE (Hand et al., 2011c) network are on the order of 2-4% yr^{-1}, but somewhat larger (~ 6% yr^{-1}) along the east coast of the USA. SO_4^{2-} declines in winter were somewhat larger than in other seasons.

These trends are consistent with average trends reported by CASTNET (2010) of -0.045 ugS m^{-3} yr^{-1} for the period 1990–2008 in the eastern US, and a decrease of CASTNET aerosol sulphate concentrations by -21% in the east and northeast, -22% in the Midwest, and -20% in the south between the two periods 1990–1994 and 2000–2004 (Sickles and Shadwick, 2007a). Indirect evidence for declining sulphate particulate concentrations is found in an analysis of SO_4^{2-} wet deposition by 20–30% over a time period of 15 years (Sickles and Shadwick, 2007b), corresponding to a trend of about –1.4% to –2.1% yr^{-1}. In Canada, aerosol sulphate concentrations from 1991–1993 declined by 30 to 45% by 2004–2006 at non-urban CAPMoN sites in the eastern half of the country. These declines are consistent with the trends of inorganic aerosol components reported by Quinn et al. (2009) at Barrow, Alaska, ranging between –2.3% yr^{-1} for SO_4^{2-} to –6.4% for NH_4. Hidy and Pennell (2010) show remarkable agreement of PM2.5 and SO_4^{2-} declines in Canada, pointing to common emission sources of PM2.5 and SO_4^{2-}

2.A.2.3.2 Black (light arborbing) and elemental carbon trends

The terms black carbon (BC), also referred to as light absorbing carbon (LAC), and elemental carbon (EC) refer to the analysis method: optical methods (aerosol light absorption) or filter measurements using thermal methods, respectively. The measurements are associated with large uncertainties; intercomparisons show differences of a factor 2–3 for optical methods, and a factor of 4 for thermal methods (Vignati et al., 2010),

which also renders quantitative comparison of LAC time series uncertain. In addition, while there is a general lack of BC/EC measurements, long-term time series are even scarcer.

In Europe, long term EC and organic carbon (OC) data are available at 2 stations (in Norway and Italy) starting in 2001 (EMEP, 2010). (Torseth et al., 2012) reports slight decreases over these 9 years, however without an assessment of statistical significance. In North America, the combined IMPROVE and CSN network (Hand et al., 2011c) is measuring elemental and organic carbon. However, trend analysis of long-term data are only reported (Hand et al., 2011c) for total carbon (TC=black carbon + organic carbon), since an upgrade in sampling techniques around 2005 led to a different measured ratio of EC and OC carbon. These TC measurements indicate highly significant ($p<0.05$) downward trends of total carbon between 2.5 and 7.5% yr^{-1} along the east and west coasts of the USA, and smaller and less significant ($p<0.15$) trends in other US regions from 1989-2008. Sharma et al. (2006) published long term measurements of equivalent BC at Alert, Canada and Barrow, Alaska, USA. Decreases were 54% at Alert and 27% at Barrow for 1989–2003; part of the trend difference was associated with changes in circulation patterns, i.e., the phase of NAO.

In China, (Han et al., 2011) report stable elemental carbon concentration in sediments at Chaohu and Lake Taihu in Eastern China until the late 1970s, followed by a sharp increase afterwards, corresponding well with the rapid industrialization of China in the last three decades. An analysis of broadband radiometer data from 1957 to 2007 (Wang and Shi, 2010) showed a slight decrease in absorption of aerosol after 1990, likely due to LAC, while there was no significant change in the scattering fraction of aerosol.

In India, at the southern station Trivandrum downward trends in BC of 250 ng m^{-3} yr^{-1} (from 4000 to 2000 ng m^{-3}) in the period 2001-2009 are reported, the largest changes occurring in 2007-2009 (Krishna Moorthy et al., 2009). At the northern station Kanpur increases of AOD in post-monson and winter are observed for 2001-2010, attributed to anthropogenic emission changes, and declining trends in pre-monsoon and monsoon season, which were attributed to changes in natural emissions (Kaskaoutis et al., 2012).

2.A.3 Quantifying Changes in the Mean: Trend Models and Estimation in Box 2.2

This appendix provides a detailed description of the method used to estimate linear trends in Chapter 2 and compares the results of this relatively simple method with those of a wide variety of other methods for fitting lines to data and estimating their uncertainty. It is demonstrated that the differences among the methods are rather small compared to the uncertainty estimates of each method. Details of the smoothing method used to produce the result shown in Box 2.2 Figure 1, are also provided.

2.A.3.1 Methods of Estimating Linear Trends and Uncertainties

Several different methods of calculating linear trends and their uncertainties are illustrated here by application to the annual mean time series of globally averaged Earth surface temperatures from HadCRUT4 data set (see Section 2.4.3 for details). The methods used are briefly described below. The conclusion of this analysis is that, for time series like the one used here, the trend line slope and its uncertainty limits are very similar for most of the methods that take into account dependency in the data sets in the form of the first-order autoregressive model AR(1). These results are similar to those obtained by the Restricted Maximum Likelihood (REML) method used in AR4. The similarity of the AR4 method results to those of the methods investigated here was determined by applying these methods to AR4 data sets and obtaining similar results for linear trends and their uncertainties (not shown). One of the simpler methods is selected for use in this Chapter.

2.A.3.2 Comparison of Trend Slope Calculation Methods

We would like to fit a straight line to a given time series of observations $\{y_i\}$ that correspond to an independent variable (instants of time) $\{x_i\}$:

$$y_i = a + bx_i + e_i, \quad i = 1, \cdots, N$$

where a and b are constant parameters to be determined, while $\{e_i\}$ represent residual variability in observations (w.r.t. the straight line $y = a + bx$). Without any additional assumptions, one can find the least

squares solution for the trend line, *i.e.,* $\hat{a}$ and $\hat{b}$ that minimize overall squared error $\sum_1^N e_i^2$ in the equation above:

$$\hat{b} = \frac{\sum_{i=1}^{N}(x_i - m_x)(y_i - m_y)}{\sum_{i=1}^{N}(x_i - m_x)^2}, \quad \hat{a} = m_y - \hat{b}m_x \tag{2.A.1}$$

where m_x and m_y are sample means of x and y, respectively:

$$m_x = \frac{1}{N}\sum_{i=1}^{N} x_i, \quad m_y = \frac{1}{N}\sum_{i=1}^{N} y_i \tag{2.A.2}$$

Data residuals (or errors in the linear fit) are

$$\hat{e}_i = y_i - (\hat{a} + \hat{b}x_i) \qquad i = 1, \cdots, N \tag{2.A.3}$$

To estimate uncertainty in $\hat{a}$ and $\hat{b}$, it is useful to view $\{e_i\}$ as a realization of some random process $\{\varepsilon_i\}$. Then the estimates of $\hat{a}$ and $\hat{b}$ can be interpreted as random variables and inferences can be made about their uncertainties, i.e., deviations from their "true" values. Assumptions made about $\{\varepsilon_i\}$ affect, in general, the estimates of $\hat{a}$ and $\hat{b}$, and, usually to a larger extent, the uncertainties (confidence intervals) for these estimates.

1. Ordinary least squares (OLS) is the best known case of this kind of analysis. It assumes that all ε_i are independent identically-distributed (i.i.d.) random variables with normal distribution $\mathcal{N}(0, \sigma_e^2)$. While σ_e is usually considered unknown, in this case its unbiased estimate can be obtained from data residuals (2.A.3) as

$$\hat{\sigma}_e^2 = \frac{1}{N-2}\sum_{i=1}^{N} \hat{e}_i^2. \tag{2.A.4}$$

Note that $N-2$ appears in the denominator instead of N because two degrees of freedom out of the original N were spent on fitting two parameters a and b.

The trend slope $\hat{b}$ estimated by equation (2.A.1) will also be normally distributed: $\mathcal{N}(0, \sigma_b^2)$, and its standard deviation σ_b can be estimated using the σ_e estimate:

$$\hat{\sigma}_b = \hat{\sigma}_e / S_x, \quad S_x^2 = \sum_{i=1}^{N}(x_i - m_x)^2. \tag{2.A.5}$$

Under the assumptions made about ε_i, the random variable defined as

$$U = \frac{\hat{b} - b}{\hat{\sigma}_b}$$

has a known probability distribution, a Student's t with $N-2$ degrees of freedom. To form a confidence interval for $\hat{b}$ such that it contains the true value of b with probability p, define

$$q = t_{\frac{1+p}{2}}(N-2) \tag{2.A.6}$$

i.e., the $\frac{1+p}{2}$-quantile of Student's $t(N-2)$ distribution. Random variables with this distribution lie in the interval $(-q, q)$ with probability p. From this statement applied to U, it is inferred that the interval $(\hat{b} - q\hat{\sigma}_b, \hat{b} + q\hat{\sigma}_b)$ contains b with probability p, or, as it is usually stated,

$$b = \hat{b} \pm q\hat{\sigma}_b \tag{2.A.7}$$

where $\hat{b}$, $\hat{\sigma}_b$, and q are given by formulas (2.A.1)-(2.A.6).

2. OLS with reduced number of degrees of freedom by Santer et al. (2008), hereafter **S2008**. The standard OLS assumption about independence of the residual deviations of data from the straight line is often

unrealistic. A better approximation to reality is a model for serially correlated error, a.k.a. first-order autoregressive model AR(1):

$$\varepsilon_{i+1} = \rho\varepsilon_i + \delta_i, \quad i = 1,\cdots,N-1 \tag{2.A.8}$$

where δ_i, not ε_i are now thought of as independent random variables. For a certain class of statistical estimation problems, this kind of data interdependence acts as if the sample size was reduced to N_r:

$$N_r = N\frac{1-\rho}{1+\rho} \tag{2.A.9}$$

For example, if calculations by formulas (2.A.1)-(2.A.5) are carried through for a large sample with data dependency due to the AR(1) model (2.A.8), replacing $N-2$ by N_r-2 in the denominator of (4) results in a correct estimate of the trend error's standard deviation σ_b by formula (2.A.5). Based on these theoretical considerations, Santer et al. (2008) employed a heuristic procedure that carries this calculation ahead using the value of ρ estimated from the sample of the OLS data residuals $\{\hat{e}_i\}$. Estimated $\hat{\rho}$ is the correlation coefficient between two $N-1$-long subsamples lagged by one time step:

$$\hat{\rho} = \frac{S_{12}}{\sqrt{S_{11}S_{22}}}, \quad S_{12} = \sum_{i=1}^{N-1}(\hat{e}_i - m_1)(\hat{e}_{i+1} - m_2) \tag{2.A.10}$$

$$S_{11} = \sum_{i=1}^{N-1}(\hat{e}_i - m_1)^2, \quad S_{22} = \sum_{i=2}^{N}(\hat{e}_i - m_2)^2 \tag{2.A.11}$$

$$m_1 = \frac{1}{N-1}\sum_{i=1}^{N-1}\hat{e}_i, \qquad m_2 = \frac{1}{N-1}\sum_{i=2}^{N}\hat{e}_{i+1} \tag{2.A.12}$$

(It is assumed that the timeseries are avalable on a uniform time grid without any gaps).
Furthermore, S2008 used N_r-2 in place of $N-2$ as a degree-of-freedom parameter for Student's t in (2.A.6). Even though in case of AR(2.A.1) error the sampling distribution of U is not that of Student's t, S2008 have calculated confidence intervals for b using formulas (2.A.1)-(2.A.7), with (2.A.4) and (2.A.6) modified by the replacement of $N-2$ by N_r-2, with N_r computed by (2.A.9) using ρ estimated according to (2.A.10)-(2.A.12). Their extensive numerical experiments suggested that this heuristic strategy results in reliable, conservative uncertainty estimates for the trend slope.

3. Generalized Least Squares (GLS). Rewrite the same problem as discussed above in matrix notation. Let $\mathbf{X} = \left[\mathbf{X}^0\ \mathbf{X}^1\right]$ be an $N\times 2$ matrix, and $\mathbf{Y}$ and $\mathbf{E}$ N-dimensional column-vectors such that

$$\mathbf{X}^0 = \left[1\cdots 1\right]^T,\ \mathbf{X}^1 = \left[x_1\cdots x_N\right]^T,\ \mathbf{Y} = \left[y_1\cdots y_N\right]^T,\ \mathbf{E} = \left[e_1\cdots e_N\right]^T$$

Let also $\mathbf{c}^T = [a\ b]$. Then the linear trend estimation problem becomes

$$\mathbf{Y} = \mathbf{X}\mathbf{c} + \mathbf{E}$$

Let $\mathbf{E}$ be a random vector from the multivariate normal distribution $\mathcal{N}(0, \mathbf{V})$, where **V** is a covariance matrix. The optimal estimator of $\mathbf{c}$ is

$$\hat{\mathbf{c}} = \left(\mathbf{X}^T\mathbf{V}^{-1}\mathbf{X}\right)^{-1}\mathbf{X}^T\mathbf{V}^{-1}\mathbf{Y}$$

and covariance matrix for $\hat{\mathbf{c}}$ is

$$\mathbf{P} = \left(\mathbf{X}^T\mathbf{V}^{-1}\mathbf{X}\right)^{-1}$$

For the practical implementation of this method, **V** is unknown. Here we assume that **V** is a covariance matrix of an AR(1) process: $\mathbf{V} = \left(v_{ij}\right)$, $v_{ij} = \sigma_e^2\rho^{|i-j|}$ where σ_e^2 and ρ are estimated as variance and lag-1 autocorrelation coefficient respectively from data residuals of the initial OLS fit, as described in equations (2.A.4) and (2.A.10)-(2.A.12).

4. Prewhitening. First OLS is performed, and $\hat{\rho}$ is estimated as in (2.A.10) above. Then the time series y is prewhitened as

$$y_i' = \frac{y_{i+1} - \hat{\rho}y_i}{1-\hat{\rho}}, \qquad i = 1,\cdots,N-1 \tag{2.A.13}$$

The the OLS is applied to timeseries $\{y_i'\}$ and corresponding times $\{x_i,\ i=1,\cdots,N-1\}$. The prewhitening scheme (2.A.13) does not change the value of the "true" trend coefficient b.

5. Sen–Theil trend estimator, or median slope method: Nonparametric estimate of the linear trend based on Kendall's τ, from Sen (1968). Relaxes the usual requirement of normal distribution of $\{\varepsilon_i\}$, but does assume i.i.d $\{\varepsilon_i\}$. No reduction of effective sample size is done.

6. Wang and Swail (2001) iterative method (WS2001). A method of trend calculation iterating between computing Sen–Theil trend slope for time series prewhitened as in equation (2.A.13), computing data residuals of the original time series with regards to the line with this new slope, estimating $\hat{\rho}$ from these residuals (as in equations (2.A.10)-(2.A.12)), prewhitening the original time series using this $\hat{\rho}$ value, etc. Zhang and Zwiers (2004) compared this method with other approaches, including Maximum Likelihood for linear trends with AR(1) error, and found it to perform best, especially for short time series.

Table 2.A.3: Trends (˚C per decade) and 90% confidence intervals for HadCRUT4 global mean annual time series for periods 1901-2011, 1901-1950, and 1951-2011 calculated by methods described in Appendix 2.A. Effective sample size N_r and lagged by one time step correlation coefficient for residuals $\hat{\rho}$ are given for methods that compute them. Note differences in the width of confidence intervals between methods that assume independence of data deviations from the straight line (OLS and Sen–Theil methods) and those that allow AR(1) dependence in the data (all other methods). Two of these methods use non-parametric tend estimation (Sen-Theil and WS2001).

Method	1901–2011			1901–1950			1951–2011		
	Trend	N_r	$\hat{\rho}$	Trend	N_r	$\hat{\rho}$	Trend	N_r	$\hat{\rho}$
OLS	0.075 ± 0.006			0.107 ± 0.016			0.107 ± 0.015		
S2008	0.075 ± 0.013	28	0.599	0.107 ± 0.026	21	0.407	0.107 ± 0.028	21	0.494
GLS	0.073 ± 0.012		0.599	0.100 ± 0.023		0.407	0.104 ± 0.025		0.494
Prewhtn	0.077 ± 0.013		0.594	0.113 ± 0.022		0.362	0.111 ± 0.026		0.488
Sen-Theil	0.075–0.006+0.007			0.113–0.019+0.019			0.109–0.017+0.019		
WS2001	0.079–0.014+0.012		0.596	0.114–0.026+0.023		0.352	0.110–0.028+0.029		0.487

2.A.3.3 Method for Calculating Linear Trends and their Uncertainties for General Use Within Chapter 2

The method applied in this chapter is a slight modification of the S2008 method. The sample size is not reduced ($N_r = N$), if the estimated $\hat{\rho}$ is negative. The method was also modified for use with time series where some data is missing. The formula (9) for the effective sample size is still used. This formula was designed to give precise results for trend error when used for long time series of fully available data. In the presence of missing data (and shorter time series) this formula underestimates N_r further and thus results in wider (more conservative) confidence intervals (compared to the cases without missing data). The final procedure is as follows.

The time series of observations $\{y_i\}$ corresponds to instants of time $\{x_i,\ i=1,\cdots,N\}$ that form a uniform grid. In some cases, observations y_i are missing. Formally, two sets of indices I_a and I_m are introduced that correspond to available and missing observations, respectively. Obviously, the union of the two sets includes all the possible data locations and the two sets do not intersect,

$$\{1,\cdots,N\} = I_a \cup I_m, \quad I_a \cap I_m = \varnothing$$

The size of I_a is N_a.

First, OLS is performed for available observations:

$$\hat{b} = \frac{\sum_{i \in I_a} (x_i - m_x)(y_i - m_y)}{\sum_{i \in I_a} (x_i - m_x)^2}, \quad \hat{a} = m_y - \hat{b} m_x$$

where m_x and m_y are sample means of x and y over I_a, respectively:

$$m_x = \frac{1}{N_a} \sum_{i \in I_a} x_i, \quad m_y = \frac{1}{N_a} \sum_{i \in I_a} y_i$$

Data residuals (or trend line misfits) are

$$\hat{e}_i = y_i - (\hat{a} + \hat{b} x_i), \quad i \in I_a$$

Lag-one correlation coefficient of $\{\hat{e}_i\}$ can be estimated over the subset of indices $I_c = \{i : i \in I_a \,\&\, (i+1) \in I_a\}$. Let N_c be the size of I_c. Then

$$\hat{\rho} = \frac{S_{12}}{\sqrt{S_{11} S_{22}}}, \quad S_{12} = \sum_{i \in I_c} (\hat{e}_i - m_1)(\hat{e}_{i+1} - m_2)$$

$$S_{11} = \sum_{i \in I_c} (\hat{e}_i - m_1)^2, \quad S_{22} = \sum_{i \in I_c} (\hat{e}_{i+1} - m_2)^2$$

$$m_1 = \frac{1}{N_c} \sum_{i \in I_c} \hat{e}_i, \qquad m_2 = \frac{1}{N_c} \sum_{i \in I_c} \hat{e}_{i+1}$$

A provision is made for not raising the effective sample size if estimated $\hat{\rho}$ is negative:

$$\hat{\rho}_+ = \max(\hat{\rho},\ 0)$$

The resulting $\hat{\rho}_+$ is used to obtain the effective sample size of the set of available observations:

$$N_r = N_a \frac{1 - \hat{\rho}_+}{1 + \hat{\rho}_+}$$

which is then used to estimate the variance of data deviations from the trend line:

$$\hat{\sigma}_e^2 = \frac{1}{N_r - 2} \sum_{i \in I_a} \hat{e}_i^2.$$

Therefore the variance of trend slope estimator is obtained:

$$\hat{\sigma}_b = \hat{\sigma}_e / S_x, \quad S_x^2 = \sum_{i \in I_a} (x_i - m_x)^2.$$

To construct a confidence interval for probability level p, let

$$q = t_{\frac{1+p}{2}}(N_r - 2)$$

be the $\frac{1+p}{2}$-quantile of Student's $t(N_r - 2)$ distribution. Finally

$$b = \hat{b} \pm q \hat{\sigma}_b$$

where $\hat{b}$, $\hat{\sigma}_b$, and q are given by formulas above.

2.A.3.4 Smoothing Spline Method

An alternative approach is to estimate local trends using non-parametric trend models obtained by penalized smoothing of time series (e.g., (Wahba, 1990; Wood, 2006), Section 6.7.2). The value in any year is considered to be the sum of a non-parametric smooth trend and a low-order autoregressive noise term. The trend is represented locally by cubic spline polynomials(Scinocca et al., 2010) and the smoothing parameter is estimated using Restricted Maximum Likelihood (REML) allowing for serial correlation in the residuals. [PLACEHOLDER FOR FINAL DRAFT: more detailed description of the smoothing spline method used for the figure and table in Box 2.2]

2.A.4 Changes in Temperature

2.A.4.1 Change in Surface In-Situ Observations Over Time

Observations are available for much of the global land surface starting in the mid-1800s or early 1900s. Availability is reduced in the most recent years due in large part to international data exchange delays. Non-digitized temperature records continue to be found in various country archives and are being digitized (Allan et al., 2011; Brunet and Jones, 2011). Efforts to create a single comprehensive raw digital data holding with provenance tracking and version control have advanced (Thorne et al., 2011b). Most historical SST observations arise from ships, with buoy measurements and satellite data becoming a significant contribution in the 1980s. Digital archives such as the International Comprehensive Ocean-Atmosphere Data Set (ICOADS, currently version 2.5, Woodruff et al., (2011)) are constantly augmented as paper archives are imaged and digitised (Brohan et al., 2009). Despite substantial efforts in data assembly, the total number of available SST observations and the percentage of the Earth's surface area that they cover remain very low before 1850 and drop drastically during the two World Wars. The sampling of land and marine records through time which form the basis for the in-situ LSAT and SST records detailed in the chapter are summarized in Figure 2.A.1.

[INSERT FIGURE 2.A.1 HERE]

Figure 2.A.1: Change in percentage of possible sampled area for land records (top panel) and marine records (lower panel). Land data comes from GHCNv3.2.0 and marine data comes from the ICOADS in-situ record.

2.A.4.2 Land Surface Temperature Dataset Innovations

Improvements have been made to the historical global data sets of land-based station observations used in AR4. Basic descriptions of the methods for the current versions of all datasets are given in Table 2.A.4. Global Historical Climatology Network (GHCN) V3 improvements (Lawrimore et al., 2011b) included elimination of "duplicate" time series for many stations, updating more station data with the most recent data, the application of enhanced quality assurance procedures (Durre et al., 2010) and a new pairwise homogenization approach for individual station time series (Menne and Williams, 2009). Two version increments to this V3 product to fix coding issues have since accrued, which have served to slightly increase the centennial timescale trends. Goddard Institute of Space Studies (GISS) continues to provide an estimate based upon primarily GHCN but with different station inclusion criteria, additional night-light-based urban adjustments and a distinct gridding and infilling method (Hansen et al., 2010). CRUTEM4 (Jones et al., 2012a) incorporates additional series and also newly homogenized versions of the records for a number of stations. It continues the model of incorporating the best available estimates for each station arising from research papers or individual national meteorological services with access to the best metadata on the assumption that such efforts have had most attention paid to them. In contrast, all other products considered in AR5 undertake a globally consistent homogenization processing of a given set of input data, although those data may well have been processed at source. A new data product from a group based predominantly at Berkeley (Rhode et al., submitted) uses a kriging technique, commonly used in geostatistics, to create a global mean timeseries accounting for time-varying station biases by treating each apparently homogeneous segment as a unique record. This is substantially methodologically distinct from earlier efforts and so helps us to better explore structural uncertainty (Box 2.1) in LSAT estimates.

Table 2.A.4: Summary of methods used by producers of global Land-Surface Air Temperature products. Basic methodological details are included to give a flavour of the methodological diversity. Further details can be found in the papers describing the dataset construction processes cited in the text.

Dataset	Start of Record	Number of Stations	Quality Control and Homogeneity Adjustments	Infilling	Averaging Procedure
CRUTEM4 (Jones et al., 2012b)	1856	5583 (4842 used in gridding)	Source specific QC and homogeneity applied generally to source data prior to collation	none	Average of the two hemispheric averages weighted 2/3 NH and 1/3 SH.
GHCNv3 (Lawrimore et al., 2011a)	1880	7280	Outlier and neighbour QC and pairwise comparison based adjustments	Limited infilling by eigenvectors (for global mean calculations only)	Average of gridboxes area weighted

GISS (Hansen et al., 2010)	1880	c.6300	Night lights based adjustments for urban influences	Averages to 40 large scale bins	Average of the bins with areal weighting.
Berkeley (Rhode et al., submitted)	1753	39028	Individual outliers are implicitly down-weighted. Neighbour-based test to identify breaks and each apparently homogeneous segment treated separately.	No gridding, but kriging produces field estimate based upon the station constraint at each timestep.	Kriged field estimate limited to maximum 1500 km distance from any station

2.A.4.3 Sea Surface Temperature Data Improvements and Dataset Innovations

2.A.4.3.1 In situ SST data records

Because of the irregular nature of sampling in space and time when observations are made from the moving platforms (ships and floating buoys), it is customary to use statistical summaries of "binned" (most commonly grid box) observations rather than individual observed values (Table 2.A.4). Means or medians of all SST values in a given bin that pass quality control procedures are generally used. Standard deviations and numbers of observations in individual bins are useful for estimating uncertainties. These procedures usually serve as an initial step for producing more sophisticated gridded SST products, which involve bias correction and, in some cases, interpolation and smoothing.

Since AR4, major innovations have primarily been around understanding of modern era biases. Beginning in the 1930s some ships began taking measurements of engine room intake (ERI) water. It is hypothesized that proximity to the hot engine often biases these measurements warm (Kent et al., 2010). Because of the prevalence of the ERI measurements among SST data from ships, the ship SSTs are biased warm by 0.12-0.18 K on average compared to the buoy data (Kennedy et al., 2011a; Kennedy et al., 2011c; Reynolds et al., 2010). Since the 1980s, drifting and moored buoys have been producing an increasingly large fraction of global SST observations and these have tended to be colder than ship-based measurements.

Although more variable than SSTs, Marine Air Temperatures (MATs) are assumed to be physically constrained to track SST variability because of the continuous air-sea heat exchange. However, there have been shown to be some longer-term variations, at least in certain locations and periods e.g., Christy et al., (2001); Smith and Reynolds, (2002) which necessitate a degree of caution. Regardless, they provide an independent measure of marine region temperature changes. Adjustments have been applied to account for the change in deck heights and for the use of non-standard practices during World War II (Rayner et al., 2003) and the 19th Century (Bottomley et al., 1990). Because of biases due to solar heating, only NMATs have so far been widely used in climate analyses. The progress on the analytical correction of solar heating biases in recent day-time MAT data allowed their use in a recent analysis (Berry and Kent, 2009; Berry et al., 2004). Table 2.A.5 gives a brief description of well-known historical SST products, organized by their type.

Table 2.A.5: Data Sets of SST and NMAT Observations Used in Section 2.4.2. These data sets belong to the following categories: a database of individual in situ observations; gridded data sets of climate anomalies (with bucket and potentially additional bias corrections applied); and globally complete interpolated data sets based on the latter products.

Data Set	Period	Space-Time Grid Resolution	Bucket/ Bias Corrections Applied
Historical Database of In Situ Observations			
International Comprehensive Ocean – Atmosphere Data Set, ICOADS, v2.5	1662 – present; 1800 – present, 1960 – present	Individual reports; 2° x 2° mon summ; 1° x 1° mon summ	No
Gridded Data Sets of Observed Climate Anomalies			
U.K.M.O. Hadley Centre SST, v.2, HadSST2	1850 – present	5° x 5° monthly	Yes, 1850–1941
U.K.M.O. Hadley Centre SST, v.3, HadSST3	1850–2006	5° x 5° monthly	Yes, 1850–2006

U.K.M.O. Hadley Centre NMAT, v.4.3 MOHMAT4.3N	1856–2007	5° x 5° monthly	Yes, 19th Century and WWII
Globally Complete Objective Analyses (Interpolated Products) of Historical SST Records			
U.K.M.O. Hadley Centre Interpolated SST, v.1, HadISST	1870 – present	1° x 1° monthly	Yes, 1870–1941
JMA Centennial in-situ Observation Based Estimates of variability of SST, COBE SST	1891 – present	1° x 1° monthly	Yes, 1891–1941
NOAA Extended Reconstruction of SST, ERSSTv3b	1854 – present	2° x 2° monthly	Yes, 1854–1941

2.A.4.3.2 Comparing different types of data and their errors

Comparisons are complicated as different measurement technologies measure somewhat different physical characteristics of the surface ocean. IR and MW radiometers sense water temperature of the top 10–20 μm and 1–2 mm respectively, whereas in situ SST measurements are made in the depth range between 10 cm and several meters and are often called "bulk" SST, with an implicit assumption that the ocean surface layer is well-mixed. This assumption is valid only for night-time conditions or when surface winds are strong. Otherwise, the surface layer is stratified and its temperature exhibits diurnal variability (Kawai and Wada, 2007; Kennedy et al., 2007), such that a measured temperature value typically depends on the depth and time of day at which the measurement is made (Donlon et al., 2007). Aside from the diurnal variability, an independent phenomenon of a thermal skin layer takes place in the top 1 mm or so of the ocean surface and results in a strong temperature gradient across this layer (usually, cooling towards the surface), especially enhanced in the top 100 μm. While all in situ and satellite measurements might be affected by diurnal variability, only IR satellite data are subject to the thermal skin effect. IR radiometers are said to measure "skin" temperature. Temperature at the bottom of the thermal skin layer is called "subskin temperature." MW radiometer measurements are close to this variable. To estimate error variance or to verify uncertainty estimates for SST observations by comparison of different kinds of SST data, data values have ideally to be adjusted for time and depth differences by modelling the skin effect and diurnal variability or for minimum geophysical errors by constraining the comparison to the night-time data only, to minimize the diurnal variability effects.

Comparisons between in situ measurements and different satellite instruments have been used to assess the uncertainties in the individual measurements. Random errors on ATSR measurements have been estimated (Embury et al., 2011; Kennedy et al., 2011a; O'Carroll et al., 2008) to lie between 0.1 and 0.2 K. The uncertainties associated with random errors for AATSR are therefore much lower than for ships (around 1–1.5 K: Kent and Challenor, (2006); Kent et al., (1999); Kent and Berry, (2005) Reynolds et al., (2002b); Kennedy et al., (2011a)) or drifting buoys (0.15–0.65 K: Kennedy et al., (2011a); Reynolds et al., (2002b); Emery et al., (2001); O'Carroll et al., (2008)).

Characterizing relative mean biases between different systems informs the procedures for homogenizing and combining different kinds of measurements. Embury et al. (2011) found average biases of less than 0.1 K between reprocessed AATSR retrievals and drifting buoy observations and of around 0.1 K between ATSR2 retrievals and buoys. Using an earlier AATSR dataset, Kennedy et al. (Kennedy et al., 2011a) found that ship measurements were warmer relative to matched satellite SSTs than drifting buoys, suggesting ship measurements were biased relative to drifting buoy measurements by 0.18 K. They hypothesized that HadSST2 contained an increasing cool bias because of a decrease in the relative proportion of warm-biased ship observations. They applied a time-varying adjustment to the HadSST2 global means in the form of 0.18 K times the fraction of drifting buoys compared to the 1991–1995 period. This correction improved the consistency between trends in global average anomalies from the in situ and ATSR data sets. However, Kennedy et al. (2011b) found a smaller relative bias between ships and drifting buoys and found that changes in the biases associated with ship measurements might have been as large, or larger than, this effect.

2.A.4.3.3 Differences in long term average temperature anomalies

Temperature differences between the periods of 1986=>2005 and 1886=>1905:
HadCRUT4: 0.66 ± 0.06˚C (90% confidence interval)
GISTEMP: 0.62˚C
NCDC: 0.65˚C

Temperature differences between the periods of 1946=>2011 and 1880=>1945:
HadCRUT4: 0.38 ± 0.04˚C (90% confidence interval)
GISTEMP: 0.35˚C
NCDC: 0.37˚C

Uncertainty estimates have been calculated using the HadCRUT4 uncertainty model. To allow estimates of coverage uncertainty to be made for these differences between long term averages, HadGEM control run fields were used in place of the NCEP reanalysis as the globally complete reference data.

[INSERT FIGURE 2.A.2 HERE]
Figure 2.A.2: Differences in long term average temperatures in pairs of periods as calculated from HadCRUT4, GISTEMP and NCDC's data. Left - temperature difference between the periods of 1986 to 2005 and 1886 to 2005. Right - temperature difference between the periods of 1986 to 2005 and 1886 and 2005. The median and confidence limits (5% and 95%)for differences calculated from HadCRUT4 are shown in black. Period differences for GISTEMP are red. Period differences for NCDC are in blue.

2.A.4.4 Technical Developments in Combined Land and SST Products

Table A2.4.3 summarizes current methodological approaches. For HadCRUT4 both the land and the ocean data sources have been updated and the product now consists of 100 equi-probable solutions (Morice et al., 2012). The post-1990s period is now more consistent with the remaining products – it exhibits a greater rate of warming than the previous version over this period. NOAA's MLOST product has incorporated GHCNv3 and ERSST3b and reinstated high-latitude land data but is otherwise methodologically unchanged from the version considered in AR4 (Vose et al., 2012b). Since AR4 NASA GISS have undertaken updates and a published sensitivity analysis focussed primarily around their urban heat island adjustments approach (Section 2.4.1.2.) and choice of product and method for merging pre-satellite era and satellite era SSTs (Hansen et al., 2010). For SST several alternative datasets or combinations of datasets were considered and these choices had an impact of the order 0.04 K for the net change over the period of record. An improved concatenation of pre-satellite era and satellite era SST products removed a small apparent cooling bias in recent times. Following the release of their code the GISS method has been independently replicated in a completely different programming language (Barnes and Jones, 2011) which builds a degree of confidence in the veracity of the processing.

Table 2.A.6: Methodological details for the current global merged surface temperature products. Only gross methodological details are included to give a flavour of the methodological diversity, further details can be found in the papers describing the dataset construction processes.

Dataset	Start Date	Land Dataset	Marine Dataset	Merging of Land and Marine	Infilling	Averaging Technique
HadCRUT4 (100 versions) (Morice et al., 2012)	1850	CRUTEM4 (100 versions)	HadSST3 (100 versions)	Weighted average based upon the percentage coverage	None, spatial coverage incompleteness accounted for in error model	Average of area weighted Northern and Southern Hemisphere averages
MLOST (Vose et al., 2012b)	1880	GHCNv3	ERSST3b	Weighted average based upon the percentage coverage	Low frequency component filtered. Anomaly spatial covariance patterns for high frequency component. Land and ocean interpolated separately.	Area weighted average of available gridbox values
NASA GISS (Hansen et al., 2010)	1880	GHCNv3, USHCNv2 plus Antarctic SCAR data	HadISST1 (1870–1981), OISSTv2 (1981–)	Priority given to land data	Radius of influence up to 1200 km for land data	After gridding, non-missing values are averaged over the zones 90°S–23.6S, 23.6°S–0°, 0°–23.6°N, 23.6°N–90°N; and the four

means are averaged with 3:2:2:3 weighting to represent their area.

2.A.4.5 Technical Advances in Radiosonde Records

There now exist five estimates of radiosonde temperature evolution, which are based upon a very broad range of methodological approaches to station selection, identification of artificial timeseries breaks and adjustments (Table 2.A.7). HadAT and RATPAC were discussed in AR4 and no further technical innovations have accrued for the operational versions of these products. Development of an automated version of HadAT and discussion of efforts to characterize the resulting parametric uncertainty are summarized in the main text. A group at the University of Vienna have produced RAOBCORE and RICH (Haimberger, 2007) using ERA reanalysis products (Box 2.3) as a basis for identifying breaks. Given the relative sparseness of the observing network this may have advantageous properties in many regions compared to more traditional intra-station or neighbour-based approaches. Breakpoints are identified through reanalysis background departures using a statistical breakpoint test for both these products. Uncertainties in adjustments arising from the use of reanalyses fields to estimate the adjustments for RAOBCORE have been addressed by several variants and sensitivity studies (Haimberger, 2004; Haimberger, 2007; Haimberger et al., 2008). The RICH products use the same breakpoint locations but have only an indirect dependency on the reanalyses as the adjustments are neighbour based. Two varieties have been developed (Haimberger et al., 2012). The first uses pairwise neighbour difference series to estimate the required adjustment. The second uses differences in station innovations relative to the reanalyses fields. Both variants have been run in ensemble mode and the resulting uncertainty estimates are discussed in the main text. Sherwood and colleagues developed an iterative universal kriging approach for radiosonde data (Sherwood, 2007) and applied this to a global network (Sherwood et al., 2008) to create IUK. The algorithm requires a set of break locations and the raw data and then fits an optimal estimate of the homogenized series based upon a number of basis functions including leading modes of variability. Breakpoint locations were defined by tests on the station series and without recourse to metadata.

Table 2.A.7: Summary of methodologies used to create the radiosonde products considered in this report. Except IUK (1960) all timeseries begin in 1958. Only gross methodological details are included to give a flavour of the methodological diversity, further details can be found in the papers describing the dataset construction processes. Between these dataset approaches a very broad range of processing choices have been considered.

Dataset	Temporal Resolution	Number of Stations	Homogeneity Test	Adjustment Method
HadAT2 (Thorne et al., 2005)	Seasonal / monthly	676	KS-test on difference series from neighbour averages together with metadata, manually interpreted	Target minus neighbour difference series based.
RATPAC (Free et al., 2005)	monthly	87	Multiple indicators and metadata assessed manually by three investigators until 1996, first difference method with t-test and metadata after 1995	Manually based adjustments prior to 1996, first difference derived breaks after 1995.
IUK (Sherwood et al., 2008)	Individual launch	527	Derived hierarchically looking 1. for breaks in 00Z-12Z series, 2. breaks in the series with twice daily measures, and 3. once daily ascents. Breakpoint detection was undertaken at the monthly timescale with no recourse to metadata	Relaxation to an iterative solution minimum given breaks and set of spatial and temporal basis functions.
RICH-obs (64 member ensemble) (Haimberger et al., 2012)	Individual launch	2881	SNHT test on the difference between the observed data and ERA reanalysis product background expectation field modified by metadata information.	Difference between station and a number of apparently homogeneous neighbours
RICH-tau (64 member ensemble)	Individual launch	2881	As above	Difference between station innovation (candidate station and reanalysis background expectation

(Haimberger et al., 2012)				field) and innovation estimates for apparently homogeneous neighbors.
RAOBCORE (Haimberger et al., 2012)	Individual launch	2881	As above	Difference between candidate station and reanalysis background expectation field

2.A.4.6 Advances in MSU Satellite Records

Gross methodological details of the MSU products are summarized in Table 2.A.8. The UAH dataset removed an apparent seasonal cycle artefact in the latter part of their record related to the introduction of AMSU in version 5.3 and changed the climatological baseline to 1981–2010 to produce version 5.4. Both changes had negligible impact on trend estimates.

Version 3.2 of the RSS product (Mears and Wentz, 2009a; Mears and Wentz, 2009b) for the first time incorporated a subset of AMSU instruments. It was concluded that an instantaneous correction is required to merge MSU and AMSU as they sense slightly different layers and that there will also be a systematic long-term impact unless real-world trends are vertically invariant (Mears et al., 2011). Using HadAT data this impact was estimated to be no more than 5% of the trend. Two more significant changes were accounting for latitudinal error structure dependencies, and a more physical handling of instrument body temperature effect issues in response to (Grody et al., 2004). In early 2011 version 3.3 was released which incorporated all the AMSU instruments and led to a de-emphasising of the last MSU instrument which still remained operational after 15 years, a trend reduction over the post-1998 period, and a reduction in apparent noise.

The new STAR analysis used a fundamentally distinct approach for the critical inter-satellite warm target calibration step (Zou et al., 2006a). Satellites orbit in a pole-to-pole configuration with typically two satellites in operation at any time. Over most of the globe they never intersect. The exception is the polar regions where they quasi-regularly (typically once every 24 to 48 hours but this is orbital geometry dependent) sample in close proximity in space (<111 km) and time (<100s). The STAR technique uses these Simultaneous Nadir Overpass (SNO) measures to characterize inter-satellite biases and the impact of instrument body temperature effects before accounting for diurnal drift. SNO estimates remain two point comparisons between uncertain measures over a geographically limited domain so cannot guarantee absolute accuracy. For humidity satellite measures the geographic domain has been shown to be an issue (John et al., 2011), but it is presently unclear whether this extends to temperature measurements. Initially they produced MT near-nadir measures since 1987 over the oceans (Zou et al., 2006a); then included more view angles and additional channels including LS and multi-channel recombinations (Zou et al., 2009); then extended back to 1979 and included land and residual instrument body temperature effects building upon the UAH methodology and diurnal corrections based upon RSS (Zou and Wang, 2010). In the latest version 2.0, STAR incorporated the AMSU observations inter-calibrated by the SNO method to extend to the present (Zou and Wang, 2011a).

Table 2.A.8: Summary of methodologies used to create the MSU products considered in this report. All time series begin in 1978–1979. Only gross methodological details are included to give a flavour of the methodological diversity, further details can be found in the papers describing the dataset construction processes.

Dataset	Inter-Satellite Calibration	Diurnal Drift Adjustments	Calibration Target Temperature Effect	MSU / AMSU Weighting Function Offsets
UAH (Christy et al., 2003)	Backbone method – adjusting all other satellites to a subset of long-lived satellites	Cross-scan differences used to infer adjustments. Measurements are adjusted to refer to the measurement time at the beginning of each satellite's mission.	Calibration target coefficients are determined as solution to system of daily equations to explain the difference between co-orbiting satellites	No accounting for differences beyond inter-satellite calibration.
RSS (Mears and Wentz,	Stepwise pairwise adjustments of all satellites based upon difference in means. Adjustments are a	Climate model output used to infer diurnal cycle. All measurements adjusted to refer to local	Values of the target temperature factors and scene temperature factors are obtained from a	Stepwise adjustment to account for the change in weighting functions.

2009a; Mears and Wentz, 2009b)	function of latitude and constant in time.	midnight.	regression using all satellites of the same type together.	
STAR (Zou and Wang, 2011b)	Simultaneous nadir overpass measures	RSS adjustments are multiplied by a constant factor to minimize inter-satellite differences.	Largely captured in the SNO satellite intercomparison but residual artefacts are removed using the UAH method.	Channel frequency shifts on each satellite estimated and adjusted for.

2.A.4.7 Stratospheric Sounding Unit Data Background

The SSU instruments provide the only long-term near-global temperature data above the lower stratosphere, extending from the upper troposphere to the lower mesosphere (Randel et al., 2009; Seidel, 2011), with the series terminating in 2006. In theory, five channels of AMSU should be able to continue this series (Kobayashi et al., 2009) but despite incipient efforts at an AMSU-only record (Mo, 2009) and plans to merge AMSU and SSU, the current long-term series ends in 2006. The raw record has three unique additional issues to those encountered in MSU dataset construction. The satellite carries a cell of CO_2 which tends to leak, causing a spurious increase in observed temperatures. Compounding this the CO_2 content within the cells varies among SSU instruments (Kobayashi et al., 2009). At the higher altitudes sensed, large diurnal and semi-diurnal tides (due to absorption of solar radiation) require substantial corrections (Brownscombe et al., 1985). Finally, long-term temperature trends derived from SSU need adjustment for increasing atmospheric CO_2 (Shine et al., 2008) as this affects radiation transmission in this band.

2.A.4.8 GPS-RO Data Background

Global Positioning System (GPS) radio occultation (RO) fundamental observations are time delay of the occulted signal's phase traversing the atmosphere. It is based on GPS radio signals which are bent and retarded by the atmospheric refractivity field, related mainly to pressure and temperature, during their propagation to a GPS receiver on a Low Earth Orbit (LEO) satellite. An occultation event occurs whenever a GPS satellite sets (or rises from) behind the horizon and its signals are occulted by the Earth's limb. The fundamental measurement is the signal phase which is based on precise timing with atomic clocks. Potential clock errors of GPS or LEO satellites are removed by differencing methods using an additional GPS satellite as reference and by relating the measurement to even more stable oscillators on the ground. Thus, GPS RO is anchored to the international time standard and currently the only self-calibrated raw satellite measurement with SI traceability, in principle (Leroy et al., 2006; Baringer et al., 2010). Subsequent analysis converts the time delay to temperature and other parameters, which inevitably adds some degree of uncertainty to the temperature data, which is not the directly measured quantity but rather inferred with the inference being dependent on the precision of available data for other dependent parameters and how the data are processed. GPS RO measurements have several attributes that make them suited for climate studies: (i) they exhibit no satellite-to-satellite bias (Hajj et al., 2004; Ho et al., 2009a), (ii) they are of very high precision (Anthes et al., 2008; Foelsche et al., 2009; Ho et al., 2009a), (iii) they are not affected by clouds and precipitation, and (iv) they are insensitive to retrieval error when used to estimate inter-annual trends in the climate system (Ho et al., 2009c). GPS-RO observations can be used to derive atmospheric temperature profiles in the upper troposphere and lower stratosphere (UT/LS) ((Hajj et al., 2004; Ho et al., 2009a; Kuo et al., 2004).

2.A.5 FAQ 2.1, Figure 2.

This material documents the provenance of the data that was input to FAQ 2.1, Figure 2 in the IPCC WG1 Fifth Assessment Report. The code will also be archived at the website along with a static version of the data files when the final report is published. As stated in the caption all publicly-available, documented, datasets known to the authors have been used. Three have been truncated (two marine air temperature and one sea surface temperature) for explicitly source documented and acknowledged significant issues but no further screening has been applied.

Land surface air temperature anomalies relative to 1961-1990:
Dark Grey: Berkeley (Rohde et al. submitted)
Green: NCDC Smith et al. (2008)
Blue: GISS Hansen et al. (2010)
Red: Lugina et al. (2005) from IPCC AR4
Pale Grey: CRUTEM4 ensemble Morice et al. (2012), Jones et al. (2012a)

Global lower tropospheric MSU-equivalent temperature anomalies relative to 1979 from satellites and radiosondes, series taken from BAMS State of the Climate 2011 except IUK from State of the Climate 2009.
Black : HadAT2 Thorne et al. (2005)
Yellow : IUK Sherwood et al. (2008)
Orange : RAOBCORE Haimberger et al. (2007)
Dark Grey: RICH Haimberger et al. (2008)
Green: RATPAC Free et al. (2005)
Blue: RSS Mears and Wentz (2009a,b)
Red: UAH Christy et al. (2003)

Sea-surface temperature anomalies relative to 1961-1990:
Yellow: NOCS Berry and Kent (2009, original climatology period is different so adjusted to average anomaly for HadSST2 over common period 1970-2009)
Orange: HadSST2 Rayner et al. (2006)
Dark Grey: ERSSTv3b Smith et al. (2007)
Green: COBE Ishii et al. (2005)
Blue: Kaplan et al. (1998)
Red: ICOADS Worley et al. (2005)
Pale Grey: HadSST3 ensemble Kennedy et al. (2011c)

Ocean heat content anomalies (0-700m) relative to 1993-2009:
Yellow: Palmer et al. (2007)
Orange: Domingues et al. (2008)
Dark Grey: Ishii and Kimoto (2009)*
Green: Willis et al. (2004)*
Blue: Lyman and Johnson (2008)*
Red: Gouretski and Reseghetti (2010)*
*Some series taken from Palmer et al. (2010).

Marine air temperature anomalies relative to 1961-1990
Orange: HadMAT Rayner et al. (2003) interpolated
Dark Grey: MOHMAT Rayner et al. (2003) uninterpolated
Green: NOCS Berry and Kent (2009, original climatology period is different so adjusted to average anomaly for MOHMAT over common period 1970-2006)
Blue: Ishii et al. (2005, uninterpolated). Series shown only after 1900 due to known but uncorrected biases in earlier data
Red: Ishii et al. (2005, interpolated). Series shown only after 1900 due to known but uncorrected biases in earlier data

Specific humidity anomalies, each data set relative to own climatology
Green: HadCRUH Willett et al. (2008)
Blue: Dai (2006)
Red: NOCS Berry and Kent (2009) [marine only]

Sea level anomalies relative to 1961-1990:
Black: Church and White (2006)
Yellow: Holgate and Woodworth (2004) from IPCC AR4
Orange: Leuliette et al. (2004) from IPCC AR4
Dark Grey: Nerem et al. (2010)
Green: Gornitz and Lebedeff (1987)*

Blue: Jevrejeva et al. (2006)*
Red: Trupin and Wahr (1992)*
Pale grey: Church and White (2011)
* series from Woodworth et al. (2008).

September Arctic sea ice extent
Green: NSIDC Fetterer et al. (2002)
Blue: HadISST1.2 Rayner et al. (2003)
Red: NASA Bootstrap Comiso (1999)

Northern Hemisphere March-April snow-cover anomalies relative to 1961-1990
Blue: from IPCC AR4 SPM based on an update of Brown (2000)
Red: Robinson and Frei (2000) used in BAMS State of the Climate

Glacier mass balance. Values are five year averages.
Dark grey Cogley (2009) interpolated
Green Cogley (2009) simple average
Blue WGMS (2009) all glaciers
Red WGMS (2009) reference set of 30 glaciers

2.A.6 Changes in Atmospheric Circulation and Patterns of Variability

[INSERT FIGURE 2.A.3 HERE]
Figure 2.A.3: Supplementary Figure: Linear trends in (left) SLP, (middle) 500 hPa GPH, and (right) 100 hPa GPH in (top) November to April 1979/1980 to 2011/2012 and (bottom) May to October 1979 to 2011 from ERA-Interim data. Trends are only shown if significant at the 90% level.

Tables

Table 2.3: Trends in various aerosol variables using data sets with at least 10 years of measurements. Unless otherwise noted, trends of individual stations were reported in % yr^{-1}, and significance level is $p < 0.05$. The standard deviation is determined from the individual trends of a set of regional stations.

Region/Aerosol Variable	Trend, % yr^{-1} (1s, standard deviation)	Period	Reference	Comments
Europe				
PM2.5	–2.9 (1.31) –3.9 (0.87)[b]	2000–2009	Adapted from (Torseth et al., 2012), Regional background sites	13 sites available, 6 sites show statistically significant results. Average change was –0.37 –0.52[b] mg m^{-3} yr^{-1}.
PM10	–1.9 (1.43) –2.6 (1.19)[b]	2000–2009		24 sites available, 12 sites show statistically significant results. Average change was 0.29 and 0.40[b] mg m^{-3} yr^{-1}.
SO_4^{2-}	–3.0 (0.82) –3.1 (0.72)[b]	1990–2009		30 sites available, 26 sites show statistically significant results. Average change was 0.29 and 0.40[b] mg m^{-3} yr^{-1}.
SO_4^{2-}	– 1.5 (1.41) –2.0 (1.8)[b]	2000–2009		30 sites available, 10 sites show statistically significant results. Average change was –0.04 and –0.04[b] mgm^{-3} yr^{-1}
PM10	–1.9	1991–2008	(Barmpadimos et al., 2012) Rural and urban sites	10 sites in Switzerland. The trend is adjusted for change in meteorology– not adjusted data did not differ strongly. The average change was –0.51 μgm^{-3} yr^{-1}.
USA				
PM2.5	–2.1 (2.08) –4.0 (1.01)[b]	2000–2009	Adapted from (Hand et al., 2011b) Regional background sites	153 sites available, 52 sites show statistically significant negative results. Only 1 site show statisticallly positive trend
PM2.5	–1.5 (1.25) –2.1 (0.97)[b]	1990–2009		153 sites available, 39 sites show statistically significant results.
PM10	–1.7 (2.00) –3.1 (1.65)[b]	2000–2009		154 sites available, 37 sites show statistically significant results.
SO_4^{2-}	–3.0 (2.86) –3.0 (0.62)[b]	2000–2009		154 sites available, 83 sites show statistically significant negative results. 4 sites showed statistical positive trend.
SO_4^{2-}	–2.0 (1.07) –2.3 (0.85)[b]	1990–2009		103 sites available, 41 sites show statistically significant results.
Total Carbon	–2.5 to –7.5	1989–2008	(Hand et al., 2011b). Regional background sites	The trend interval includes sites mainly located along the east and west coasts of the USA, fewer sites were situated in the central part of the continent.
Arctic				
EBC[a]	–3.8 (0.7) P<0.1	1989–2008	(Hirdman et al., 2010)	Alert, Canada 62,3° W 82,5° N
SO_4^{2-}	–3.0 (0.6) P<0.1	1985–2006		
EBC[a]	Not sig. P<0.1	1998–2008		Barrow, Alaska, 156,6° W 71,3° N

SO_4^{2-}	Not sig. P<0.1	1997–2008		
EBC[a]	–9.0 (5.0) P<0.1	2002–2009		Zeppelin, Svalbard, 11,9° E 78,9° N
SO_4^{2-}	–1.9 (1.7) P<0.1	1990–2008		
Global Assessments				
Scattering coefficient		2001–2010	Adapted from (Collaud Coen et al., 2012); Regional background sites	Trend study including 24 regional background sites with more than 10 years of observations. Regional averages for 2001–2010. Parenthesis show total number of sites and number of sites with significant trend.
Europe (4/1)	+0.6 (1.9) +2.7[b]			
USA (14/10)	–2.0 (2.5) –2.9 (2.4)[b]			
Mauna Loa (1/1)	+2.7			
Arctic (1/0)	+2.4			
Antarctic (1/0)	+2.5			
Absorption coefficient		2001–2010	Adapted from (Collaud Coen et al., 2012) Regional background sites	Trend study of aerosol optical properties at 24 regional background sites with more than 10 years of observations. Regional averages for 2001-2010. Parenthesis show total number of sites and number of sites with significant trend.
Europe (3/0)	0.32 (0.4)			
USA (1/1)	–2.03			
Mauna Loa (1/1)	+9.0			
Arctic (1/1)	–6.47			
Anarctic (1/1)	–0.07			
Particle number concentration				
Europe (4/2)	–0.9 (1.7) –2.3 (1.0)[b]	2001–2010	Adapted from (Collaud Coen et al., 2012) regional background sites	Trend study of particle number concentration at 17 regional background sites. Regional averages of particle number concentration for last 10 years.. Parenthesis show total number of sites and number of sites with significant trend.
N. America and Caribbean (4/3)	–5.3 (2.8) –5.8 (1.1)[b]			
Mauna Loa (1/0)	–3.5			
Antarctica (2/2)	2.7 (1.4)			

Notes:
(a) Equivalent Black Carbon
(b) Trend numbers refer to a subset of stations with significant changes over the time - generally in regions strongly influenced by anthropogenic emissions; Figure 2.11.

Box 2.5, Table 1: Established indices of climate variability with global or regional influence. Columns are: (1) name of a climate phenomenon, (2) name of the index, (3) index definition, (4) primary references, (5) comments, including when available, characterization of the index or its spatial pattern as a dominant variability mode.

Climate Phenomenon		Index Name	Index Definition	Primary References	Characterization / Comments
El Niño – Southern Oscillation (ENSO)	Traditional indices of ENSO-related Tropical Pacific climate variability	NINO3	SST anomaly averaged over [5°S–5°N, 150°W–90°W]	Rasmusson and Wallace (1983), Cane (1986)	Traditional SST-based ENSO index, "devised by the Climate Analysis Center of NOAA [*now: Climate Prediction Center*] because a warming in this region strongly influences the global atmosphere" Cane et al. (1986).
		NINO1	Same as above but for [10°S–5°S, 90°W–80°W]		Introduced along with NINO3 by NOAA's Climate Analysis Center (now: Climate Prediction Center) circa 1983–1984 to describe other details of ENSO-related tropical Pacific SST variability.
		NINO2	Same as above but for [5°S–0°, 90°W–80°W]		
		NINO1+2	Same as above but for [10°S–0°, 90°W–80°W]		
		NINO4	Same as above but for [5°S–5°N, 160°E–150°W]		
		NINO3.4	Same as above but for [5°S–5°N, 170°W–120°W]	Trenberth (1997)	Used by W MO, NOAA to define El Niño / La Niña events. Detrended form is close to the 1st PC of linearly detrended global field of monthly SST anomalies (Deser et al., 2010a)
		Troup SOI	Standardized for each calendar month MSLP difference: Tahiti minus Darwin, x10	Troup (1965)	Used by Australian Bureau of Meteorology
		SOI	Standardized difference of standardized MSLP anomalies: Tahiti minus Darwin	Trenberth (1984)	Maximizes signal to noise ratio of linear combinations of Darwin / Tahiti records
		Darwin SOI	Standardized Darwin MSLP anomaly	Trenberth and Hoar (1996)	Introduced to avoid use of the Tahiti record, considered suspicious before 1935.
		Equatorial SOI (EQSOI)	Standardized difference of standardized MSLP anomalies over equatorial [5°S–5°N] Pacific Ocean: [130°W–80°W] minus [90°E–140°E]	Bell and Halpert (1998)	
	Indices of ENSO events evolution and for identifying different types of events	Trans-Niño Index (TNI)	Standardized NINO1+2 minus standardized NINO4	Trenberth and Stepaniak (2001)	Nearly uncorrelated with NINO3.4
		El Niño Modoki Index (EMI)	SSTA: [165°E–140°W, 10°S–10°N] minus ½[110°W–70°W, 15°S–5°N] minus ½[125°E–145°E, 10°S–20°N]	Ashok et al. (2007)	Defines "typical El Niño Modoki events" as those with the seasonal EMI value (JJAS or DJF means) no less than 0.7σ, where σ is the seasonal EMI std.
		Indices of Eastern Pacific (EP) and Central	EP Index: leading PC of the tropical Pacific SSTA with subtracted predictions from a linear regression on NINO4; CP index:	Kao and Yu (2009)	

		Pacific (CP) types of ENSO events	same as EP but with NINO1+2 used in place of NINO4.		
		E and C Indices	45° orthogonal rotation of the two leading PCs of the equatorial Pacific SSTA. Approximate formulas: C=1.7*NINO4 - 0.1*NINO1+2, E = NINO1+2 - 0.5*NINO4	Takahashi et al. (2011)	Constructed to be mutually uncorrelated; many other SST-based ENSO indices are well approximated by linear combinations of E and C.
Pacific Decadal and Interdecadal Variability		Pacific Decadal Oscillation (PDO)	1st PC of monthly N. Pacific SST anomaly field [20°N–70°N] with subtracted global mean; sign is selected to anti-correlate with NPI	Mantua et al. (1997); Zhang et al. (1997)	
		Intedecadal Pacific Oscillation (IPO)	Projection of a global SST anomaly field onto the IPO pattern, which is found as one of the leading EOFs of a low-pass filtered global SST field; sign is selected to correlate with PDO	Folland et al. (1999); Power et al. (1999) ; Parker et al. (2007)	IPO pattern was the 3rd EOF for 1911–1995 period and half power at 13.3 years; 2nd EOF for 1891–2005 data and 11 years half power
		North Pacific Index (NPI)	SLP [30°N–65°N; 160°E–140°W]	Trenberth and Hurrell (1994)	
NAO		Lisbon/ Ponta Delgada-Stykkisholmur/ Reykjavik North Atlantic Oscillation (NAO) Index	Lisbon/Ponta Delgada minus Stykkisholmur/ Reykjavik standardized MSLP anomalies	Hurrell (1995b)	A primary NH teleconnection both in MSLP and 500 hPa geopotential heigh (Z500) anomalies (Wallace and Gutzler, 1981); one of rotated PCs of NH Z700 (Barnston and Livezey, 1987). MSLP anomalies can be monthly, seasonal or annual averages, resulting in the NAO index of the same temporal resolution (Hurrell, 1995). In Jones et al. (1997) definition, temporal averaging is applied to monthly NAO index values. NAO index is typically interpreted for boreal winter season (e.g., DJFM or NDJFM means).
		Gibraltar – South-west Iceland NAO Index	Gibraltar minus South-west Icealnd / Reykjavik standardized monthly surface pressure anomalies	Jones et al. (1997)	
		PC-based NAO Index	Leading PC of MSLP anomalies over the Atlantic sector [20°N–80°N, 90°W–40°E]; sign is selected to correlate with station-based NAO indices.	Hurrell (1995b)	
		Summer NAO (SNAO)	Leading PC of daily MSLP anomalies for July and August over the North Atlantic region [25°N–70°N, 70°W–50°E]; sign is selected to correlate with station-based (winter) NAO indices.	Folland et al. (2009)	Calculations with daily, 10-day, or July-August mean MSLP data result in the same spatial pattern "characterized by a more northerly location and smaller spatial scale than its winter counterpart."

		Model-oriented NAO index	DJF SLP difference between averages [90°W–60°E, 20°N–55°N] minus [90°W–60°E, 55°N–90°N].	Stephenson et al. (2006)	NAO index which is less sensitive to climate models' shifts of locations of maximum variability.
Annular modes	Arctic Oscillation (AO), a.k.a. Northern Annular Mode (NAM)	PC-based NAM (AO) index	1st PC of the monthly mean MSLP anomalies poleward of 20°N; sign is selected to correlate with NAO indices.	Thompson and Wallace (1998; 2000)	Closely related to the NAO
	Antarctic Oscillation (AAO), a.k.a. Southern Annular Mode (SAM)	PC-based AAO index	1st PC of 850hPa or 700hPa height anomalies south of 20°S; sign is selected to correlate with grid-based AAO and SAM indices	Thompson and Wallace (2000)	
		Grid-based AAO index: 40°S–65°S difference	Difference between normalized zonal mean MSLP at 40°S and 65°S, using gridded SLP fields	Gong and Wang (1999)	
		Grid-based SAM index: 40°S–70°S difference	Same as above but uses latitudes 40°S and 70°S	Nan and Li (2003)	
		Station-based SAM index: 40°S–65°S	Difference in normalized zonal mean MSLP at 40°S and 65°S, using station data	Marshall (2003)	
Pacific/North America (PNA) atmospheric teleconnection		PNA index based on centers of action	¼[Z(20°N, 160°W) - Z(45°N, 165°W) + Z(55°N, 115°W) - Z(30°N, 85°W)], Z is the location's standardized 500 hPa geopotential height anomaly	Wallace and Gutzler (1981)	A primary NH telecon-nection (Wallace and Gutzler, 1981) in MSLP and in 500 hPa geopotential height anomalies (Z500); 2nd leading rotated PC of the NH Z700 (Barnston and Livezey, 1987)
		RPC-based PNA	Amplitude of the PNA pattern in the decomposition of the 500 hPa geopotential (Z500) anomaly field into the set of leading rotated EOFs obtained from the RPCA analysis of the NH Z500 monthly anomalies; sign is selected to correlated with the centers of action PNA index	Barnston and Livezey (1987).	
Pacific/South America (PSA) atmospheric teleconnection		PSA1 and PSA2 mode indices (PC-based)	2nd and 3rd PCs respectively of SH 500 hPa seasonal geopotential height anomaly	Mo and Paegle (2001)	Calculation was done with NCEP-NCAR reanalysis for Jan 1949 - Mar 2000. First three PCs were explaining 20%, 13%, and 11% of the total variance, respectively. There many published variations on this procedure, involving temporal filtering, using austral winter data only, PC rotation, different variables (e.g., 200 hPa streamfunction). PSA1 is positive during El Niño events (sign-selecting convention).

		PSA index based on centers of action from the 1972-1982 El Niño events composite	[-Z(35°S, 150°W) + Z(60°S, 120°W) - Z(45°S, 60°W)], Z is the location's JJA 500 hPa geopotential height anomaly	Karoly (1989)	Approximates PSA1 of the previous definition
		PSA index based on centers of action and La Niña response sign	-[-Z(45°S, 170°W) + Z(67.5°S, 120°W) - Z(50°S, 45°W)]/3, Z is the location's 500 hPa geopotential height anomaly	Yuan and Li (2008)	Approximates (–1)*PSA1 of the PC-based definition above
Atlantic Ocean Multidecadal Variability		Atlantic Multidecadal Oscillation (AMO) index	10-yr running mean of de-trended Atlantic mean SST anomalies [0°–70°N]	Enfield et al. (2001)	Called "virtually identical" to the smoothed leading rotated N. Atlantic PC
		Revised AMO index	As above, but subtracts global mean anomaly instead of de-trending	Trenberth and Shea (2006)	
Tropical Atlantic Ocean variability	Atlantic Niño	ATL3	SST anomalies averaged over [3°S–3°N, 20°W–0°]	Zebiak (1993)	Identified as the two leading PCs of detrended tropical Atlantic monthly SSTA (20°S–20°N): 38% and 25% variance respectively for HadISST1, 1900–2008 (Deser et al. 2010a)
		PC-based Atlantic Niño Index	1st PC of the detrended tropical Atlantic monthly SSTA (20°S–20°N); sign is selected to correlate with ATL3	Deser et al. (2010a)	
	Tropical Atlantic Meridional Mode (AMM)	AMM Index	2nd PC of the detrended tropical Atlantic monthly SSTA (20°S–20°N)		
Tropical Indian Ocean variability	Indian Ocean Basin (IOB) Mode	IOB basin mean index	SST anomalies averaged over [40°–110°E, 20°S–20°N]	Yang et al. (Yang et al., 2007)	
		IOB Mode, PC-based Index	The 1st PC of the IO detrended SST anomalies (40°E–110° E, 20°S–20°N); sign is selected by correlation with IOB basin mean index	Deser et al. (2010a)	Identified as the two leading PCs of detrended tropical Indian Ocean monthly SSTA (20°S–20°N): 39% and 12% of the variance, respectively, for HadISST1, 1900–2008 (Deser et al. 2010a)
	Indian Ocean Dipole (IOD) Mode	IOD Mode PC-based index	The 2nd PC of the IO detrended SST anomalies (40°E–110° E, 20°S–20°N); sign is selected to correlate with DMI		
		DMI	SST anomalies difference: [50°E–70°E, 10°S–10°N)]-[90°E–110°E, 10°S–0°]	Saji et al. (1999)	

1

Chapter 2: Observations: Atmosphere and Surface

Coordinating Lead Authors: Dennis L. Hartmann (USA), Albert Klein Tank (Netherlands), Matilde Rusticucci (Argentina)

Lead Authors: Lisa Alexander (Australia), Stefan Broennimann (Switzerland), Yassine Abdul-Rahman Charabi (Oman), Frank Dentener (EU / Netherlands), Ed Dlugokencky (USA), David Easterling (USA), Alexey Kaplan (USA), Brian Soden (USA), Peter Thorne (USA / UK), Martin Wild (Switzerland), Panmao Zhai (China)

Contributing Authors: Robert Adler (USA), Richard Allan (UK), Robert Allan (UK), Donald Blake (USA), Aiguo Dai (USA), Robert Davis (USA), Sean Davis (USA), Markus Donat (Australia), Vitali Fioletov (Canada), Erich Fischer (Switzerland), Leopold Haimberger (Austria), Ben Ho (USA), John Kennedy (UK), Stefan Kinne (Germany), James Kossin (USA), Norman Loeb (USA), Cathrine Lund-Myre (Norway), Carl Mears (USA), Christopher Merchant (UK), Steve Montzka (USA), Colin Morice (UK), Joel Norris (USA), David Parker (UK), Bill Randel (USA), Andreas Richter (Germany), Matthew Rigby (UK), Ben Santer (USA), Dian Seidel (USA), Tom Smith (USA), David Stephenson (UK), Ryan Teuling (Netherlands), Junhong Wang (USA), Xiaolan Wang (Canada), Ray Weiss (USA), Kate Willett (UK), Simon Wood (UK)

Review Editors: Jim Hurrell (USA), Jose Marengo (Brazil), Fredolin Tangang (Malaysia), Pedro Viterbo (Portugal)

Date of Draft: 5 October 2012

Notes: TSU Compiled Version

Figures

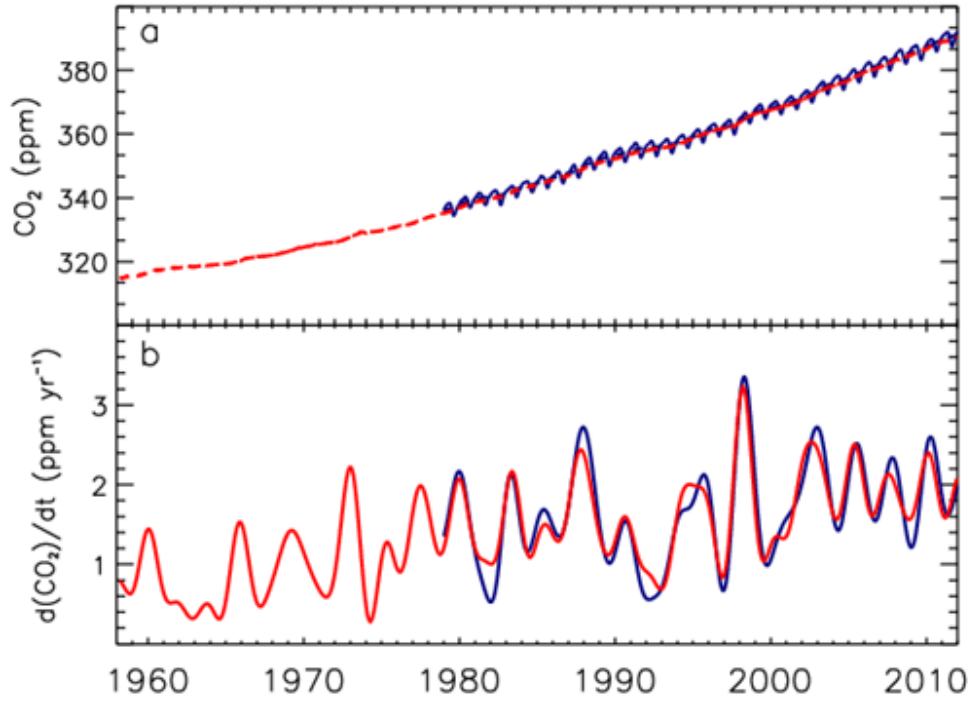

Figure 2.1: a) Globally averaged CO_2 dry air mole fractions from Scripps Institution of Oceanography (SIO) at monthly time resolution based on measurements from Mauna Loa, Hawaii and South Pole (red) and NOAA/ESRL/GMD at quasi-weekly time resolution (blue). SIO values are deseasonalized. b) Instantaneous growth rates for globally averaged atmospheric CO_2 using the same colour code as in (a). Growth rates are calculated as the time derivative of the deseasonalized global averages.

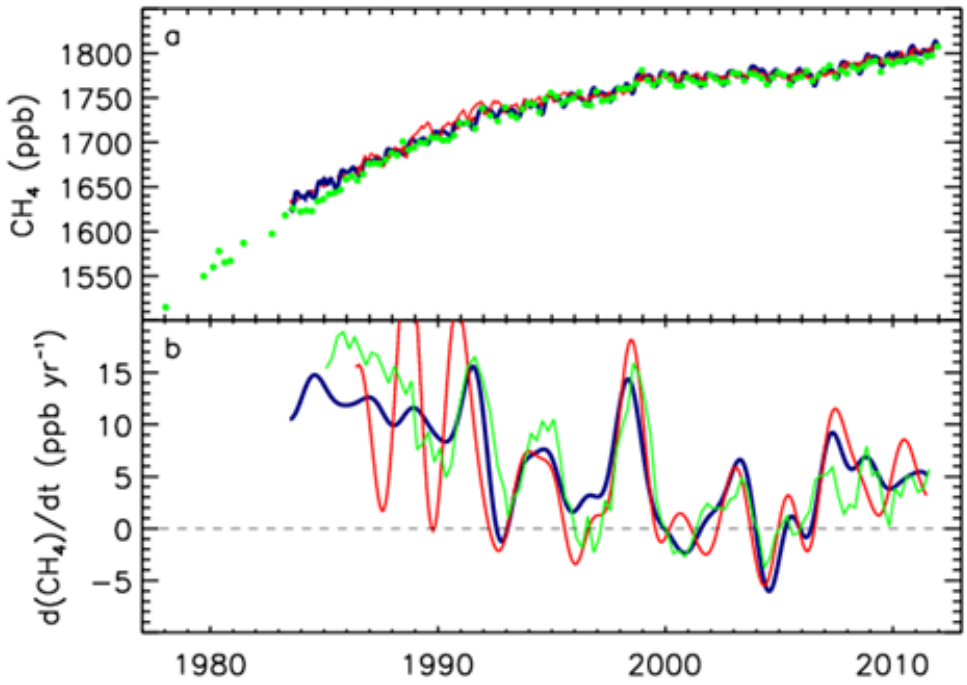

Figure 2.2: a) Globally averaged CH_4 dry air mole fractions from UCI (green), AGAGE (red), and NOAA/ESRL/GMD (blue) b) Instantaneous growth rate for globally averaged atmospheric CH_4 using the same colour code as in (a). Growth rates were calculated as in Figure 2.1.

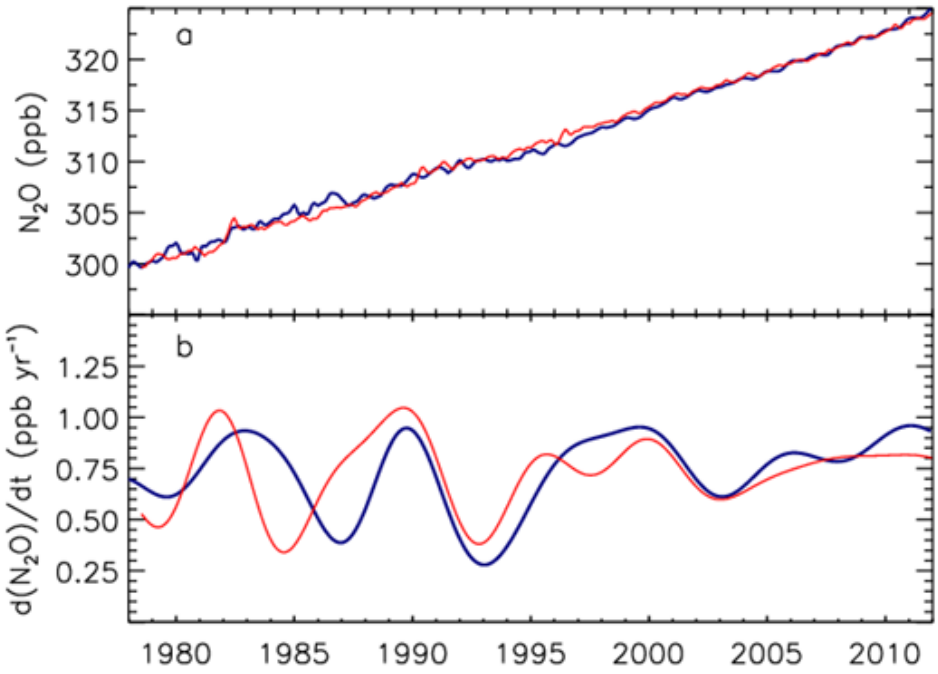

Figure 2.3: a) Globally averaged N_2O dry air mole fractions from AGAGE (red) and NOAA/ESRL/GMD (blue). b) Instantaneous growth rates for globally averaged atmospheric N_2O. Growth rates were calculated as in Figure 2.1.

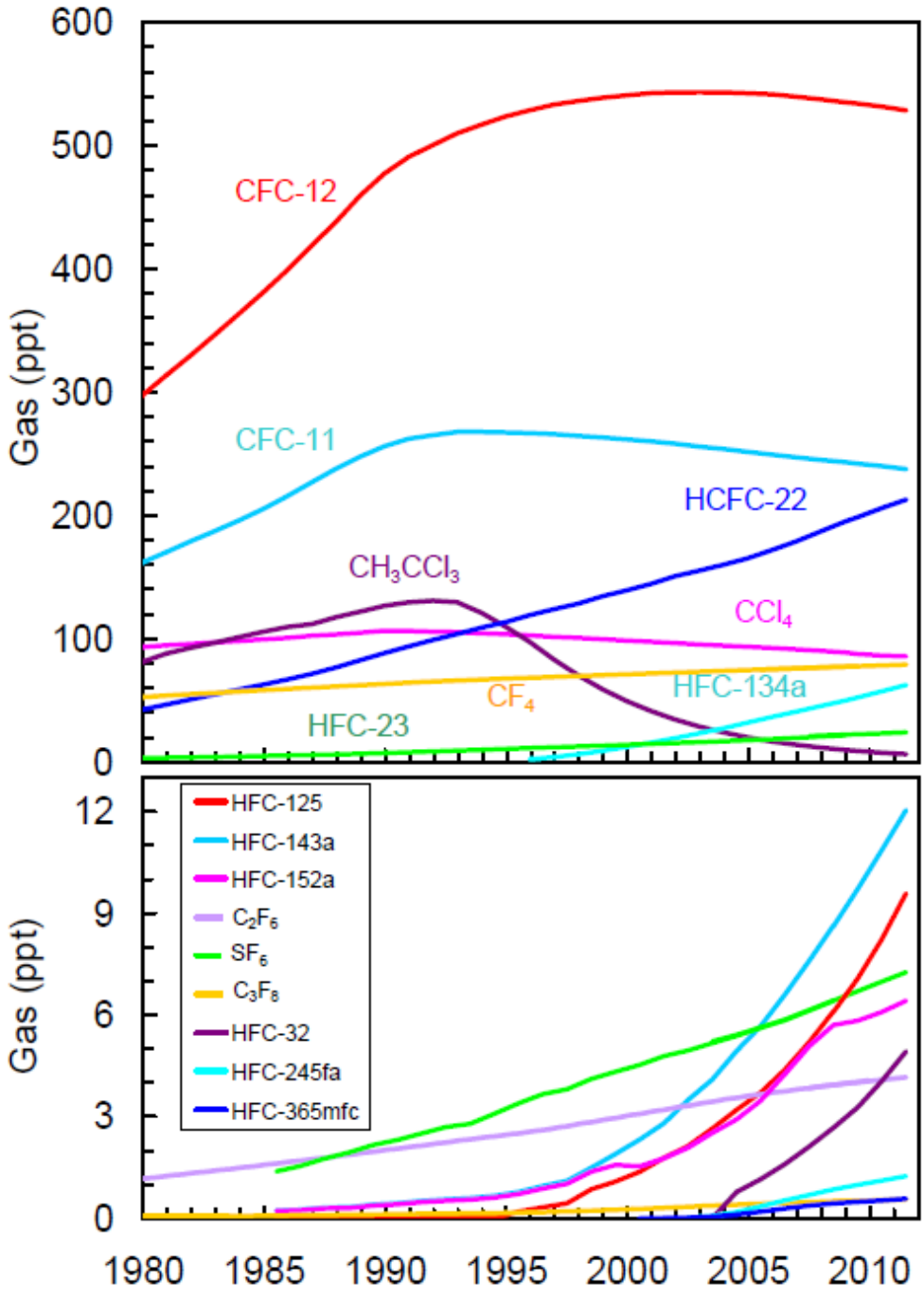

Figure 2.4: Globally averaged dry air mole fractions at Earth's surface of the major halogen-containing LLGHGs. These are derived mainly using monthly mean measurements from the AGAGE and NOAA/ESRL/GMD networks. For clarity, only the most abundant chemicals are shown in different compound classes and results from different networks have been combined when both are available. While differences exist, different network measurements agree reasonably well (except for CCl_4 (differences of 2–4% between networks) and HCFC-142b (differences of 3–6% between networks)) (see also (WMO, 2011) Chapter 1).

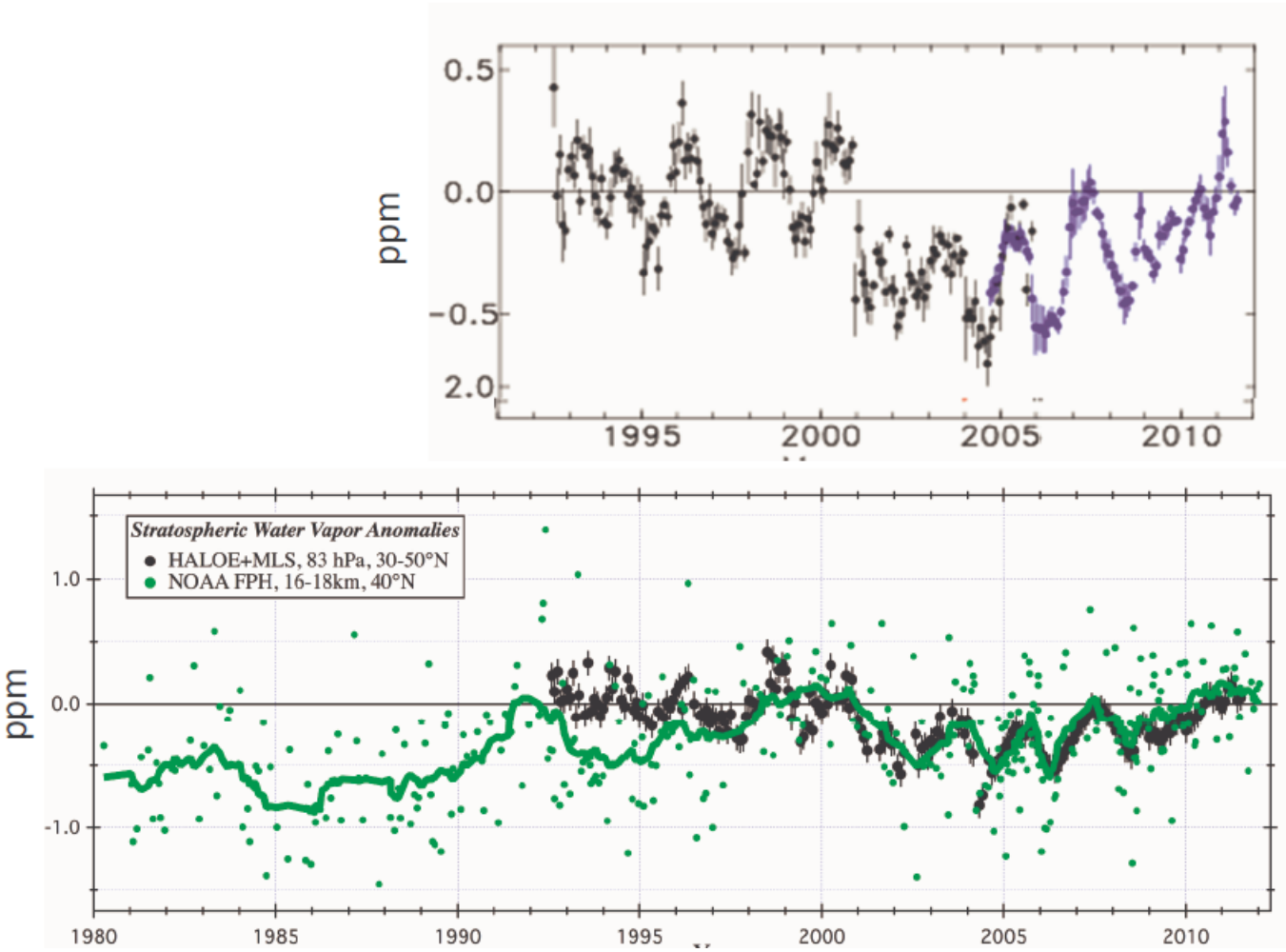

Figure 2.5: Top: De-seasonalized near-global water vapour anomalies in the lower stratosphere (16–19 km) from merged HALOE (black) and MLS (blue) measurements (updated from (Randel, 2010). Bottom: Balloon-borne measurements of stratospheric water vapour from Boulder, Colorado (green dots, with green curve showing smoothed variations), compared with monthly HALOE+MLS satellite measurements over 30–50°N. Both data sets have been de-seasonalized and normalized for the period 2000–2011.

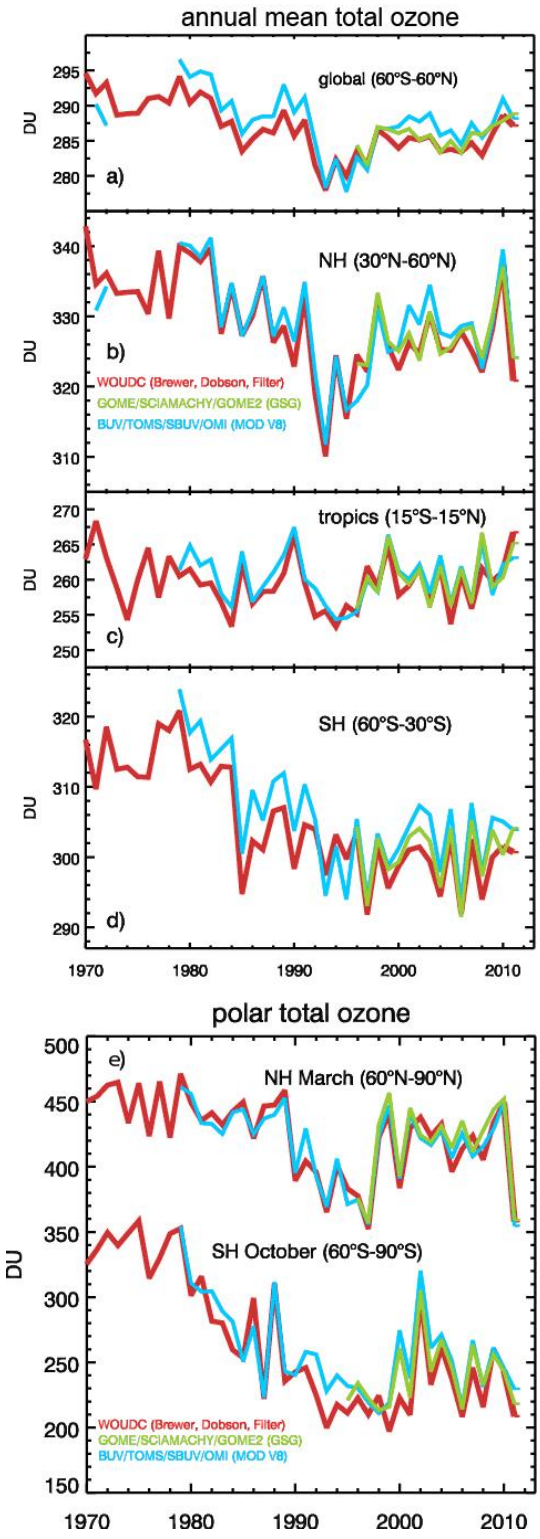

Figure 2.6: Zonally averaged, annual mean total column ozone in Dobson Units (DU; 1 DU = 2.69 × 10^{16} O_3 cm^{-2}) of ground-based measurements combining Brewer, Dobson, and filter spectrometer data (red), merged BUV/SBUV/TOMS/OMI MOD V8 (blue) and GOME/SCIAMACHY/GOME-2, 'GSG' (green), for a) 60°S–60°N, b) 30°N–60°N (NH), c) 15°S–15°N (tropics), and d) 30°S–60°S (SH). e) March and October polar total column ozone in the NH and SH, respectively. Adapted from Weber et al. (2012).

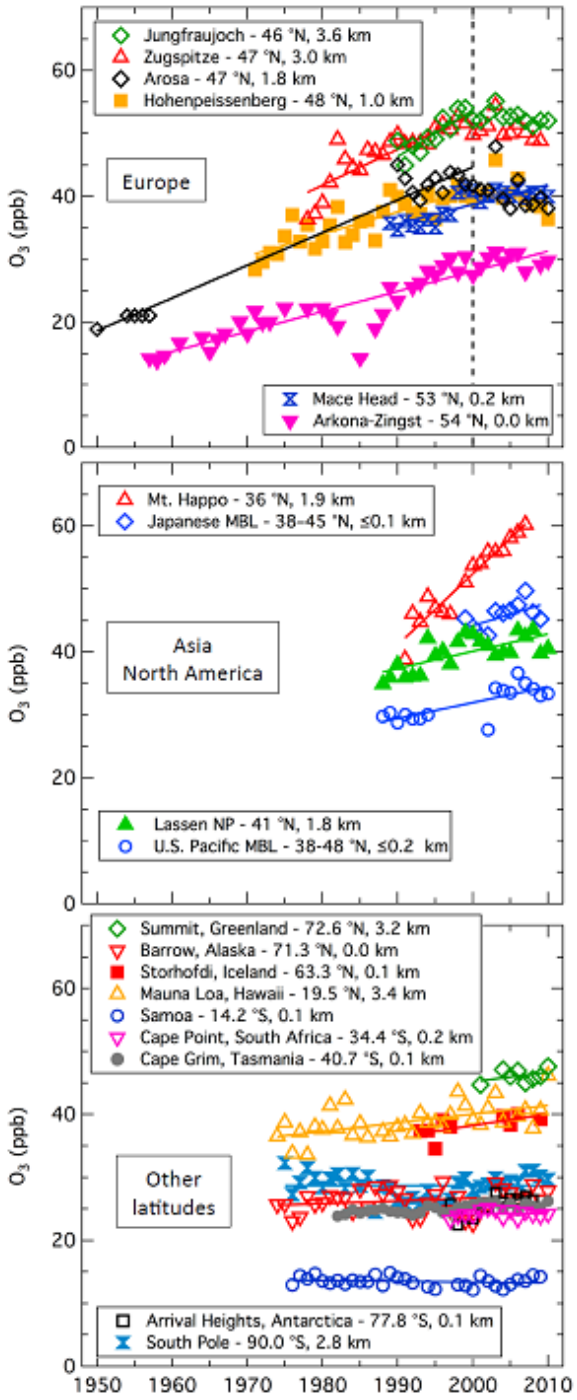

Figure 2.7: Annually averaged surface ozone mixing ratios from regionally representative monitoring sites around the world. Top: Europe with trend lines fit through the data prior to 2000 when ozone was generally increasing. Middle: East Asia and western North America. Bottom: Remote sites in the NH and SH. Time series include data from all times of day and trend lines are linear regressions described in Parrish et al. (2012).

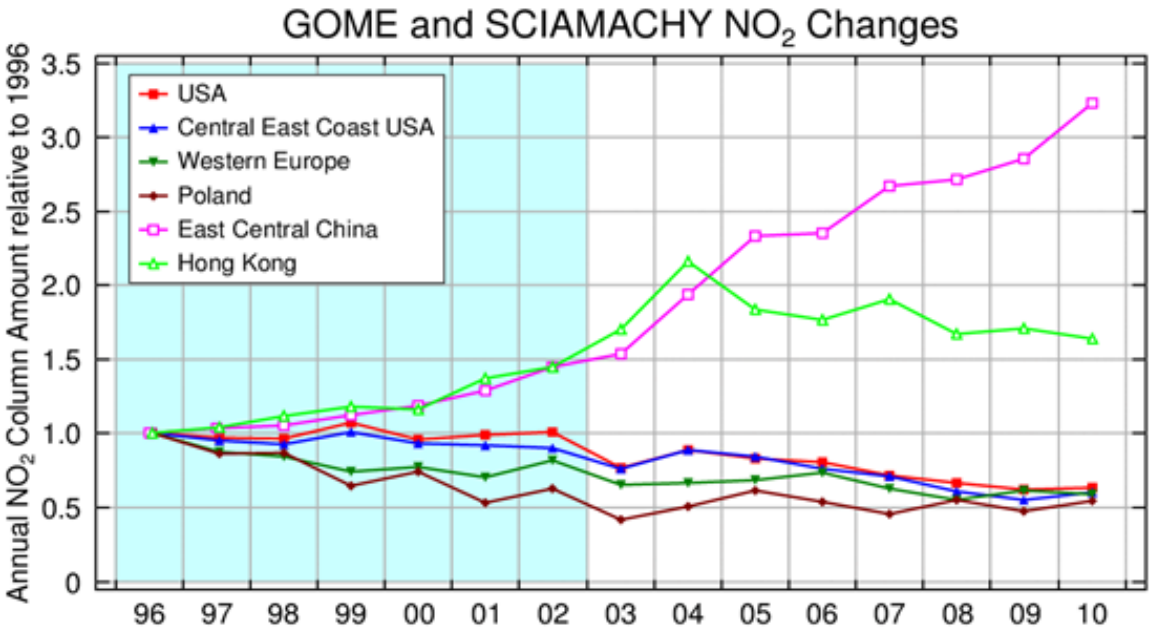

Figure 2.8: Relative changes in tropospheric NO_2 column amounts, normalized for 1996, derived from two instruments, the Global Ozone Monitoring Experiment (GOME) from 1996 to 2002 and the Scanning Imaging Spectrometer for Atmospheric Cartography (SCIAMACHY) from 2003 to 2010. Updated from (Richter et al., 2005).

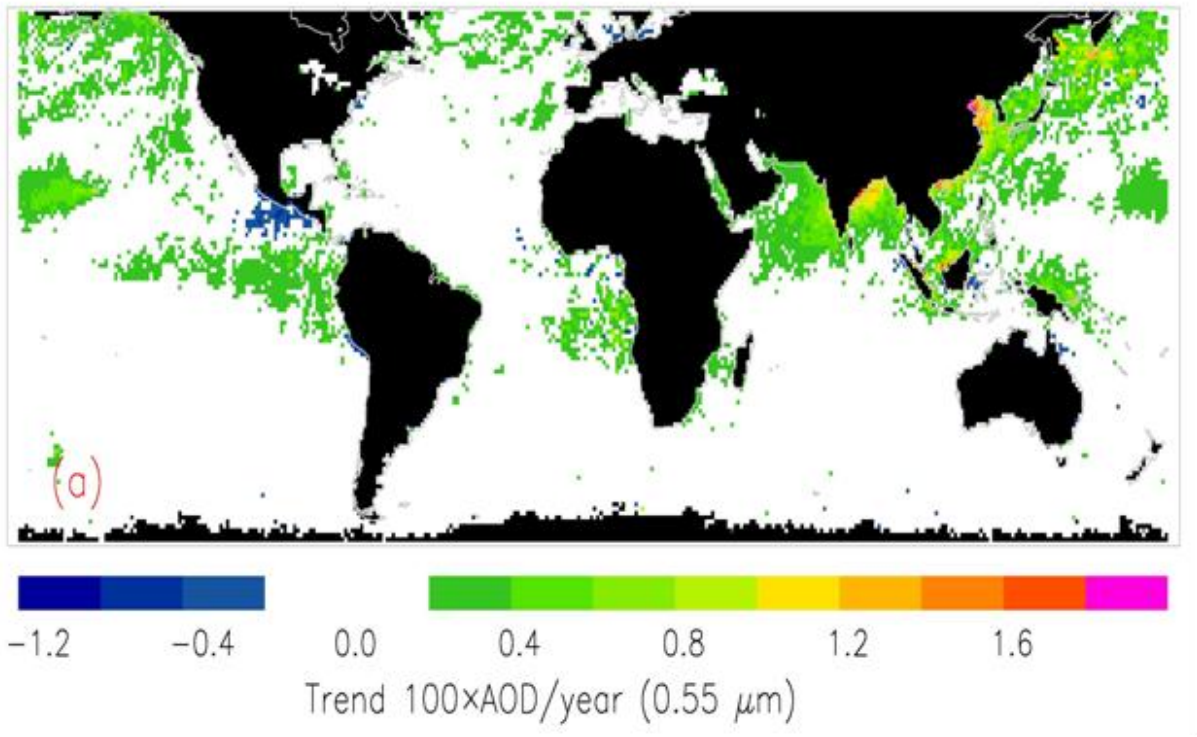

Figure 2.9: Trends in aerosol optical depth (AOD) for the ten-year period 2000–2009, based on de-seasonalized, conservatively cloud-screened MODIS aerosol data over oceans (Zhang and Reid, 2010). Negative AOD trends off Mexico are due to enhanced volcanic activity at the beginning of the record. Most non-zero trends are significant at 95% confidence levels (Zhang and Reid, 2010).

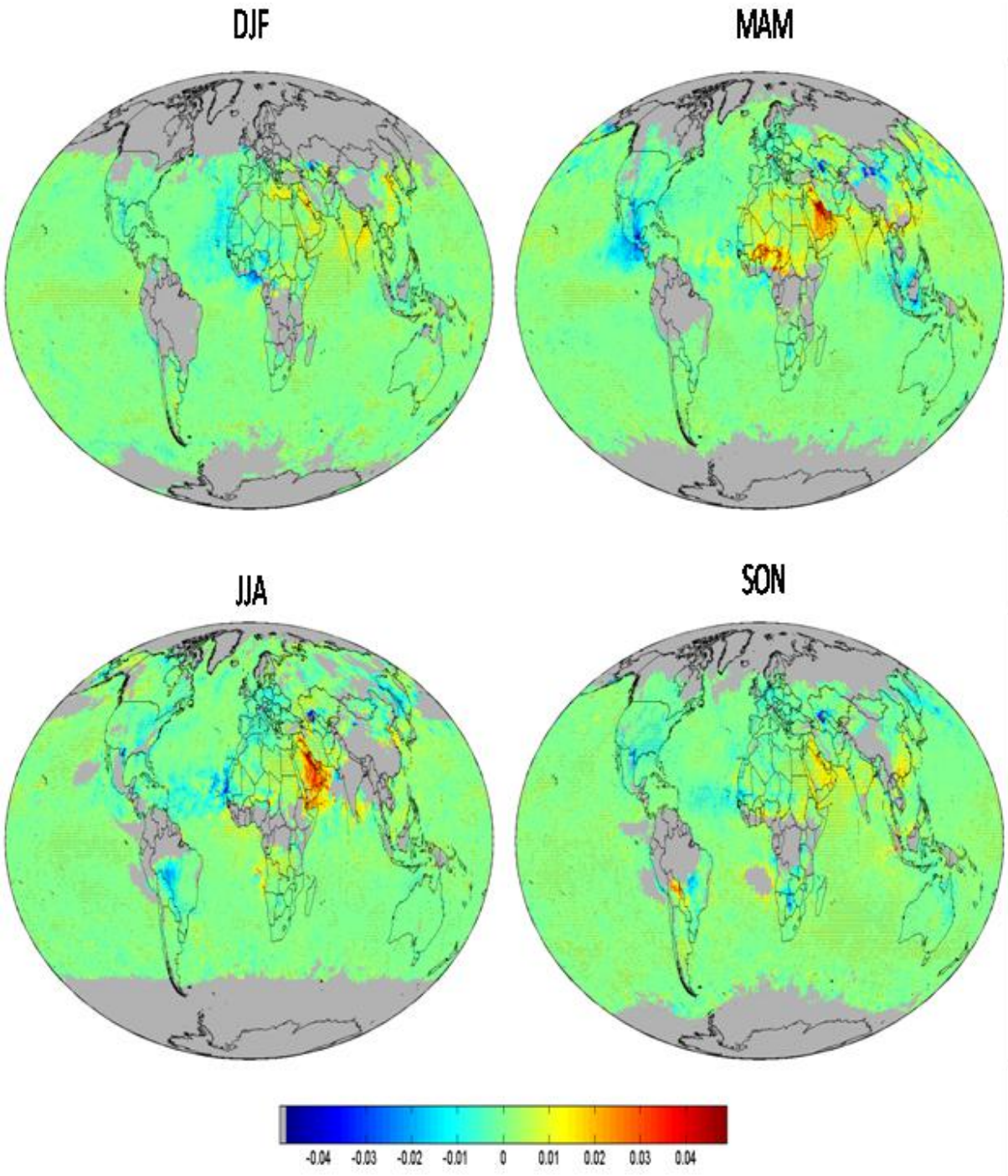

Figure 2.10: Trends in aerosol optical depth (AOD) using SeaWiFS data from 1998 to 2010 (Hsu et al., 2012).

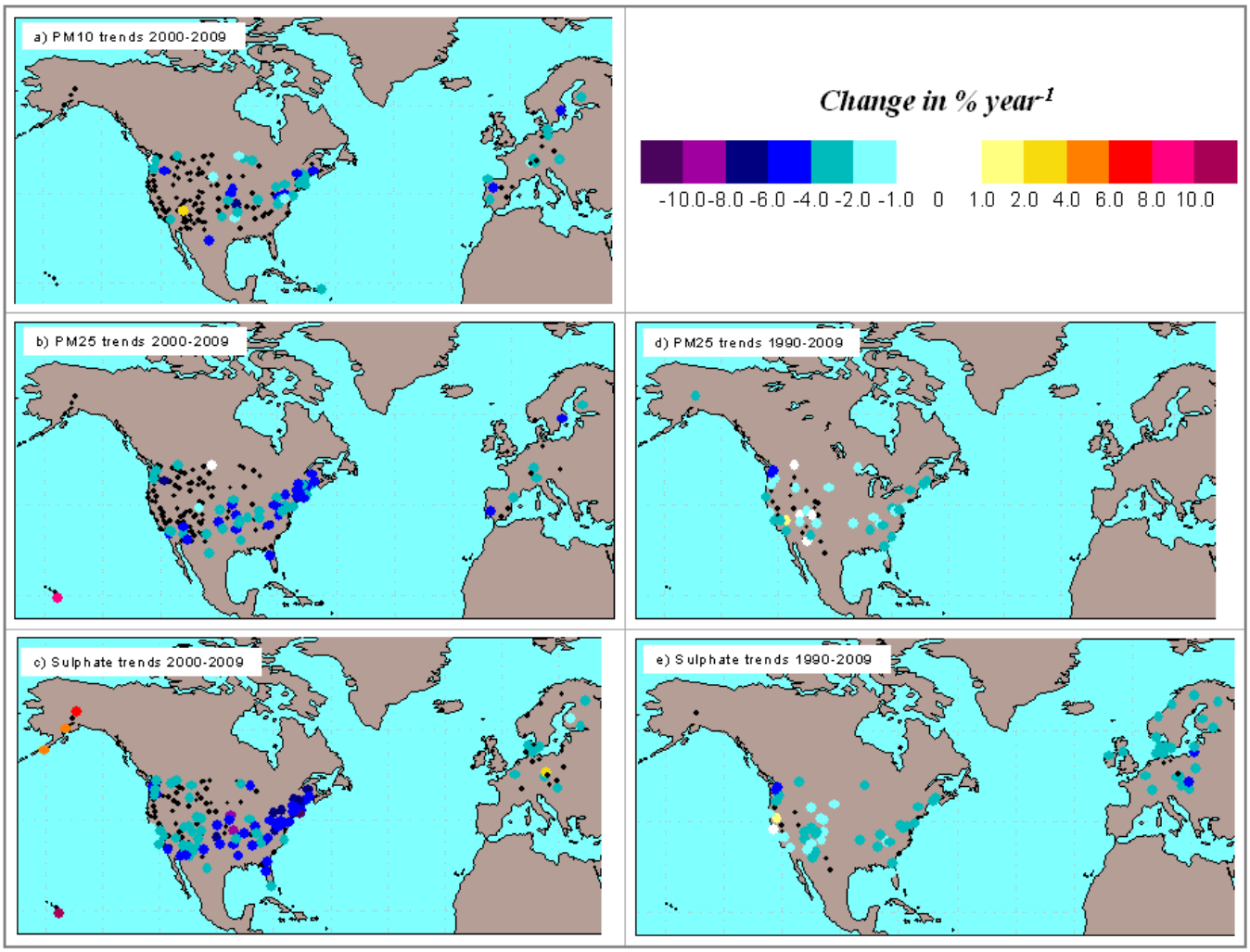

Figure 2.11: Trends in particulate matter (PM) and sulphate in Europe and USA. The trends are based on measurements from the EMEP (Torseth et al., 2012) and IMPROVE (Hand et al., 2011) networks in Europe and USA, respectively. Sites with significant trends to p = 0.05 or better are shown in colour codes, the black dots are sites with non-significant trends.

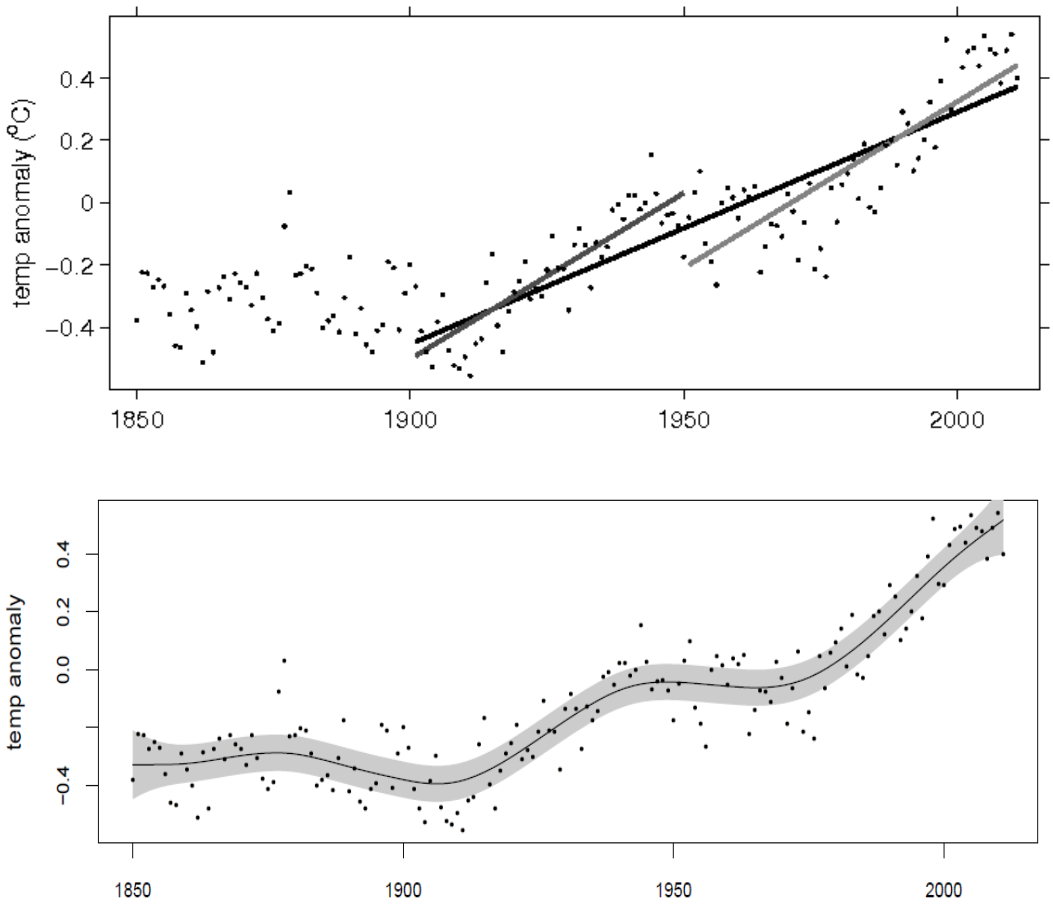

Box 2.2, Figure 1: Top: Global mean surface temperature anomalies relative to a 1961–1990 climatology based on HadCRUT4 annual data (dots). The straight black lines are Least Squares trends for 1901–2011, 1901–1950 and 1951–2011. Bottom: Same data as top, with Smoothing Spline (solid curve) and the 90% confidence interval on the smooth curve (shading).

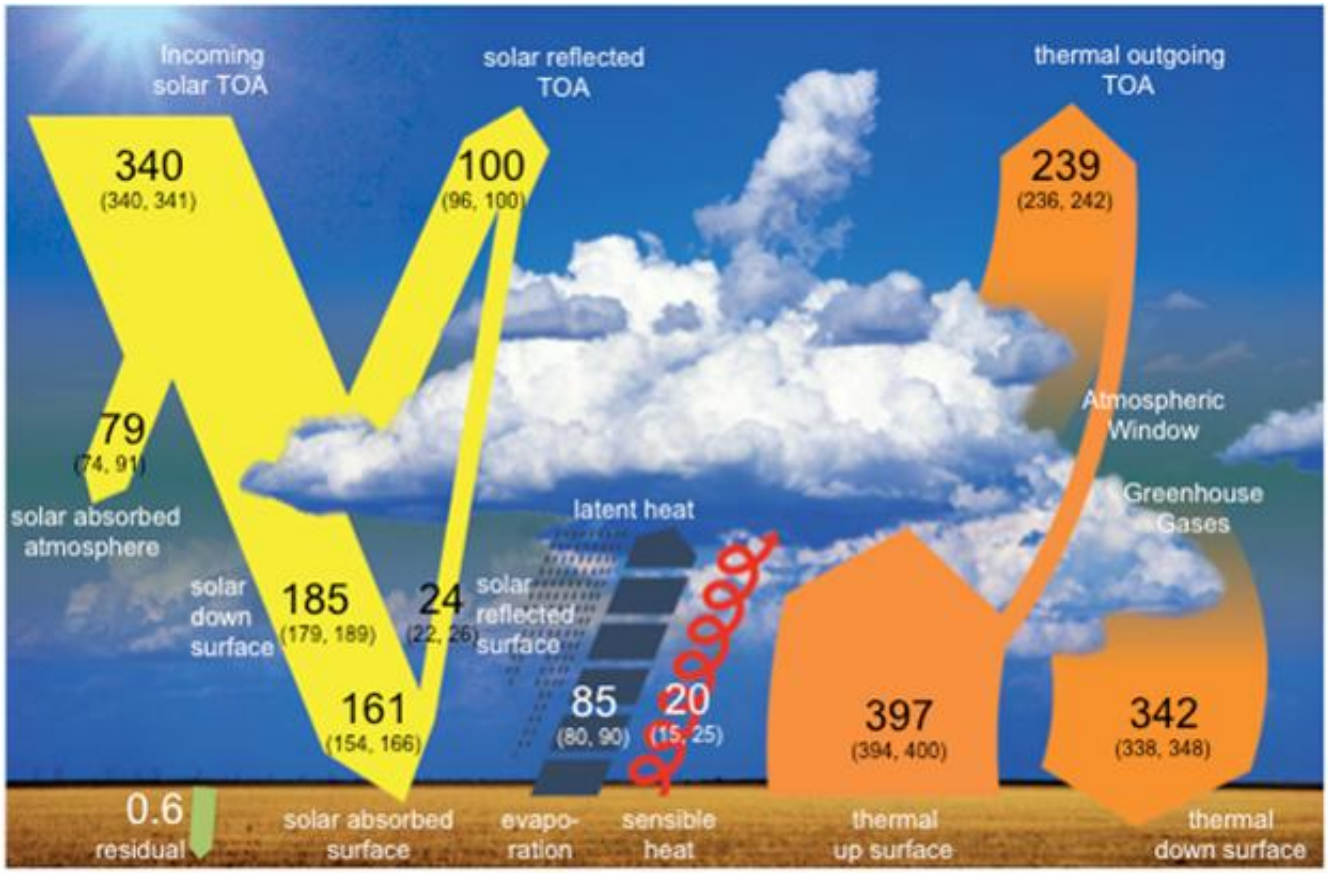

Figure 2.12: Global mean energy budget under present day climate conditions. Numbers state magnitudes of the individual energy flows in Wm^{-2}, adjusted within their uncertainty ranges to close the energy budgets. Numbers in parentheses attached to the radiative fluxes cover the range of values in line with observational constraints (based on Loeb et al., 2009; Stephens et al., in press; Trenberth and Fasullo, 2012; Wild et al., submitted).

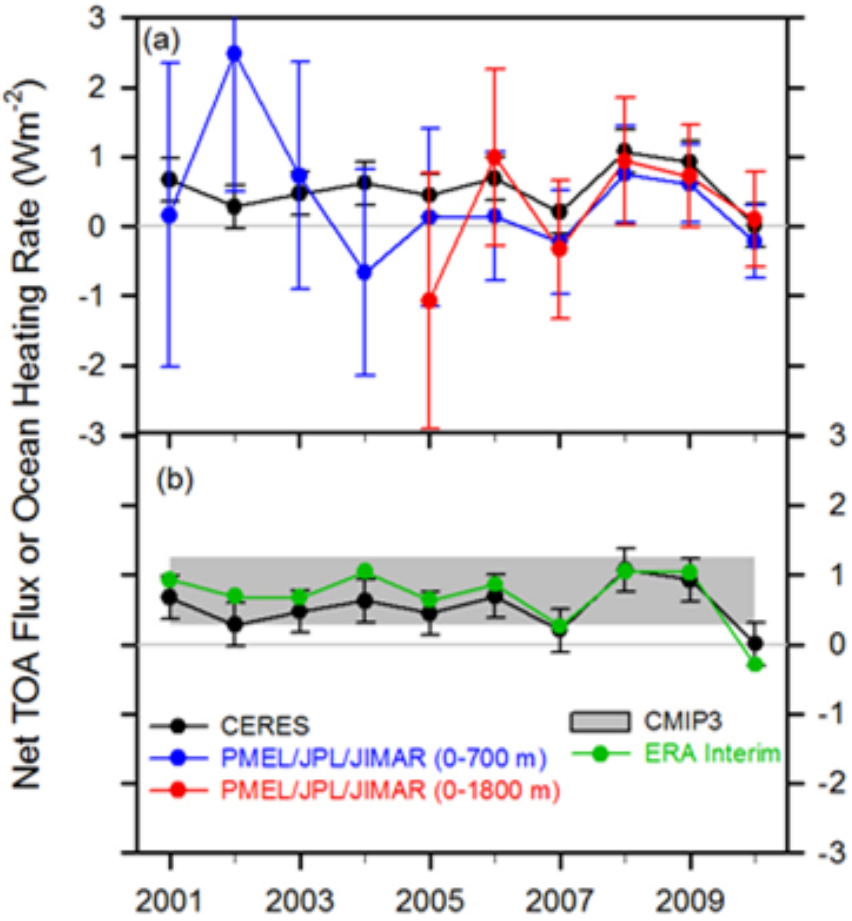

Figure 2.13: Comparison of net TOA flux and upper ocean heating rates. Global annual average net TOA flux from (a) CERES observations (based upon the EBAFTOA_ Ed2.6 product) and (b) ERA Interim reanalysis are anchored to an estimate of Earth's heating rate for 2006–2010. The Pacific Marine Environmental Laboratory/Jet Propulsion Laboratory/Joint Institute for Marine and Atmospheric Research (PMEL/JPL/JIMAR) ocean heating rate estimates (a) use data from Argo and World Ocean Database 2009; The gray bar (b) corresponds to one standard deviation about the 2001–2010 average net TOA flux of 15 CMIP3 models. From Loeb et al.(2012).

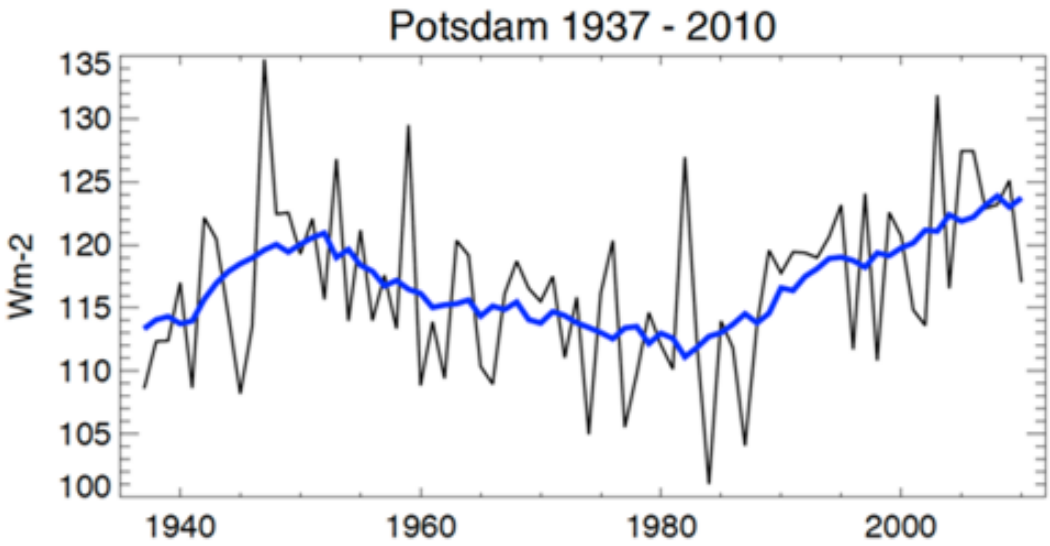

Figure 2.14: Annual mean surface solar radiation (in W m^{-2}) as observed at Potsdam, Germany, from 1937 to 2010. Five year moving average in blue. Updated from Wild (2009) and Ohmura (2009).

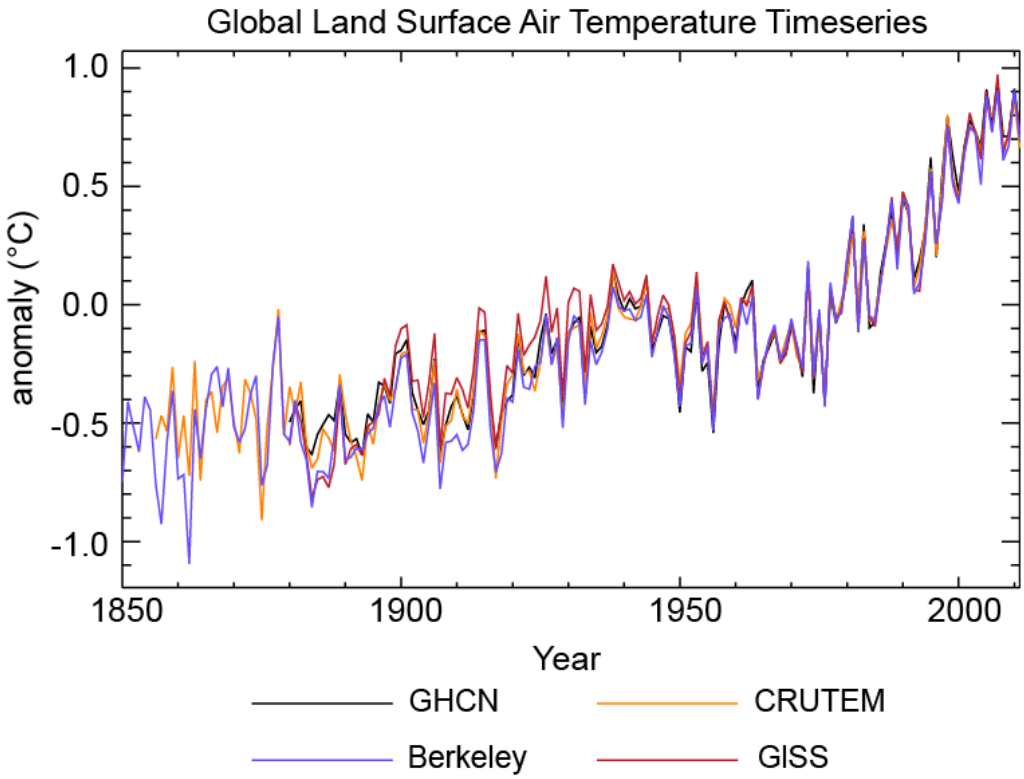

Figure 2.15: Global annually averaged LSAT anomalies relative to a 1961–1990 climatology from the latest versions of four different data sets.

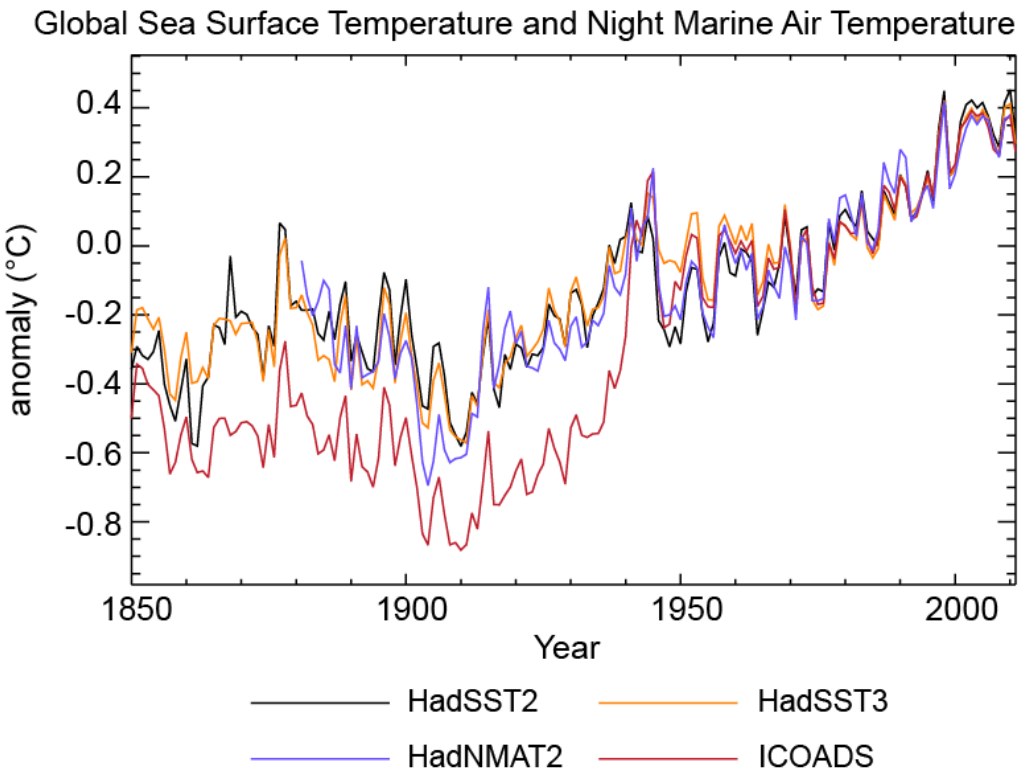

Figure 2.16: Global annually averaged SST and NMAT relative to a 1961-1990 climatology from gridded data sets of SST observations (HadSST2 and its successor HadSST3), the raw SST measurement archive (ICOADS, v2.5) and night marine air temperatures data set HadNMAT2 (Kent et al., Submitted). Both HadSST2 and HadSST3 are based on SST observations from versions of the ICOADS data set, where some measurement biases were corrected. Largest corrections are applied to the period before 1941 and are informed, in particular, by night marine air temperature data. In HadSST3 biases are adjusted for the entire period (Kennedy et al., 2011).

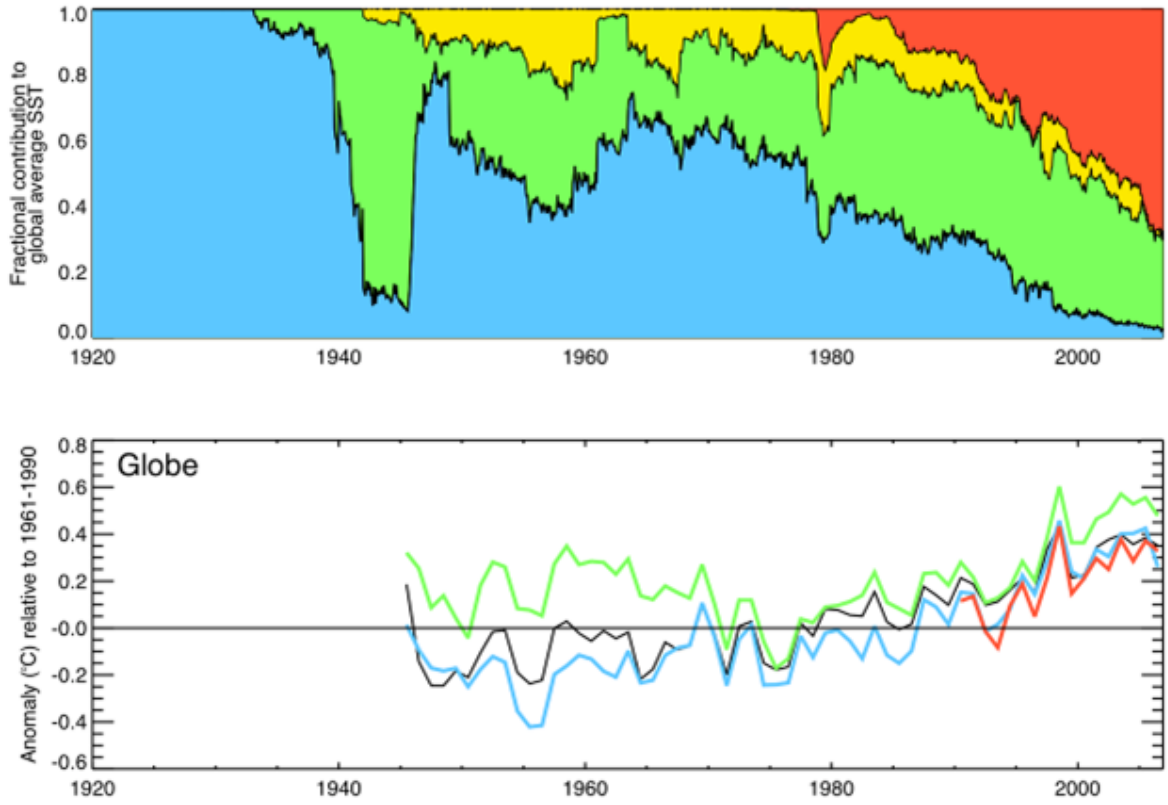

Figure 2.17: Temporal changes in the prevalence of different measurement methods in the ICOADS. Top: fractional contributions of observations made by different measurement methods: bucket observations (blue), ERI and hull contact sensor observations (green), moored and drifting buoys (red), and unknown (yellow). Bottom: Global annual average SST anomalies based on different kinds of data: engine room intake (ERI) and hull contact sensor (green), bucket (blue), buoy (red), and all (black). Averages are computed over all times and locations where both ERI and hull measurements, (but not necessarily buoy data) were simultaneously available. Adapted from Kennedy et al. (2011).

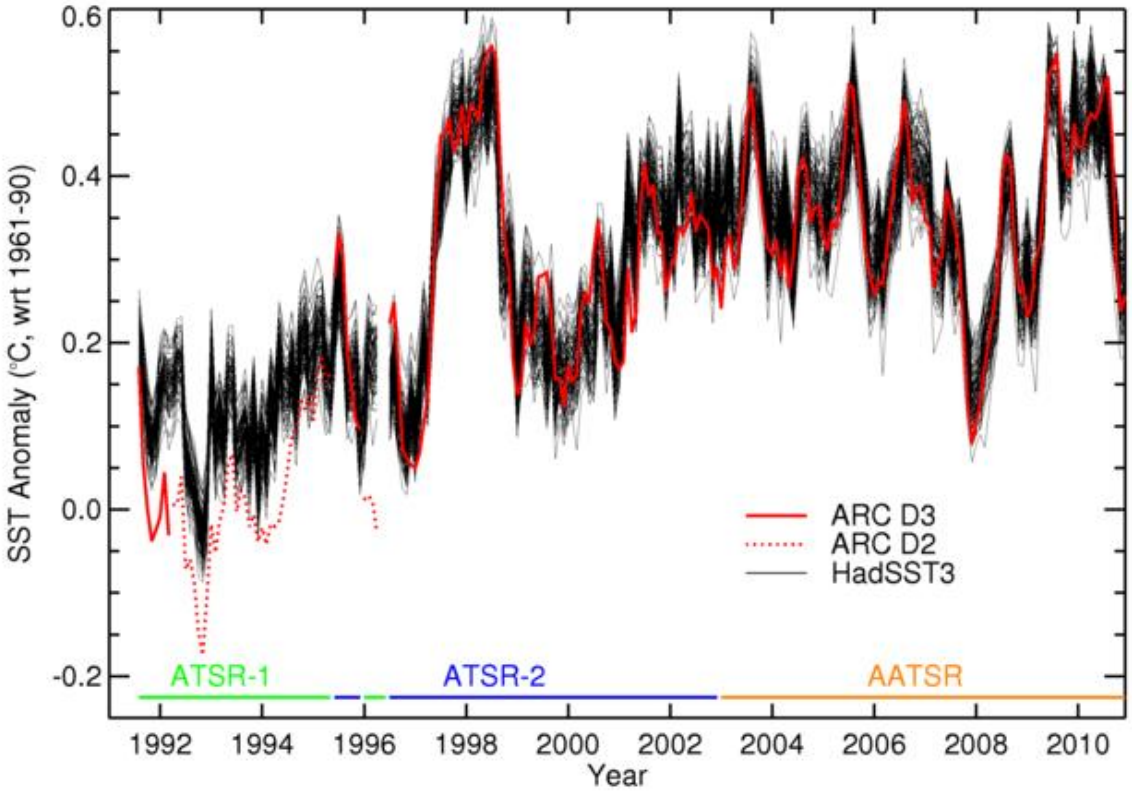

Figure 2.18: Global monthly mean SST anomaly from satellites (ATSRs) and *in situ* records (HadSST3). Black lines: the 100 member HadSST3 ensemble. Red lines: ATSR night-time $SST_{0.2m}$ estimates from the ATSR Reprocessing for Climate (ARC) project. Retrievals based on three spectral channels (D3, solid line) are more accurate than retrievals based on only two (D2, dotted line). Contributions of the three different ATSR missions to the curve shown are indicated at the bottom. The *in situ* and satellite records were co-located within 5° × 5° monthly grid boxes: only those where both data sets had data in the same month were used in the comparison. Adapted from Merchant et al. (Submitted).

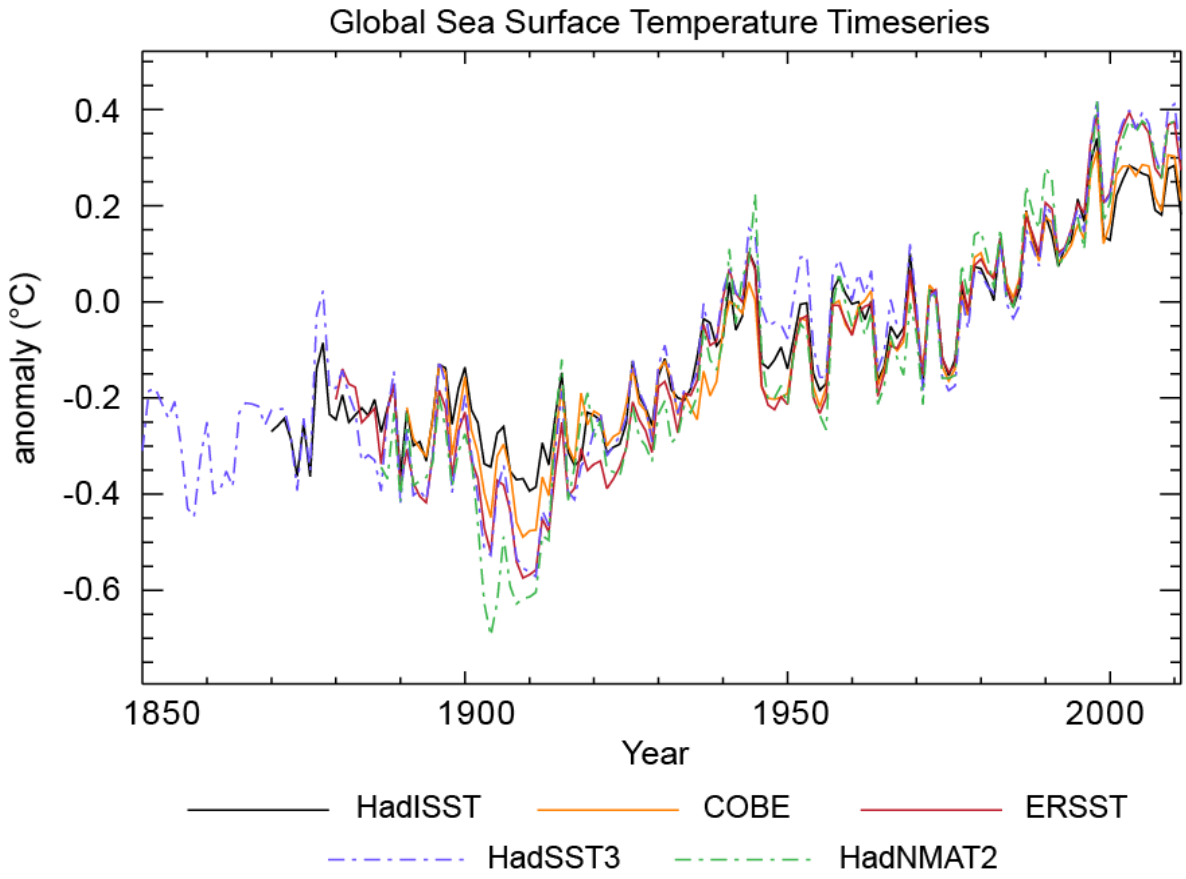

Figure 2.19: Global annually averaged SST and NMAT relative to a 1961–1990 climatology from state of the art datasets. Interpolated products are shown by solid lines; non-interpolated products by dashed lines.

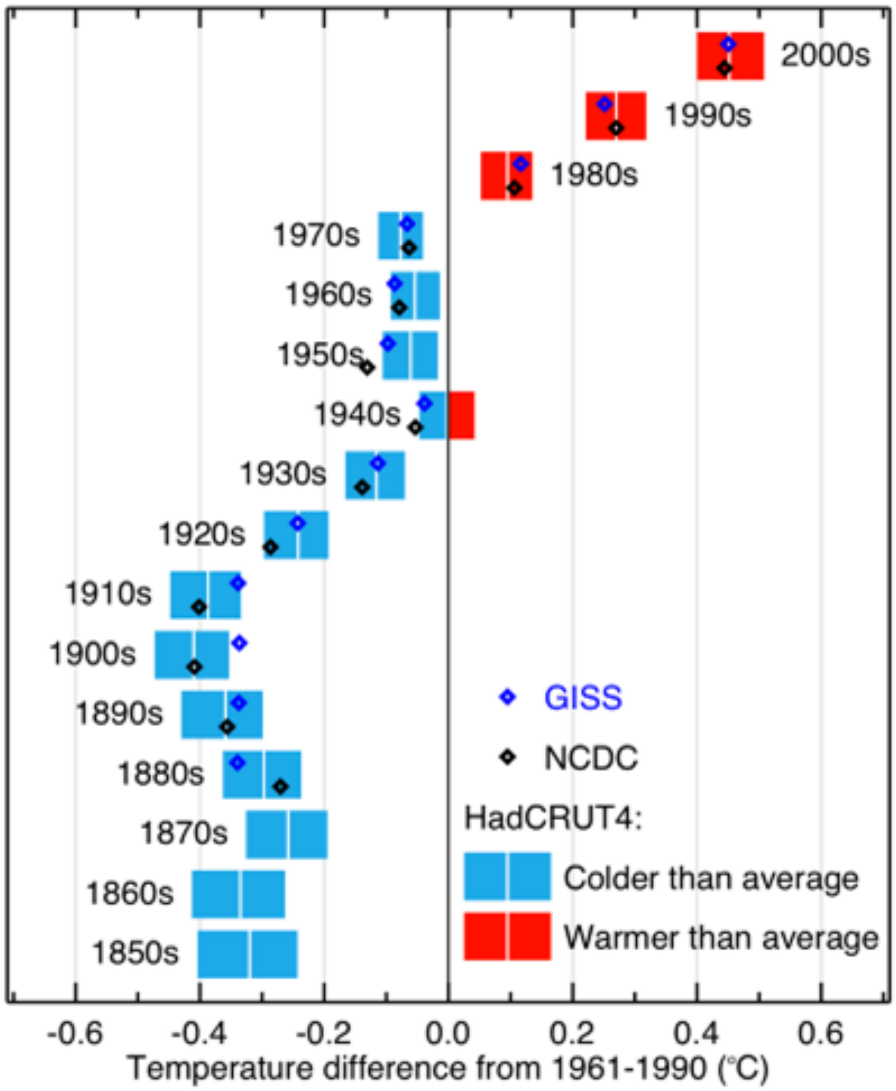

Figure 2.20: Decadal mean temperature anomalies (white vertical lines) and their uncertainties (5–95 percentile ranges as coloured blocks) based upon the LSAT and SST combined HadCRUT4 ensemble (Morice et al., 2012). Anomalies are relative to a 1961–1990 climatology. 1850s indicates the period 1850-1859, and so on. NCDC MLOST and GISS dataset best-estimates are also shown.

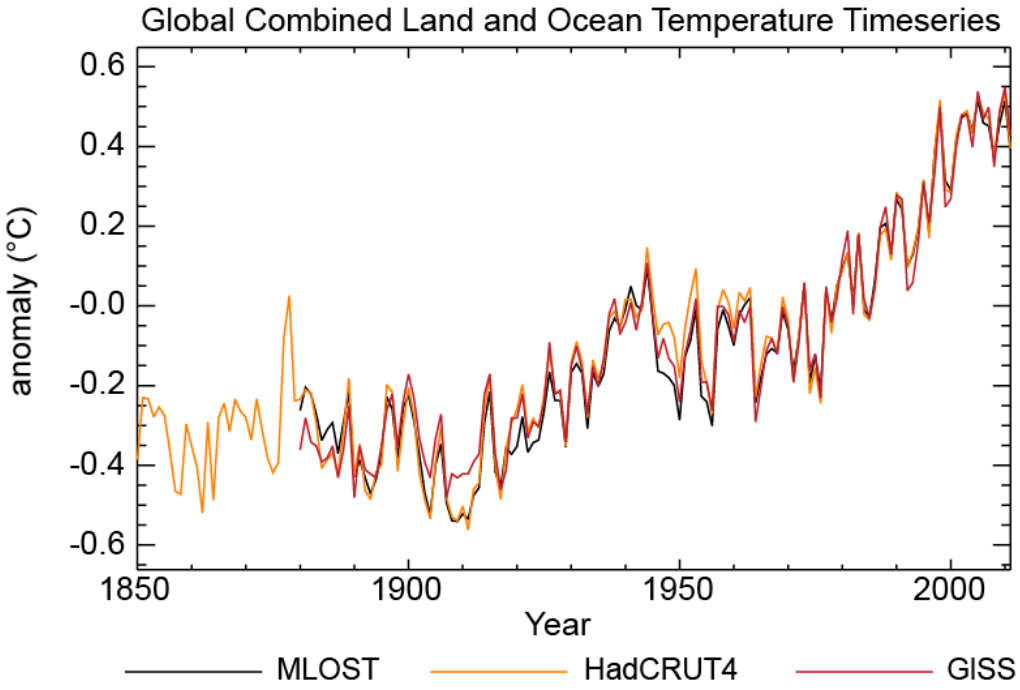

Figure 2.21: Global mean surface temperature anomalies relative to a 1961–1990 climatology from the latest version of the three combined LSAT and SST data sets.

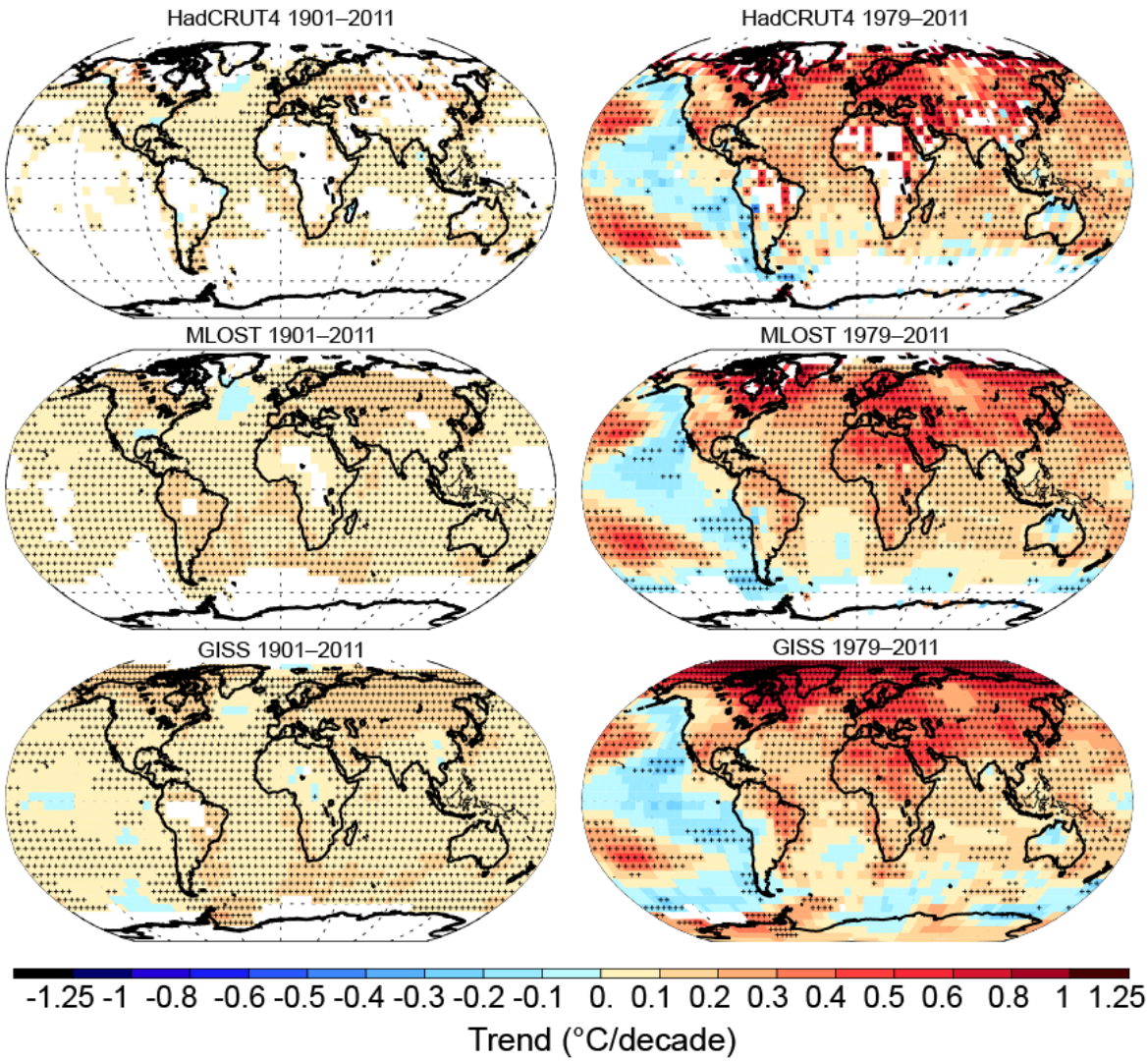

Figure 2.22: Trends in surface temperature from the three global datasets for 1901–2011 (left hand panels) and 1979–2011 (right hand panels). Trends have been calculated only for those grid boxes with greater than 70% complete records and more than 20% data availability in first and last decile of the period. Grid boxes where the trend is significant at the 10% level are indicated by a +. Differences in coverage primarily reflect the degree of interpolation undertaken by the dataset providers ranging from none (HadCRUT4) to substantial (GISS).

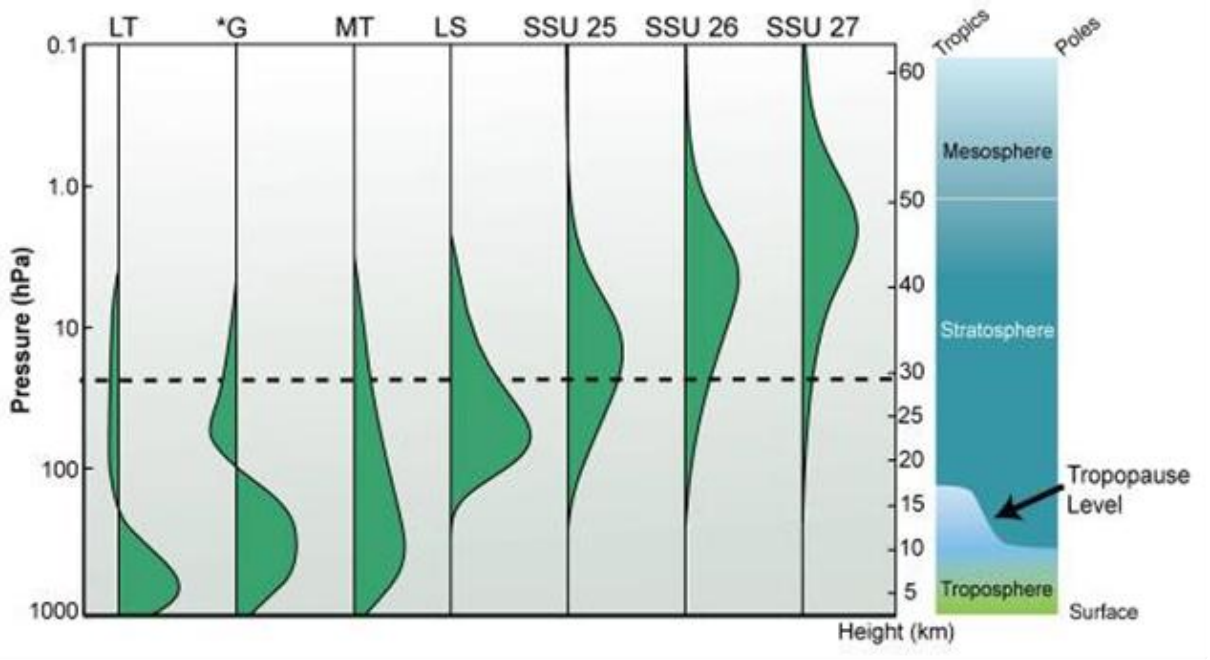

Figure 2.23: Vertical weighting functions for those satellite temperature retrievals discussed in this chapter (modified from Seidel et al. (2011)). The dashed line indicates the typical maximum altitude achieved in the historical radiosonde record. The three SSU channels are denoted by the designated names 25, 26 and 27. LS (Lower Stratosphere) and MT (Mid Troposphere) are two direct MSU measures and LT (Lower Troposphere) and *G (Global Troposphere) are derived quantities from one or more of these that attempt to remove the stratospheric component from MT.

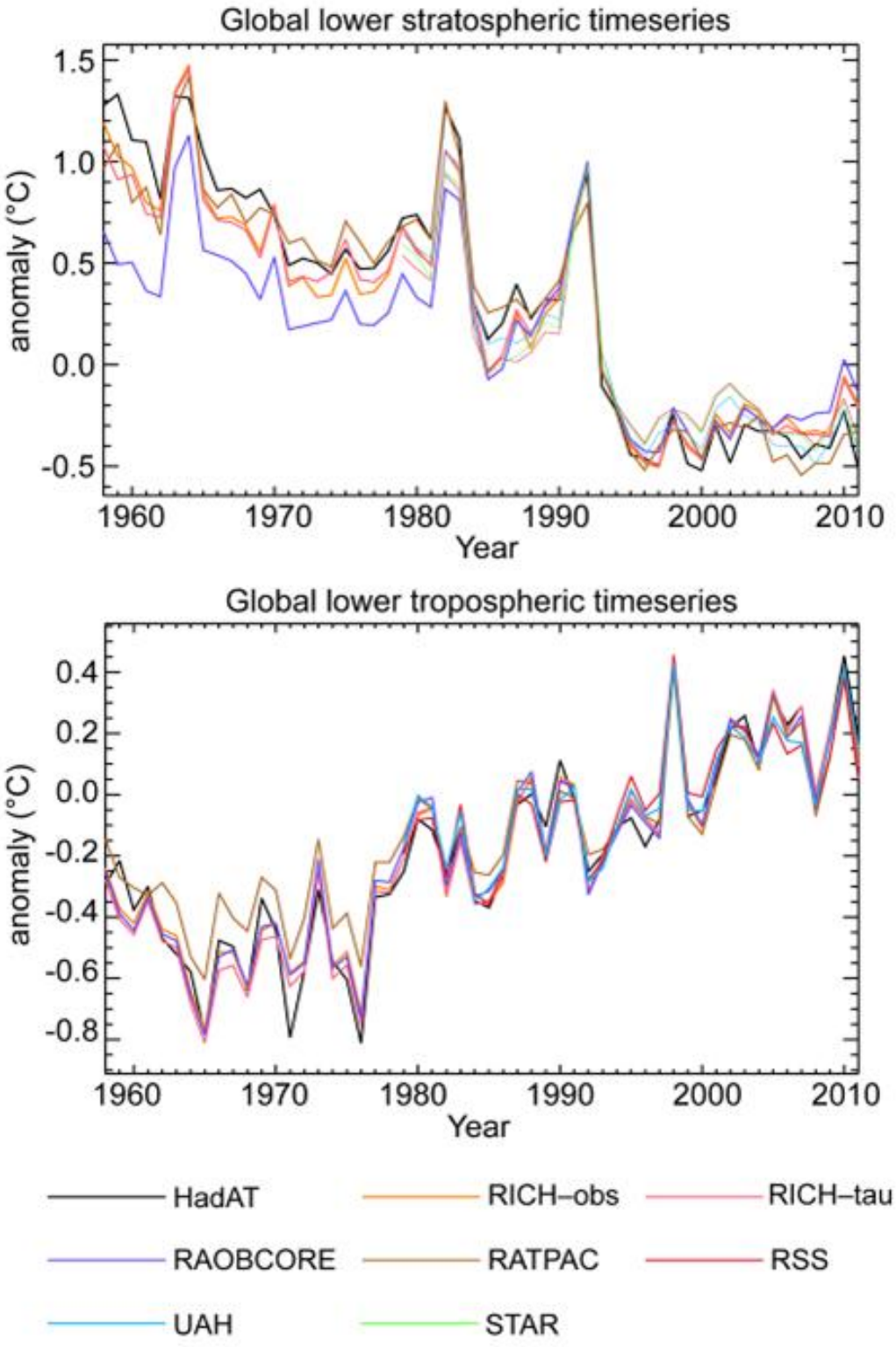

Figure 2.24: Global average lower stratospheric (top) and lower tropospheric (bottom) temperature anomalies relative to a 1981–2010 climatology from different data sets. STAR does not produce a lower tropospheric temperature product. Note that the y-axis resolution differs between the two panels.

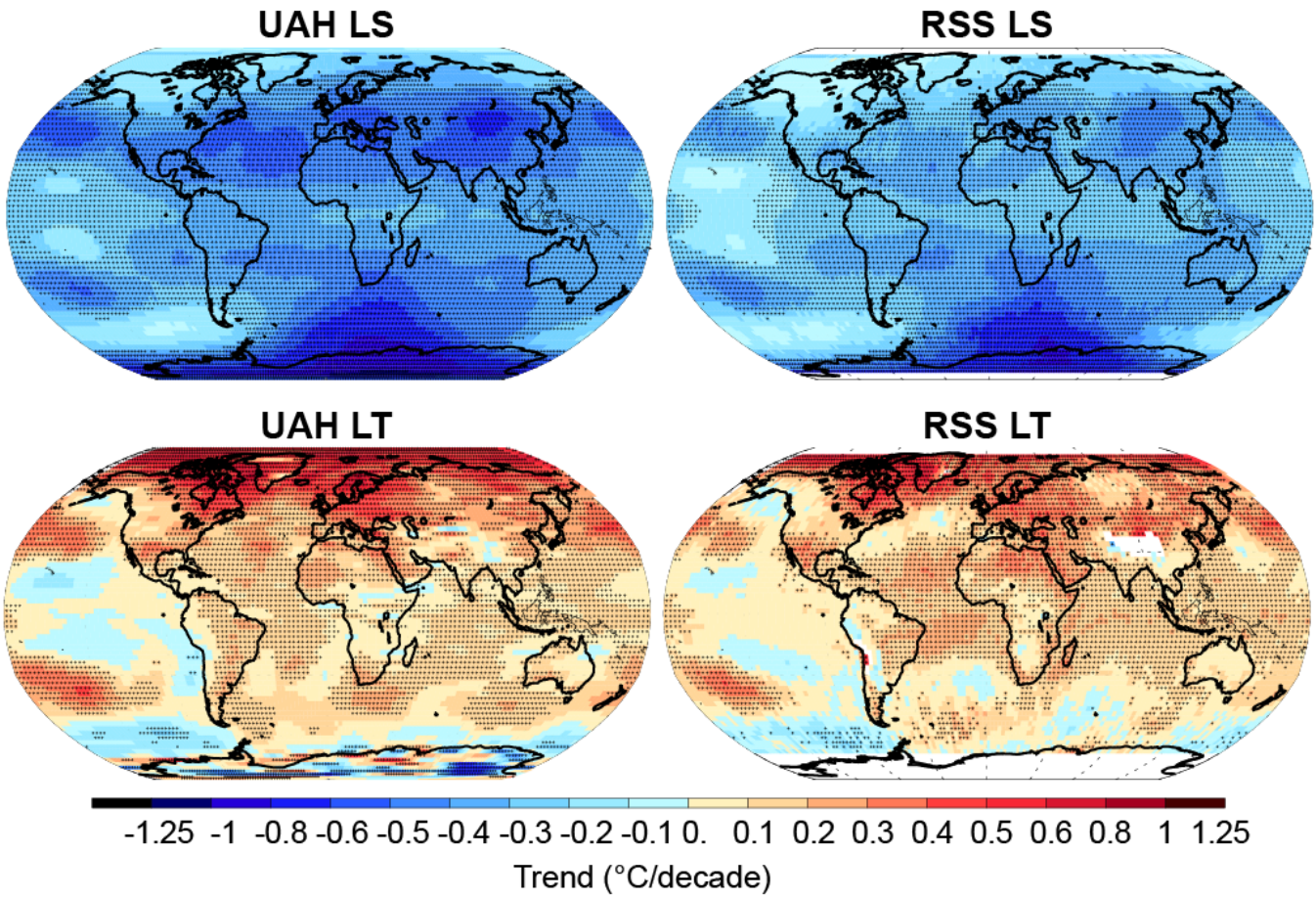

Figure 2.25: Trends in MSU upper air temperature over 1979 to 2011 from UAH (left hand panels) and RSS (right hand panels) and for LS (top row) and LT (bottom row). Data are temporally complete within the sampled domains for each dataset. Grid boxes where the trend is significant at the 10% level are highlighted by a +.

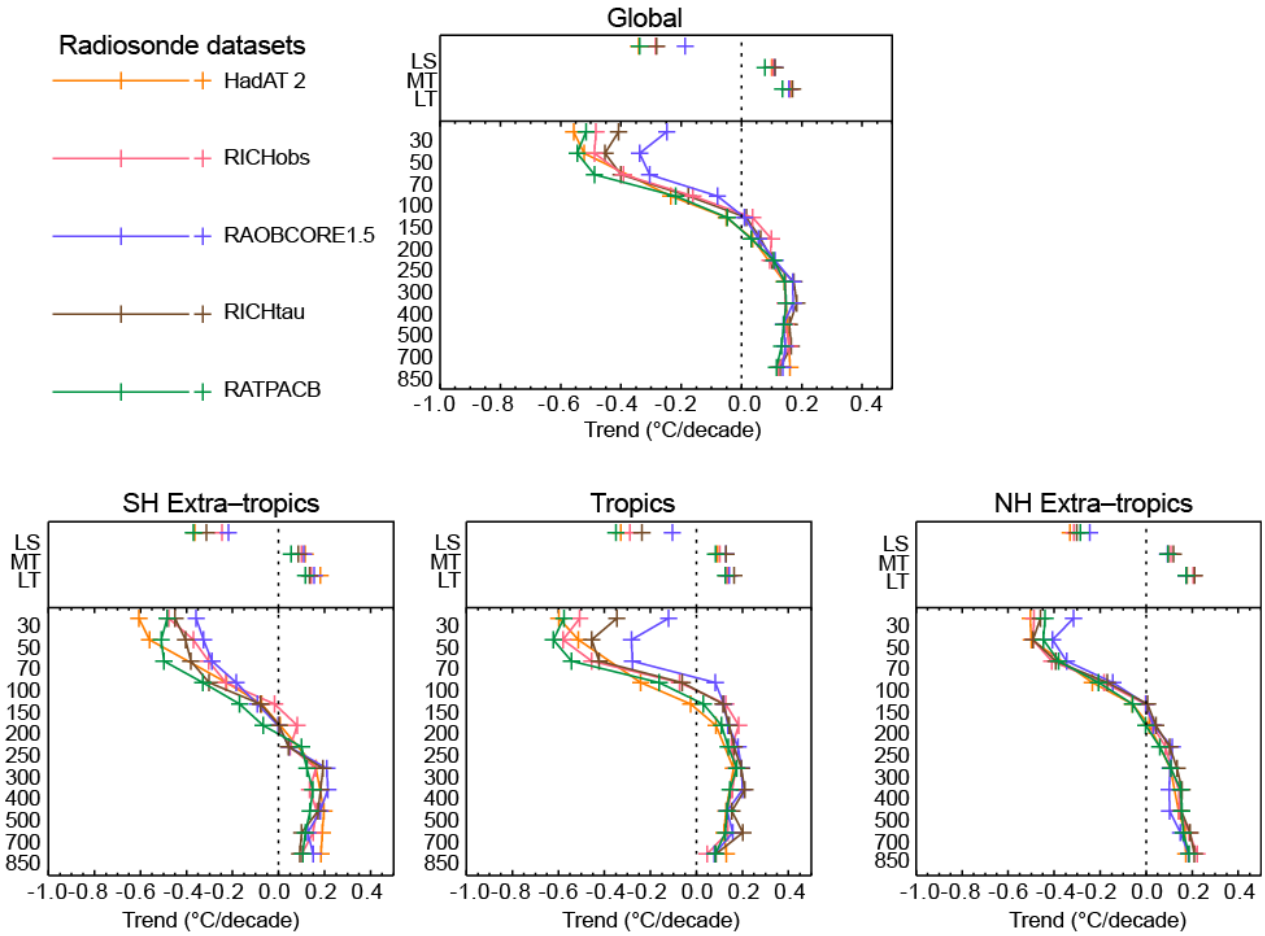

Figure 2.26: Linear temperature trend estimates for all available radiosonde data products that contain records for 1958–2010 for the globe (top) and tropics (20°N–20°S) and extra-tropics (bottom). The bottom panel trace in each case is for trends on distinct pressure levels. Note that the pressure axis is not linear. The top panel points show MSU layer equivalent measure trends. MSU layer equivalents have been processed using the method of Thorne et al. (2005). No attempts have been made to sub-sample to a common data mask.

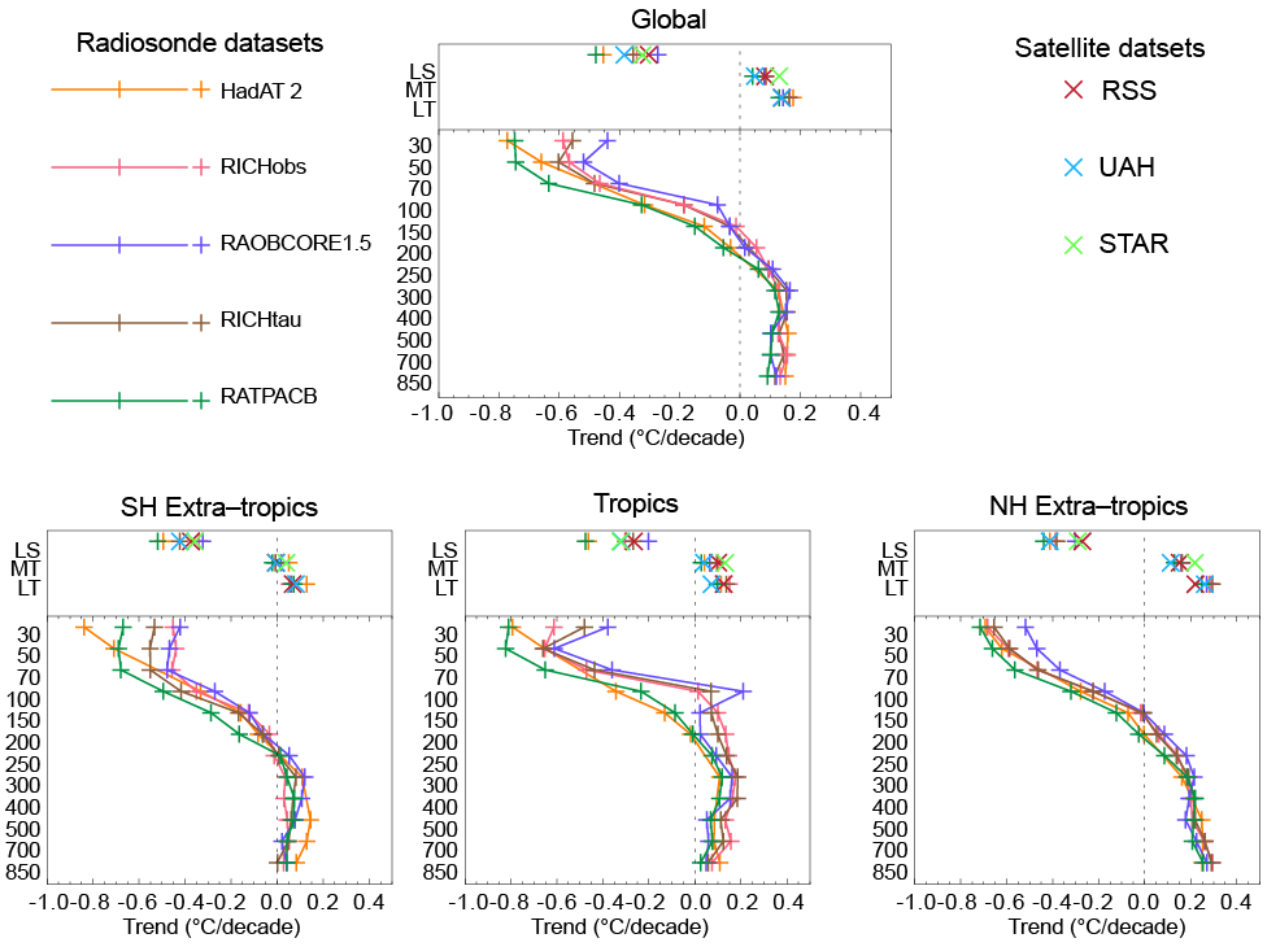

Figure 2.27: As Figure 2.26 except for the satellite era 1979–2010 period and including MSU products.

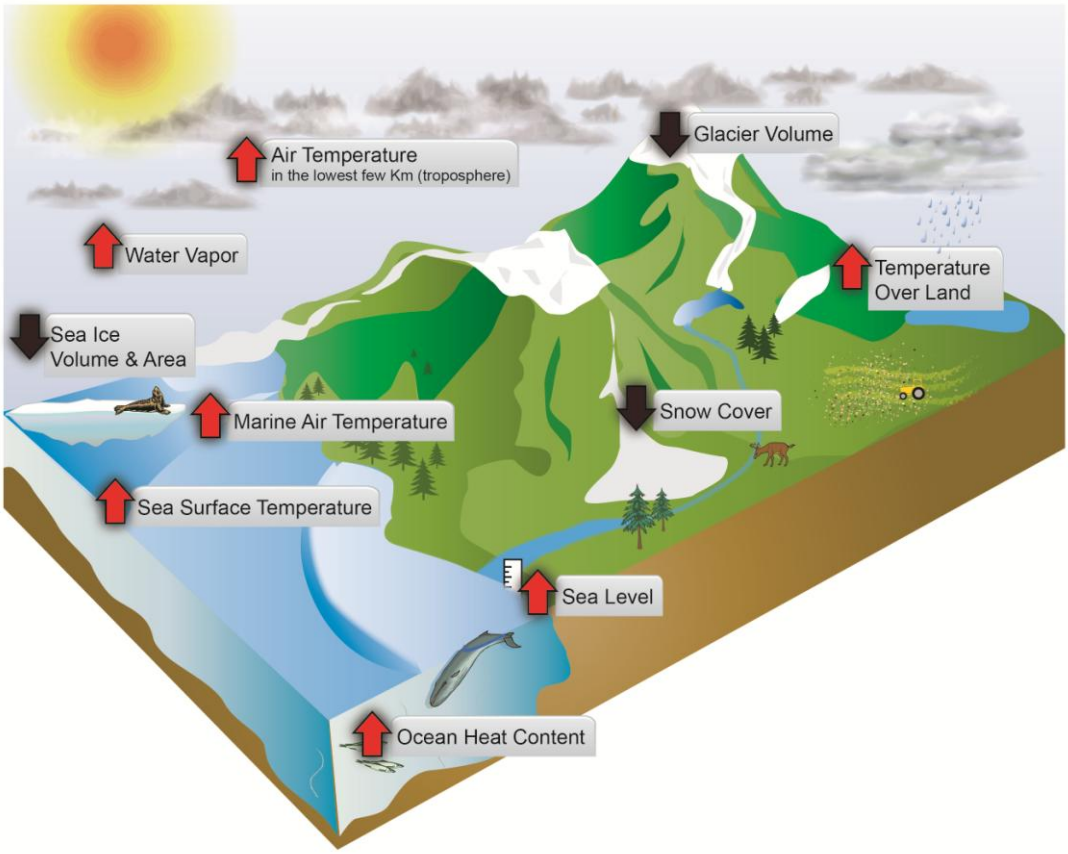

FAQ 2.1, Figure 1: Repeated analyses of independently measured components of the climate system which would be expected to change in a warming world, exhibit trends consistent with warming (arrow direction denotes the sign of the change), as shown in FAQ 2.1, Figure 2.

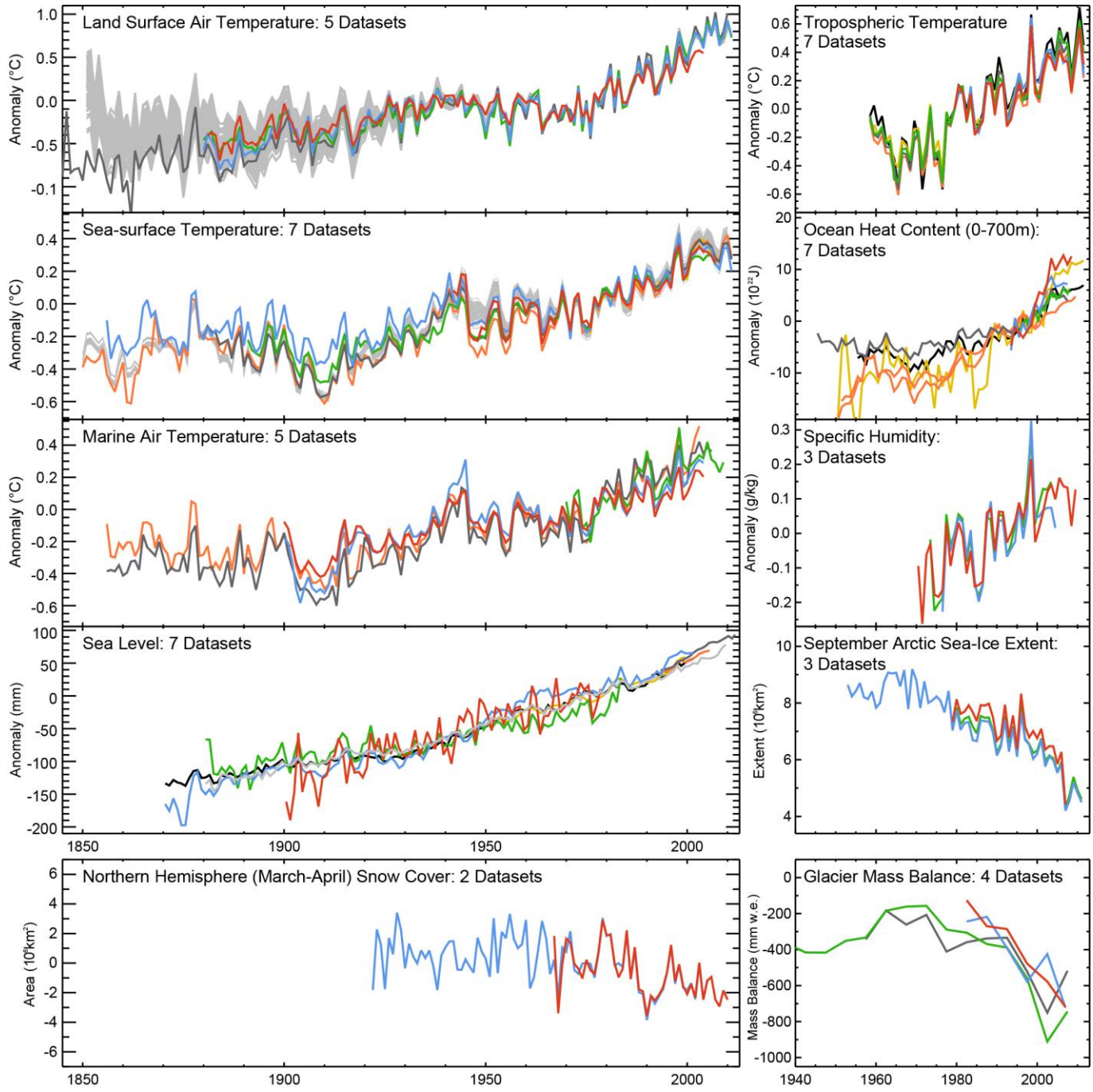

FAQ 2.1, Figure 2: Multiple redundant indicators of a changing global climate. Each line represents an independently-derived estimate of change in the climate element. All publicly-available, documented, datasets known to the authors have been used in this latest version. In each panel all datasets have been normalized to a common period of record. Further details are given in Arndt et al. (2010). A full detailing of which source datasets go into which panel is given in Appendix 2.A.

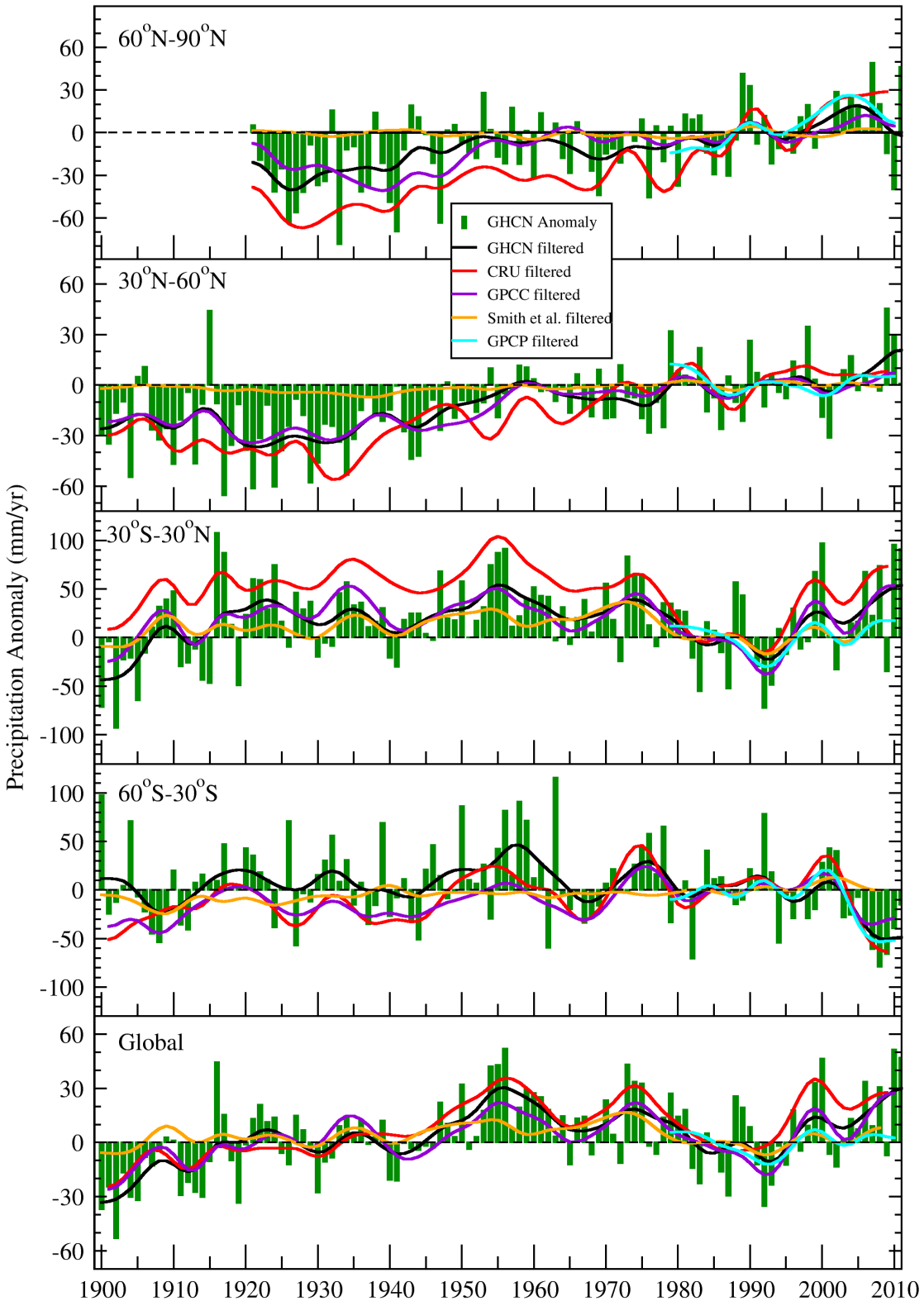

Figure 2.28: Annual precipitation anomalies averaged over land areas for four latitudinal bands and the globe from GHCN (green bars) relative to a 1981–2000 climatology. Smoothed curves (see Appendix 3.A from (Trenberth et al., 2007) for GHCN and other global precipitation data sets as listed.

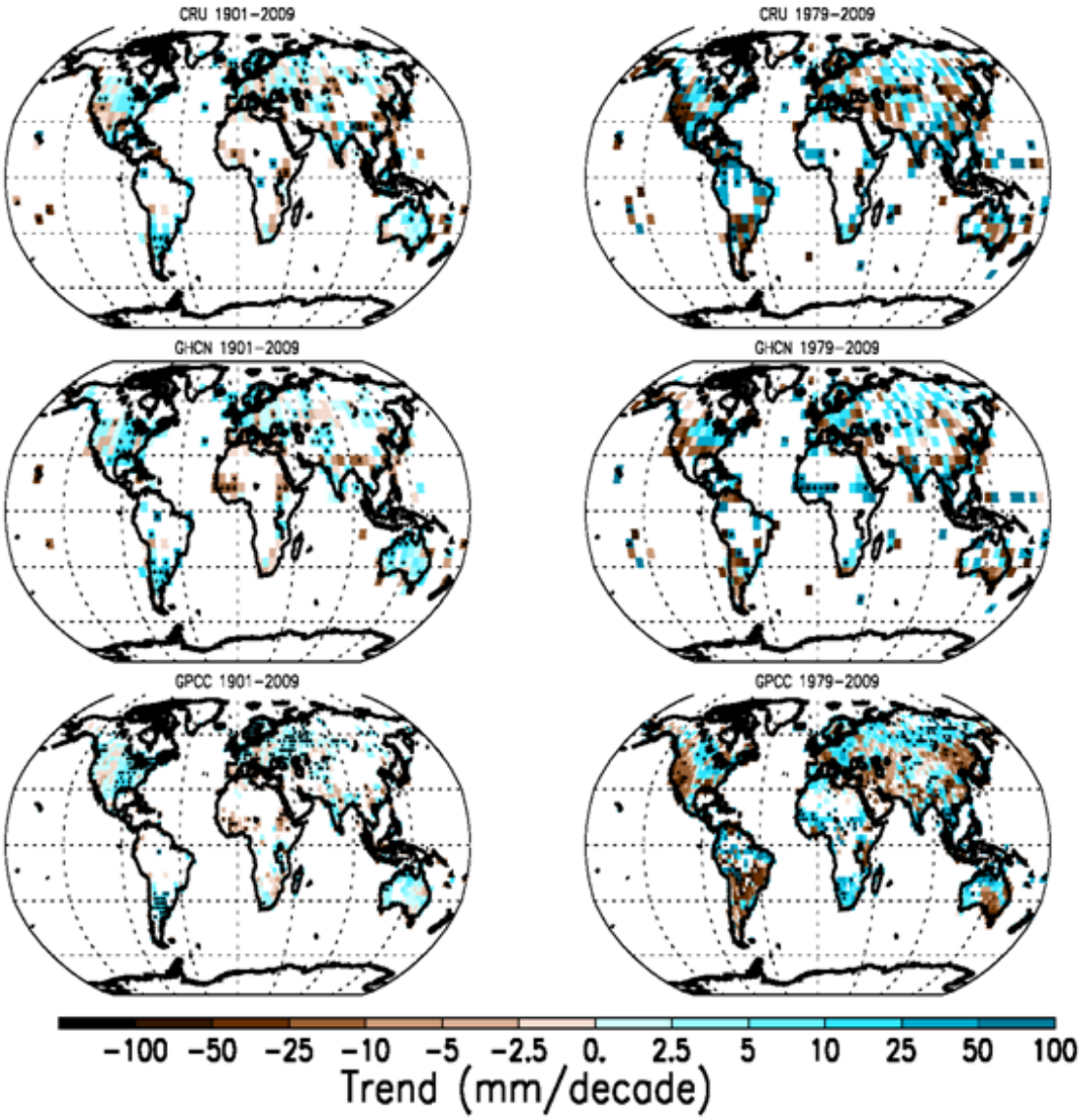

Figure 2.29: Trends in precipitation from the CRU, GHCN and GPCC data sets for 1901–2009 (left hand panels) and 1979–2009 (right hand panels). Grid boxes with statistically significant trends at the 10% level are indicated by a +.

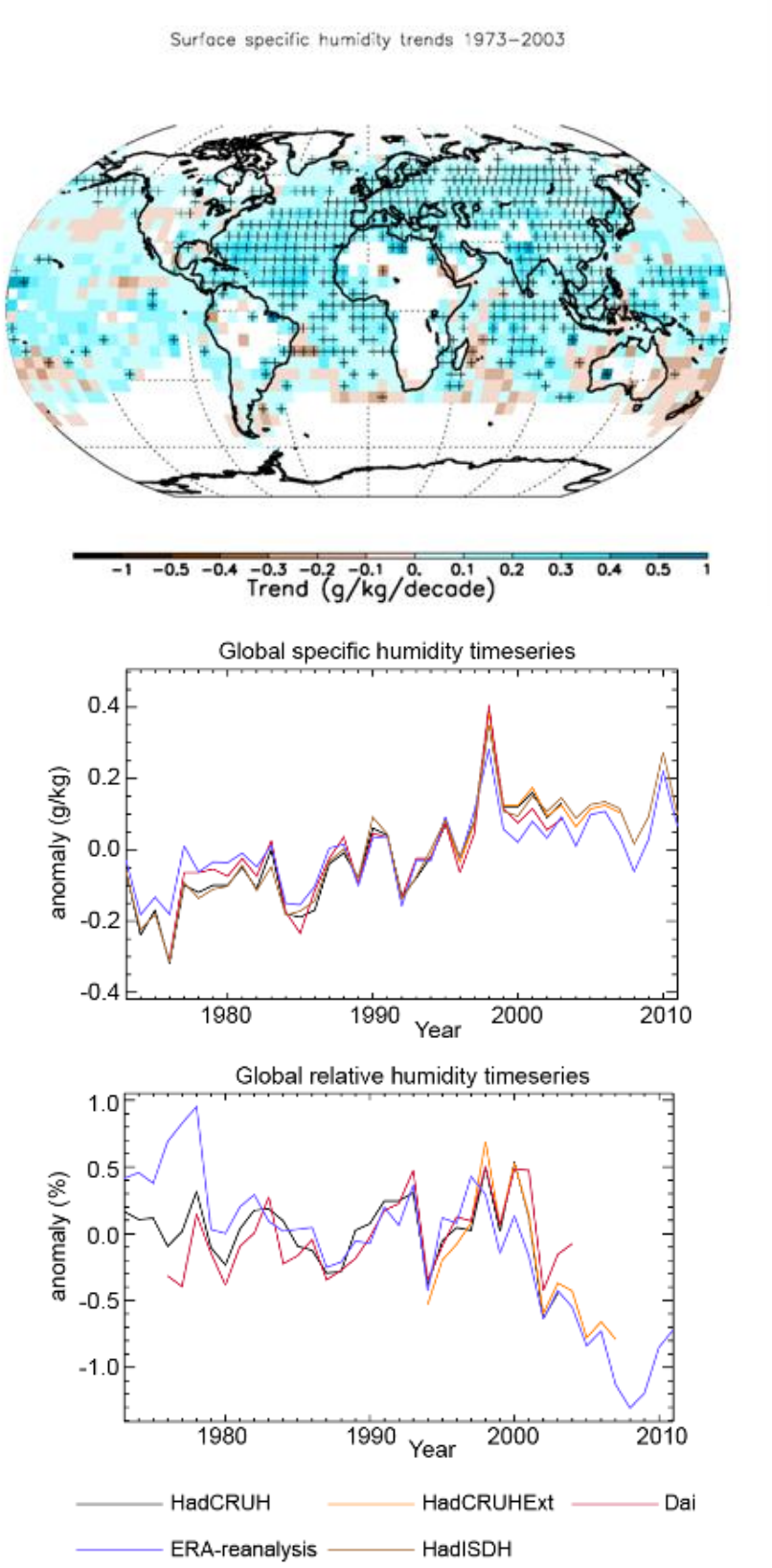

Figure 2.30: a) Trends in surface specific humidity from HadCRUH over 1973–2003. Grid boxes with statistically significant trends at the 10% level are indicated by a +. b) Global anomalies in land surface specific humidity from HadCRUH, HadCRUHExt, (Dai, 2006), and ERA-interim (Simmons et al., 2010), c) As b) but for relative humidity.

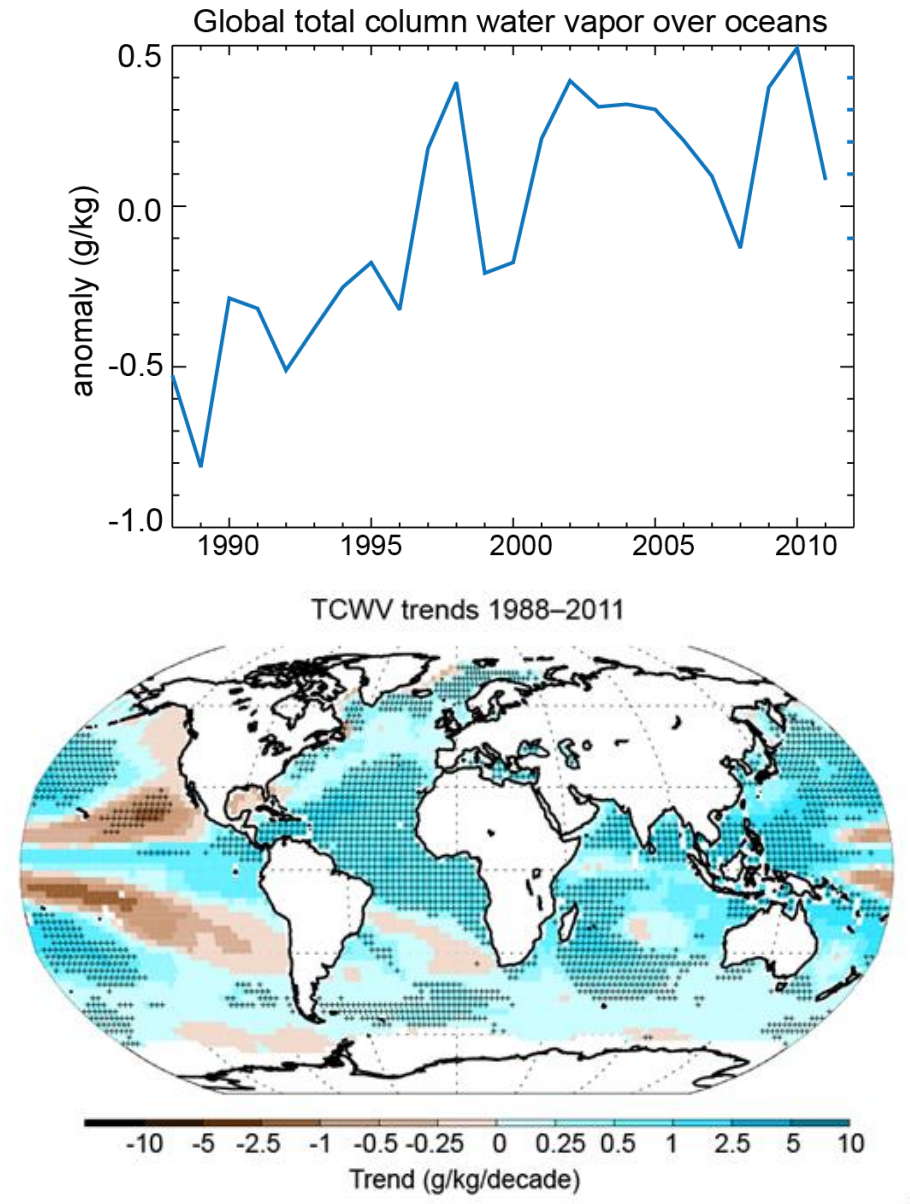

Figure 2.31: Top**:** Global anomalies in column integrated water vapour averaged over ocean surfaces. Bottom: Trends (kg m^{-2} per decade) in column integrated water vapour from Special Sensor Microwave Imager, (Wentz et al., 2007) for the period 1988–2010. Grid boxes with statistically significant trends at the 10% level are indicated by a ♦.

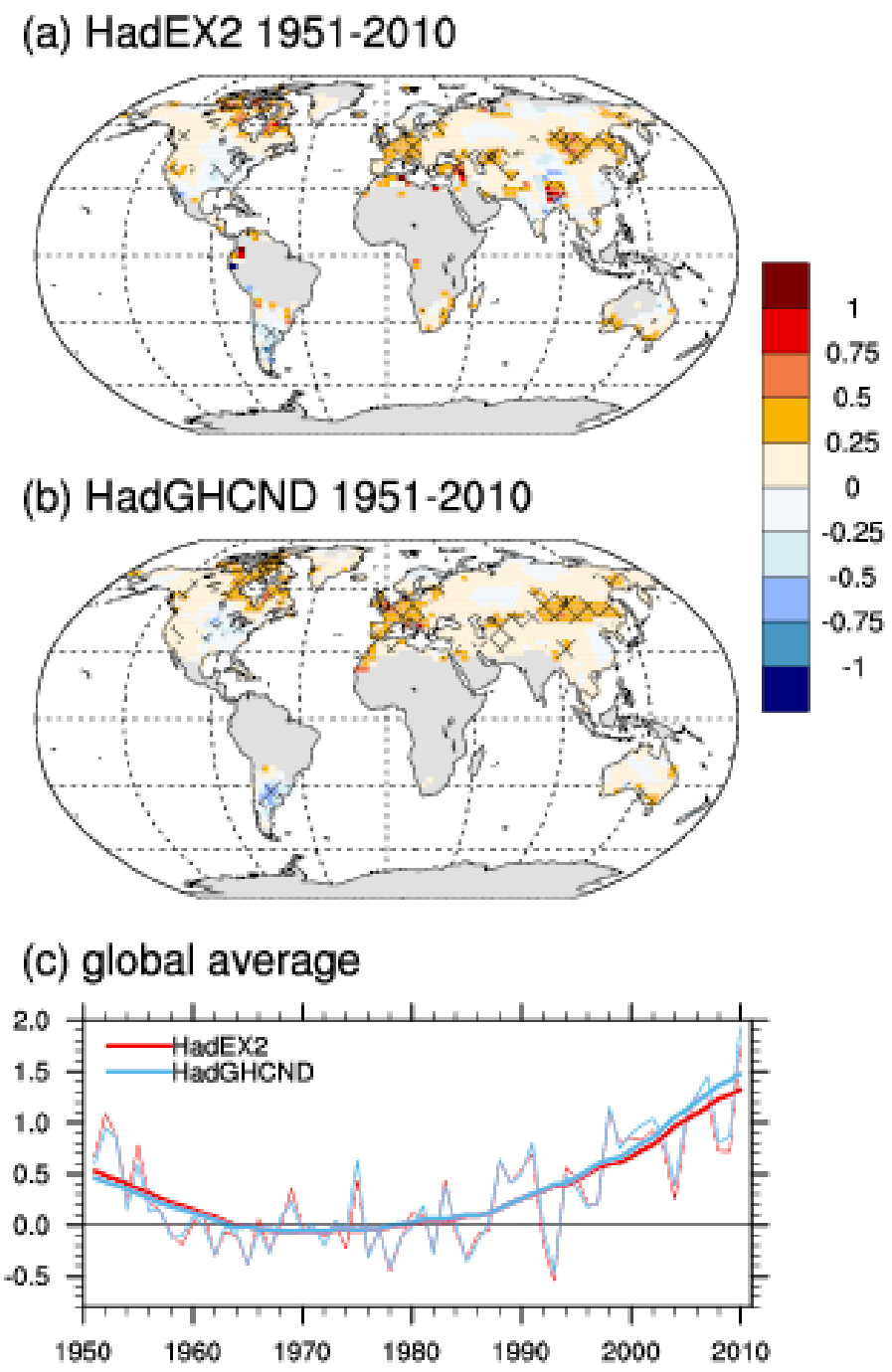

Box 2.4, Figure 1: Trends (°C per decade) in the warmest day of the year using different datasets for the period 1951–2010. The datasets are (a) HadEX2 (Donat et al., 2012a), (b) HadGHCND (Caesar et al., 2006) using data updated to 2010 (Donat et al., 2012b) , and (c) Globally averaged annual anomalies (thin solid lines) for each dataset with associated decadal variations (thick solid lines). Hatching on maps indicates gridboxes where trends are significant at 10% level. Annual anomalies are only calculated using gridboxes where both datasets have data and where 90% of data are available.

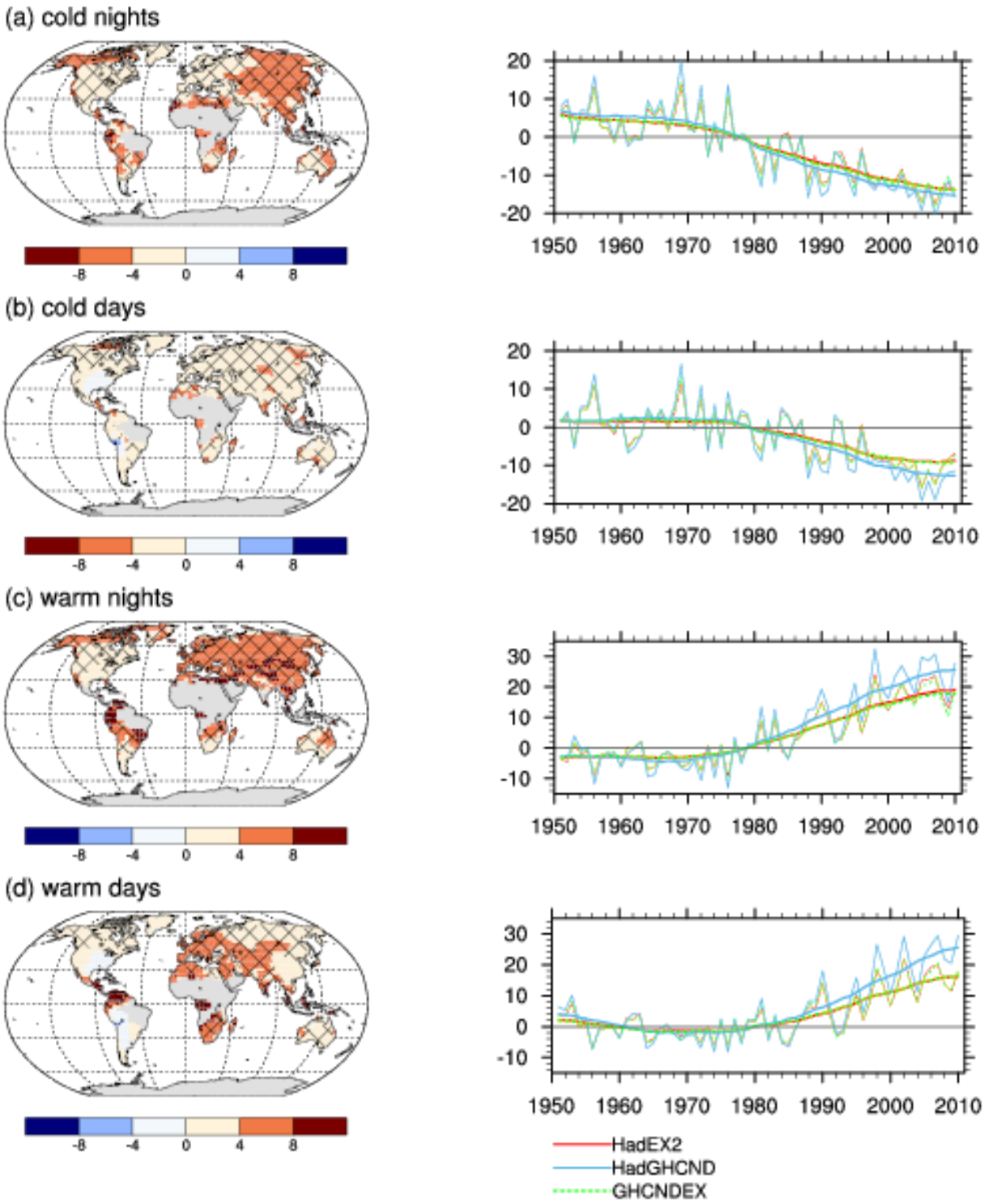

Figure 2.32: Trends (days per decade) in the annual frequency of extreme temperatures, over the period 1951 to 2010, for: (a) cool nights (10th percentile), (b) cool days (10th percentile), (c) warm nights (90th percentile) and (d) warm days (90th percentile). Trends were calculated only for grid boxes that had at least 40 years of data during this period and where data ended no earlier than 2003. Hatching indicates gridboxes where trends are significant at the 10% level. The data source for trend maps is HadEX2 (Donat et al., 2012a). Beside each map are the global annual time series of anomalies with respect to 1961 to 1990 (thin lines) along with decadal variations (thick lines) for three global datasets: HadEX2; HadGHCND (Caesar et al., 2006) and updated to 2010 and GHCNDEX (Donat et al., 2012b). Global averages are only calculated using gridboxes where all three datasets have at least 90% of data over the time period. Trends are significant at the 5% level for all the global indices shown.

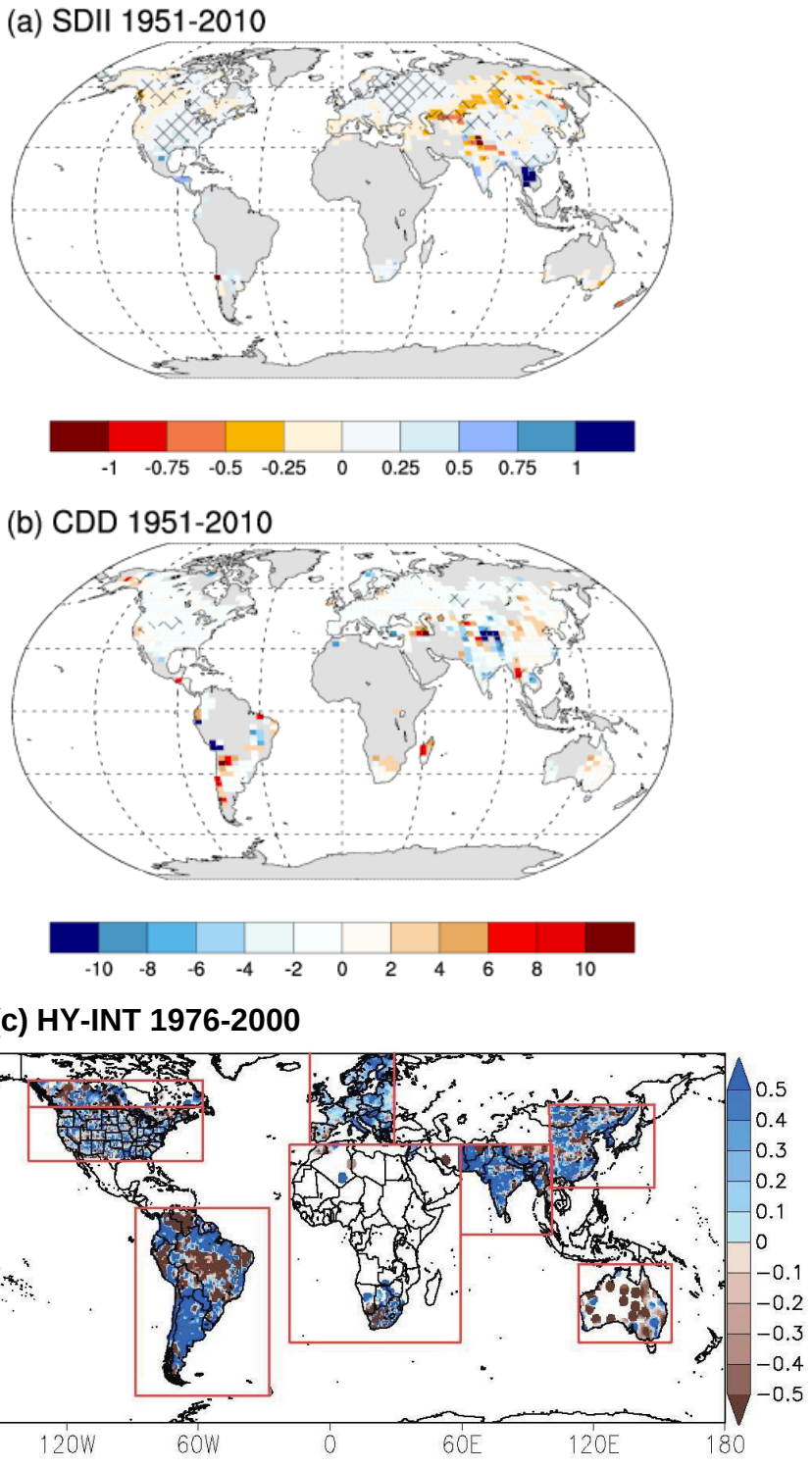

Figure 2.33: (a) Trends (mm day^{-1} yr^{-1}) in daily precipitation intensity and (b) trends (days per year) in the frequency of the annual maximum number of consecutive dry days. Trends were calculated only for grid boxes that had at least 40 years of data during this period and where data ended no earlier than 2003. Hatching indicates gridboxes where trends are significant at the 10% level. The data source for trend maps is HadEX2 (Donat et al., 2012a). (c) Trends in hydroclimatic intensity (HY-INT: a multiplicative measure of length of dry spell and precipitation intensity) over the period 1976 to 2000 (from Giorgi et al. (2011)). An increase (decrease) in HY-INT reflects an increase (decrease) in the length of drought and /or extreme precipitation events.

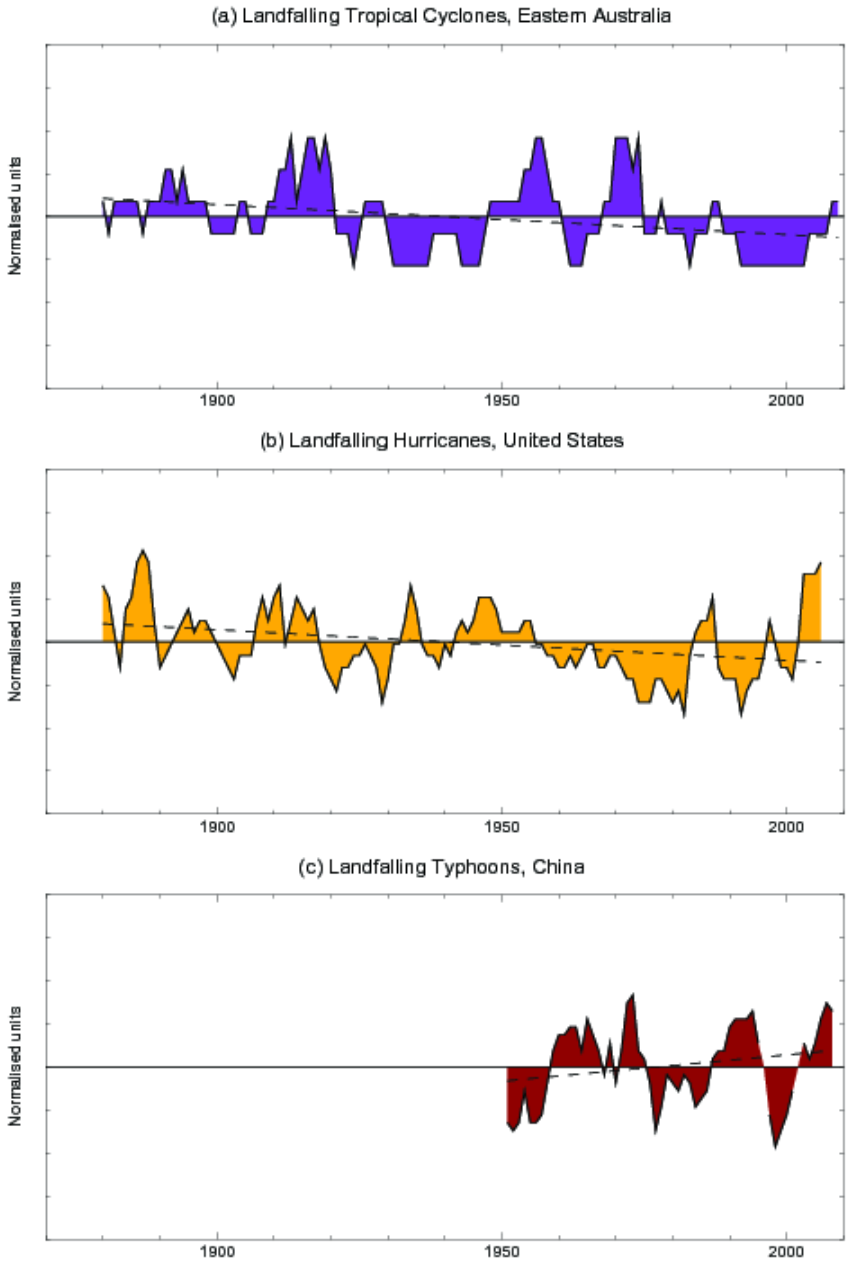

Figure 2.34: Normalized 5-year running means of the number of (a) adjusted land falling eastern Australian tropical cyclones (adapted from (Callaghan and Power, 2011) and updated to include 2010/2011 season) and (b) unadjusted land falling U.S. hurricanes (adapted from (Vecchi and Knutson, 2011) and (c) land-falling typhoons in China. Vertical axis ticks represent one standard deviation, with all series normalized to unit standard deviation after a 5-year running mean was applied. The dashed lines are trends calculated using ordinary least squares regression.

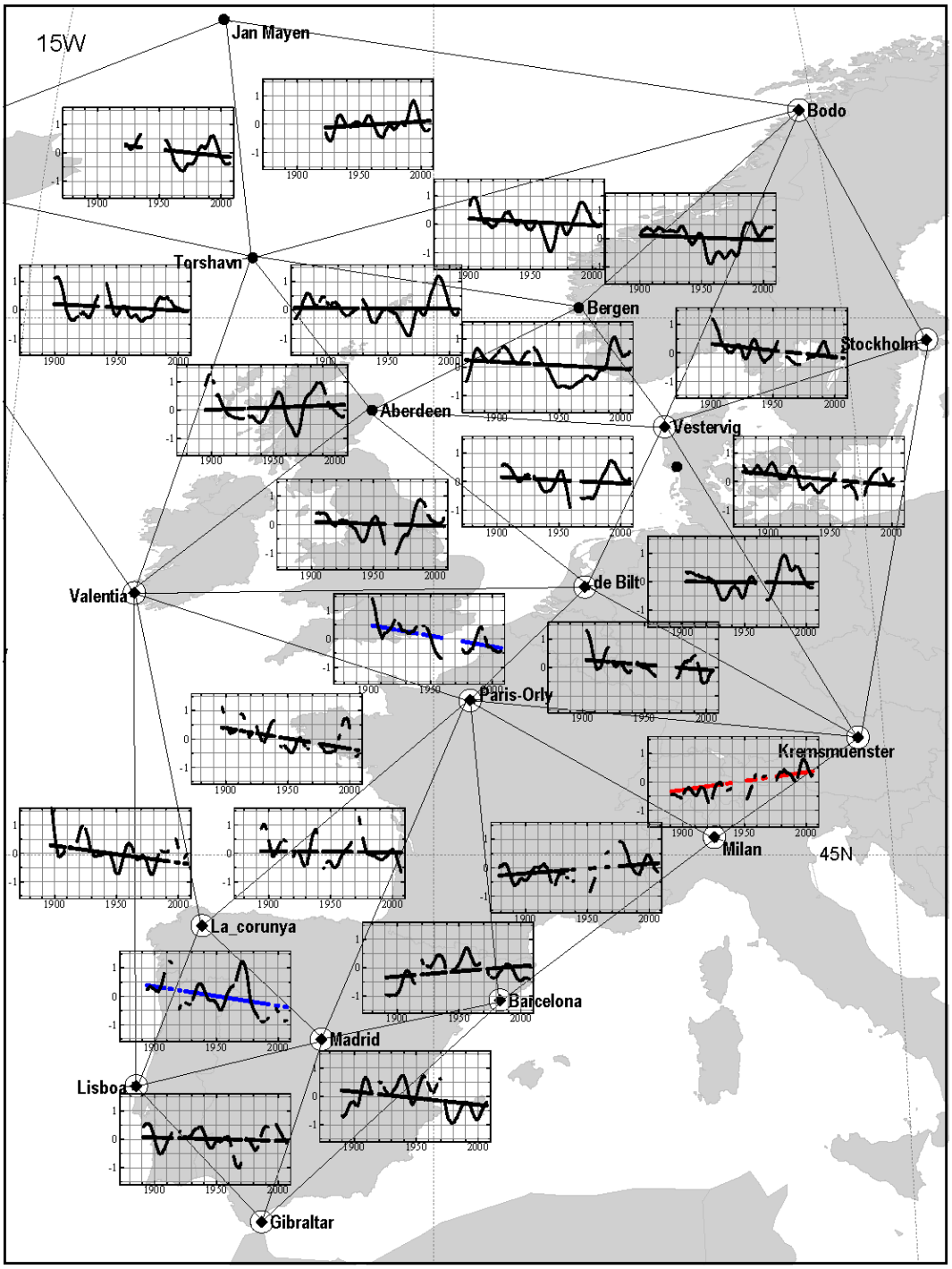

Figure 2.35: 99th percentiles of geostrophic wind speeds for winter. Triangles show regions where geostrophic wind speeds have been calculated from in situ surface pressure observations. Within each pressure triangle, Gaussian low-pass filtered curves and estimated linear trends of the 99th percentile of these geostrophic wind speeds for winter are shown. The ticks of the time (horizontal) axis range from 1875 to 2005, with an interval of 10 years. Disconnections in lines show periods of missing data. Red (blue) trend lines indicate upward (downward) trends of at least 5% significance. From Wang et al. (2011).

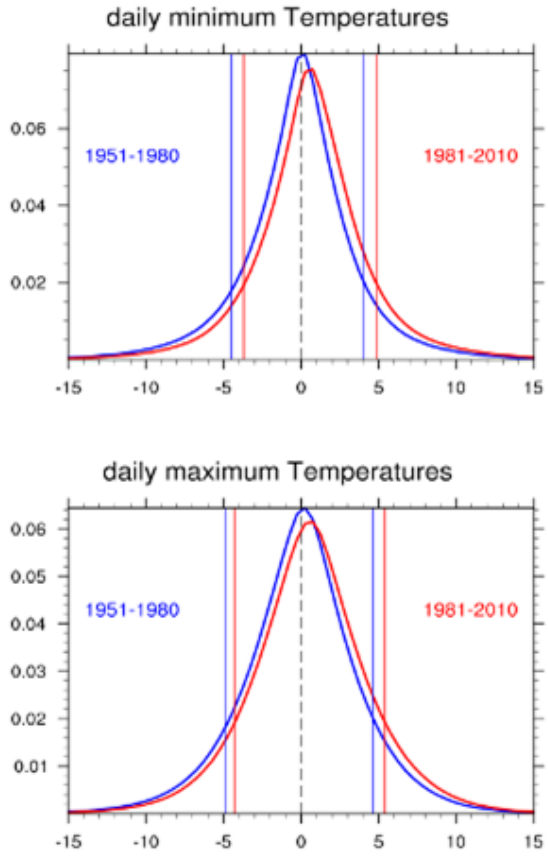

FAQ 2.2, Figure 1: Distribution of (a) daily minimum and (b) daily maximum temperature anomalies relative to a 1961–1990 climatology for two periods: 1951–1980 (blue) and 1981–2010 (red) using the HadGHCND data set. The vertical blue and red lines indicate the 10th (left-hand side) and 90th (right-hand side) percentiles for both periods.

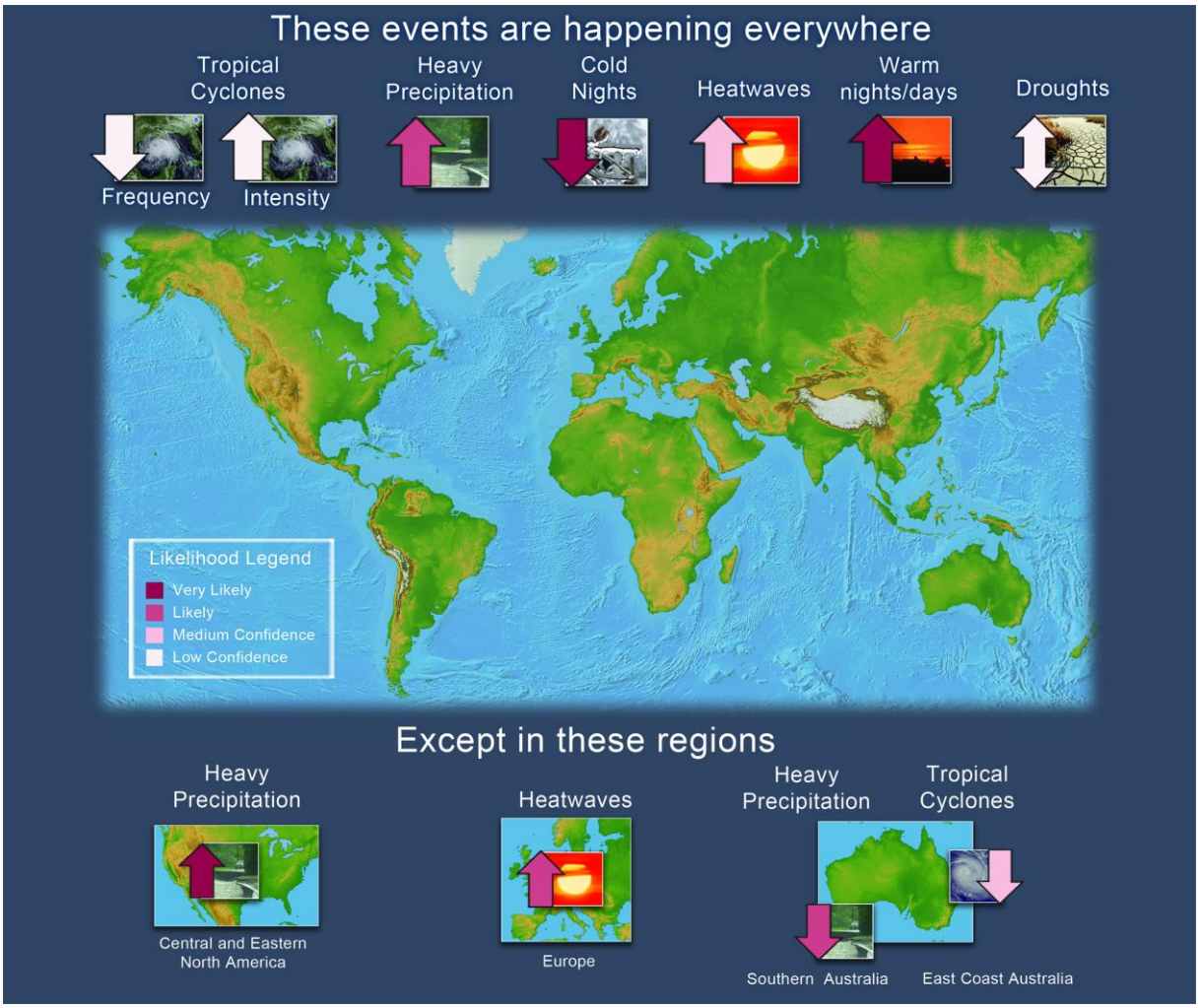

FAQ 2.2, Figure 2: The likelihood and direction of trend in the frequency (or intensity) of various climate extremes since the middle of the 20th century. Where the trend goes both up and down, this implies that there is regional variation in the sign of the trend, or that studies using different measures of dryness do not agree. Large regions that differ from the 'global' conclusion—either with respect to sign of, or confidence in, the trend—are also highlighted.

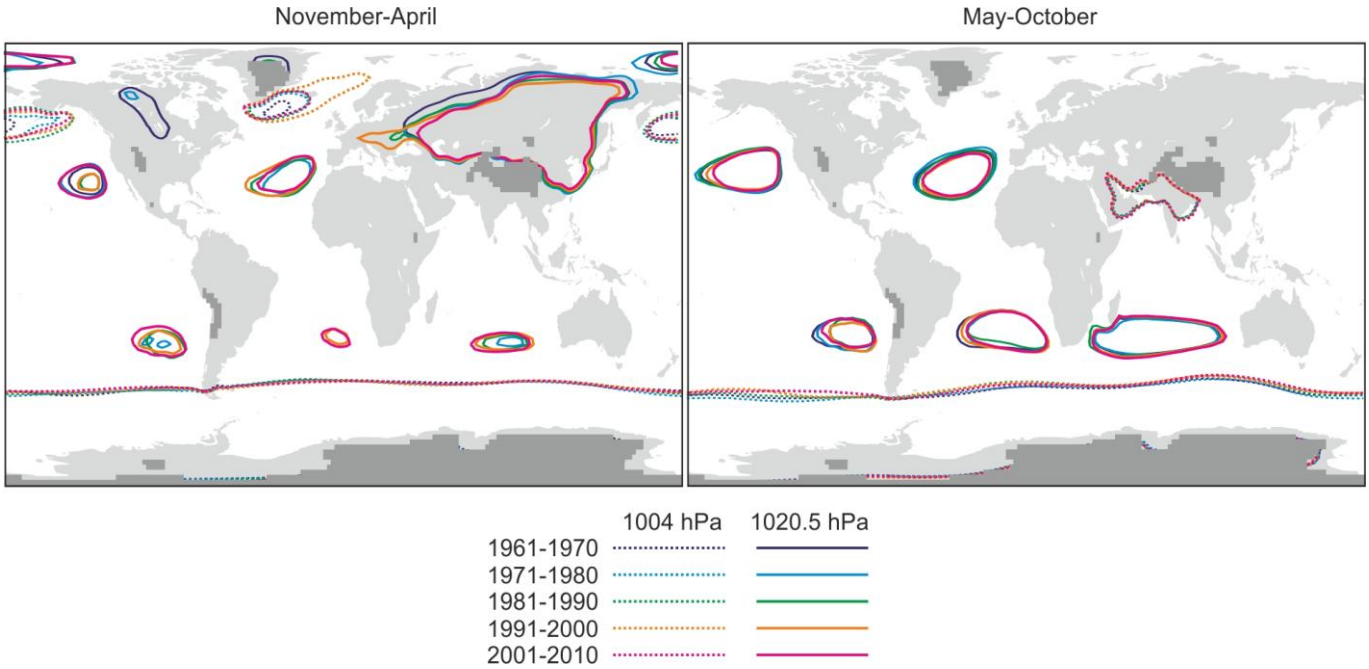

Figure 2.36: Decadal averages of SLP from the 20th Century Reanalysis (20CR) for (left) November of previous year to April and (right) May to October shown by two selected contours. Topography above 2 km above sea level in 20CR is shaded in dark grey.

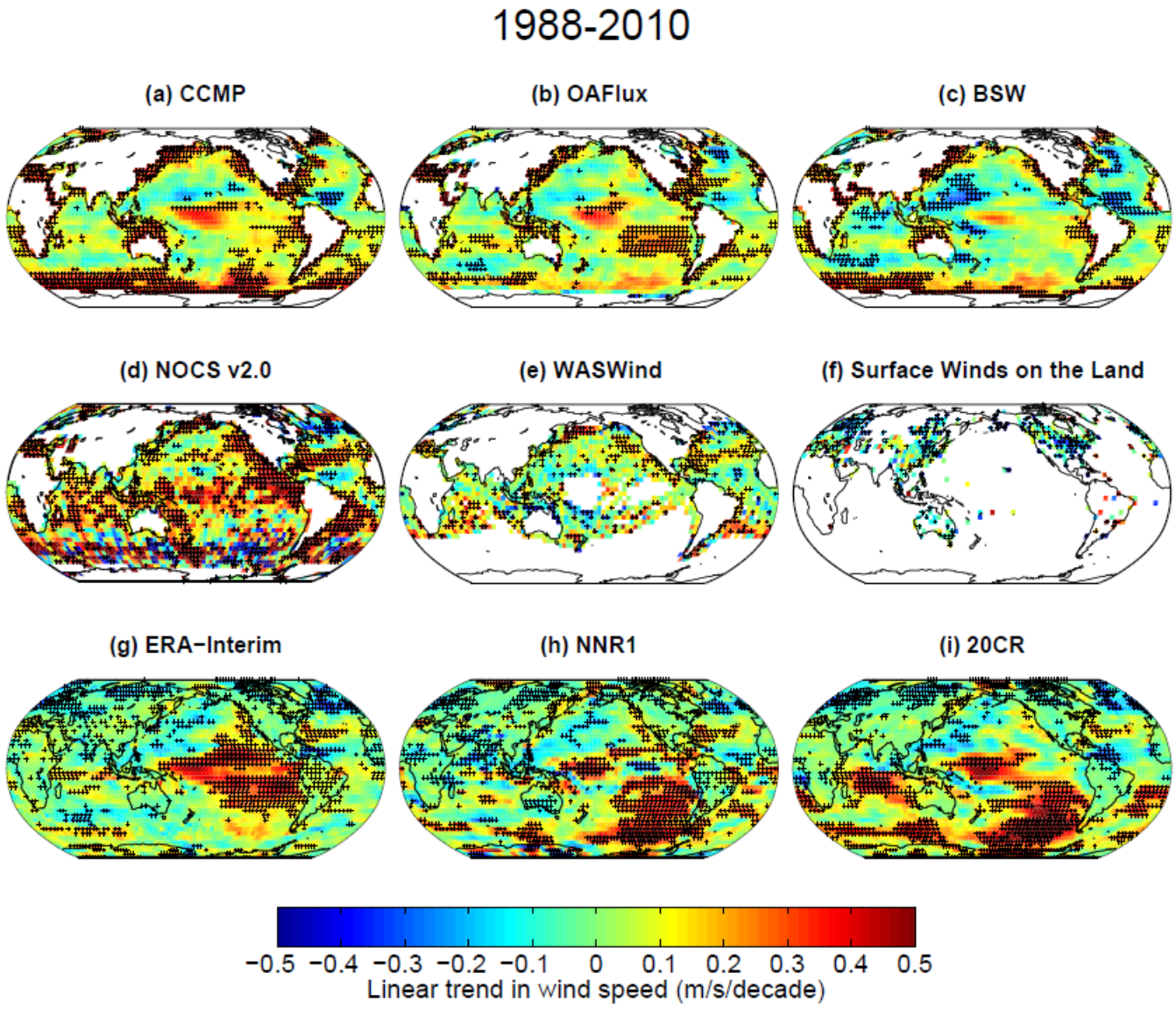

Figure 2.37: Surface wind speed trends for 1988–2010. Shown in the top row are data sets based on the satellite wind observations: (a) Cross-Calibrated Multi-Platform wind product (CCMP, Atlas et al., 2011); (b) wind speed from the Objectively Analyzed Air-Sea Heat Fluxes data set, release 3 (OAFlux); (c) Blended Sea Winds (BSW, Zhang et al., 2006); in the middle row are data sets based on surface observations: (d) wind speed from the Surface Flux Data Set, v.2, from NOC, Southampton, U.K. (Berry and Kent, 2009); (e) Wave- and Anemometer-based Sea Surface Wind (WASWind, (Tokinaga and Xie, 2011a)); (f) Surface Winds on the Land (Vautard et al., 2010); and in the bottom row are surface wind speeds from atmospheric reanalyses: (g) ERA-Interim; (h) NCEP-NCAR, v.1 (NNR1); and (i) 20th Century Reanalysis (20CR, Compo et al., 2011). Wind speeds correspond to 10 m heights in all products. Land station winds (panel f) are also for 10 m (but ananometer height is not always reported) except for the Australian data where they correspond to 2 m height. To improve readability of plots, all data sets (including land station data) were averaged to the 4° × 4° uniform longitude-latitude grid. Linear trend slopes and their uncertainties were computed for the annually averaged timeseries of 4^{o}x4^{o} cells by the method described in Appendix 2.A For all data sets except land station data, an annual mean was considered available only if monthly means for no less than eight months were available in that calendar year. Trend values were computed only if no less that 70% of all years (17) had a values and no less than 20% of first and last 10% of the annual record were available as well (i.e., at least one year available out of the first three and the last three years each). Black plus signs (+) indicate areas where linear trends slopes are different from zero at 10% significance level.

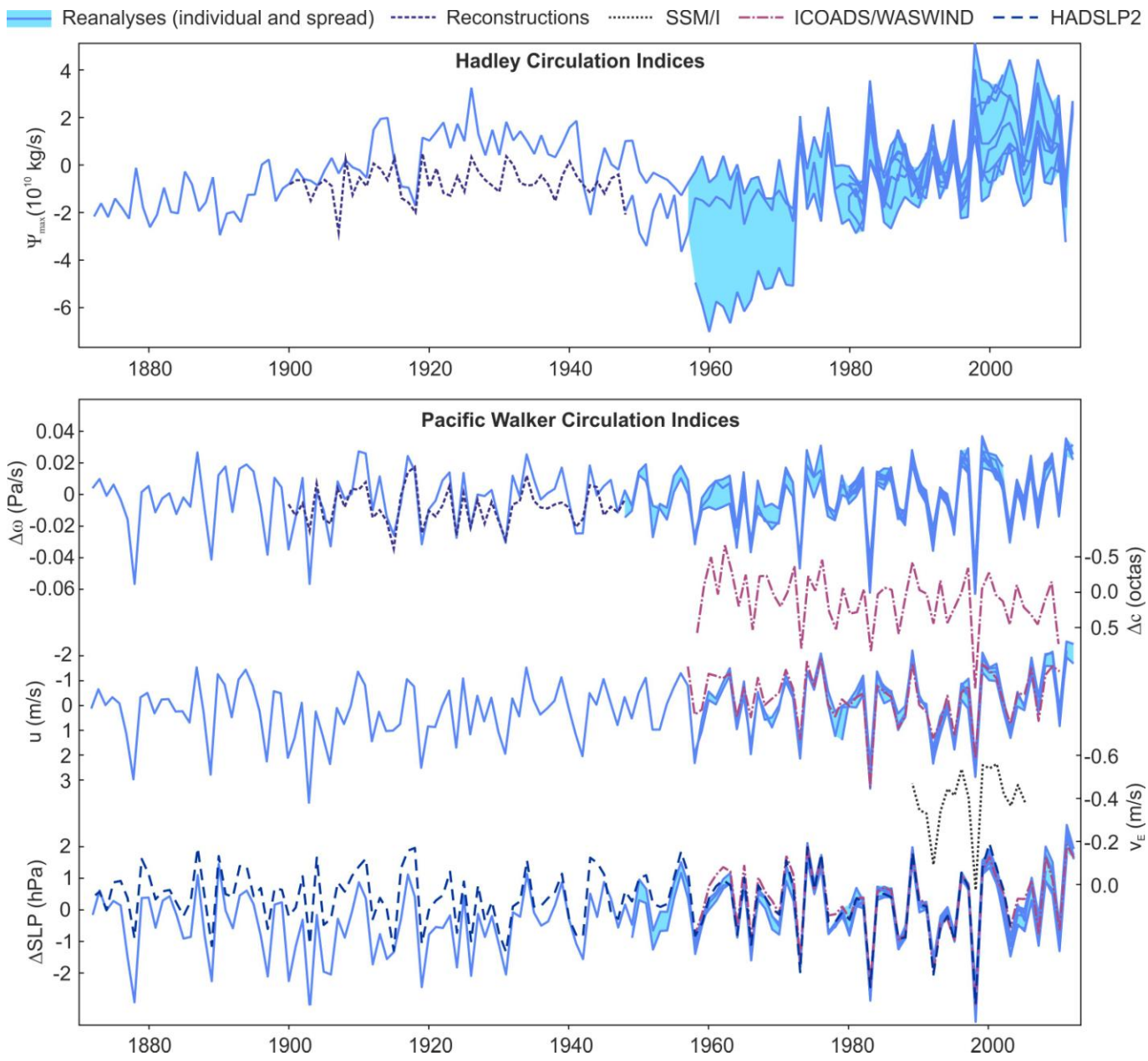

Figure 2.38: Top: Indices of the strength of the northern Hadley circulation in December to March (Ψ_{max} is the maximum of the meridional mass stream function at 500 hPa between the equator and 40°N, updated from Broennimann et al. (2009)). Bottom: Indices of the strength of the Pacific Walker circulation in September to January ($\Delta\omega$ is the difference in the vertical velocity between [10°S to 10°N, 180°W to 100°W] and [10°S to 10°N, 100°E to 150°E] as in Oort and Yienger (1996), updated from Broennimann et al. (2009)), Δc is the difference in cloud cover between [6°N–12°S, 165°E–149°W] and [18°N–6°N, 165°E–149°W] as in Deser et al. (2010), v_E is the effective wind index, updated from Sohn and Park (2010), u is the zonal wind at 10 m averaged in the region [10°S–10°N, 160°E–160°W], ΔSLP is the SLP difference between [5°S–5°N, 160°W–80°W] and [5°S–5°N, 80°E–160°E] as in Vecchi et al. (2006)). Time series based on ICOADS data are only shown from 1957 to 2009. All reanalysis data sets listed in Box 2.3 are used, if available until March 2012, except for the zonal wind at 10 m (20CR, ERA-Interim, ERA-40, NCEP2). Where more than one time series was available, anomalies from the 1979/1980 to 2001/2002 mean values of each series are shown.

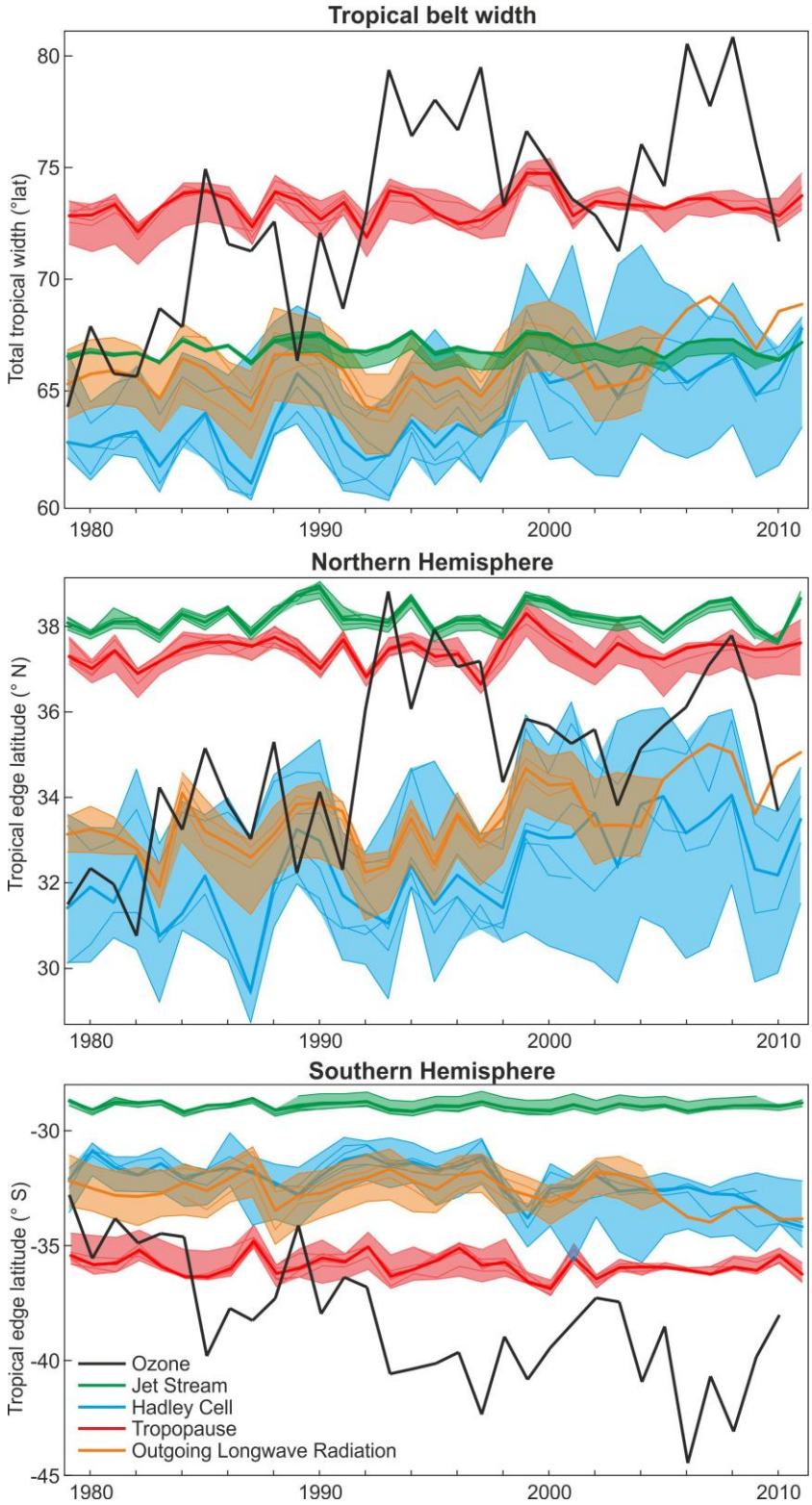

Figure 2.39: Annually averaged tropical belt width (top) and tropical edge latitudes in each hemisphere (middle and bottom). The tropopause, Hadley cell, and jet stream metrics are based on reanalyses (see Box 2.3); outgoing longwave radiation and ozone metrics are based on satellite measurements. The ozone metric refers to equivalent latitude (Hudson, 2011; Hudson et al., 2006). Adapted and updated from Seidel et al. (2008) using data presented in Davis and Rosenlof (2011) and (Hudson, 2011; Hudson et al., 2006). Where multiple datasets are available for a particular metric, all are shown as light solid lines, with shading showing their range and a heavy solid line showing their median.

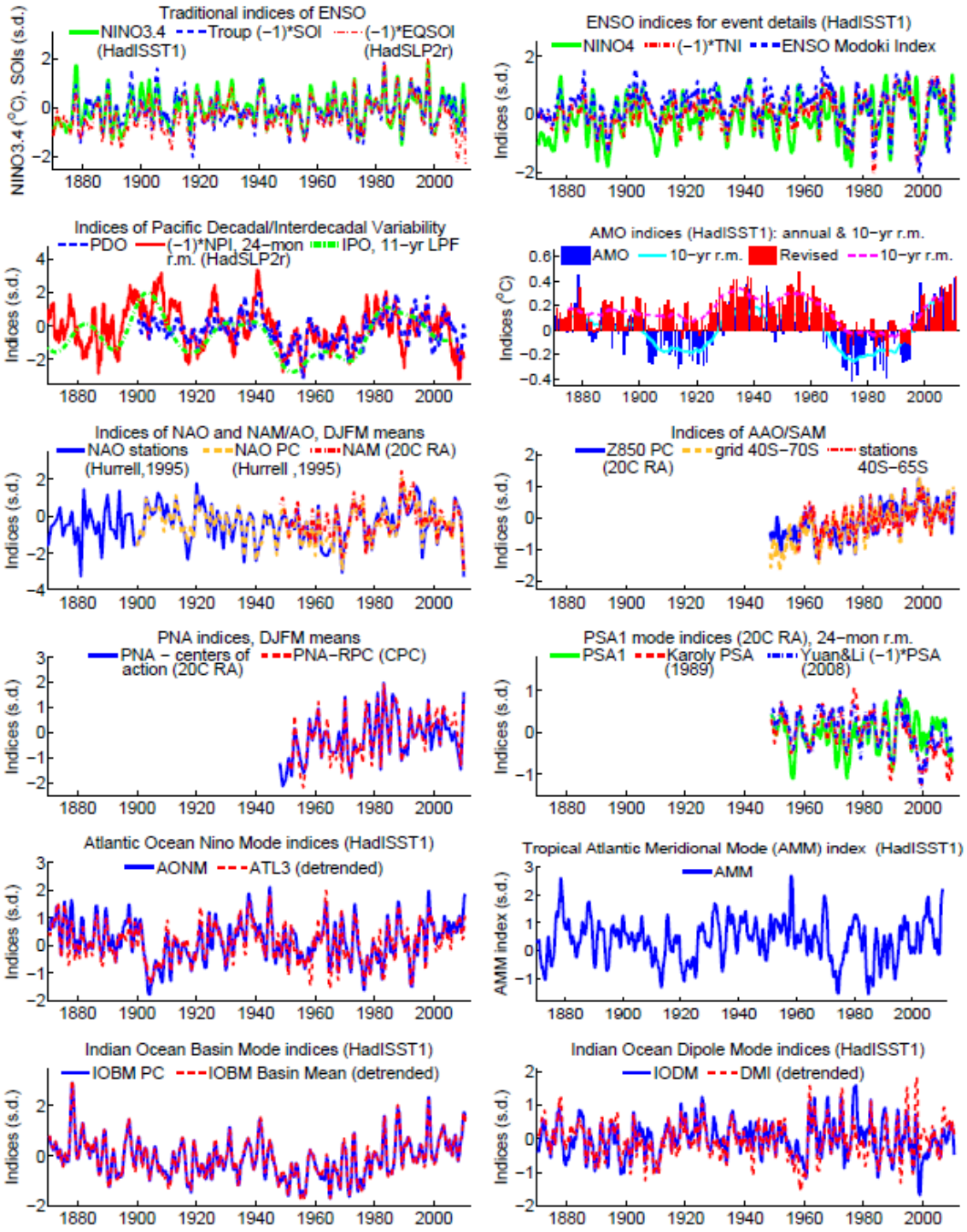

Box 2.5, Figure 1: Some indices of climate variability, as defined in Table 1. Where 'HadISST1', 'HadSLP2r', or '20C RA' are indicated, the indices were computed from the SST or MSLP values of the former two data sets or from 500 or 850 hPa geopotential height fields from the 20th Century Reanalysis, version 2. A data set reference given in the title of each panel applies to all indices shown in that panel. 'CPC' indicates an index timeseries publicly available from the NOAA Climate Prediction Center. Where no data set is specified, a publicly available regularly updated version of an index from the authors of a primary reference given in Table 1 was used. (Citations are given in panel legends only when needed for unambiguous identification of a particular index definition from Table 1; their presence or absence does not mean that the index values obtained from the authors were or were not used here). All indices are shown as 12-month running means (r.m.) except when the temporal resolution is explicitly indicated (e.g., 'DJFM' for December-to-March averages) or smoothing level (e.g., 11-year LPF for a low-pass filter with half-power at 11 years).

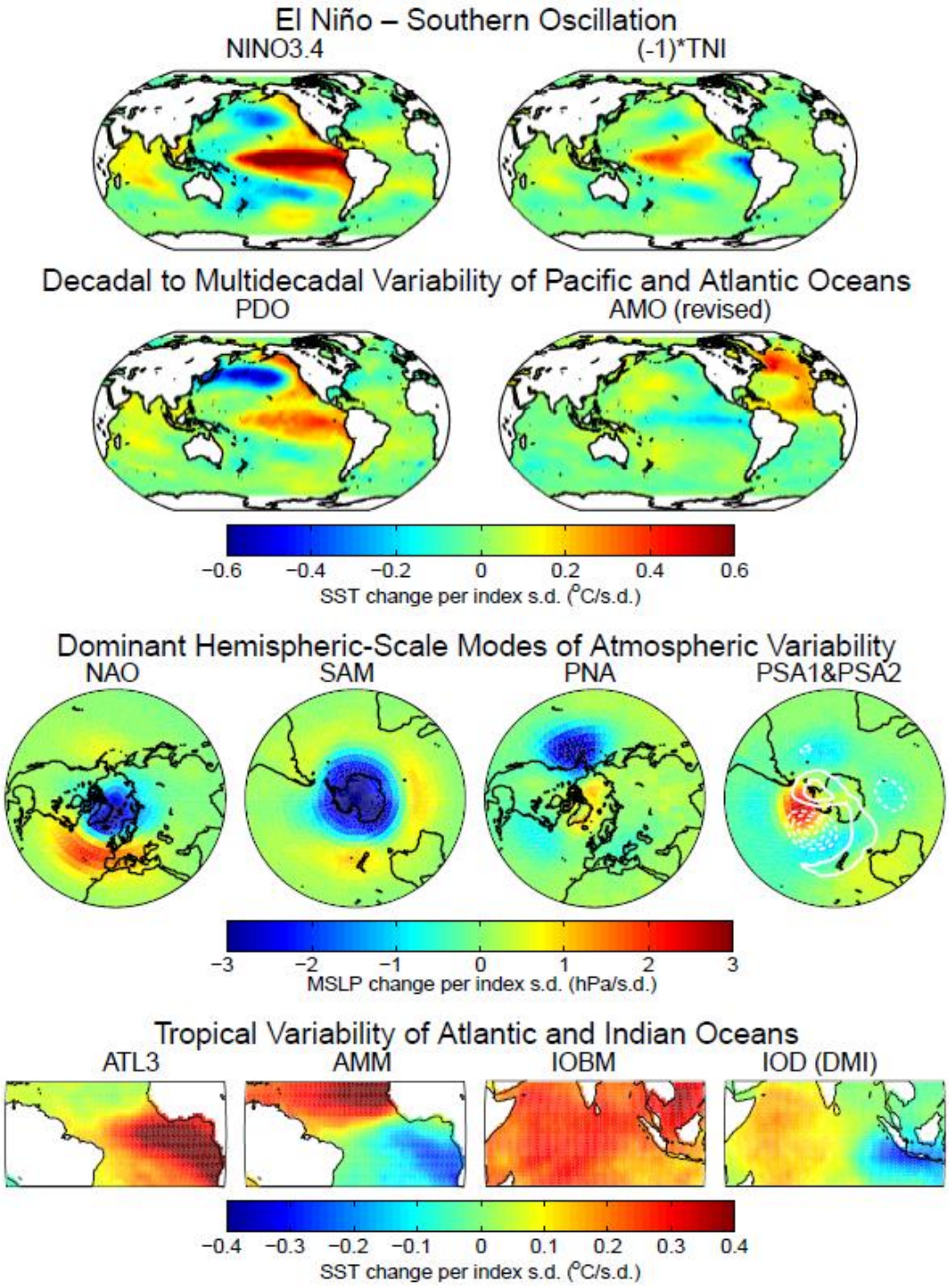

Box 2.5, Figure 2: Spatial patterns of climate modes listed in Table 1. All patterns shown here are obtained by regression of either SST or MSLP fields on the standardized index of a climate mode. For each climate mode one of the indices shown in Figure 1 was used. SST and MSLP fields are from HadISST1 and HadSLP2r data sets (interpolated gridded products based on data sets of historical observations). All SST-based patterns are results of monthly regressions for the 1870–2010 period except for the PDO regression pattern, which was computed for 1900–2010. The MSLP-based patterns of NAO and PNA are regression coefficients of the DJFM means; PSA1 and PSA2 patterns are regressions of seasonal means; SAM pattern is from a monthly regression. All SLP-based patterns are results of the 1948–2010 regression, except for the PDO regression pattern which is from 1876–2010 regression. For each pattern the time series was linearly de-trended over the regression interval. All patterns are shown by color plots, except for PSA2, which is shown by white contours over the PSA1 color plot (contour steps are 0.5 hPa, zero contour is skipped, negative values are indicated by dash).

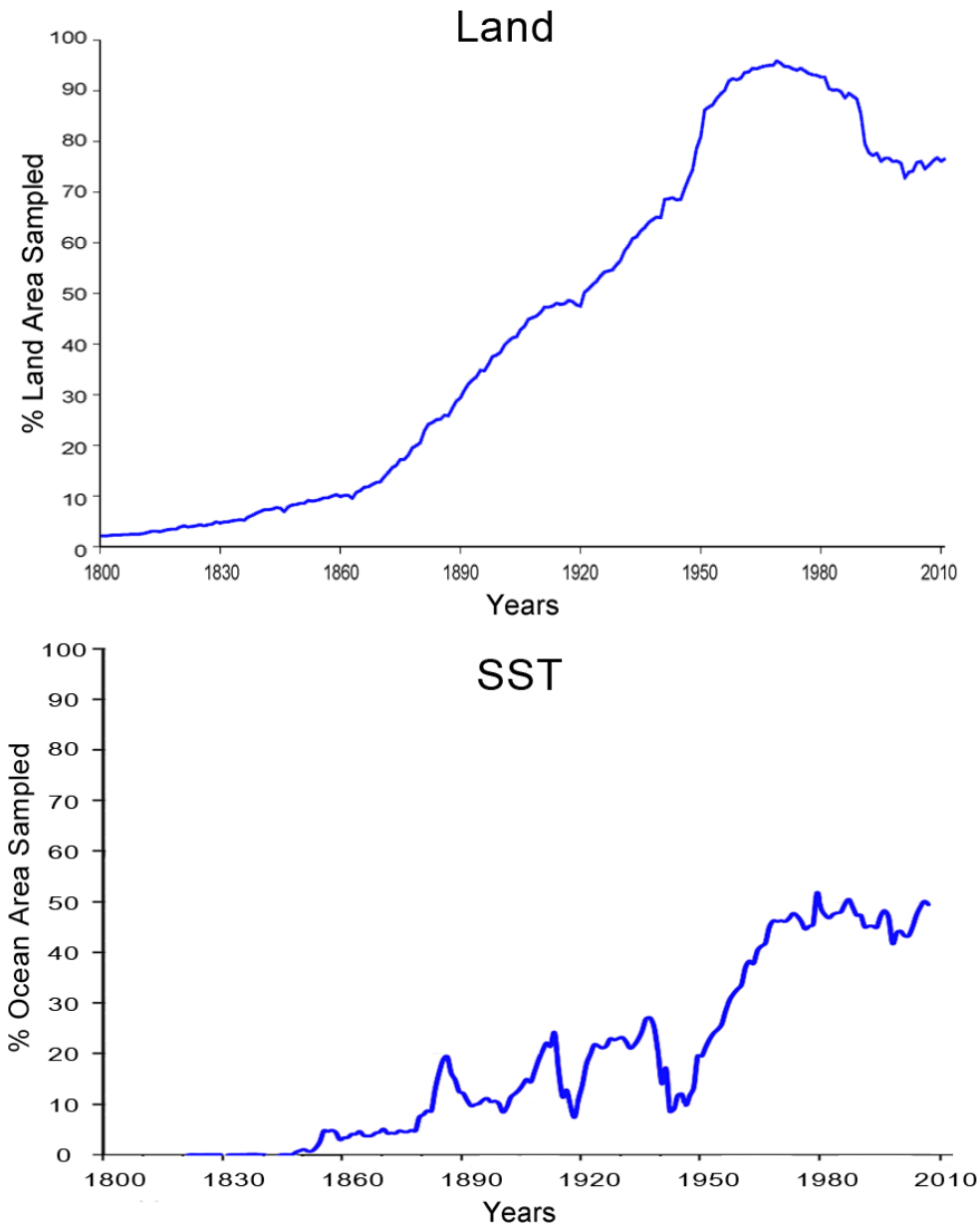

Figure 2.A.1: Change in percentage of possible sampled area for land records (top panel) and marine records (lower panel). Land data comes from GHCNv3.2.0 and marine data comes from the ICOADS in-situ record.

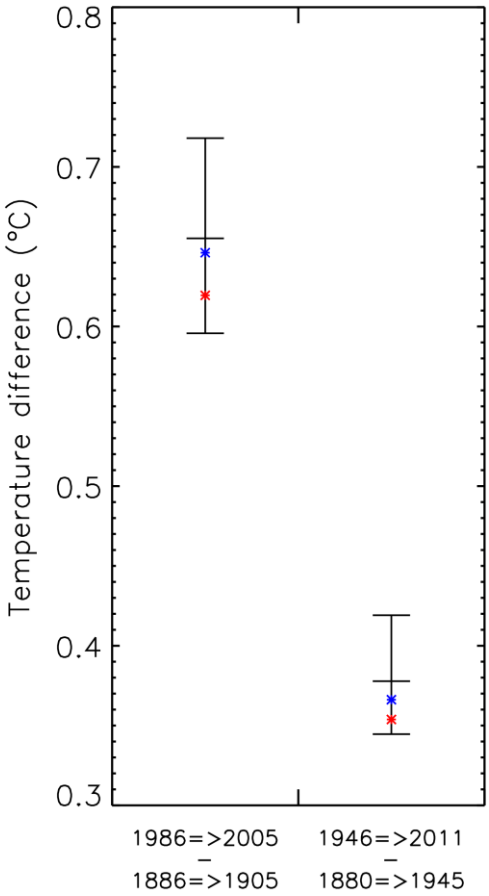

Figure 2.A.2: Differences in long term average temperatures in pairs of periods as calculated from HadCRUT4, GISTEMP and NCDC's data. Left - temperature difference between the periods of 1986 to 2005 and 1886 to 2005. Right - temperature difference between the periods of 1986 to 2005 and 1886 and 2005. The median and confidence limits (5% and 95%)for differences calculated from HadCRUT4 are shown in black. Period differences for GISTEMP are red. Period differences for NCDC are in blue.

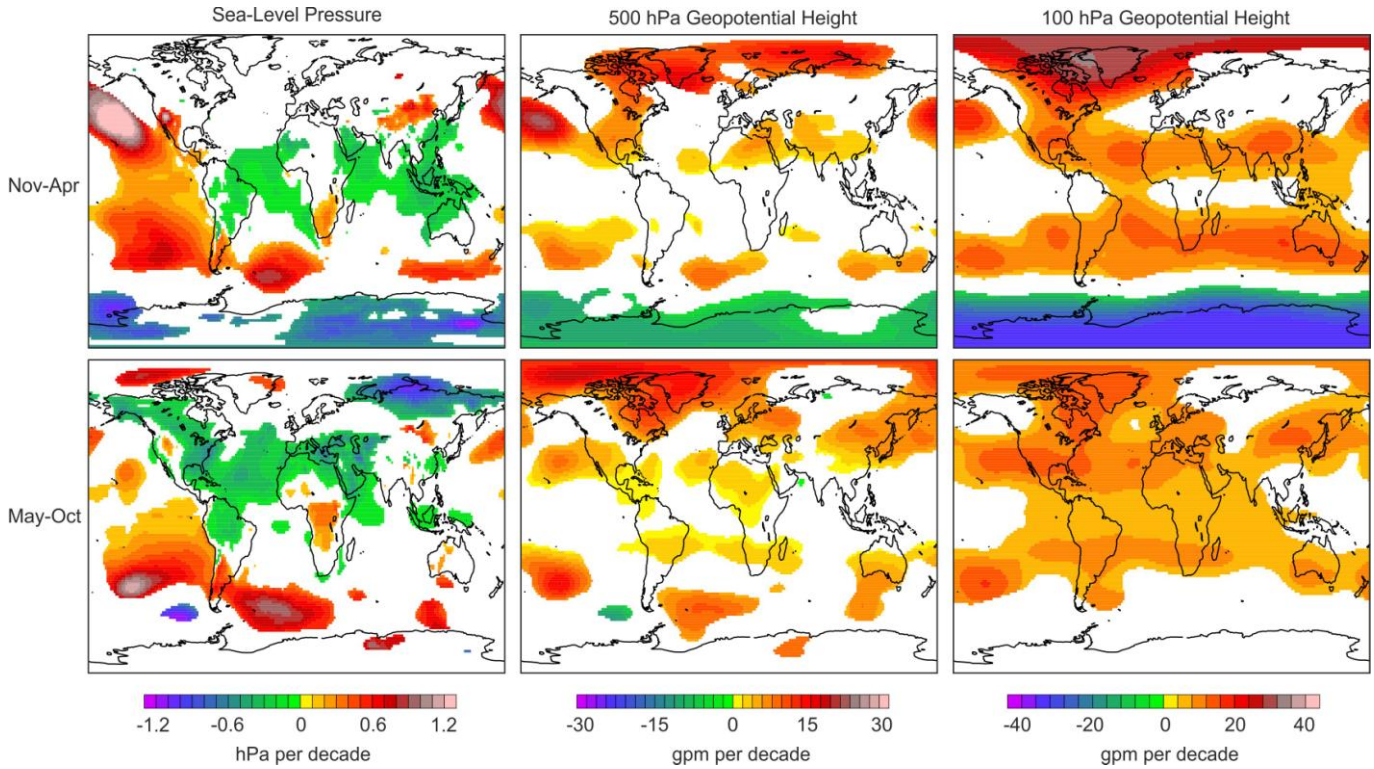

Figure 2.A.3: Supplementary Figure: Linear trends in (left) SLP, (middle) 500 hPa GPH, and (right) 100 hPa GPH in (top) November to April 1979/1980 to 2011/2012 and (bottom) May to October 1979 to 2011 from ERA-Interim data. Trends are only shown if significant at the 90% level.